# Scale-down Characterisation and Modelling of Harvest Operations in Mammalian Cell Culture Processes


**Adrian Victor Allen Joseph**

Advanced Center for Biochemical Engineering

University College London

This dissertation is submitted for the degree of

*Biochemical Engineering EngD*

April 2017

I would like to dedicate this thesis to my wonderful parents, Marie Joseph and Lionel Felix.

They were my inspiration.

# Declaration

I hereby declare that except where specific reference is made to the work of others, the contents of this dissertation are original and have not been submitted in whole or in part for consideration for any other degree or qualification in this, or any other University. This dissertation is the result of my own work and includes nothing which is the outcome of work done in collaboration, except where specifically indicated in the text.

Adrian Victor Allen Joseph

April 2017

# Acknowledgements

Firstly, I would like to acknowledge my supervisor Prof. Nigel Titchener-Hooker. His experience and extensive knowledge in the region of primary recovery provided great guidance throughout this programme. I am very grateful for his support. He has always encouraged my research, and helped me grow and express myself as a scientist. I would also like to acknowledge Prof. Suzanne S Farid and Dr. Stephen Goldrick who were both heavily involved in multiple publication efforts. Along with Prof. Titchener-Hooker they spent endless hours reviewing these publications and provided valuable feedback. Additionally, I would like to acknowledge the Department of Biochemical Engineering which was home for over 5 years. Paula Thomas assisted in organising numerous secondments and meetings. Derrick Abraham and Imran Sayed helped notably with financing of travel and placing of other unique expenses.

Secondly, I would like to acknowledge David Gruber, Michael Mollet, Brian Kenty, Jean Bender, Jim Dyre, Steve Rose, Ramin Afrasiabi, Ken Lee, Waikeen Chung, Kumar Singarapu and Morenje Mlawa. They all provided advice during numerous industrial placements at MedImmune Gaithersburg and Cambridge. I would also like to thank MedImmune as an organisation for embracing me with open arms and offering comfort during many occasions of failed experiments.

Finally, I would like to acknowledge my warm-hearted mother (Marie Joseph), my motivating father (Lionel Felix) and my exceptionally intelligent sister (Agatha Joseph) for their continued support throughout the EngD. They provided a great environment for me to work and more importantly words of comfort when arriving home late after numerous challenging days during the programme. I would also like to thank my landlady and friend

Mary Bracho who welcomed me to her home providing me lodging and much needed conversation when experiments failed during my industrial placement in Gaithersburg. I would like to specially acknowledge my mesmerizing fiancée (Anjali Kuperan) who supported me throughout this programme across multiple continents. She has encouraged me and picked me up on a frequent basis (singing *"Lean on me" by Bill Withers*, on the phone) when there were difficult times throughout this programme.

# Abstract

Disk-stack centrifugation and depth filtration are often used in combination for the removal of cells and cellular debris during the production of biopharmaceutical products. Process development and characterisation of these unit operations are often conducted at pilot-scale so as to best mimic the performance of commercial-scale equipment. However, this requires large volumes of material and significant levels of effort for successful characterization. This thesis describes scale-down methods for centrifugation and depth filtration that were developed to minimize test volumes when conducting characterization studies. The scale-down method for centrifugation uses a capillary shear device to mimic the shear created in commercial-scale centrifuges. This method consists of a two-stage process in which the culture is exposed to a shear device with a known energy dissipation rate and then separated by a lab-scale centrifuge. The methodology showed on multiple occasions to create mimic centrates with similar turbidities. The scale-down depth filtration method developed in this thesis uses a model based approach to translates constant pressure data to provide constant flow predictions. The method proposed uses constant pressure filter fouling data fitted to common filter fouling models to identify the best fitting model. The best fitting model's optimized coefficients were then correlated with the filter capacities from constant flow studies. The developed scale-down method for depth filtration was able to predict constant flow capacity with in an accuracy of ± 15%. Scale-down methods enable drastic reduction in both material and time requirements for process characterisation studies. Additionally, they allow a much wider design space to be tested than is currently possible at pilot-scale for such studies. In the case of the scale-down method developed this thesis for depth filtration there was on average an 80% reduction in processing time and an additional 70% reduction in feed material required when performing depth filter characterisation studies. While the scale-down centrifugation method enabled studies to be conducted with few millilitres of material compared to the pilot scale method which may require tens of hundreds of litres. With scale-down methods for centrifugation and depth filtration developed, these tools were used to quantify the effect of a range of cell culture conditions on the process performance of the harvest sequence.

# Table of contents

# List of figures

# List of tables

# Nomenclature

**Roman Symbols**

| | |
|---|---|
| $\Delta P$ | pressure increase (Pa) |
| $\mu$ | viscosity of the process fluid (Pa.s) |
| $\nu$ | the kinematic viscosity ($m^2.s^{-1}$) |
| $\nu_\infty$ | the tangential tip velocity ($m.s^{-1}$) |
| $\omega$ | angular velocity ($s^{-1}$) |
| $\rho$ | density of the process fluid ($Kg.m^{-3}$) |
| $\Sigma_{ds}$ | equivalent disk stack centrifuge settling area ($m^2$) |
| $\Sigma_{lab}$ | equivalent laboratory centrifuge settling area ($m^2$) |
| $\tau_{max}$ | the shear stress distribution in the boundary layer ($Kg.m^{-1}.s^{-2}$) |
| $\varepsilon_{max}$ | maximum energy dissipation rate ($W.Kg^{-1}$) |
| $A$ | available membrane frontal area ($m^2$) |
| $a'', b''$ | dimensionless coefficients for the linearized intermediate pore blockage model |
| $c$ | correction factor to allow for flow conditions not considered in the theoretical derivation of $\Sigma$ for large-scale centrifuges |

$CF_{Cap,i}$ filter capacity at constant flow for a given pressure (L.m$^{-2}$)

$D$ diameter of the capillary (m)

$dU/dr_w$ the shear rate at the pipe wall (Kg.m$^{-1}$.s$^{-2}$)

$J$ flux (m.s$^{-1}$)

$J_v(0)$ initial flux (m.s$^{-1}$)

$J_v(t)$ flux relative to available membrane area (m.s$^{-1}$)

$K_A$ complete blocking constant

$K_{Com}$ complete blocking constant

$K_C$ cake filtration constant

$K_I$ intermediate blocking constant

$K_S$ standard blocking constant

$l$ length of the capillary (m)

$LDH_{NS}$ absorbance of no shear sample at 450 nm

$LDH_{SS}$ absorbance of sheared sample at 450 nm

$N$ rotational speed of the disk (RPS)

$OD_f$ optical density of feed at 600 nm

$OD_o$ optical density of well spun sample at 600 nm

$OD_s$ optical density of supernatant at 600 nm

$P$ power input (W)

$P_{max}$ predicted capacity at 10 psi for constant flow operations (L.h$^{-1}$)

$Q$ flow rate (m$^3$.s$^{-1}$)

$Q_0$ initial volumetric filtrate flow rate (L.h$^{-1}$)

$Q_{ds}$ flow rate of pilot scale disk-stack centrifuge (L.h$^{-1}$)

$R_1$ radius to sample surface in an individual tube (m)

$r_1$ inner radius of centrifuge discs (m)

$R_2$ radius to sample base in an individual (m)

$r_2$ outer radius of centrifuge discs (m)

$R_{filter}$ specific resistance to filtration (m$^{-1}$)

$S$ solids remaining in processed samples (%)

$T$ applied torque (Kg.m$^2$.s$^{-2}$)

$t$ filtration time (h)

$t_{lab}$ laboratory centrifugation time (h)

$V$ total filtrate volume per filter area (L.m$^{-2}$)

$V_{lab}$ volume of suspension in individual tubes (L)

$V_{max}$ predicted maximum volume filtered per unit area for constant pressure operations (L.m$^{-2}$)

$X$ the distance from the edge of the rotating shear device disc (m)

$x$ fraction of overall centrifugation time for deceleration phase

| | |
|---|---|
| $y$ | fraction of overall centrifugation time for acceleration phase |
| $Z$ | number of discs in disc-stack centrifuge |
| CDR | complimentary determining region |
| CIP | cleaning in place |
| COGS | cost of goods sold |
| CPP | critical process parameters |
| CQA | critical quality attributes |
| Fab | fragment antigen-binding |
| Fc | fragment crystallizable |
| FDA | food and drug administration |
| HAMA | human anti-mouse antibody |
| hcDNA | host cell deoxyribonucleic acid |
| HCP | host cell protein |
| Ig | immunoglobulin |
| mAbs | monoclonal antibodies |
| TFF | tangential flow filtration |

# Chapter 1

# Literature Review

With an increased number of biopharmaceutical products transitioning to clinical trials there is a greater requirement to conduct process development studies within short time lines. Platform processes have become popular in the biopharmaceutical industry as a result. Extensive research in upstream has enabled higher titres to be reached during the the fermentation process [Kunert & Reinhart, 2016]. This, coupled with an increasing trend to complex biologics has meant that the robustness of the platform process is often tested to its limits. Scale-down experimental techniques allow for better understanding of large scale process performance. Furthermore, these techniques allow for the acceleration of process development for these products [Titchener-Hooker *et al.*, 2008]. This thesis explores development and validation of novel scale-down tools and methodologies in the primary recovery region of drug purification.

The literature review provides a brief introduction about monoclonal antibodies (mAbs) and how biopharmaceutical companies have profited from this product. It delves further into the high costs associated with drug development and the importance of process development. The thesis is based on the development of scale-down devices in

the primary recovery region and hence the literature review gives a detailed overview and critique of the current scale-down methodologies that are currently available.

## 1.1 Monoclonal Antibody Commercial Success

The first biopharmaceutical to gain approval was recombinant human insulin, by the late 1980's the types of products being approved were hormones and cytokines [Walsh, 2014]. Over the last three decades the approval of biopharmaceuticals and their market value has increased considerably. By 2012 market sales had been estimated to reach 50 billion USD with an annual compound growth rate expected to exceed the predicted 8% [Reichert & Valge-Archer, 2007]. This was associated with the emergence of monoclonal antibody (mAb) based products [Liu, 2014].

MAbs have been financially lucrative and have had a significant influence on patient health across a wide range of disease segments which include; respiratory, cancer, cardiovascular and transplant rejection [McCamish & Woollett, 2012]. Products like Humira (AbbVie) have been able to generate billions of dollars in sales [Aggarwal, 2011]. Worldwide sales of all drugs have surpassed the trillion dollar mark; Information Management Services (IMS) forecasts a 1.3 trillion dollar market by 2018 [Looney, 2016]. Figure 1.1 shows its growth in sales over years 2005 to 2009. With such sales mAbs have been touted to replace the pharmaceutical industries best selling drugs such as Lipitor (Pfizer) and Plavix (BMS) by 2016 [Table 1.1].

## 1.2 Monoclonal Antibody Structure

During the early 1960's Milstein began looking into understanding the structure of antibodies and by the mid 1960's he had worked with Brenner to understand the diversity

**Table 1.1:** Predicted sales of world's top drugs in 2014 [Hirschler, 2010]

| Consensus forecast for 2010 | | | |
|---|---|---|---|
| Drug | Target | Manufacturer | Sales (Bln USD) |
| Lipitor | Cholesterol | Pfizer | 11.7 |
| Plavix | Anti-clotting | Sanofi/ Bristol | 9.6 |
| Advair | Asthma/COPD | Glaxo Smith Kline | 9 |
| Remicade | Artheritis | Merck/ J&J | 7.4 |
| Enbrel | Artheritis | Pfizer/ Amgen | 7.1 |
| Humira | Artheritis | Abbott | 6.8 |
| Avastin | Cancer | Genentech/Roche | 6.7 |
| Rituxan | Cancer | Genentech/Roche | 6.1 |
| Diovan | Hypertension | Novartis | 6 |
| Crestor | Cholesterol | AstraZeneca | 5.8 |
| **Consensus forecast for 2014** | | | |
| Drug | Target | Manufacturer | Sales (Bln USD) |
| Avastin | Cancer | Roche | 8.9 |
| Humira | Artheritis | Abbott | 8.5 |
| Enbrel | Artheritis | Pfizer | 8 |
| Crestor | Cholesterol | AstraZeneca | 7.7 |
| Remicade | Artheritis | Merck | 7.6 |
| Rituxan | Cancer | Genentech/Roche | 7.4 |
| Lantus | Diabetes | Sanofi-Aventis | 7.1 |
| Advair | Asthma/COPD | Glaxo Smith Kline | 6.8 |
| Herceptin | Cancer | Genentech/Roche | 6.4 |
| NovoLog | Diabetes | Novo Nordisk | 5.7 |

among antibodies [Brenner, 1966]. Later Köhler collaborated with Milstein to create a method for producing antibodies by fusing an antibody producing plasma with a rodent myloma tumour [Ozato *et al.*, 1980]. Since then single human B cell cloning techniques to clone directly and express immunoglobulin (Ig) genes from antigen-specific B cells have been developed. Early mAb products were in vivo murine-based products, typically immunogenic in humans inducing Human Anti-Mouse Antibody (HAMA) responses and furthermore had poor abilities to induce human immune effector responses, thereby limiting their clinical applicability [Tjandra *et al.*, 1990]. Genetic manipulation in the late

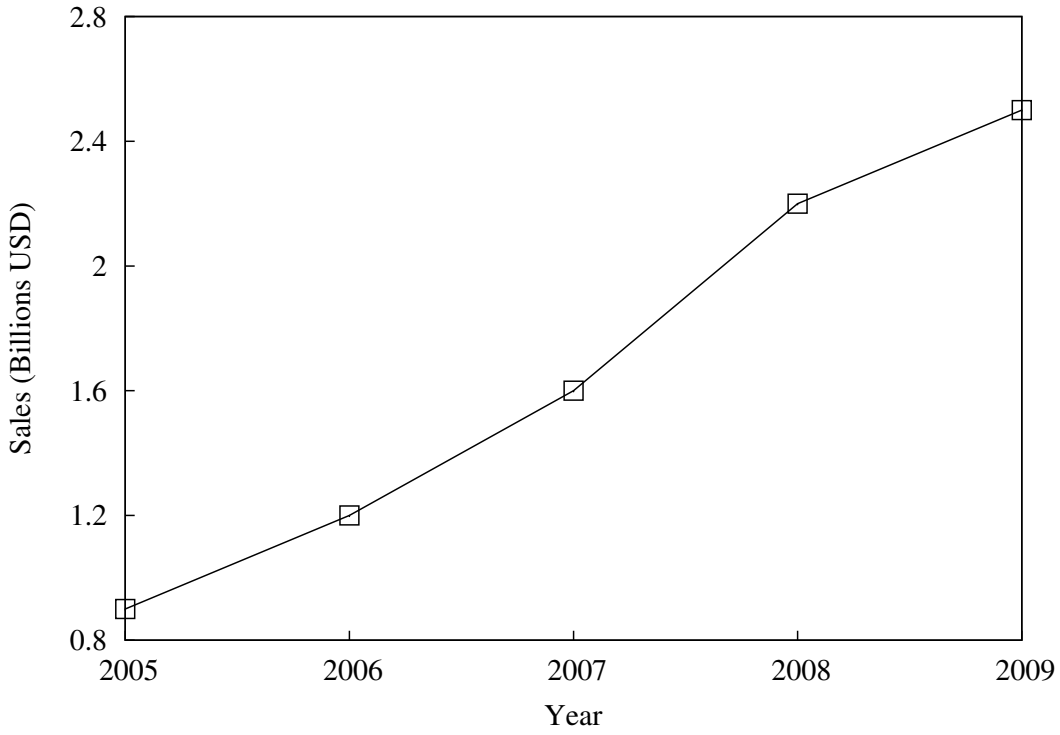


**Fig. 1.1:** Sales growth of Humira (AbbVie) between years 2005-2009 [Aggarwal, 2011]

1980's enabled the removal of the murine sequence of the mAb [Werner, 2004]. Currently there are fully humanised antibodies such as Humira (AbbVie) that are available in the market. The removal of the murine content from the mAb sequence had allowed for the reduction of HAMA response and increased effectiveness of the mAb [Werner, 2004]. The past century has witnessed the evolution of the "magic bullet" from concept to clinical reality. The attributes of target specificity, low toxicity and the ability to activate the immune system suggest the continuing promise of therapeutic antibodies. Monoclonal antibodies (mAbs) are proteins naturally produced by the immune system and can be divided up into five classes; IgG, IgM, IgA, IgD and IgE. Each have distinctive structures, type of activity and specified locations in the body to provide immunity against pathogens of varying types. In this thesis the class of interest was IgG. These have subclasses of IgG 1, 2, 3 and 4. All IgGs share a distinct Y shaped structure [Figure 1.2] which is made up of two identical polypeptide chains each containing one heavy and one light chain. These

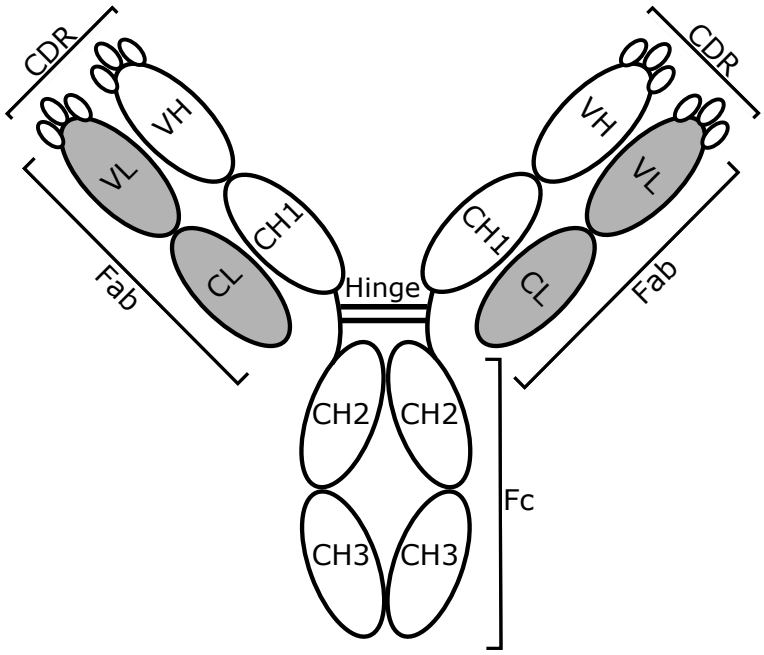


**Fig. 1.2:** Basic structural schematic of IGg class antibody

chains are made up of multiple domains, four make up the heavy chain and while two make up the light chain [Jefferis, 2009]. All the domains are held together by hydrogen bonded anti-parallel $\beta$ strands in the form of a bilayer structure. This structure is further stabilised by a combination of covalent and disulphide bonds.

The bilayer structure of a mAb can also be separated into Fragment antigen-binding (Fab) and Fragment crystallizable (Fc) fragments [Figure 1.2]. Though all domains can be described as either constant or variable, only regions of the Fab fragment towards the N terminal contain the two variable domains in both heavy and light chains. In the variable domain upto 30% amino acid residues can vary between mAbs but it is the Complimentary Determining Region (CDR) which experiences the most variability. In each of the variable domains there are three CDRs which together form a pocket which is responsible for the antigen-antibody binding. This binding is very specific and is heavily based around the middle CDR's ability to act as an antigen determinant. Side chains of the CRDs are

influenced by Van der Waals forces, hydrogen bonds and electrostatic forces. These forces enable the depressions and protrusion of the antigen to be filled. Binding to the antigen is further facilitated by the hinge. This allows for the mAb to rotate between the two Fab and Fc regions. Polypeptide links connect the variable and constant domains in the Fab region, creating flexibility and better antigen binding [Presta, 2008]. Unlike the Fab region the Fc region of the mAb is made up of four constant domains and as a result is less involved in antigen interaction. The Fc region is essential in providing long half-lives.

Once the mAb structure and antigen binding are determined for a particular therapeutic indication, the next step is to develop the manufacturing process to supply material for the clinical trials and eventually commercial market. The following section describes the typical pressures faced during drug development.

## 1.3 MAb Development

**Table 1.2:** Bioprocess development considerations

| Time Spans | Safety & Environment | Economic |
|---|---|---|
| Process development | Batch contamination | Cost of development |
| Batch process time | Cross contamination | Manufacturing CoG |
| Meeting clinical demand | Waste material handling | Facility cost |
| | | Sales Expectations |
| **Quality & Regulation** | **Operational Performance** | **Legal** |
| GMP standards | Titres | |
| Validation | Yields | Patent infringement |
| Quality of raw material | Purity | Biologic licence application |
| Batch consistency | Resource utilisation | |
| Product characterisation | Scale-up | |

Monoclonal antibody (mAb) development requires the expertise of many hundreds of professionals steering the drug candidate through pre-clinical and clinical testing, man-

ufacturing, regulatory affairs, approval and marketing [McCafferty, 2010]. There are a number of considerations such as product quality, economics, safety, legal and regulatory constraints when taking a mAb to market. Upon the analysis of these factors an informed decision can be taken to determine whether the process is worthy of further development based upon its capabilities and or the identification of its limitations [Farid, 2001].

### 1.3.1 Economic and Time Pressure

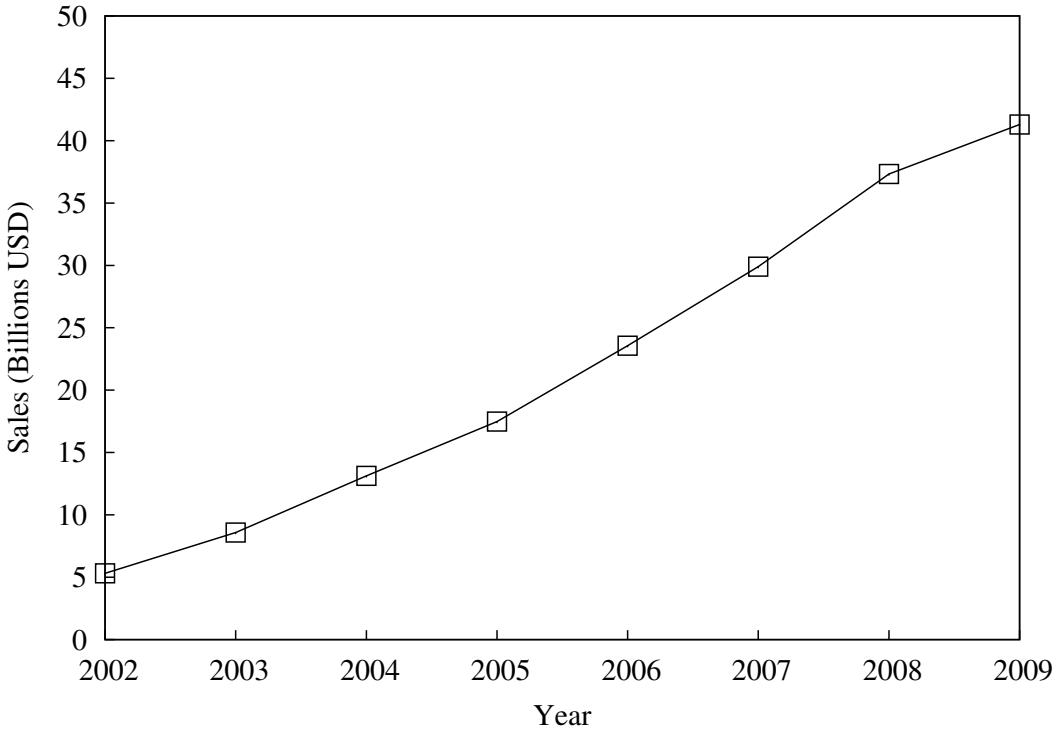


**Fig. 1.3:** MAb sales growth over years 2002-2009 [Howard, 2011]

The development of a mAb is an increasingly lengthy, costly and risky process [Werner, 2004].Biopharmaceutical companies continually invest in ways to reduce the escalating costs of bringing a drug to market. Any progress in reducing the cost of goods sold (COGS) helps ensure wider distribution of the drug to patients. However, optimization of COGS

may result in a increased drug development time. As a result decisions made regarding drug development are made in a climate where there often a good deal of pressure to make the correct decision but typically there is little information available to make that decision [Farid, 2008]. Figure 1.3 shows the consistent growth in sales for mAb based products over the last decade. The development cost has been valued at $1.6 billion and this cost has been subjected to a considerable rise over the last decade [Pharmaceuticals, 2014]. This increase in cost has been influenced by the pressures of competition and regulatory guidelines that require a thorough understanding of the characteristics of the product. Drugs need to transition between phases of clinical trials before gaining approval. The cumulative approval rate of the FDA (Food and Drug Administration) for human mAbs is estimated at 17.5%. As a result larger capital backing is needed to sustain the drug development process due to the multiplied risk factors that account for the chances of failure at each stage [Pharmaceuticals, 2014].

Development of biologics is estimated to take around 7-12 years, from discovery to patient [Krishna, 2012]. These timelines involve non-clinical, pre clinical and clinical development. The non-clinical and pre-clinical developments are aimed at generating a supply of the drug and to provide sufficient information for its safe use during the costly task of clinical development. Development delays could potentially be severe, and can incur a large losses in revenue [Farid, 2001]. All biopharmaceutical companies aim to release their drug out to the market swiftly in order to obtain the largest possible market share. The swiftness has particular importance in the biopharmaceutical industry because of the finite patent lifetime of drugs [Pharmaceuticals, 2012]. It is said that each day lost from the drug being on the market results in a loss of 1 million USD of possible revenue [Farid, 2001]. Also with increased competition drugs have a shortened life cycle meaning that the time for a company to recoup its research and development costs is reduced

[Jungbauer & Göbel, 2012].

Some companies put an emphasis to just concentrate on the clinical demands in order to make it to market first so as to obtain the largest market share. Historically this strategy was common place in the biopharmaceutical industry because reaching the market first provided attractive returns [Farid, 2008]. As the biopharmaceutical industry continues to mature, this culture promoting first to market is slowly changing due to reduction in the pricing flexibility, higher manufacturing costs and shorter patent exclusivity for the product.

### 1.3.2 Quality and Regulation

Along with the development costs and pressures to be first to market, biopharmaceutical drug development has always been strictly regulated to ensure patient safety and product efficacy. These regulations are enforced by the FDA (Food and Drug Administration) and other regulatory agencies [Reichert *et al.*, 2005]. These agencies require the drug manufacturer to have understood the molecule through structural characterisation. They also require understanding of the effects of CPPs (Critical Process Parameters) and CQAs (Critical Quality Attributes) in relation to the purity and levels of impurity accumulated using the manufacturing process [Goetze *et al.*, 2010]. The regulatory agencies have close oversight of the candidate drug during all stages of clinical development. Once the drug has successfully met target criteria in the clinic, the regulatory agency can grant approval. However, regulatory agencies also have the power to terminate applications if products are found to offer no significant improvement in mortality or quality of life.

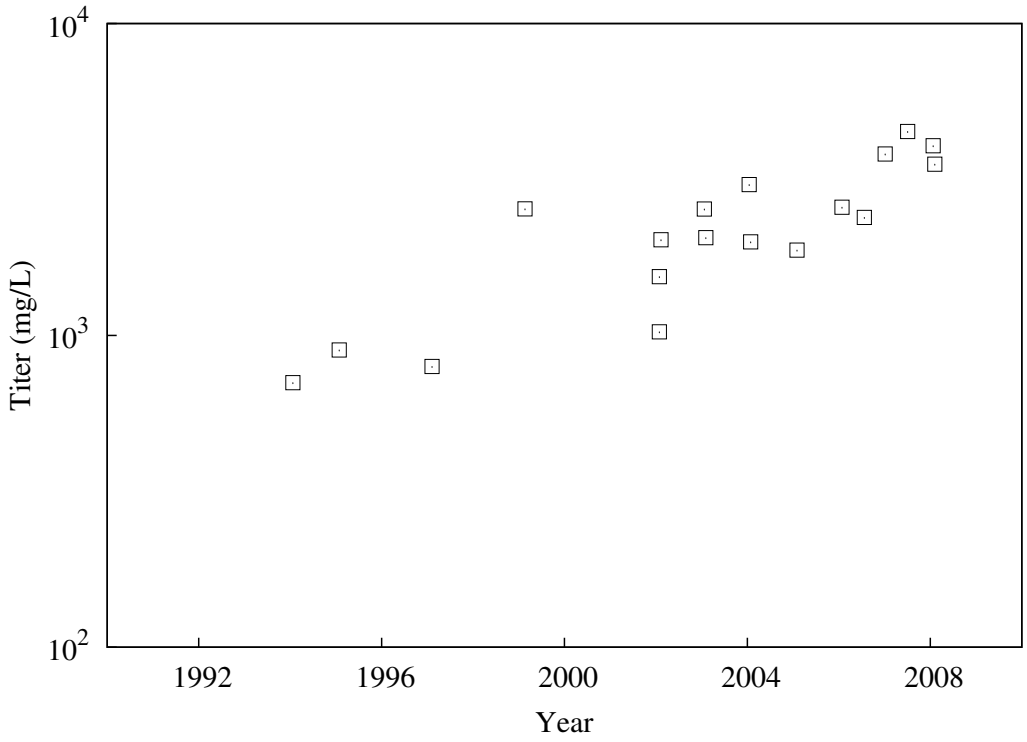


**Fig. 1.4:** Titre increases in different types of antibodies over the last 2 decades [Howard, 2011]

### 1.3.3 Process Consideration

The manufacturing process can also significantly impact the COGS. In particular, the amount of mAb produced in a single batch, or product titre, has an inversely proportional relationship with the cost of goods ($/g). As a result of this driver titres have increased by three orders of magnitude over the last 20 years [Figure 1.4]. These increases have been achieved though upstream developments in the expression technology, process optimisation and especially with the development of longer fed batch cultures processes [Birch & Wood, 1985]. However, these advances have resulted in the generation of higher levels of impurities. Higher levels of impurities such as host cell protein (HCP), host cell DNA (hcDNA) and product aggregates make the purification process more challenging [Farid, 2008]. Consistently removing higher levels of these impurities has to be addressed as part of the process development effort. Others process considerations include the

removal of complex aggregate formations, antibody fragments and product variants. These process development steps also need to be conducted in a timely fashion to accelerate the progress of antibodies to the clinic.

## 1.4 Monoclonal Antibody (mAb) Process Development

Most biopharmaceutical companies have more than one potential drug candidate in their pipeline at any given time and there is a desire to produce multiple products within one clinical manufacturing site for similar products such as mAbs. Consistent processes are clear drives for utilization of a template approach within process development [Pisano, 1997]. The mAb product class offers some level of biochemical similarities and hence enables the utility of a template purification platform. A typical platform process assumes the sequence of operations has the ability to purify all mAbs. However, even though mAbs share a product class, significant physiochemical differences exist within. Molecules can differ significantly from each other in their affinity and elution behaviours. In some cases this leads to the platform process being rendered impractical. The platform serves as a guide for the overall scheme of the down stream process and identifies a range of operating conditions for individual unit operations. A platform approach enables biopharmaceutical companies to speed up the time required to take a product to clinic through reducing the time and resource requirements for process development [Ghose *et al.*, 2005]. This approach also lays down a guide that can be adopted across multiple manufacturing sites. Following a platform can also speed the transfer of the process to multiple manufacturing sites.

Figure 1.5 illustrates a commonly used mAb platform process. Different companies have different approaches to the platform [Table 1.3]. The final process developed can change depending on the type of molecule or the experience within company in the pu-

rification of the molecule. In a typical mAb platform cell culture undergoes an initial solid liquid separation step for the removal of cells and cellular debris utilizing a combination of centrifuge and depth filtration operations. The Protein-A column then allows for the removal of aggregates and concentration of the product. The following two chromatographic steps of cation and anion exchange allow for the reduction of process and product related impurities. The success of a typical platform is determined by the level of selective capture enabled by using the Protein-A step and removal of impurities remove impurities in the later cation and anion exchange steps. A detailed description of each of the unit operations illustrated in Figure 1.5 is found in Table 1.4.

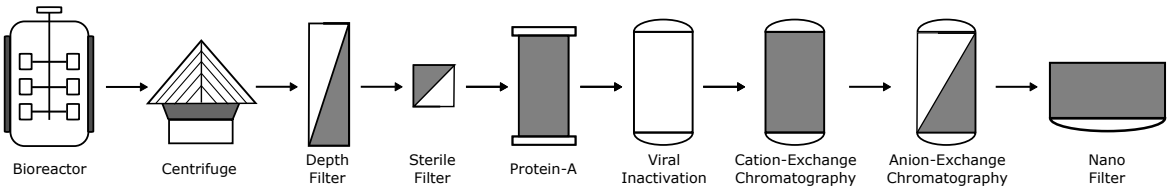


**Fig. 1.5:** Illustration of a commonly used mAb downstream process platform

**Table 1.3:** Comparisons of different production process where number indicates position in the downstream process [Sommerfeld & Strube, 2005]

| | Herceptin | Rituxan | MabCampath | Synagis | Remicade |
|---|---|---|---|---|---|
| Cell Harvest | 1 | 1 | 1 | 1 | 1 |
| Protein A | 2 | 2 | 2 | | 2 |
| Virus Inactivation | 3 | 3 | 3 | 4 | 3 |
| Cation Exchange | 4 | 5 | 4 | 3 | 4 |
| Anion Exchange | 5 | 4 | | 2 & 6 | 6 & 7 |
| Hydrophobic Interaction | 6 | | | | |
| Size Exclusion | | | 5 | 8 | |
| Virus Clearance | | 6 | 6 | 5 & 6 | 5 |
| Sterile Filtration | 7 | 7 | 7 | 9 | 8 |

**Table 1.4:** Functions and limitations of common unit operations in the purification process [Liu *et al.*, 2010]

| Unit Operation | Function | Limitation |
|---|---|---|
| Centrifugation | Separation of the host cells from the culture medium | System design is required to minimise shear damage |
| Depth Filtration | Separation of the host cells from the culture medium<br>Utility to reduce hcDNA & HCP load | When processing large cell culture volumes requires large filter areas |
| Protein-A | Used to capture the mAb from the cell culture fluid<br>Effective way of removing process related impurities | mAb binding capacity and high cost. |
| Cation-Exchange & Anion-Exchange | Used as a step to remove product variants and aggregates<br>Removal of residual amounts of HCP & hcDNA | Binding capacity, plant constraints and limited regeneration |
| Nano Filtration | Removes broad sizes of viruses. | High cost, prone to fouling and limiting through put. |

## 1.5 What are the Challenges?

Upstream process commonly achieve cell densities >1× $10^7$ cells/mL. This introduces high levels of impurities, and places an increased demand on the downstream making it difficult to apply the platform process for all biologics [Westoby *et al.*, 2011a]. The challenge is to remove both process related and product related impurities and this is compounded by the increasing demand for more complex mAb products [Liu *et al.*, 2010].

### 1.5.1 Manufacturing Capacity

The medical need for high doses over an extended period has meant that production capacity for mAbs is typically seen a limiting factor [Samaranayake *et al.*, 2009]. Examples

of products not being able to meet consumer demand include Enbrel (Amgen, Thousand Oaks, CA, USA) which was a Fc fusion protein released in 1988 [DePalma, 2004]. However with the future of the industry trending towards specialised and niche products the lack of agile manufacturing capacity now has the potential to become another bottleneck [McGlaughlin, 2010]. These are some examples of capacity limiting the ability of the drug to meet market demand. Other factors when considering process capacity include production process times, number of cycles, facility flexibility and the ability to be compliant with cGMP regulations [Liu *et al.*, 2010].

### 1.5.2 Removal of product related impurities

Heterogeneity of antibody structure is common in mammalian cell culture processes [Pilbrough *et al.*, 2009]. Product related impurities are expected in all mAb processes and this includes dimers, aggregates and various isoforms. However, with larger titres produced upstream the concentration of these process related impurities increase [Trexler-Schmidt *et al.*, 2009]. Typically the use of a Protein-A capture step followed by chromatographic steps is a sufficiently robust platform for impurity removal [Trexler-Schmidt *et al.*, 2009]. Yet this process is being increasingly challenged by the large volume of high impurity load causing reductions in the processes' purity and yield. This results in the need for additional polishing steps or the development of alternative purification strategies [Li *et al.*, 2007].

### 1.5.3 Removal of Process Related Impurities

Process-related impurities include cell culture media components, HCPs, hcDNA or chromatographic media such as leached protein-A [Flatman, 2011]. FDA guidelines state that these impurities should be minimised by use of well controlled manufacturing processes [Li *et al.*, 2007]. Most biotechnology products reviewed by the FDA contain host

cell protein levels of 1–100 ppm [Champion *et al.*, 2005]. HCPs have recently generated much interest due to their product safety implications with responses ranging from negligible to fairly severe [Shukla & Kandula, 2008]. Most purification processes use Protein-A column followed by two other chromatography polishing steps. Protein-A is capable of successfully clearing most HCPs produced in the cell culture process, with reductions seen from 10000ppm to 100ppm. However, the ability of the protein-A step to remove HCPs is being tested with the trend towards high cell density cell culture processes [Tait *et al.*, 2012].

## 1.6 Harvest

Mammalian cells secrete the soluble mAb product to the cell culture broth with only a negligible amount of the mAb product remaining within the cell [Marichal-Gallardo & Alvarez, 2012]. This provides both opportunity and restrictions in creating a process for the removal of the solid content from the cell culture broth. While typical cell densities of mammalian cells producing monoclonal antibodies have increased they have not reached cell densities similar to those for *Ecoli* and yeast cultures. Existing equipment is hence still widely applicable for the harvest of mammalian cell cultures. However mammalian cells are shear sensitive making them more susceptible to cellular damage unlike *Ecoli* and yeast cultures. Furthermore, the broths of mammalian cell cultures are nutrient rich making them more susceptible to contamination during the harvest step.

Solids liquid separation is common place across many industries and hence a large wealth experience is available for this harvest step. The harvest step is designed to handle a high particulate loading and a wide particle size distribution [Yavorsky *et al.*, 2003]. The approach of a platform process is ubiquitous across the entire sequence and the harvest section of the process platform is no exception. The red box marked in Figure 1.6 shows a

typical primary recovery step for the purification of a mAb. The primary recovery process can be separated into two sections; primary clarification and secondary clarification. Primary clarification is the first phase of the primary recovery process. This removes the bulk of the large particles, whole cells and cell debris. This step is usually performed by centrifugation and depth filtration but less commonly with tangential flow filtration (TFF). Secondary clarification is used for the removal of colloidal material, lipids, hcDNA, HCP and other material not removed in the primary clarification. This is typically performed by a depth filter with a tighter cut-off [Yavorsky *et al.*, 2003]. A successful harvest is one that consistently delivers particulate-free material with good product quality and high yield. However, with an increase in quality there is a potential for product loss through a loss in yield. Early primary recovery sequences were based on TFF systems [Zydney & Ho, 2002] but the centrifugation and depth filtration combination has emerged to be more common place in industry at commercial-scale. This is due to the robustness of such a pairing while handling large quantities of variable materials [Roush, 2008]. The choice of primary recovery sequence is dependent on three main factors; scale, operation and objective. Other factors include capital cost, equipment size, speed of separation, operation temperature and CIP (Cleaning in Place) needs. Typically as a rule of thumb for large scale processes (>2000L) centrifugation is used as the primary clarification step. For smaller volumes (<2000L) depth filtration is the preferred unit operation [Yavorsky *et al.*, 2003]. The latter sections explore in detail the technical aspects of harvest operations that are specific to mammalian cell culture.

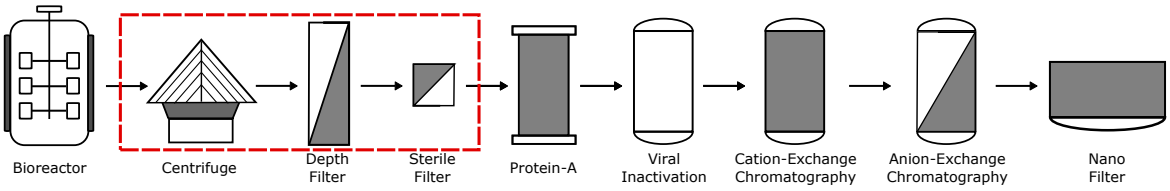


**Fig. 1.6:** Primary recovery sequence in a typical mAb process platform highlighted within a red box

### 1.6.1 What are the Challenges?

Improved cell stability, media characterisation, supplementation, optimized bioreactor controls along with longer cell culture durations have all contributed to the attainment of higher titres [Kelly, 2009]. The general mAb titre is typically around 3-5g/L with some titres reaching 9g/L using an extended fed batch cell culture process [Jagschies *et al.*, 2006]. With extended durations often comes reduced cell viability, increased levels of cell debris and a rise in the overall organic constituents in the cell broths. The variable colloidal nature of the cell broth complicates the separation process [Yavorsky *et al.*, 2003].

With an increase in variability in the feed broth there is a burden placed on the primary recovery step to remove larger quantities of general cell debris and a larger concentration of process and product related impurities. Harvest operations are being looked into as an alternative method to reduce the ever increasing loads of HCPs and hcDNA. These process related impurities that are not removed create a knock on effect on the performance of the chromatographic steps. New primary recovery methods that are more robust are currently being developed to combat the variability created by the cell broth. These include chemical pre-treatments to the broth, changes in pH, as well as addition of flocculants, precipitants and salts [Li *et al.*, 2007].

## 1.7 Centrifugation

Centrifugation is a unit operation that utilizes density difference to separate a mixture by accelerating the settling that would occur during gravity sedimentation. The more dense particles (solids) in the mixture move away from the axis of rotation whilst the less dense particles (liquid) remain closer to the axis of rotation. Continuous centrifugation is often used for the separation of a variety of biologics with an extensive history when processing

yeast cultures and dairy products. Typically the separations of mammalian products are often conducted through the use of a disk-stack centrifuge [Kempken *et al.*, 1995].

### 1.7.1 Disk-Stack Centrifugation

Disk-stack centrifugation is typically used for the separation of most yeast and bacterial fermentation broths. They are also often the start of many harvest sequences when processing mammalian cell culture broths. This is because they allow for efficient separation in a continuous fashion. In the past these centrifuges were seen to generate high shear regions and early studies identified the high shear regions caused cell damage resulting in cell lysis. However newer designs generate significantly lower levels of shear in the centrifuge through modifications to the inlet feed zone in-order to eliminate air-liquid interface. Fully hermetic, hyrdohermetic and reconfigured hermtic centrifuges all have feedzones which avoid the air-liquid interface.

Disk-stack centrifuges consist of a number of conical disks that are separated by ribs. The culture is fed into the rotating bowl by a central pipe and the culture is accelerated to the speed of the bowl [Kempken *et al.*, 1995]. The centrifugal force causes the solids to be separated. The cells and cellular debris are accelerated through the narrow channel between disks and are captured at the periphery of the bowl. The clarified centrate travels to the top of the bowl and product containing supernatant is collected in a continuous fashion. Disk-stack centrifuges are easily cleaned through Clean in Place (CIP) systems unlike membrane processes making them more suitable for usage in a manufacturing setting.

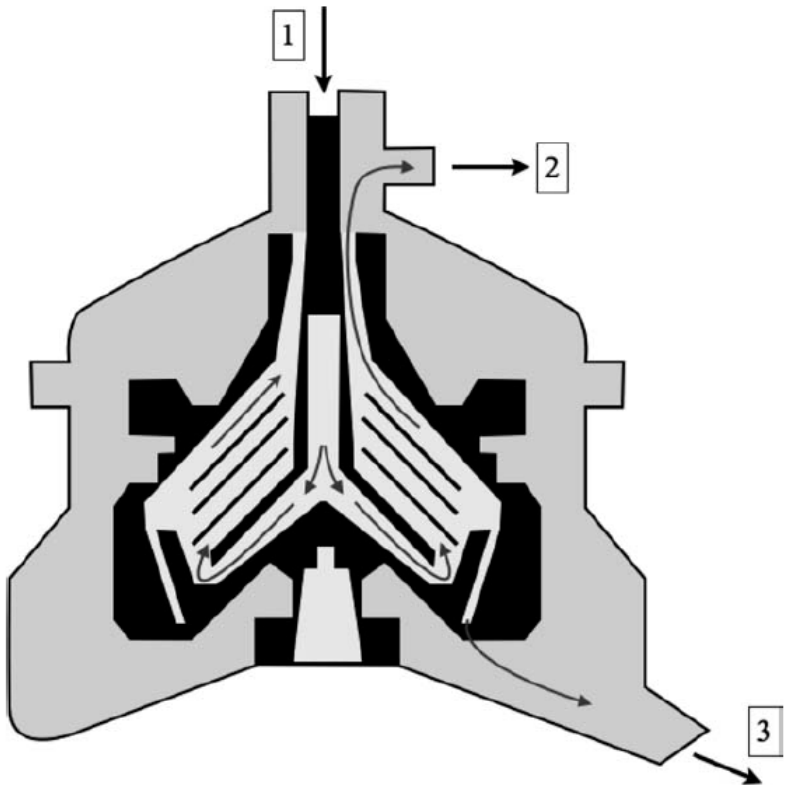


**Fig. 1.7:** Disk-stack centrifuge basic schematic [Marichal-Gallardo & Alvarez, 2012]

### 1.7.2 Centrifugation Theory

Separation in the case of centrifugation is based on exploiting the density difference between the cells and the media in which they grow. When cell broths are left to stand without mixing the cells will eventually sediment under the force of gravity. The sedimentation of particles utilizing centrifugal force is centrifugation. This is often thousands of times greater than that of the force of gravity. Higher densities of larger particles such as cells and cellular debris result in these species settling the fastest. The rate at which these particles settle is referred to as the settling velocity. Stoke's law [Equation 1.1] defines the settling velocity ($u_c$) under the assumption that the particles are isolated and spherical in an infinite fluid medium in a non-turbulent environment. The settling velocity ($u_c$) is a function of paticle diameter ($d$), densities of solid ($\rho_s$) and liquid ($\rho_l$) of the mixture , fluid

viscosity ($\eta$), the distance from the axis of rotation ($r$) and the angular velocity ($\omega$).

$$u_c = \frac{d^2(\rho_s - \rho_l)\omega^2 r}{18\eta} \tag{1.1}$$

The separation performance of a centrifuge is a function of many parameters. These include cell culture properties, centrifuge feed flow rate, centrifuge geometry and rotational speed. The geometry and the rotational speed are both accounted by the Sigma factor ($\Sigma$). This translates to the area of a gravity settling tank that would be required to achieve the same level of separation performance as the centrifuge. The Sigma factor for a disk-stack centrifuge is shown in Table 1.5. This is developed under the assumptions of Stoke's law . The Sigma theory ($\Sigma$) is used to compare centrifuges of different types. The correction coefficient (c) accounts for the deviation from the assumptions of the Stoke's Law. Lower values of c indicate a larger deviation away from Stoke's Law. Different centrifuges have different c values. Tubular bowl, multi chamber and disk stack centrifuges have been quoted to have a c value of 0.9, 0.8 and 0.4 respectively.

$$\frac{Q_{ds}}{c_{ds}\Sigma_{ds}} = \frac{V_{lab}}{t_{lab}c_{lab}\Sigma_{lab}} \tag{1.2}$$

With lower $Q/\Sigma$ values a better clarification is typically achieved, this allows for less dense particles to separated, achieving increased clarification through the centrifuge.

### 1.7.3 Centrifuge Process Development and Characterisation

Typically when operating a disk-stack centrifuge the cell culture feed stream is fixed meaning the quality of the cell culture at the start of operation will likely be the same as that sampled at the end of operation. Characterisation studies for centrifugation often require understanding the effect of altering the unit operation's process parameters of flow rate and bowl speed on its process performance attributes. The centrifugation step's process

**Table 1.5:** Sigma relationship for tubular bowl, disk-stack and bench top centrifuges

| Machine Type | Sigma Relationship | Definition |
|---|---|---|
| Tubular bowl [Boychyn *et al.*, 2001] | $\frac{\pi\omega^2 L(r_2^3-r_1^3)}{g\ln(2r_2/(r_2+r_1)}$ | $L$ = length of bowl<br>$\omega$ = angular velocity<br>$r_1$ = inner radius of the bowl<br>$r_2$ = outer radius of the bowl |
| Disk-stack [Hutchinson *et al.*, 2006] | $\frac{2}{3g}\pi N\omega^2\cot\theta(r_2^3-r_1^3)$ | $\theta$ = angle of the disk<br>$N$ =number of disks |
| Bench top [Hutchinson *et al.*, 2006] | $\frac{V_{lab}\omega^2(3-2x-2y)}{6g\ln(2R_2/(R_2+R_1)}$ | $x$ = acceleration fractional times<br>$y$ = deceleration fractional times<br>$V$ = volume of material<br>$R_1$ = inner radius<br>$R_2$ = outer radius |

performance is typically inferred by the turbidity of the centrate.

Most process characterisation studies are often conducted using laboratory scale or pilot scale equipment. However, the scaling of centrifuge is difficult making it critical that process development runs to be conducted on a machine with similar geometry and size to that of the commercial-scale centrifuge. Furthermore, the process development work on the centrifuge must be conducted using representative cell culture broths. Typically process development studies for centrifuges are conducted using both representative and worst case cell broth so that centrifuge is characterised to handle any scenarios beyond the expected broth conditions. One of the process parameters that can be altered when operating the centrifuge is the flow rate. Operation of the disk-stack centrifuge under low flow rates often give better clarification performance through the removal of small cellular debris. However, the low flow rates results in longer process times which often creates an opportunity for bio-burden growth and with increases in processing time the productivity of the process also decreases. Another parameter that can be altered is the bowl speed. Higher bowl speeds result in better clarification through the application of a

larger centrifugation force hence aiding separation. However, some studies have shown increase in bowl speed can result in the breakage of shear sensitive mammalian cells and the release of intra cellular proteases, HCPs and hcDNA that could potentially make the downstream purification of the conditioned media more difficult.

The separation step can have a knock on effect on subsequent purification steps further downstream and have a very immediate effect on the performance of the subsequent depth filtration step. Hence process parameters of the disk-stack centrifuge need to be carefully considered during process development studies. Optimisation efforts from such studies have been mostly conducted at pilot-scale due to some parameters being difficult to mimic at a smaller scale. These parameters include include shear stress and solids discharge. However, progress has been made with the advent of devices that mimic the levels of shear observed in pilot and commercial scale disk-stack centrifuges.

### 1.7.4 Centrifugation: Scale-down Approaches

Process characterization of commercial scale centrifuges is typically accomplished through the use of pilot-scale machines. This is a material intensive and time consuming process. These characterization studies often only capture a narrow design space and hence the quality of information generated from these studies is limited. High throughput scale-down techniques now enable the rapid generation of extensive experimental data representative of large-scale performance, both in the upstream and downstream manufacturing process. Such large experimental data sets generated through these techniques allows for better identification of the effects and interactions of the input parameters on the process performance and product quality [Titchener-Hooker *et al.*, 2008]. While the use of scale-down tools is the norm in most upstream and downstream operations, there have been challenges in integrating scale-down methods for process characterization

for operations within the harvest sequence. Typically, Sigma theory is used to scale centrifuges irrespective of size, geometry and type [Ambler, 1959]. However, Sigma theory does not take into account the generation of small particles through cell damage in the high shear regions of centrifuge feed zones. In order to capture accurately these effects at laboratory-scale, the shear generated in the feed zone needs to be mimicked [Boychyn *et al.*, 2001].

The Rotating Shear Device (RSD) contains a chamber with a centrally mounted disk where cell culture can be inserted via a sample sample port. The disk is attached to a motor that enables controlled rotational speeds between 1000 - 15,000 RPM to be delivered resulting in energy dissipation rates developed to reproduce the prevailing shear conditions in such feed zones [Boychyn *et al.*, 2001].

Analytical solutions to the equations of motion for flow over the rotating disk suggest that maximum shear stresses are observed at the boundary layer. Equation 1.3 describing the shear stress distribution in the boundary layer $\tau_{max}$, was obtained from Schlichting & Gersten [2003]: where $X$ is the distance from the edge of the disc and $v_\infty$ is the tangential tip velocity. Integration of 1.3 over the diamter of the disk provides the applied torque ($T$) shown in Equation 1.4 where $R$ is the radius of the disk.

$$\tau_{max} = 0.322\mu v_\infty \left(\frac{\rho v_\infty}{\mu X}\right)^{1/2} \tag{1.3}$$

$$T = 0.664\pi\mu v_\infty \left(\frac{\rho v_\infty}{\mu X}\right)^{1/2} \left(\frac{16R^{5/2}}{15}\right) \tag{1.4}$$

With the applied torque known [Equation 1.4] the power input $P$ can be calculated using Equation 1.5 where $N$ is the rotational speed of the disk. In order to calculate the maximum energy dissipation rate ($\varepsilon_{max}$, Equation 1.6) in the boundary region the volume is needed. The volume of the maximum energy dissipation region is calculated using Equation 1.7. Boychyn *et al.* [2001] and Levy *et al.* [1999] confirmed with CFD (Computational Fluid Dynamic) studies that equations described provide a good estimation of the shear related parameters in the boundary region.

$$P = 2\pi NT \tag{1.5}$$

$$\varepsilon_{max} = \frac{P}{\rho V} \tag{1.6}$$

$$V = 2\pi \left[ 5R^2 \left( \frac{\mu R}{\rho \nu_\infty} \right)^{1/2} - \left( \frac{10R\rho\nu_\infty}{\mu} \right) \left( \frac{\mu R}{\rho \nu_\infty} \right)^{3/2} + \left( \frac{\mu R}{\rho \nu_\infty} \right)^{5/2} \left( \frac{\rho \nu_\infty}{\mu} \right)^2 \right] \tag{1.7}$$

Operated in combination with a bench-top centrifuge, this has been shown successfully to predict the clarification efficiency of mammalian cell culture in a pilot-scale disk-stack centrifuge [Hutchinson *et al.*, 2006]. The RSD has also been used in conjunction with micro-well plates using sub-millilitre volumes to successfully model pilot-scale centrifugation performance [Tait *et al.*, 2009].

Extensive publications have shown the utility of the RSD to help map the impact of exposure to various levels of shear as might be experienced in the centrifugal step at pilot to manufacturing-scale [Boychyn *et al.*, 2001, Hutchinson *et al.*, 2006, Tait *et al.*, 2009]. However, the rotating shear devices are custom made and have a hold up volume of 20mLs which is often times insufficient material for subsequent depth filtration studies which

might require 1L or more of material. The production of 1L of material in 20mL batches is a time consuming task.

Alternative methods to the RSD have also shown to create levels of shear similar to those seen in disk stack centrifuges [Westoby *et al.*, 2011b, Chan *et al.*, 2006]. These devices are capillary-based and can vary the level of Energy Dissipation Rates (EDRs) exerted through changes in flow rate or changes in capillary diameter. EDR is the irreversible rate of increase in internal energy within a system [Bird *et al.*, 1960]. It is often measured in terms of unit of power per unit volume or mass. The effect of EDR on cell culture properties has been used in previous studies to characterise bioprocess related scenarios such as centrifugation [Boychyn *et al.*, 2001, Westoby *et al.*, 2011b] and cross flow filtration [Vickroy *et al.*, 2007]. Under laminar flow conditions of capillary operation the maximum energy dissipation occurs at the capillary wall. The maximum energy dissipation rate ($\epsilon_{max}$) for a Newtonian fluid can be described using Equation 1.8 where $\nu$ is the kinematic viscosity and $dU/dr_w$ is the shear rate at the pipe wall.

$$\varepsilon_{max} = \nu \left( \frac{dU}{dr_w} \right)^2 \tag{1.8}$$

The shear rate can be also be calculated experimentally when the pressure drop across a capillary and the capillary's geometry is known using Equation 1.9.

$$\frac{dU}{dr_w} = \frac{D\Delta p}{4l\mu} \tag{1.9}$$

Combining Equations 1.8 and 1.9 energy dissipation rate $\epsilon_{max}$ can be described as a function of pressure increase ($\Delta P$), where; $l$ and $D$ are the length and diameter of the capillary and $\mu$ and $\rho$ are the viscosity and density of the process fluid.

$$\epsilon_{max} = \frac{D^2 \Delta P^2}{16 l^2 \mu \rho} \tag{1.10}$$

Capillary systems allow experiments to be scaled readily without the need for custom fabrication. Also with the capillary-based method being continuous it allows for varying amounts of material to be processed. This is especially useful when determining filter sizing which requires larger volume of material to establish filter capacity [Westoby *et al.*, 2011b].

The Capillary Shear Device (CSD) has also shown to be a preparative device with the ability to develop a a range of EDRs. Flow through the capillary specifically enables the generation of EDRs equivalent to those found in disk-stack centrifuge feed zones [Westoby *et al.*, 2011b]. Furthermore, this methodology has shown that centrates obtained from it can generate a particle size distribution equivalent to that from a large-scale centrifuge [Westoby *et al.*, 2011b].

## 1.8 Depth Filtration

Centrifugation and depth filtration are a commonly used pairing in industry. Over the years centrifuge designs have been adapted to create lower levels of shear at the feed-zone enabling better clarification of cell culture broths. However, disk-stack centrifuges find it difficult to remove cell debris <1$\mu$m. Depth filters separate such cellular debris by forcing the suspension through a porous medium while the debris are retained in the porous structure. Depth filters are not limited to use in conjunction with disk stack centrifuges.

Some depth filter processes are designed to be used as a primary cell removal method, but these configurations are best suited for processing smaller batch volumes (< 2000L). Depth filters are often attractive at such a scale as they can require lower capital costs, are easy to use and are disposable. These single-use depth filter cartridges often only need a holder to secure the filters and a pump to drive material through the filter. The operation of such filters requires no complex control loops and only require monitoring of pressure and turbidities. Furthermore, the single-use nature of the filters remove the need for cleaning and reuse validation which are common place for other type of filtration operations.

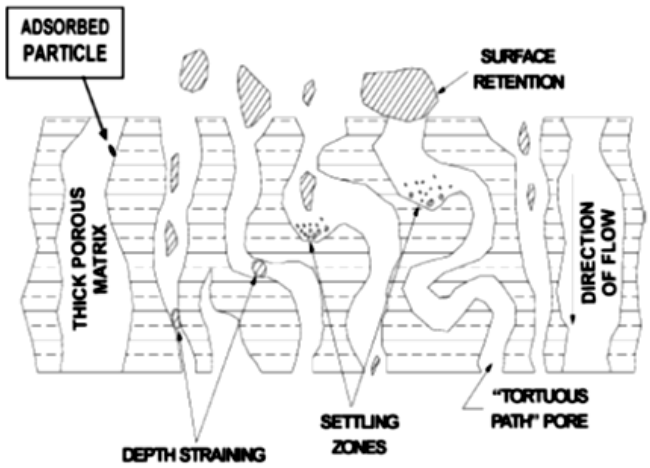


**Fig. 1.8:** Cross sectional schematic of depth filter [Shukla & Kandula, 2008]

Depth filters do not behave like absolute filters because they retain particles throughout their porous structure. This is due to the fact that they are made up a matrix of fibres (often cellulose) that are positively charged. This feature allows them to capture a wide range of particle sizes within the tortuous path created by the matrix. There are at least two ways that depth filters capture particulates. One of which is using size exclusion and the other is adsorption [Roush, 2008]. Figure 1.8 illustrates the mechanisms of solid retention by a depth filter. Depth filters are designed to utilise the entire membrane matrix rather

than just the surface of the membrane. This enables the trapping of cells and cellular debris within the structure of the membrane. The characterization of the filter to trap particulates within the pores is sometimes referred to as the ”dirt holding” capacity of the depth filter [Singh *et al.*, 2013]. Though pore size might often be looked at as the obvious property to characterize the depth filter these values however should not be interpreted as absolute values as those used for typical membrane filters. Depth filter media with high permeabilities are often associated with the removal of a wide range of particles as seen in mammalian cell culture broths. On the other hand depth filters with low permeabilities on the other hand are used to remove materials containing small particulates similar to those with the properties of centrate process streams.

The multilayer structure of a depth filter is essential to its ability to capture a range of particle sizes and increase filtration capacity. Adsorption is made possible due to multilayer structures with charged and hydrophobic characteristics. Depth filters that have a positive charge enabling the to significantly reduce endotoxins from water and in some cases to achieve the removal of virus particles [Gerba & Hou, 1985]. More recently the use of depth filters for the processing of mAbs has enabled the reduction of hcDNA and HCP through hydrophobic and ionic interactions present in the matrix [Roush, 2008]. The filter matrix is composed of diatomaceous earth, perlite and activated carbon so as to improve the performance of the adsorptive properties of the filter. The removal of HCPs and hcDNA is of particular importance as the reduction of these impurities allow for the protection and prolonging of the life of subsequent chromatographic operations.

### 1.8.1 Depth Filter Theory

Normal flow or dead end flow is a configuration in which a membrane filtration process can be operated. An alternative configuration is tangential flow. Depth filters are typically

operated under normal flow where flow occurs normal to the membrane and a pressure is applied across the filter in order for the separation process to occur. This configuration is applied to media that are difficult to process; the particles retained in the feed settle on the membrane surface or within the pores of the membrane, creating an accumulation of foulant. The foulant properties in terms of voidage and compressibility will determine the fouling of the membrane [Shirato *et al.*, 1986].

The mass transfer of water through a porous structure is represented by Darcy's Law. Most normal flow filtration models are derived from this relationship between the flow rate ($dV/dt$) and the pressure drop ($\Delta P$) created by the flow through a porous membrane. Equation 1.11 describes Darcy's law where $\mu$ is the process liquid viscosity and $k$, $L$ and $A$ describe filter properties of bed permeability, filter thickness and filter area respectively. Darcy's Law assumes that the process fluid is Newtonian and that the filter pores are uniform cylinders. However, there are difficulties applying these assumptions to complex biological fluids that often have feed streams with multiple particle size distributions and filters that have non uniform tortuous paths. This makes modelling approaches for quantifying depth filtration performance difficult. As a result experimentally measuring pressure drop as a function of flow rate is more commonplace for process development studies.

$$\frac{dV}{dt} = \frac{kA\Delta P}{\mu L} \tag{1.11}$$

### 1.8.2 Depth Filter Process Development and Characterisation

Depth filtration characterisation studies are often conducted using small-scale filter capsules. These capsules enable experimental determination of pilot-scale depth filter performance. Such studies are often easy to conduct and when tested with feed stock with

the same properties (cell density and cell viability) provide an accurate representation of performance at pilot-scale. There are a number of methods available to test depth filter performance. Most depth filtration experiments are conducted at constant flow rate and the rise of pressure across the filter is monitored as a function of the filtrate collected. This approach is known as the $P_{max}$ methodology [Yavorsky *et al.*, 2003]. In addition to the pressure drop and filtrate turbidities (NTU), product concentrations are also recorded for the duration of the $P_{max}$ studies. It is also important to monitor product concentration as there maybe instances of product binding to the filter due to the depth filter's adsorptive capabilities. This can cause large drops in yield in the process stream.

The choice in the correct sizing method requires an understanding of the filter being used, the application of the filter within the process and an appropriate experimental design. Currently there are a few methods in which filters are screened and sized. All have the aim of maximising the capacity of the filter without a break through of solids or an increase in pressure. Table 1.6 summarises the methods that are commonly used, their advantages and disadvantages and their applications.

Currently each of the parameters that influences the performance of a depth filter is tested sequentially. This form of experimentation requires a large amount of material to test so as a result is often combined with statistical design methodologies to minimize the amount of materials needed in order to test the wide range of parameters. The ability to change this sequential method to a high throughput one would, in principle allow for a wider range of parameters to be tested. The following section discusses scale-down approaches.

**Table 1.6:** Summary of filter sizing strategies

| Method | Advantage | Disadvantage | Application |
|---|---|---|---|
| $T_{max}$ and $P_{max}$ | Independent of plugging model<br>Experimentally determined<br>Provides bais for filter train selection<br>Mimics pilot-scale processing time | Requires long testing time<br>Requires large pool of material | Adsorptive depth filter |
| $V_{max}$ | Rapid Testing<br>Requires small volumes | Assumes pore plugging<br>Not consistent with pilot-scale | Sterile filters |

### 1.8.3 Scale-down Depth Filtration

Choosing a correct membrane for the filtration process is a difficult task because this is depends on many parameters. Depth filters come in many different forms of polymers and pore sizes. They require specific buffers at optimum pH and ionic strength. Both of these parameters could determine the stability and selectivity of the product. They also require examination of the operating range in terms of transmembrane pressure and flux. This is done so that the filter is able to achieve a high throughput while minimizing fouling [Chandler & Zydney, 2004]. However, most mAb manufacturers employ a platform process where filter type and filter operational conditions are fixed. This strategy enables faster process development times lines with only the filter capacity requiring to be characterized. The advent of cell lines robust enough for cell culture broths to reach cell densities of $30 \times 10^6$ cells/mL poses challenges for the performance of depth filters. The challenges associated with high cell densities are compounded by low cell viabilities and variability in the broth properties. This is mainly due to the high solid content associated with a varied particle size distribution of the broth which drastically decreases the performance of the depth filter [Schirmer *et al.*, 2010].

Currently the influence of starting material on the performance of a depth filter is tested sequentially at constant flow. This mode of conducting experimentation requires large pools of material and extensive time to test so as a result it is combined with sta-

tistical designs so as to minimise the number of experiments. This may often allow for a narrow range of materials to be tested. The potential development of a method that minimises time and material requirements but that would enable a high throughput method allowing for a wider range of parameters to be tested is very exciting. Another advantage of developing a high throughput method is that it would reduce the material requirement from previous unit operations like the centrifuge.

A number of high throughput normal flow filtration systems can be found in literature [Table 1.7], and there are also other systems that are commercially available [Table 1.8]. The filtration systems described in the literature are typically operated at constant pressure. This method of operation for understanding filtration performance is often quicker and requires less material when compared to operating at constant flow. These advantages mean that systems operating at constant pressure are more suitable for a high through put screening studies. However, this method of operation does not mimic actual usage which is typically constant flow at pilot-scale. Additionally all the constant pressures systems that are described in literature generate the required pressure by vacuum, this limits the maximum pressure that the system can exert. Commercially available filtration systems that are able to mimic pilot-scale filters operate in constant flow mode.

The constant pressure methods found in literature use considerably less material and are less time intensive than their commercial counter parts. This makes them ideal to be used as a basis for a scale-down high throughput system. The work by Chandler & Zydney [2004] used a custom manifold that was able to incorporate a standard 96well filter plate with a pressurised reservoir [Chandler & Zydney, 2004]. Changing the pressure in the reservoir allowed accumulating flux data at different pressures to be recorded. A similar methodology for small scale filter studies was employed by Vandezande *et al.*

**Table 1.7:** High throughput hardware for normal flow filtration operated in constant pressure described in literature

| | Chandler and Zydney 2004 | Jackson et al. 2006 | Vandezande et al. 2005 |
|---|---|---|---|
| Pressure mode | Negative | Negative | Negative/Positive |
| Equipement type | Multiscreen filter plate | Custom filter | Custom filter |
| Filter area ($cm^2$) | 0.28 | 0.79 | 4.52 |
| Max samples | 96 | 8/24 | 16 |

[2005]. In comparison to the 96 well filter plates the system developed by Vandezande *et al.* [2005] was only able to process 16 samples at a time. However, this system allowed for changing of the filter type so as to assess different filters simultaneously. Both of these methodologies were able to give representative scale up data in larger scale laboratory experiments for filter media of similar geometry and flow paths.

Work done by Jackson *et al.* [2006] looked to automate this process by using a TECAN (Mannedorf, Switzerland) based platform. This process had an automated vacuum manifold that could be controlled through the TECAN platform. A customised housing was utilized to fit 8 or 24 wells that could hold removable filter inserts in place. Flux was measured through measuring the permeate volume at the start and the filtrate volume at the end of the filtration run. The filtration run had to be stopped intermittently to obtain filtrate volume data and hence volumetric readings during the filtration were kept to a minimum [Jackson *et al.*, 2006]. This technique was further developed when assessing sterile filtration properties in DNA based vector feeds [Kong *et al.*, 2010]. Here the system was able to automate feeding and liquid sensing; meaning the changes in volume can be tracked frequently (reading every 15 seconds) on permeate side. This system of automation reduces the errors associated with a micro scale system. The throughput for this system is lower than the other methods. However, this system provides a basis for integration with other high throughput processes.

**Table 1.8:** High through put hardware for normal flow filtration operated in constant flow found commercially

| | Scilog FilterTec Station | PendoTECH |
|---|---|---|
| Mode of operation | Constant pressure and flow | Constant pressure and flow |
| Max sample | 3 | 4 |
| Measurable parameters | Pressure, volume & flowrate | Pressure, volume & flowrate |

# Chapter 2

# Aim of the Thesis

With an increasing number of biopharmaceutical drugs transitioning through clinical trials there has been a huge pressure placed on the process development for a drug. The process development is often subjected to shorter time lines. Decisions regarding the process are often made with very little specific information and process material to determine the optimum platform configuration for the process. Platform processes have been extremely popular mainly as a result of these pressures. Extensive research and development in upstream has resulted in large increases in titres over the last few decades. This is beneficial as it has meant a reduction in the overall cost of goods. Higher titres are mainly obtained as a result of longer culture durations and higher cell densities. However, this has created a larger and a more variable feed solid content containing culture fluid creating challenges for process development and characterisation of the solid liquid separation step.

This thesis looks into the development of scale-down devices and novel methods that will enable more efficient and robust process characterisation of the harvest sequence. This will aid process development in this region by allowing for a wider design space to be tested utilizing lower volumes of materials at a faster rate than was possible utilizing

legacy methods. With the methods generated in this thesis process development scientists are able to better charcterise the harvest sequence and are additionally able to conduct process development studies at an earlier stage of the development cycle. The methods developed in this thesis also allows for the generation of quantitative and qualitative information with regards to the harvest process and the potential influence of the harvest sequence on subsequent downstream operations.

The development of scale-down tools for the harvest sequence was at the center of this thesis. The use of such scale-down tools with high throughput analytical systems and design of experiment methods have created opportunities to evaluate a wider range of process parameters in short periods of time [Micheletti & Lye, 2006]. Extensive studies have been conducted on scaling down centrifugation and depth filtration. This has allowed for the reduction of sample requirement to milliliters. The evolution of these scale-down devices is described in detail in the Literature review section (Chapter 1). Chapter 3 discuss the development of a unique device that attempts to mimics the levels of shear observed in the disk-stack centrifuge. This device was leveraged in Chapter 4 to create a scale-down mimic of the disk-stack centrifuge and additionally provide unlimited materials for subsequent depth filtration steps. With the requirement of large quantities of material for typical depth filter characterisation studies, Chapter 5 explores an alternative mode of filtration in order to reduce the material and time requirements for such studies. Conclusion, future works and the potential validation implications of the studies conducted in this thesis are discussed in Chapters 7 and 6 respectively.

## Publications

The work conducted in this thesis has resulted in a three publications (Appendix A), one book chapter and two conference presentations. The first two publications enabled the

development of an automated, high throughput and easy to setup shear device. The shear device in conjunction with a lab centrifuge was used to develop an accurate scale down mimic of a pilot scale centrifuge. The third publication was based on a novel method to characterize filter capacity utilizing a fraction of the material and time when compared to existing capacity determining techniques.

- Adrian Joseph, Brian Kenty, Michael Mollet, Kenneth Hwang, Steven Rose, Stephen Goldrick, Suzanne Farid and Nigel Titchener-Hooker. *A Scale-down Mimic for Mapping the Process Performance of Centrifugation, Depth and Sterile Filtration* Biotechnology & Bioengineering 113(2016) 1934–1941

- Adrian Joseph, Stephen Goldrick, David Gruber, Michael Mollet, Richard Turner, Suzanne Farid and Nigel Titchener-Hooker *Lab-scale methodology for the Generation of Sheared Mammalian Cell Culture Samples* Biotechnology Journal, Special Issue: Biotech Methods and Advances **In Press**

- Stephen Goldrick*, **Adrian Joseph***, David Gruber, Michael Mollet, Richard Turner, Suzanne Farid and Nigel Titchener-Hooker *Predicting Performance of Constant Flux Depth Filtration using Constant Pressure Filtration Data* Journal of Membrane Science **In Press** ***Authors contributed equally to this work**

- Jean Bender, Richard Turner & Adrian Joseph *Manufacturing of Proteins and Antibodies, Downstream Processing Technologies, Harvest Operations* Advances in Biochemical Engineering / Biotechnology, Special Issue: New Bioprocess Strategies **Submitted**

## Conference Presentations

- Adrian Joseph & Brian Kenty, Michael Mollet, Kenneth Hwang, Steven Rose & Jean Bender *Continuous Centrifuge Characterization and Scale-Down Model* at Harvest Industry Summit Development (2014), San Francisco, CA, USA

- Adrian Joseph, Michael Mollet & Jean Bender *Leveraging Scale-down Methods to Accelerate Harvest Characterization* at Harvest Industry Summit Development (2016), Indianapolis, IN, USA

# Chapter 3

# Capillary Shear Device Development

## 3.1 Introduction

Monoclonal antibody (mAb) purification platforms often begin with the processing of cell culture material for the removal of cells and cellular debris. Disk-stack centrifuges are frequently used at manufacturing scale because of their perceived high robustness. They also enable processing in a continuous fashion utilizing the functionality of semi-continuous solids discharge [Axelsson, 2002]. However, most disk-stack centrifuge designs have high levels of shear present in feed zones. This results in breakage of shear sensitive mammalian cells creating sub micron particles [Jain *et al.*, 2005]. In the past in order to understand the potential effects of sub micron particles on subsequent unit operations, pilot scale studies had to be conducted. These studies are often material, time and resource intensive. Scale down methods allow for a reduction of these requirements and enable such studies to be conducted at laboratory scale. Methods incorporating Sigma Theory [Ambler, 1959] and correction factors [Mosqueira *et al.*, 1981] allow scaling down and subsequent comparisons between centrifuges of varying types, geometries and sizes. These methods however do not consider the effect of shear seen in the feed zones typically

associated with disk-stack centrifugation [Boychyn *et al.*, 2001].

Two separate methodologies have been shown to have the ability to mimic the levels of shear seen in hydro hermetic disk-stack centrifuges. The first being the rotating disk shear device developed at UCL [Boychyn *et al.*, 2001] and the second being the capillary shear device [Westoby *et al.*, 2011b]. Each have their advantages and disadvantages [Table 3.1]. A detailed description of each can be found in the literature review [Chapter 1].

**Table 3.1:** Summary of shearing methodologies; Rotating Shear Device (RSD) and Capillary Shear Device (CSD)

| | Advantages | Disadvantages |
|---|---|---|
| CSD | Automatable<br>Processing large volumes<br>Parts easily sourced<br>Cheap to build | Not well published<br>Requires setup |
| RSD | Well Published<br>Established methodology<br>Commercially available | Cost of $10,000<br>Difficult to automate<br>Process volume of 20mL/run |

This chapter describes the generation and fine tuning of the CSD methodology in order to generate a method with the ability to explore the sensitivity of cell cultures across a range of shear levels encountered in pilot-scale disk stack centrifuges. When developing this device it was important to consider the requirement specification (summarised in Table 3.2).

It was essetntial that the developed device had the key ability to create a range of sheared samples and the levels of shear be quantified. This was so that the effect of shear in the device could ultimately be correlated to the shear levels prevalent in a given centrifuge. A range of shear levels can be generated through changes in capillary geometry.

Hence, it was necessary to integrate capillaries of differing internal diameter sizes and different operational flow rates through the capillaries. In this thesis the flow rate was the main parameter used to manipulate and set the shear rates within the CSD. It was also imperative that the CSD was user friendly allowing for shorter experimental times and a reduction in manual handling. With the desired requirements of the CSD identified the following section describes the evolution of the CSD methodology and the integration of the design requirements into each version of the device.

**Table 3.2:** Requirements of the CSD device

| Category | Details |
|---|---|
| Tasks | Generate a range of shear |
| | Quantify the level of shear |
| Ease of use | Automation |
| | Quantified collection |
| | Performance feedback |

## 3.2 Capillary Shear Device Tool Versions

This section gives a detailed description of the operating conditions and individual parts required for each version of the CSD device utilised through out this thesis. Table 3.3 summarises the capabilities and the operational specifications of the CSD versions.

In Table 3.3 force generator describes the mechanism used in the device to drive the sample through the capillary. Version-1 used a syringe pump as a force generator while Version 2 and 3 used the piston pumps of an AKTA Explorer (GE Healthcare, Little Chalfont, UK). Syringe pumps are limited in the force they can generate and can only handle limited back pressures (1 MPa). The AKTA Explorer's piston pump had the ability to supply higher back pressures beyond 4 MPa, but due to the safety rating of the "Super Loop" was limited to 4 MPa. Some versions of the CSD were more user friendly than the others; the ease of use

of the device was determined based on the ability for automation, quantified collection of sheared material and online performance feed back from the device. Versions 1 and 3 of the CSD device were able to operate without manually placing the cell culture within the device while, Version 2 required the material to be manually inserted using a syringe into the Super Loop chamber (detailed methods of operations can be found under individual sections of the CSD versions). The CSD device also needed to be able to produce 1 L pools of sheared samples so that subsequent filter capacity studies could be conducted. Versions-1 and 3 had the ability to be programmed to produce defined volumes (>1 L) of sheared samples while Version 2 limited the user to generate 10 mL of sample per run and hence needed multiple repeat cycles to achieve the 1 L target. Performance feed back of the device refers to the ability of the system to identify and isolate failings in the system. The piston pump based Versions 2 and 3 were able to monitor back pressure readings utilizing the AKTA Explorer's functionality allowing for performance feed back unlike the syringe pump of Version-1.

**Table 3.3:** CSD device evaluation summary

| Attribute | Version 1 | Version 2 | Version 3 |
|---|---|---|---|
| Force Generator | Syringe Pump | AKTA Explorer | AKTA Explorer |
| Back Pressure (MPa) | 0-1 | 0-4 | 0-4 |
| Automation | Yes | No | Yes |
| Quantified Collection | Yes | No | Yes |
| Performance Feed back | No | Yes | Yes |

### 3.2.1 CSD Version 1: Syringe Pump based CSD

Version 1 of the Capillary Shear Device (CSD) consisted of a Harvard syringe pump (Harvard Apparatus, Cambridge, UK), 0.01″ ID 10 cm long Polyetheretherketone (PEEK) tubing, a 10 mL glass syringe and check valves as set out in Figure 3.1 and Table 3.4. The cell culture was delivered from a sealed vessel to the glass syringe via a check valve (ID-6).

Subsequently the flow through the capillary passed another check valve (ID-7) with the syringe pump in infuse mode. Variations in the level of shear was achieved by adjusting the flow rate through the capillary. This relationship has been developed in more detail in previous studies [Westoby *et al.*, 2011b]. The culture was kept well mixed using a stir plate and stir bar. The sheared material was collected in a sealed vessel.

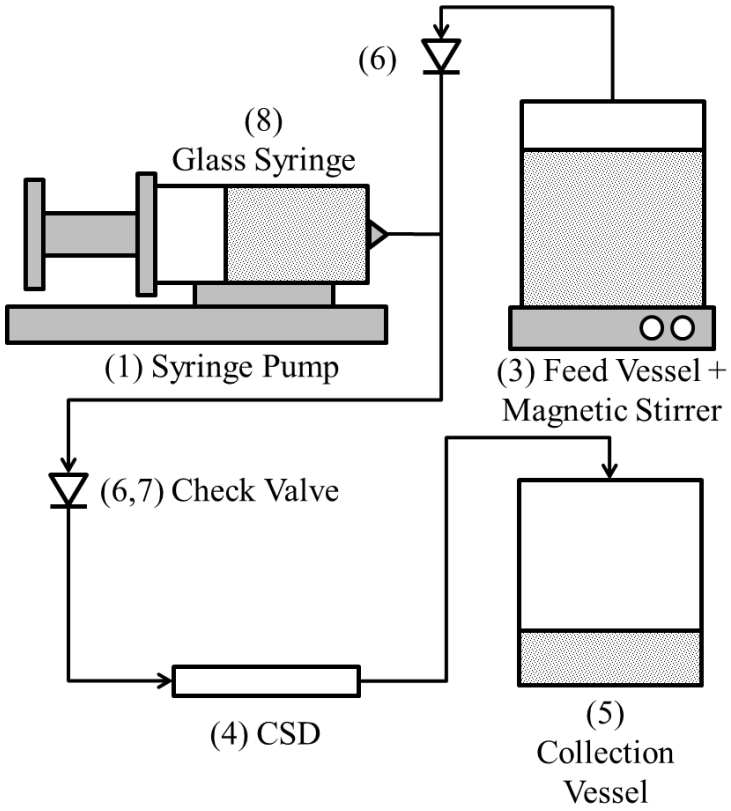


**Fig. 3.1:** Schematic of CSD Version 1

### 3.2.2 CSD Version 2: Manual AKTA based CSD

Version 1 of the CSD employed a syringe pump to prepare sheared material but in Version 2 the setup was altered and the delivery system of an AKTA Explorer (GE Healthcare, Little Chalfont, UK) was used instead of the syringe pump. Previous studies had shown that significant shear may be generated in the piston pump of the AKTA hence the ATKA

**Table 3.4:** CSD Version 1 part description

| Description | Make | ID |
|---|---|---|
| Syringe Pump (703007) | Harvard Apparatus | 1 |
| Stirrer (SP131325Q) | Thermo Scientific Cimarec | 2 |
| Vessel (EW-34516-08) | Kimex | 3&5 |
| 10cm Steel Capillary (U-112) | IDEX Health & Science | 4 |
| Check Valve (CV-3320) | IDEX Health & Science | 6 |
| Check Valve (CV-3321) | IDEX Health & Science | 7 |
| 10mL Glass Syringe (2607224) | ILS | 8 |

configuration was modified using a Super Loop (GE Healthcare, Little Chalfont, UK). This enabled the cell culture to avoid exposure to the shear of the AKTA piston pump. Material to be sheared was manually inserted into the Superloop using a syringe and subsequently the AKTA was used to generate flow through the Super Loop and CSD. The schematic and supplier details of the updated device is shown in Figure 3.2 and Table 3.5

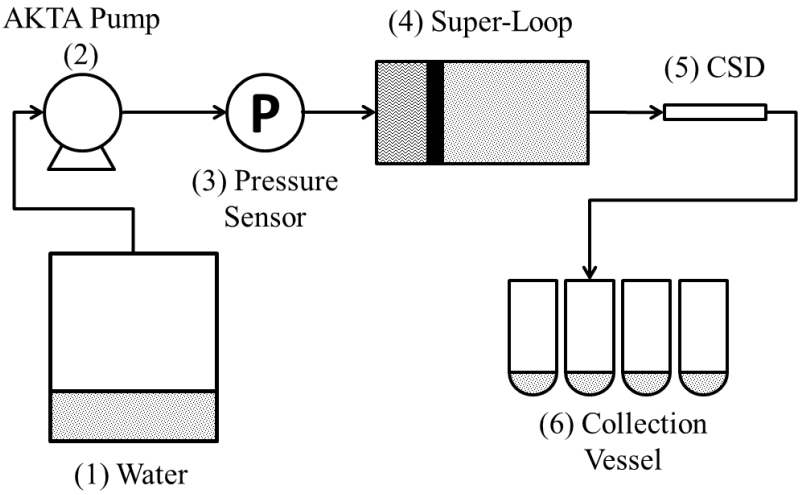


**Fig. 3.2:** Schematic of CSD Version 2

### 3.2.3 CSD Version 3: Automated AKTA based CSD

Version 2 of the CSD Setup required significant levels of sample handling. This included the use of a syringe in order to manually fill the Super Loop. The automated setup described

**Table 3.5:** CSD Version 2 part description

| Description | Make | ID |
|---|---|---|
| Pump (P-901) | GE Life Sciences | 2 |
| Pressure Sensor (P-901) | GE Life Sciences | 3 |
| Superloop (18-1113-81) | GE Life Sciences | 4 |
| 10cm Steel Capillary (U-112) | IDEX Health & Science | 5 |
| 50 mL tube (352070) | BD Biosciences | 6 |

in Figure 3.3 and Table 3.6 was able to load, pump and collect automatically. Material was drawn into the Super Loop through check valve (ID2) using the AKTA P-960 pump with the injection valve in Load mode and sample valve set to S1 where a blank ferrule was placed. The latter was to ensure material passes through to the Super Loop and not through to the CSD. Once the material had been loaded, Pumps A and B were engaged and the injection valve switched to inject mode whist the sample valve was set to S2 to provide flow through the CSD device. The material was then transported through the outlet valve into the fraction collector to collect the desired volume of material. The coding for the programming of the process was generated using the AKTA UniCorn platform. Alterations to the script could be made to alter the process either by changing the flow rate through the capillary or to accommodate multiple capillaries attached to a common sample valve.

**Table 3.6:** CSD Version 3 part description

| Description | Make | ID |
|---|---|---|
| Pump (P-901) | GE Life Sciences | 2 |
| Pressure Sensor (P-901) | GE Life Sciences | 3 |
| Superloop (18-1113-81) | GE Life Sciences | 4 |
| 10cm Steel Capillary (U-112) | IDEX Health & Science | 5 |
| Fraction Collector (Frac-950) | GE Life Sciences | 6 |
| Stirrer (SP131325Q) | Thermo Scientific Cimarec | 7 |
| Pump (P-960) | GE Life Sciences | 8 |
| Check Valve (CV-3320) | IDEX Health & Science | 9 |

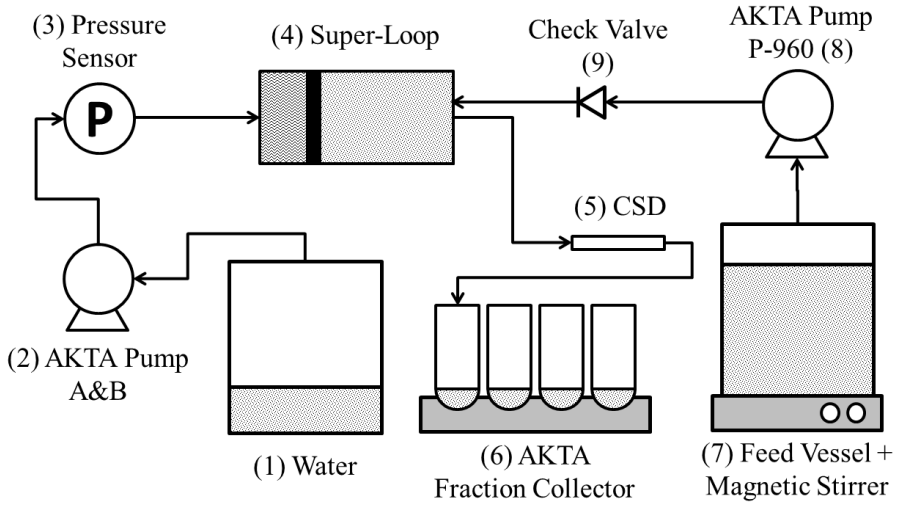


**Fig. 3.3:** Schematic of CSD Version 3

## 3.3 Materials and Methods

### 3.3.1 Cell Culture

Cell culture used in the experiments were generated using CHO cell lines expressing monoclonal antibody products. The cultures produced had a range of cell densities and viabilities measured on the day of harvest as summarised in Table 3.7. Bench-scale cell culture operations were conducted in 3 and 5 L bioreactors whilst pilot-scale cell culture operations were performed in 100 L bioreactors. All cultures were harvested between days 11-14 during the decline phase of growth. Cell density and cell viability of the culture were measured through the industrial standard trypan blue dye exclusion method (ViCell, Beckman Coulter, High Wycombe, UK).

**Table 3.7:** Chapter 1 experimental cell culture properties

| Material | Bio Reactor Size (L) | Cell Density $\times 10^6$ (cells/mL) | Cell Viability (%) |
|---|---|---|---|
| Culture-A | 100 | 21.9 | 74 |
| Culture-B | 3 | 32.2 | 39 |
| Culture-C | 100 | 18.2 | 71 |
| Culture-D | 3 | 22.2 | 66 |
| Culture-E | 100 | 24.5 | 68 |
| Culture-F | 5 | 20.8 | 94 |
| Culture-G | 5 | 23.3 | 63 |

### 3.3.2 Experimental Equipment

#### Rotating Shear Device (RSD)

The design, theory and application of the rotating shear device to mimic levels of shear found in centrifuge feed zones has been thoroughly covered in previous studies [Maybury *et al.*, 2000, Boychyn *et al.*, 2004, Hutchinson *et al.*, 2006]. The material to be sheared was held in a cylindrical chamber with a diameter of 50 mm and a height of 10 mm. A

rotating disk located within the chamber creates the shear and has a diameter of 40 mm and a thickness of 1 mm. The correlation of the rotating speed of the disk to the levels of energy dissipation has been developed in previous studies [Boychyn *et al.*, 2004]. In the experiments conducted for this chapter the rotating shear device was run at a range of speeds (6000 -9000 RPM). This provided conditions that enabled to identify the equivalent shear generated in both the Capillary shear device (CSD) and the pilot-scale centrifuge. Material was subjected to shear in the chamber for 20 seconds to ensure that the total content was equally exposed to shear generated by the rotating disk [Hutchinson *et al.*, 2006].

**AKTA Explorer**

HPLC systems such as the AKTA Explorer (GE Healthcare, Little Chalfont, UK) are common place in laboratories. Through the use of accurate piston pumps the AKTA Explorer is capable of generating flow rates up to 100 mL/min with an accuracy of ±2%. It was also configured with monitors for multi-wavelength detection, conductivity and pressure. In this application the pressure sensors and piston pumps were of particular interest because the former helps ensure the shear rates developed were consistent and reproducible while the latter develops high flow rates at increased pack pressures (>2 MPa). The flow rates were set and controlled through the Unicorn 5.31 software (GE Healthcare, Little Chalfont, UK).

**Super Loop**

Super loops (GE Healthcare, Little Chalfont, UK) are often used in a chromatographic setting for sample injection and collection while for the experiments conducted in this chapter they were used for the injection of cell culture material through the capillary.

### 3.3.3 Centrifugation

Centrifugation for this chapter was conducted in a Beckman J-HC centrifuge with a JS 4.2A rotor (Brea, CA, USA). Immediately following exposure to capillary shear, the sheared cell culture material was placed into a series of 50 mL polypropylene tubes and centrifuged with varying rotor speeds, liquid heights and for varying durations in order to generate the required range of V/tΣ.

### 3.3.4 Analytical Techniques

#### Solids Remaining

The performance of a centrifuge in removing solids at any given set of operating conditions may be described by calculating the percentage of solids remaining in the supernatant ($S$).

$$S = \left( \frac{OD_s - OD_o}{OD_f - OD_o} \right) \times 100 \tag{3.1}$$

Where $OD_s$ is the filtrate clarity post depth filtration, $OD_o$ is the base line for a well clarified centrate (obtained by extended centrifugation for 30 minutes at 16,000 g [Tait *et al.*, 2009]) $OD_f$ refers to the clarity of the feed stream prior to depth filtration. All optical densities were measured at 600 nm.

#### Turbidity

Another method to quantify the performance of the centrifuge to remove cell and cellular debris was achieved by measuring the turbidity [Westoby *et al.*, 2011b] of the centrate in a Orion Thermo Scientific (Waltham, Massachusetts, USA) turbidity meter. Centrates were placed in clear 10 mL glass vials and illuminated at a wavelength of 450 nm. The intensity of transmitted light received by the detector was quantified as nephelometric

units (NTU). Centrates with high cell debris content translate to > 100 NTU and similarly low cell debris content translate to < 100 NTU.

#### Characterisation of Cell Lysis

Lactate dehydrogenase (LDH) is an intracellular enzyme that is only released during cell rupture. LDH increase was used to characterise the extent of cell lysis occurring during the centrifugation process [Petersen *et al.*, 1988, Ma *et al.*, 2002]. It was also used to establish comparability between the established scale-down method for generating defined levels of shear (RSD) and the preparative CSD method explored in this study for the generation of filter feed volumes. Following assay protocols provided in the BioVision Kit (Milpitas, CA) samples that had been exposed to shear in either device were immediately centrifuged at 10,000 g for 15 minutes for the separation of cell debris from the sample. The supernatant was removed and combined with Nicotinamide adenine dinucleotide (NADH) and pyruvate solutions. The sample mixture was then aliquoted into a micro-well plate and a micro-plate reader used to measure the absorbance change. The LDH increase $LDH_{INC}$ was calculated by dividing the change in LDH activity in the non-sheared sample ($LDH_{NS}$) and sheared sample ($LDH_{SS}$) by that of the non-sheared sample.

$$LDH_{INC} = \left( \frac{LDH_{SS} - LDH_{NS}}{LDH_{NS}} \right) \times 100 \tag{3.2}$$

## 3.4 Theoretical Considerations

### 3.4.1 Energy Dissipation Rate

The ability of the AKTA Explorer to measure back pressures in CSD Versions 2 and 3 enabled the quantification of the Energy dissipation rates (EDRs) imposed on cell culture samples. EDR is the irreversible rate of increase in internal energy within a system. It

is often measured in terms of unit of power per unit volume or mass. The effect of EDR on cell culture has been used in previous studies to characterise bioprocess related scenarios such as centrifugation [Boychyn *et al.* [2001]; Westoby *et al.* [2011b] and cross flow filtration [Vickroy *et al.*, 2007]. Under laminar flow conditions of capillary operation the maximum energy dissipation ($\epsilon_{max}$) occurs at the wall. This can be described as a function of pressure increase ($\Delta P$), where; $l$ and $D$ are the length and diameter of the capillary and $\mu$ and $\rho$ are the viscosity and density of the process fluid.

$$\epsilon_{max} = \frac{D^2 \Delta P^2}{16 l^2 \mu \rho} \tag{3.3}$$

## 3.5 Results

### 3.5.1 Syringe Selection

The sourcing of the correct materials of construction was important for the development of a robust CSD device. During the development of Version-1 of the CSD it was found that the material of construction of the syringe played a huge part in the ability to generate sheared material. There was often a torquing effect of the plunger observed in the plastic syringe such that a portion of the force exerted by the syringe pump was lost to the torquing of the plunger. When using the plastic syringe at higher speeds more torquing was exhibited. This effect was not seen with glass syringes. The consequence of this loss of force was the reduction of the effective flow rate produced when using a plastic syringe and hence reduced levels of shear. Figure 3.4 shows the LDH release of a typical cell culture post passage through CSD Version-1 using both plastic and glass syringes. The plastic syringe showed no real increase in LDH with speed whereas with the glass syringe there was a clear increase in LDH increase with flow rate. This suggests the use of the glass syringe ensured the full force of the delivery system being applied to the cell culture. Due

to this glass syringes were chosen over the plastic syringes for the construction of CSD Version-1.

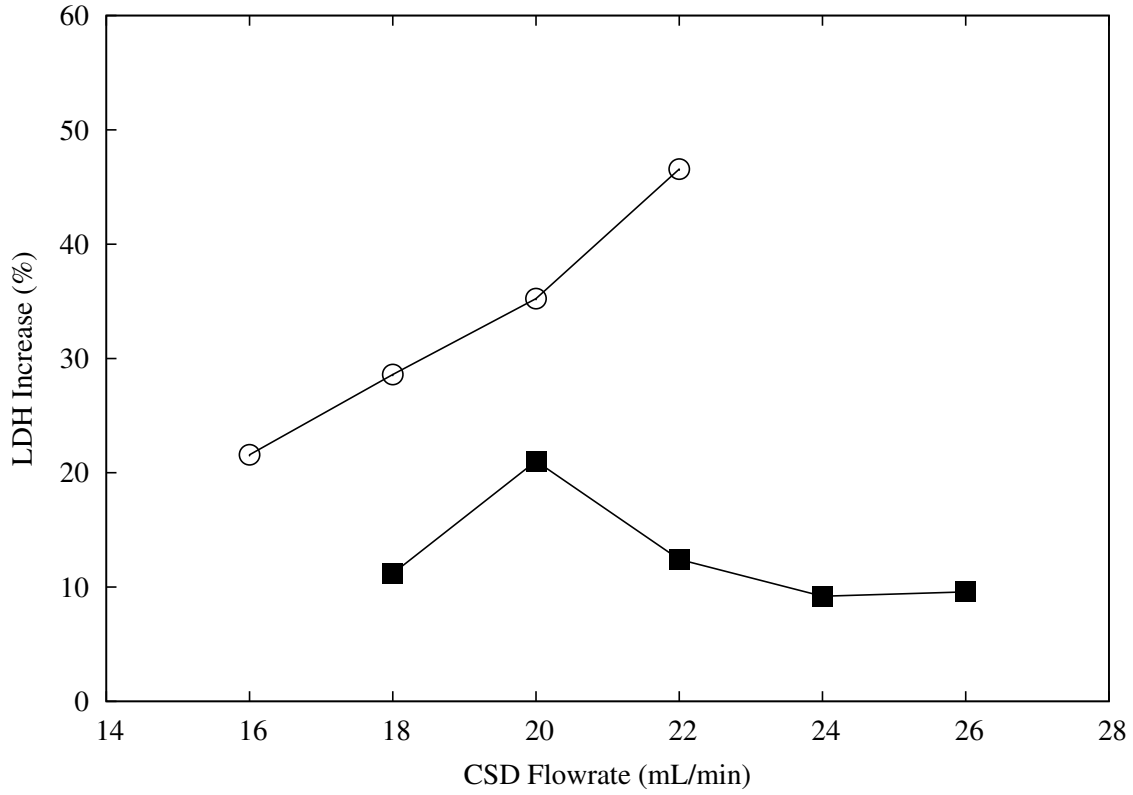


**Fig. 3.4:** Examination of the effect of material of CSD construction on the % LDH increase. Culture-A (Table 3.7) samples processed at flow rates (16-26 mL/min) with CSD Version-1 utilising BD (Franklin Lakes, NJ) 10 mL plastic (■) and ILS (Stutzerbach, Germany) 10 mL glass syringes (○)

### 3.5.2 Check Valve Selection

In order to generate large volumes of sheared samples Version-1 of the CSD device needed to be capable of automation. In particular there was a need to develop a method to fill the syringe with new cell culture and subsequently to remove the sheared cell culture. In order achieve these operational factors check valves were used. The first set of check valves incorporated into the CSD were low pressure check valves. However, it was found that material was diverted through the one-way check valve that was designed to bring clean

cell culture material into the syringe barrel. This meant the flow rate through the capillary was not representative of the flow rate set by the syringe pump. Figure 3.5 shows the use of high pressure check vales akin to those found in chromatographic systems enabled for the generation of higher levels of solids when compared to the low pressure check vales when operated at the equal flow rate. This suggests that when using the high pressure check valves, cell culture to be sheared was being directed to the capillary instead of being diverted to the source (Figure 3.1, ID 6) to bring clean cell culture to the CSD. The use of these check valves prevented material leakage which was an issue with low pressure check valves since their integrity was compromised. This led to the generation of lower levels of shear, and hence less cellular damage. Ultimately the use of chromatographic check valves produced elevated amounts of solids remaining after centrifugal separation. High pressure check valves were incorporated into all CSD designs.

### 3.5.3 Stability Study

In order to mimic large scale disk-stack centrifugation using a laboratory scale centrifuge the effects of shear and separational ability needed to be addressed independently. During the laboratory experimental procedure cell culture material was expected to be sheared first before it was centrifuged. With mammalian cells there is always a concern that any delay between shearing and centrifugation might allow the sample to degrade the sample leading to a loss in viability. Figure 3.6 shows the viable cell density over a period of 1 hour at room temperature for sheared material and a control of non-sheared material. The reduction in the viable cell density over 1 hour was very minimal in both cases. This suggests that the cell culture was very stable and not prone to significant levels of degradation over a period of time typical of the lab-scale separations. Clearly different materials will exhibit loss in viability at different rates. The developed methodology ensured material was sheared and centrifuged within the space of less than 30 minutes.

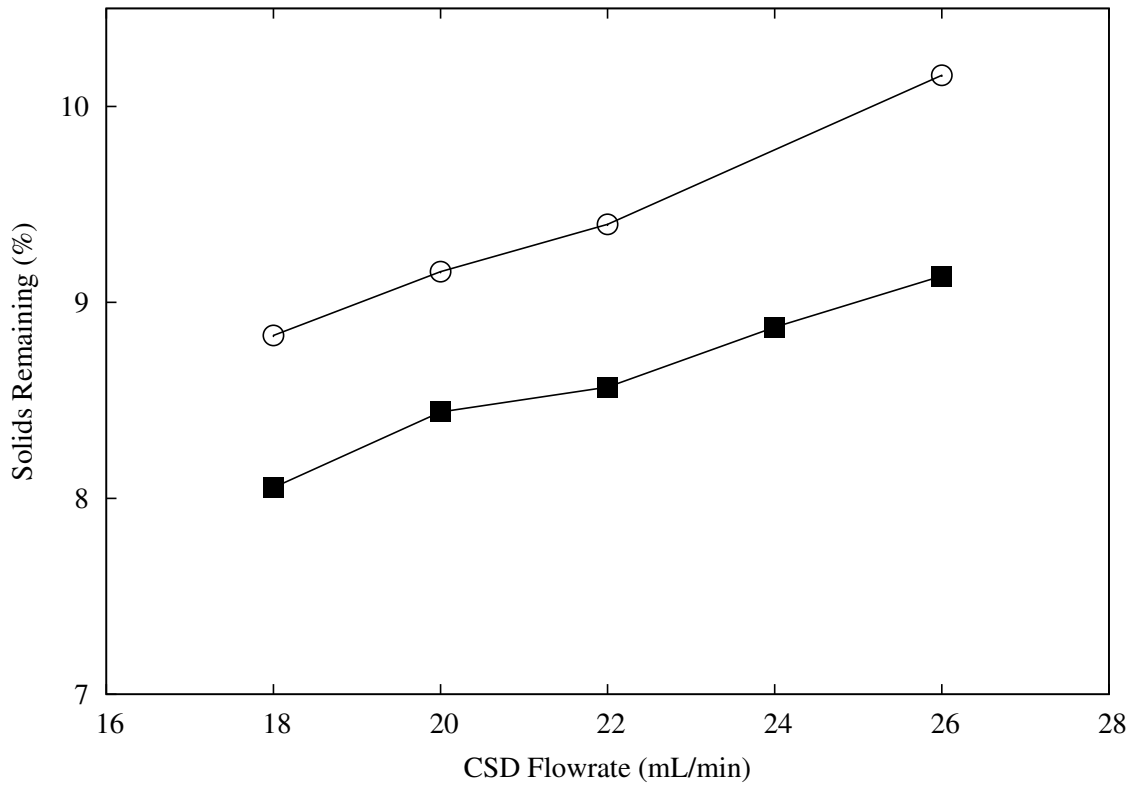


**Fig. 3.5:** Examination of the impact of check valve construction on centrate quality. % Solids remaining was used as an assay to determine centrate quality and cell culture for the study was sourced from Culture-B (Table 3.7). Cell culture was sheared at 15 mL/min using CSD Version-1 utilising VWR (Radnor, PA) low pressure check valve (■) and Upchurch Scientific (Oak Harbor, WA) high pressure check valve (○). Centrates were generated through processing the sheared material through a lab centrifuge at V/tΣ of $2.20\times10^{-8}$ (m/s).

Furthermore, once sheared the material was kept on ice to reduce further the impact and consequences of material degradation.

### 3.5.4 Bridging Study: RSD and CSD Version-1

Experiments were conducted to determine the flow rates through CSD Version-1 needed to generate levels of shear comparable to that developed in the standard RSD. The latter had already been shown to match shear levels found in the feed zone of industrial disk-stack centrifuges. Figure 3.7 shows the LDH increase for a typical cell culture broth sheared using the CSD Version-1 at flow rates from 12-20 mL/min and the RSD at rotational speeds

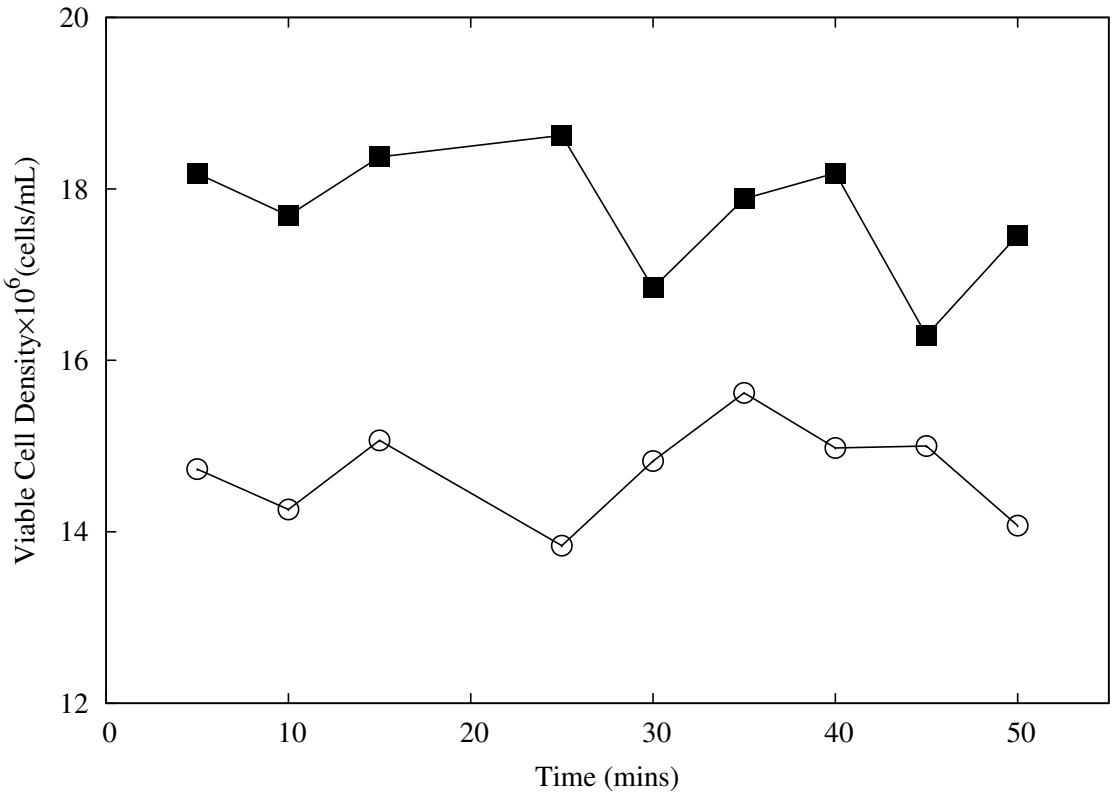


**Fig. 3.6:** Examining the impact of exposure time on cell culture quality. Viable cell densities of Culture-C (Table 3.7) are measured pre (■) and post shear (○). Sheared material was generated by processing Culture-C using CSD Version-1 at a flow rate of 20 mL/min. Both sheared and non-sheared cell culture are observed over an exposure time of 50 minutes.

between 6000-9000 RPM. A linear increase in LDH release was observed in both cases. The data from both systems overlapped each other suggesting similar levels of energy dissipation could be generated using the two devices. These results encompass those flow rates reported in the literature and shown to mimic the shear in a hydro-hermatically sealed centrifuge for operation of a CSD [Westoby *et al.*, 2011b] and the range of rotational speeds used in the RSD to achieve the same mimic [Boychyn *et al.*, 2004]. This dataset validated Version-1 of the CSD against the well established RSD and verified the use of the CSD Version-1 for the shearing of cell culture to mimic centrifugation processes.

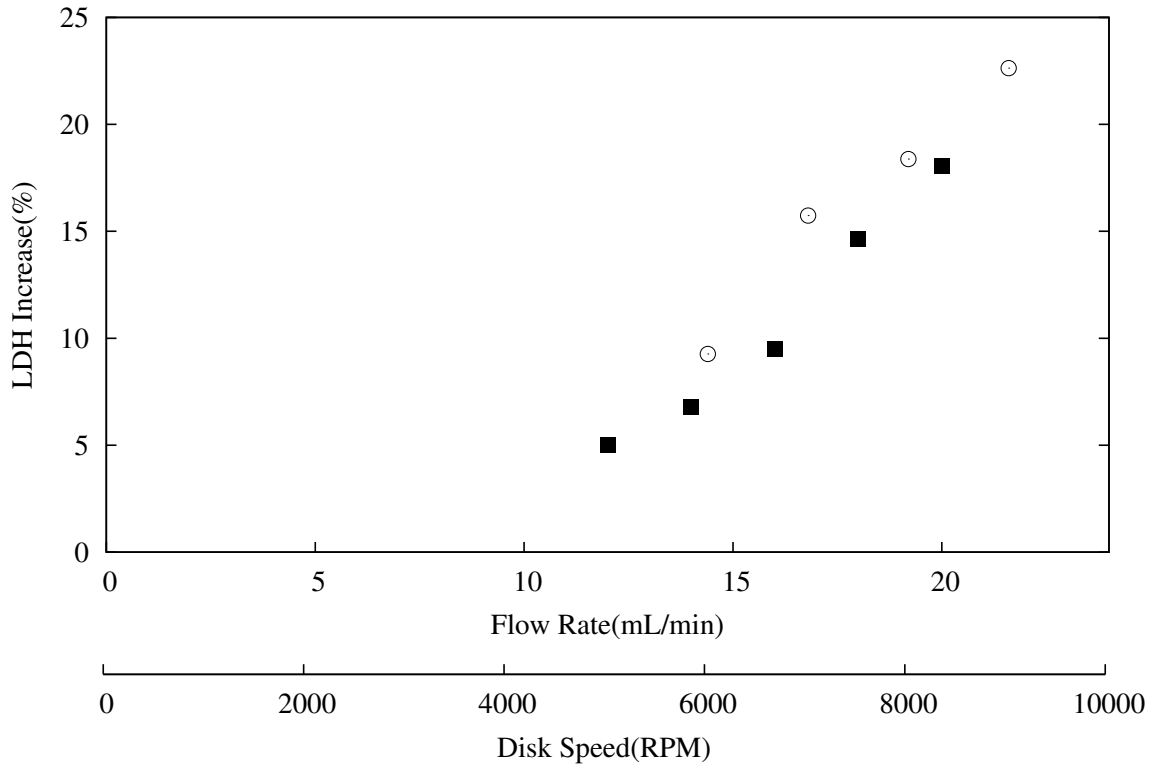


**Fig. 3.7:** Study examining the shear effects produced by two alternative shear devices as measured by the extent of LDH release: capillary shear device (CSD,■) and rotating shear device (RSD, ◯). The ranges tested for the rotational speed and flow rate incorporate literature values that have been shown previously to mimic the shear damage generated in a centrifuge equipped with an hyrdo-hermetic feed-zone. The feed material for this study was sourced from Culture-E (Table 3.7)

### 3.5.5 Effect of Capillary ID on Back Pressure

A key advantage of using the AKTA Explorer as a delivery system was that it enabled higher flow rates to be reached unlike typical syringe pumps which were unable to maintain a set flow rate at the presence of high back pressures. Furthermore, it had the utility of generating performance feed back through back pressure readings. With this functionality Figure 3.8 examines the effect of changes in capillary diameter and operational flow rates on the prevailing back pressure. The relationship between capillary internal diameter and pressure increase is a very well understood phenomenon [Bird *et al.*, 1960]. It was found that increasing operational flow rate resulted in higher back pressures and this relationship

between flow rate and back pressure became more pronounced with narrower internal capillary diameters. Furthermore, the pressures found in this study when processing mammalian cell culture through a capillary with an ID of 0.01″ confirming consistency with earlier published data.

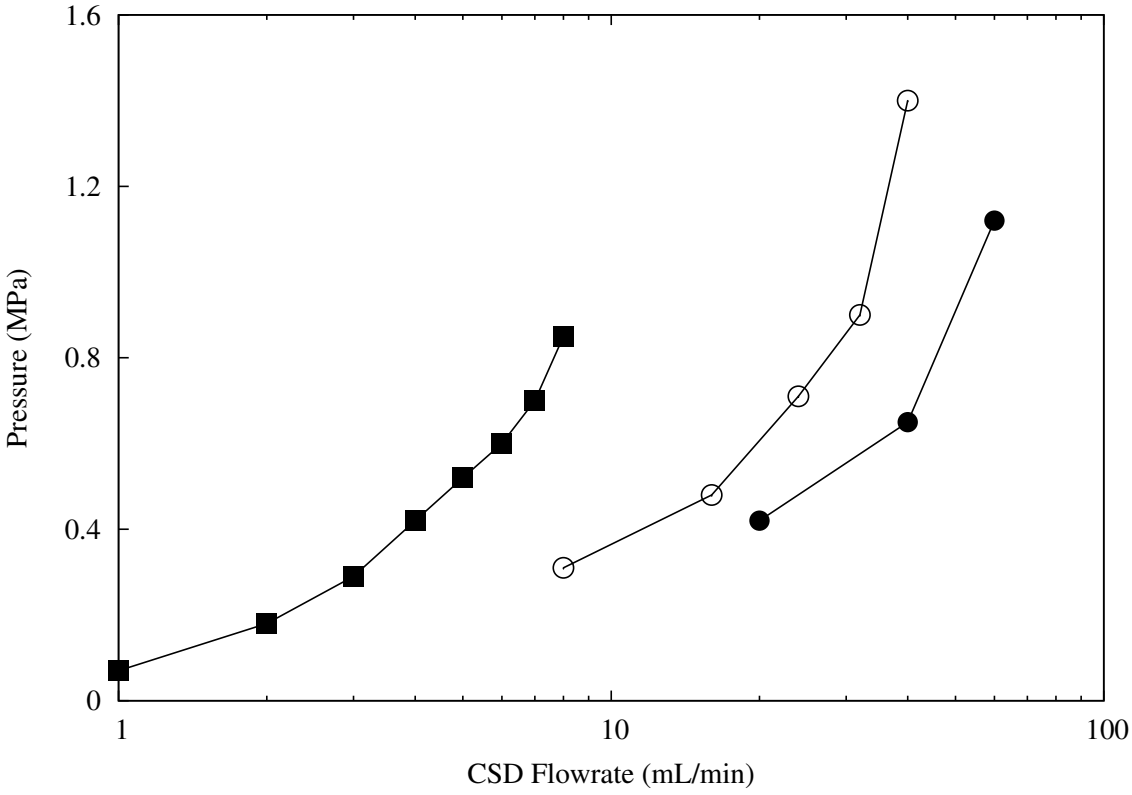


**Fig. 3.8:** Study examining the effect of capillary size over a flow rate range of 1-60 mL/min on the back pressure produced in CSD Version 2. Capillary sizes: 0.007″ (■), 0.01″ (○) 0.02″ (●)

### 3.5.6 Effect of Capillary ID on Centrate Turbidity

With higher levels of cellular damage higher levels of cellular debris are expected to be generated leading to increased centrate turbidities. Figure 3.9 shows the extent of small cellular debris created as assessed through centrate turbidity for two capillaries of different diameters but constant lengths. An increase in turbidity was expected with increased CSD flow rates for both capillaries but there was significantly more damage when the

material was passed through the 0.007″ capillary compared to the 0.01″ capillary. This was due to the higher levels of energy dissipation created using the narrower 0.007″ capillary which results in higher levels of turbidity. Furthermore, Figure 3.9 suggests in order for the 0.01″ capillary to generate equivalent amounts of energy dissipation to that of the 0.007″ capillary so that the same levels of damage was created the operational flow rate of the 0.01″ capillary would be required to increase significantly.

### 3.5.7 Bridging Study: CSD Version 2 and Version 3

A third, automated version of the CSD (Version 3) was created where cell culture material was loaded to the Super Loop using the P-960 pump. This was to reduce experimental time by removing the the syringe based manual loading of cell culture into the Super Loop using a syringe. A study was conducted in which material was sheared at the same rate using both of the CSD design variants. Subsequently all sheared material was centrifuged at the same conditions and the turbidities of the supernatants measured. Figure 3.10 shows that the turbidities obtained in each case were identical suggesting that the Automated CSD design provides a viable match to previous designs.

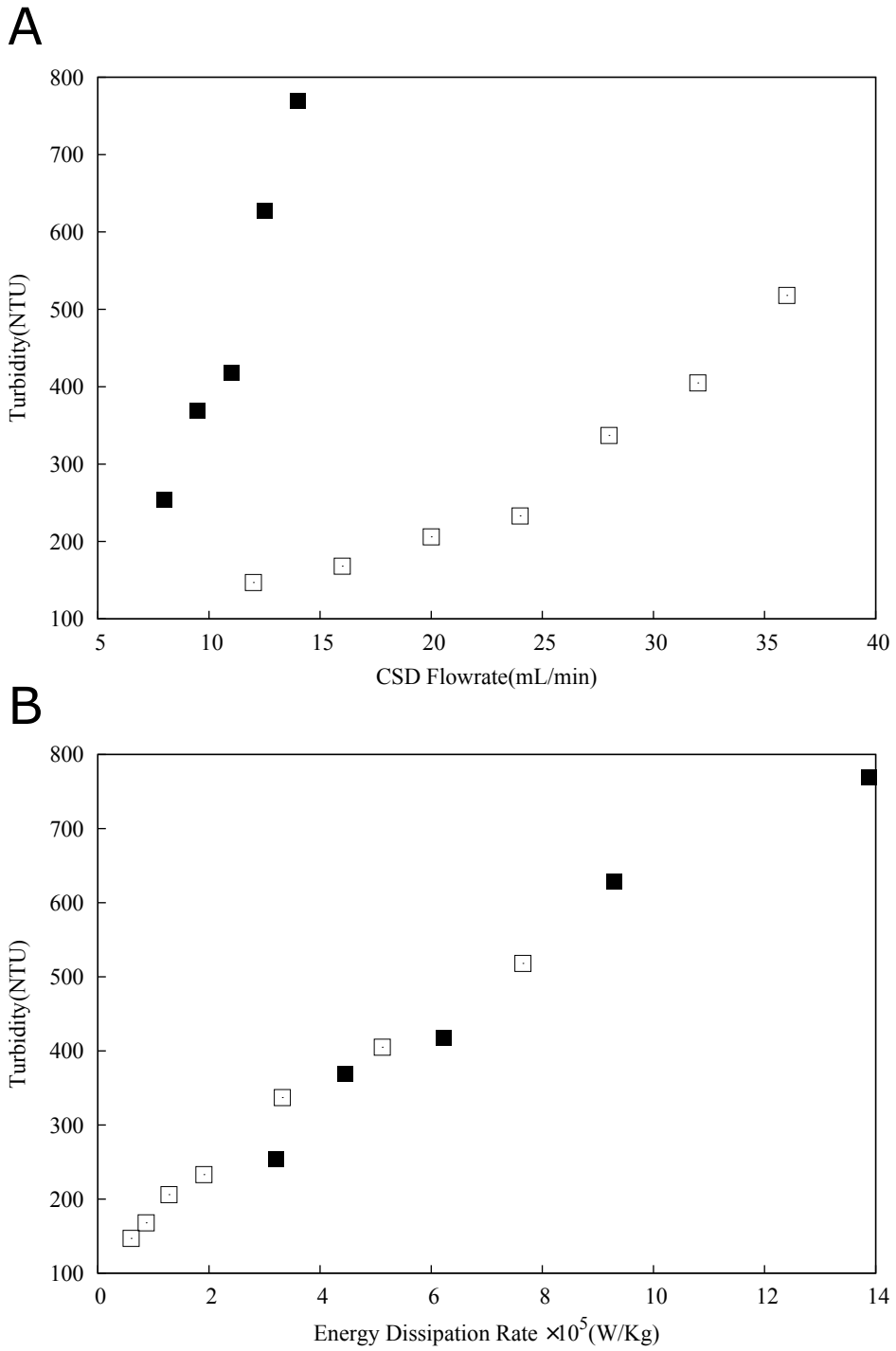


**Fig. 3.9:** Examining the effect of (**A**) flow rates and (**B**) EDR on centrate turbidity using capillary sizes 0.007″ ■ and 0.01″ □. A range of EDR were generated using CSD Version-2 by processing Culture-F. The sheared material was subsequently centrifuged at V/tΣ 2.41 $\times 10^{-8}$ (m/s).

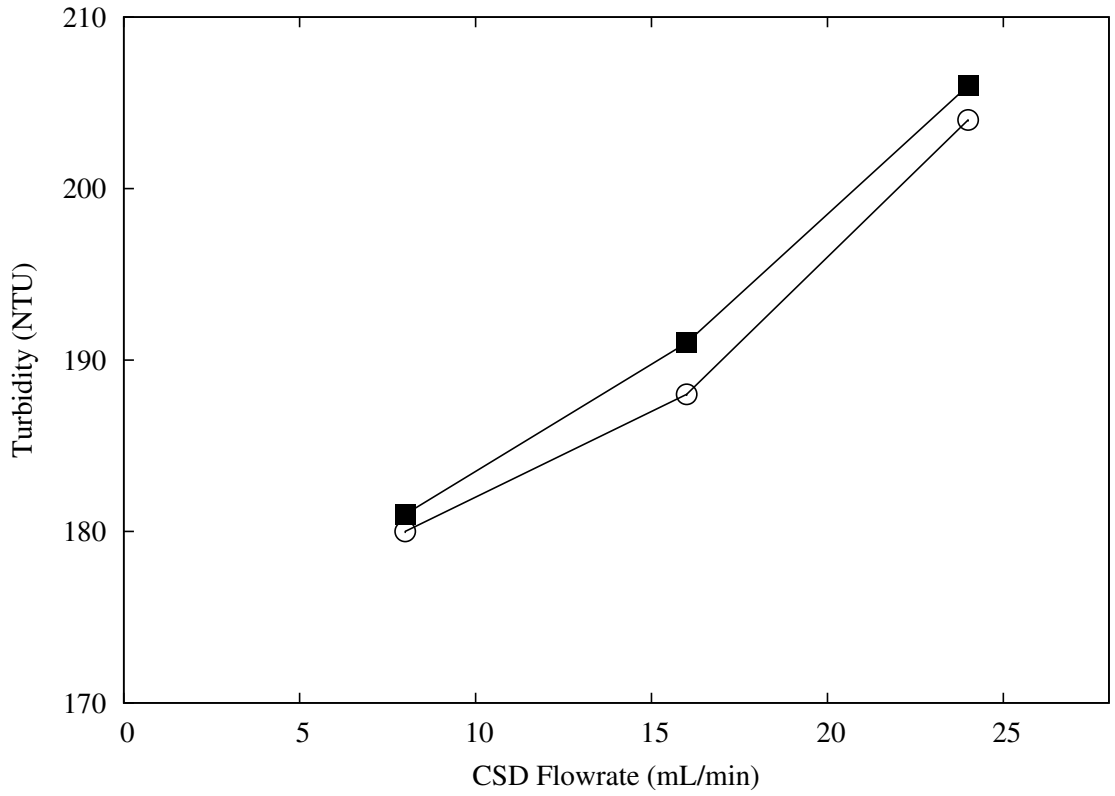


**Fig. 3.10:** Study examining the shear effects produced by CSD Version-2 (○) and Version-3 (■). The shear exerted was measured by the turbidity of sheared and centrifuged samples sourced from Culture-G (Table 3.7). A range of sheared samples were generated at flow rates of 8-24 mL/min using Version 2 and 3 of the CSD. Subsequent to shear all samples are centrifuged at V/tΣ of $2.20\times10^{-8}$ (m/s).

## 3.6 Conclusion

The aim of this chapter was to develop a device and a set of operating methodologies to provide an alternative to the rotating disk shear device (RSD) for creating varying levels of shear. Three versions of the capillary shear device (CSD) were developed. Version 1 of CSD was designed with the aim of creating similar levels of shear to those developed in the RSD and provide large pools (>1 L) of sheared samples for subsequent filter characterisation studies. The design of the CSD Version 1 was able to fulfil its aims through the selection of robust parts such as a glass syringe and high pressure check values. In an attempt to move away from the expensive and unreliable syringe pumps which were limited both in the achievable flow rate due to low back pressure (<1MPa) and force it could generate, CSD Versions 2 and 3 were developed. The AKTA Explorer (GE Healthcare, Little Chalfont, UK) is common place in downstream processing laboratories. The AKTA Explorer was incorporated in design Versions 2 and 3. It was adapted through bypassing loading of the cell culture through the piston pump and instead utilising a combination of Super Loop and P-960 peristaltic pump for the loading of material for subsequent exposure to shear. Version 2 of the CSD was used to characterise the influence of flow rate and internal capillary diameter on cellular damage. Studies were also conducted to quantify the stability of the cell culture and to confirm the cellular damage was all attributed to shear generated in the CSD. The following Chapter 4 utilised the CSD devices developed to identify the levels of shear present within the feed zone of the pilot-scale centrifuge and subsequently generate centrates using the CSD to mimic those found at pilot-scale.

# Chapter 4

# Scale-Down Centrifugation Process Development

## 4.1 Introduction

Quality by Design (QbD) regulatory initiatives over the last decade have required that biopharmaceutical manufacturers develop a thorough understanding of a product's quality attributes and manufacturing process through the generation of design spaces [Rathore & Mhatre, 2011]. High throughput scale-down techniques now enable the rapid generation of extensive experimental data representative of large-scale performance, both in the upstream and downstream manufacturing process. Such large experimental data sets generated through these scale-down techniques allow for better identification of the effects and interactions of the input parameters on the process performance and product quality during process development studies [Titchener-Hooker *et al.*, 2008]. Typically process development of centrifuge operations are material, time and resource intensive. Scale down methods allow for a reduction of these requirements and enable such studies to be conducted at laboratory scale. The laboratory scale methods published in the literature to mimic pilot-scale centrifugation utilize a combination of lab-scale centrifuge and a Rotat-

ing Shear Device (RSD). The experimental protocols utilising the RSD have been described in detail in numerous publications [Boychyn *et al.*, 2001; Hutchinson *et al.*, 2006; Tait *et al.*, 2009]. The previous chapter considered the development of a bespoke CSD which had the ability to generate similar levels of shear to that of the RSD. This chapter aims to develop an experimental methodology that incorporates CSD in order to predict and characterize pilot scale centrifugation performance. Furthermore, this chapter explores the impact and interaction of centrifugal separation on subsequent filter capacity so as to determine the best integration between the steps of centrifugal solids removal and sub micron particulate elimination by depth filtration. This chapter also examined the impact of primary recovery process parameters and cell culture conditions on the performance of subsequent centrifugal harvest and both depth and sterile filtration as a process sequence. Chapter 4 commences with establishing experiments to determine bench-scale conditions to mimic the performance of three pilot-scale centrifuges. Flow rates through the CSD Versions 1 & 2 were identified to generate equivalent levels of shear to those found in the feed zone of industrial disk-stack centrifuges. Once the level of shear had been identified the separation performance of the centrifuge was investigated to identify the correction factor (c) for the disk stack centrifuge. With the separation capabilities and the shear within the feed zone of the centrifuge characterised the next step was to characterise the subsequent unit operation in the process sequence, the filtration step. This step required adequate volumes of centrates to be generated. Accordingly, CSD Version 1 was utilised to provide the large pool of sheared sample for the generation of 1L of centrate which was subsequently filtered. CSD Version 1 was also used to create centrate mimics at multiple values of $Q/\Sigma$ from the pilot scale centrifuge in order to identify the effect on subsequent filtration processes. Further studies were conducted to explore how culture and harvest conditions impact the performance of the whole primary recovery sequence.

## 4.2 Materials and Methods

### 4.2.1 Cell Culture

Cell culture used in the experiments in this chapter were generated in a similar fashion to those in Chapter-1. The cultures produced had a range of cell densities and viabilities measured at the day of harvest as summarised in Table 4.1. Bench-scale cell culture was conducted in 3 L bioreactors whilst pilot-scale cell culture was performed in 50, 100 and 2000 L stainless steel bioreactors.

**Table 4.1:** Chapter 2 experimental cell culture properties

| Material | Bio Reactor Size (L) | Cell Density $\times 10^6$ (cells/mL) | Cell Viability (%) |
|---|---|---|---|
| Culture-H | 100 | 26.8 | 58 |
| Culture-I | 2000 | 14.9 | 74 |
| Culture-J | 100 | 23.9 | 90 |
| Culture-K | 100 | 20.3 | 96 |
| Culture-L | 2000 | 12.2 | 45 |
| Culture-M | 2000 | 16.0 | 70 |
| Culture-N | 3 | 30.8 | 31 |
| Culture-O | 50 | 11.6 | 72 |
| Culture-P | 50 | 27.4 | 84 |
| Culture-Q | 200 | 17.4 | 88 |
| Culture-R | 50 | 27.5 | 23 |
| Culture-S | 50 | 15.9 | 83 |
| Culture-T | 50 | 19.2 | 49 |

### 4.2.2 Centrifugation

#### Pilot-Scale Centrifuge: Alfa Laval LAPX-404 and BTPX-305

Continuous flow Alfa Laval LAPX-404 and BTPX-305 disk-stack centrifuges (Lund, Sweden) were used to clarify the cell culture at large-scale. In the experiments conducted with the LAPX-404 flow rates were set at 90-120 L/h and the rotational speed of the bowl was

varied to generate between 6000 to 10,000 g whilst the larger BTPX-305′s flow rate and bowl speed were maintained at 480 L/h and 12,500 g respectively.

#### Pilot-Scale Centrifuge: Wesfalia SO1

A continuous flow Wesfalia SO1-06-107 disk-stack centrifuge (Oelde, Germany) was also used to generate centrates. The experiments were conducted at a set bowl speed of 11,000 RPM and flow rates were varied between 0.3-0.9 L/min in order to generate Q/cΣ values of 2.92-4.00$\times 10^{-8}$ m/s.

### 4.2.3 Analytical Techniques

#### Particle Size Distribution (PSD)

% Solids remaining and turbidity are commonly used outputs to characterize centrate quality. Particle size distribution is another technique that is also used to characterise centrate quality. The intensity weighted particle size distributions based on dynamic light scattering was determined using a Zetasizer Nano S (Malvern Instruments, UK) equipped with a monochromatic coherent 4 mW Helium Neon laser (633 nm) as the light source. The particles were all assumed to be spherical and in this thesis. PSD readings were measured as a volume percent of total detected solids volume.

### 4.2.4 Centrifugation Experimental Methodologies

#### Scale-Down Experimental Strategy

In some cases, it is difficult to develop scale down models for unit operations using only principles of geometric similarity. In such scenarios additional aspects need to be evaluated to establish a model that can mimic performance across scales. In the case of disk-stack centrifugation the aspects that need to be characterised were the high shear

region in the feed zone and the solid liquid separation capabilities of the centrifuge. The shear in the feed zone was mimicked through the use of the shear device developed in the Chapter 3. On the other hand, the development of mimicking the separation capabilities of the disk stack centrifuge was based on the well understood process matching of equivalent settling area using a lab scale centrifuge. The methods to establish bench scale conditions in order to quantify and model the levels of shear in the disk stack centrifuge and the subsequent characterisation of separational properties of the pilot scale machines is described in detail in later sections of this chapter. Figure 4.1 illustrates the experimental strategy for the methods developed in this chapter utilising the shear device used in combination with the laboratory centrifuge to best mimic the performance of the pilot centrifuge.

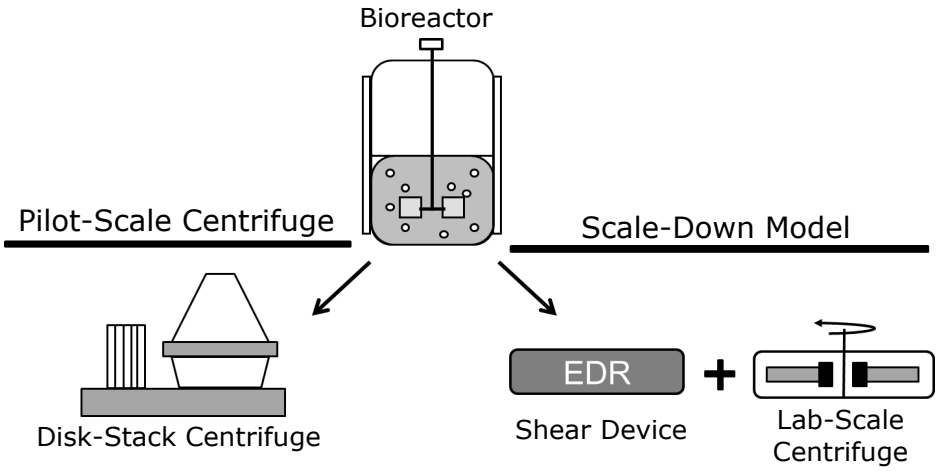


**Fig. 4.1:** Strategy for scaling down of large-scale centrifugal recovery achieved with the CSD Versions 1 and 2 in combination with lab-scale batch centrifuge with a swing out rotor.

### Identification of Pilot-scale Centrifuge Shear

In order to identify the levels of shear generated at a range of different flow rates and Energy Dissipation Rates (EDRs) through CSD Version-1 and CSD Version-2 respectively, the Lactate dehydrogenase (LDH) concentration in the cell culture was measured before and after shearing. LDH is an intracellular enzyme that is released upon cell rupture (details of

quantifying LDH is described in Chapter 3). Increased levels of LDH concentration were expected to accompany increasing levels of shear. The relationship between the level of LDH increase as a function of flow rate ($Q$) and maximum EDR ($\epsilon_{max}$) was established and used to calculate the flow rate in CSD Version 1 and the maximum EDR in CSD Version 2 that resulted in an equivalent level of % LDH increase in the pilot-scale centrifuge.

#### Identification of Pilot-Scale Centrifugation Correction Factor

Correction factors ($C_{ds}$) of ≈ 0.4 have been used in the past to describe the separation performance of industrial disk-stack centrifuges; however, not all centrifuges of the same basic design behave identically. To estimate the correction factor of the pilot-scale centrifuges examined in this chapter, sheared material was generated using the CSD Versions 1 and 2 under conditions which corresponded to the level of shear observed in the centrifuge. Subsequently, the sheared material was centrifuged in a bench top centrifuge at a range of V/t$\Sigma$ values. The supernatants from the range of centrifuged samples were then analysed for the extent of solids remaining and turbidity. This data set was used as a basis to identify the best value for the effective centrifuge correction factor $C_{ds}$.

### 4.2.5 Depth and Sterile Filtration Experimental Methodologies

The centrate clarification experiments were conducted using a Millistak+ X0HC depth filter (EMD Millipore, Massachusetts, USA) with a nominal pore size ranging from 0.1-2 $\mu$m. Sterilising grade SHC filters (EMD Millipore, Massachusetts, USA) were used to filter the depth filtered material. The SHC has a bilayer structure with a pore size rating of 0.5/0.2 $\mu$m.

Depth filtration capacity (L/m$^2$) was identified by observing the change in filter pressure at a constant flow rate. This approach is known as the $P_{max}$ methodology [Yavorsky

*et al.*, 2003]. In this study $P_{max}$ was defined as the capacity at which a pressure drop of 10 psi was reached. The experimental runs were conducted using a 23 $cm^2$ filter capsule at 200 LMH. Pressure drops and filtrate turbidities (NTU) were recorded for the duration of the experiment. In cases where the feed pool of centrate had been exhausted and a pressure of 10 psi had not been attained an intermediate pore blockage model was linearised [Equation 4.1] to predict theoretically the volume of filtrate per filter area ($V$) required to reach a pressure ($\Delta P$) of 10 psi [Hlavacek & Bouchet, 1993]. In the linearised equation $a''$ and $b''$ were used as dimensionless coefficients.

$$Ln(\Delta P) = a''V + b'' \tag{4.1}$$

The capacity of SHC sterile filters required to filter the X0HC filtrate was established through the $V_{max}$ methodology [Badmington, 1995]. Experiments were conducted with a 3.5 $cm^2$ filter area at a constant pressure of 10 psi and the flux decline was monitored over time. The $V_{max}$ method is a linearised form [Equation 4.2] of the pore constriction model used to compute theoretically the maximum volume of filtrate per unit filter area ($V_{max}$) that can be obtained before complete fouling through plugging occurs [Zydney & Ho, 2002, Kong *et al.*, 2010, Lau *et al.*, 2013].

$$\frac{t}{V} = \frac{1}{Q_0} + \left(\frac{1}{V_{max}}\right) t \tag{4.2}$$

Where $V$ is the total volume of filtrate volume per unit filter area collected over time ($t$) and $Q_0$ is the initial specific volumetric filtrate flow rate per unit filter area.

## 4.3 Results

### 4.3.1 Centrifuge Characterisation

Table 4.2 shows the summary of the bench top operating conditions run in order to mimic pilot scale operation at a range of operating settings. The operating settings of the pilot scale centrifuge encompasses a wide range of flow rates and bowl speeds.

**Table 4.2:** Operational settings for pilot-scale centrifuges and corresponding CSD Version-1 and lab-scale centrifuge settings

| Condition | Centrifuge | Pilot-Scale Centrifuge | | Capillary Shear Device (CSD) | |
|---|---|---|---|---|---|
| | | Flow Rate (L/h) | Relative Centrifugal Force (g) | $Q/c\Sigma$,$V/t\Sigma \times 10^{-8}$ m/s | CSD Flowrate (mL/min) |
| 1 | LAPX-404 | 90 | 6000 | 4.90 | 16.63 |
| 2 | LAPX-404 | 105 | 7900 | 2.92 | 17.57 |
| 3 | LAPX-404 | 120 | 10,000 | 1.65 | 18.03 |
| 4 | BTPX-305 | 480 | 12,500 | 2.20 | 17.08 |

#### Identification of Shear

Having established the comparability of the industrially accepted RSD and CSD Version-1 from the previous chapter, the next step was to utilise CSD Version-1 to match the levels of shear present in pilot-scale centrifuges; Alfa Laval LAPX-404 and BTPX-305 (Lund, Sweden). CSD Version-1 was used as a proxy to approximate the levels of shear to which the material was exposed inside the centrifuge at 6000, 7900 and 10,000 g for the LAPX-404 and at 12,500 g for the BTPX-305 respectively. Data shown in Figure 4.2 provided a correlation connecting the operating flow rate within the CSD Version-1 to the conditions of operation in the LAPX-404 centrifuge [Table 4.2] via levels of LDH increase ($LDH_{INC}$). Regression analysis of the modelling dataset and matching of the LDH increase showed that the levels of shear in the feed zone of the LAPX-404 and BTPX-305 were equivalent to the levels of shear created at a flow rate range of 16.6-18.0 mL/min in CSD Version-1

(Table 4.2). This result is highly consistent with earlier published data [Westoby *et al.*, 2011b]. Similar to CSD Version-1, CSD Version-2 was also used as a proxy to approximate the level of shear in the LAPX-404 and Wesfalia-SO1. The levels of LDH increase was a function of the EDR developed in CSD Version-2 is described in Figure 4.3 and 4.4. This correlation provided the levels of EDR required from CSD Version-2 to match the shear found in the feed zone of the LAPX-404 and Wesfalia-SO1. Values of 2.5 $\times 10^5$ W/Kg and 2.4 $\times 10^5$ W/Kg were identified to describe the shear in the LAPX-404 and Wesfalia-SO1 respectively. Values found in these studies matched closely with earlier published data from Boychyn *et al.*, 2001 where CFD analysis of a Wesfalia CSA-1 reported an EDR of $2.0 \times 10^5$ (W/Kg) and as such validated the methodology developed to identify levels of shear prevailing within a centrifuge.

**Identification of Correction Factor ($C_{ds}$)**

With the shear in the pilot-scale centrifuge identified in the earlier section through the use of CSD Version-1 and 2 the next step was the prediction of pilot-scale centrifuges process performance in order to identify the effective centrifuge correction factors ($C_{ds}$). The relationship between turbidity and V/t$\Sigma$ [Figure 4.5] was determined empirically. The $C_{ds}$ value of the Alfa Laval LAPX-404 was found to be in the region of 0.31 whilst a correction factor of 0.55 was established to describe the BTPX-305. The correction factor for a disc stack centrifuge, $C_{ds}$ values have been quoted in the range 0.4-0.5 [Pinheiro, 1993], based on industry experience and are widely applied for design purposes. However, with assuming a fixed value it is important to note that deviations in the prediction of performance can arise from variations in $C_{ds}$ [Hutchinson *et al.*, 2006]. The experimentally calculated correction factors estimated in this study for the pilot-scale centrifuges were consistent with the ranges suggested in literature [Hutchinson *et al.*, 2006] and hence validated the experimental method used to calculate the correction factor. Incorporating

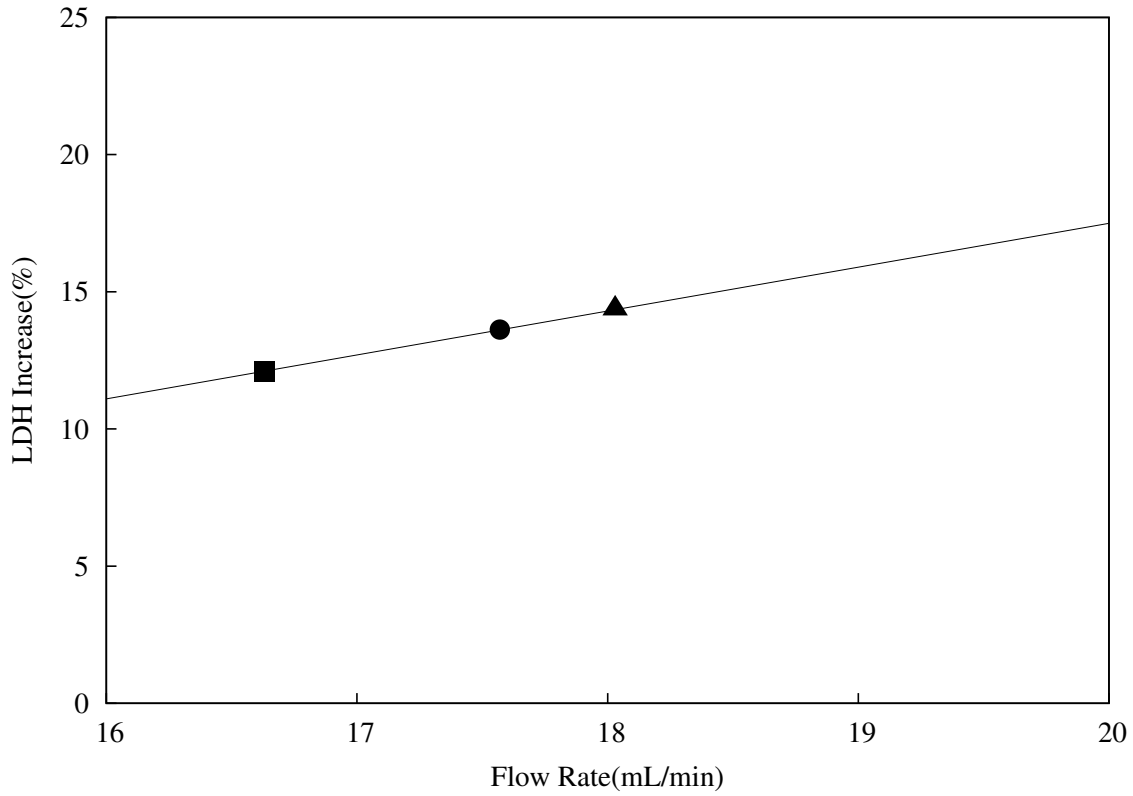


**Fig. 4.2:** Study examining the correlation between % LDH increase and operating flow rate of CSD Version-1 so as to match the shear generated in the LAPX-404 at a range of Q/Σ values. % LDH increase for the modelling dataset (□) generated by shearing Culture-H (Table 4.1) using the CSD Version-1. Regression analysis (—) was used to identify the shear in the LAPX-404 centrate at conditions 1(■), 2(●) and 3(▲) (Table 4.2) determine the following relationship between % LDH increase ($LDH_{Inc}$) and flow rate (Q) for Culture-H : $LDH_{Inc}$=1.60Q - 14.49, $R^2$=0.98.

experimentally identified LAPX-404 $C_{ds}$ with the sigma value of the continuous centrifuge allows for the calculation of bench-top centrifuge operation conditions required to mimic the pilot scale centrifuge. These values are summarised in Table 4.2.

### 4.3.2 Centrifuge Characterisation: Centrate Quality

With scoping of the shear and the separation capabilities of the pilot scale centrifuge complete, the scale-down methodology based on the CSD Version-1 and 2 and a lab-scale centrifuge was then used to mimic a set of V/tΣ in the LAPX-404 and BTPX-305 machines [Table 4.2]. To ensure the samples generated through the scale down methodology were

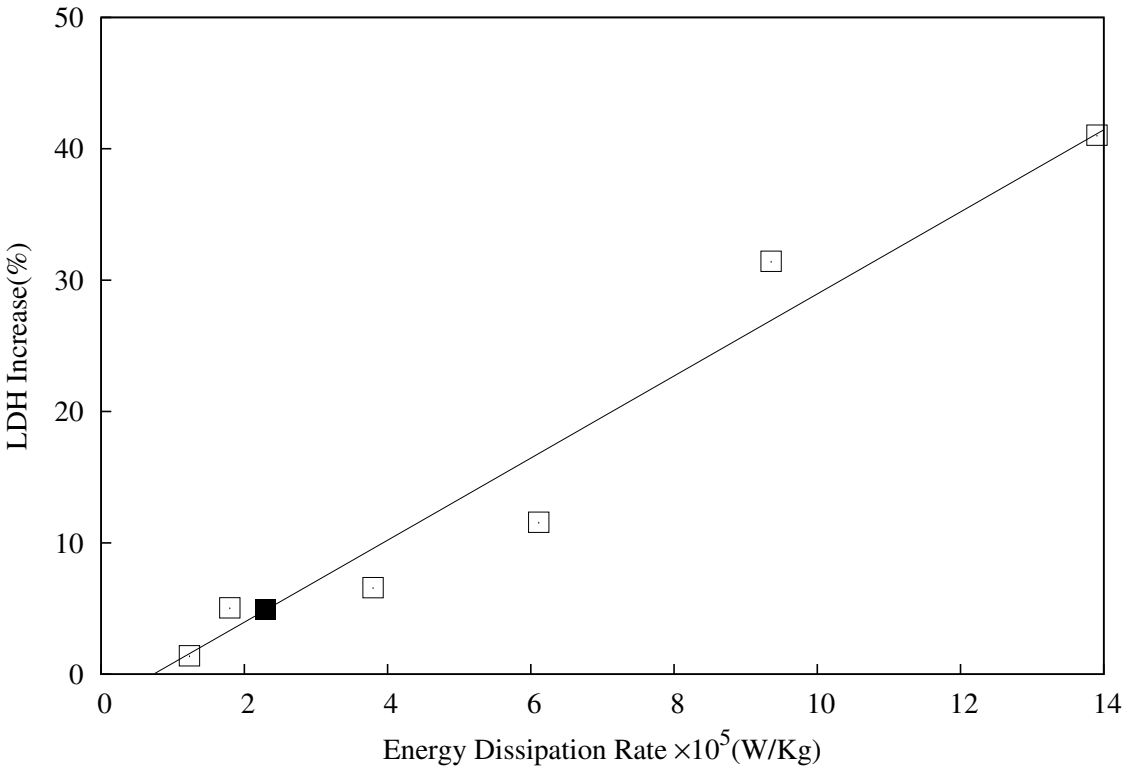


**Fig. 4.3:** Study examining the correlation between % LDH increase (measure of cell damage) and EDR generated through CSD Version-2 so as to identify the cell damage occurring in the LAPX-404. The % LDH increase for the modelling dataset (□) generated by shearing material Culture-P (Table 4.1) using the CSD Version-2 at a range of EDRs. Regression analysis (—) was used to determine the following relationship between LDH increase ($LDH_{Inc}$) and EDR ($\epsilon_{max}$) in order to identify the shear produced in the LAPX-404 at operating conditions with a bowl speed of 7900g and flow rate of 120L/hr (■): $LDH_{Inc} = 3.12\epsilon_{max} - 2.29$, $R^2$=0.96

representative mimics of the pilot scale centrifuge markers of % solids remaining, turbidity and particle size distribution were used. The % solids remaining [Figure 4.6] and turbidity [Figure 4.7] for samples generated using the scale-down method closely resembled the solids remaining in samples generated by the pilot-scale centrifuges. Furthermore, samples generated from the scale down methodology had almost identical particle size distributions [Figure 4.8] to those of the centrates created using the pilot scale centrifuge. With all markers creating very close matches to the pilot-scale machine, the validity of

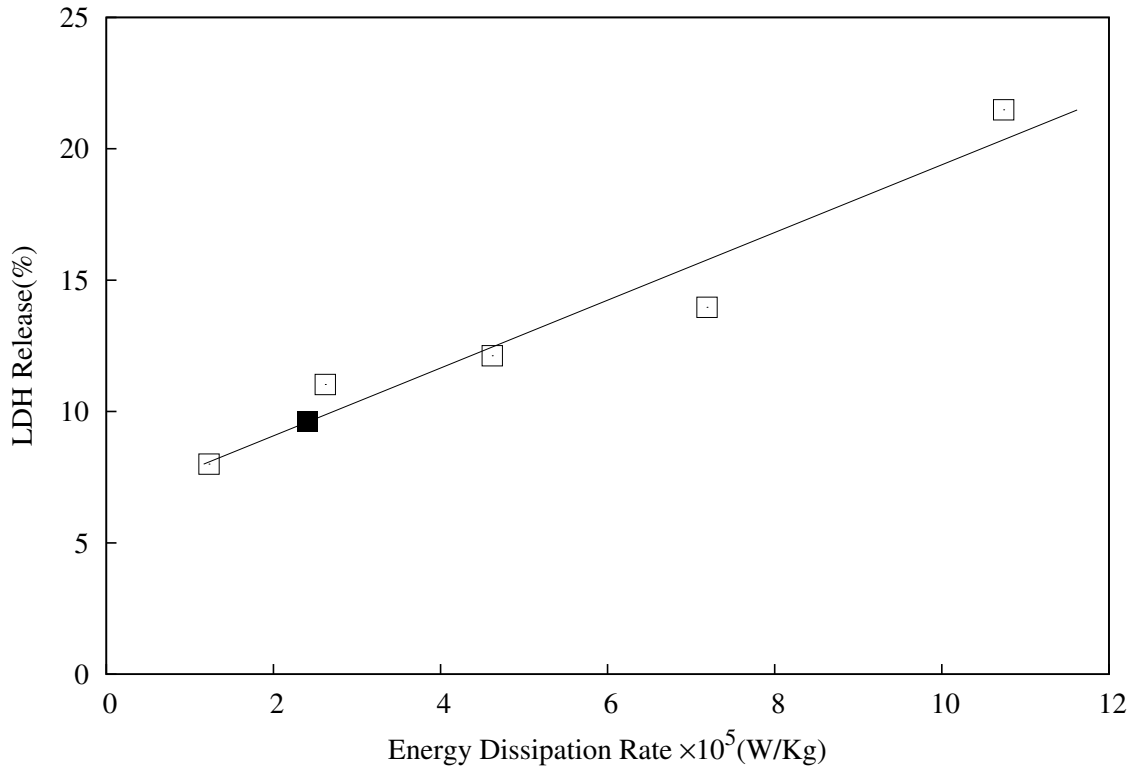


**Fig. 4.4:** Study examining the correlation between the % LDH increase (Measure of cell rupture) and EDR of CSD Version-2 so that cell damage in the feed zone of the Wesfalia SO1-06-107 at a bowl speed of 11,000 RPM can be quantified. LDH increase for the modelling datasets (□) was generated by shearing material (Culture-J) (Table 4.1) using the CSD Version-2. Regression analysis (—) was used to determine the following relationship between LDH Release ($LDH_{Rel}$) and EDR ($\epsilon_{max}$) to identify the levels of shear generated in the Wesfalia SO1-06-107 centrifuge (■): $LDH_{Rel}$=1.29$\epsilon_{max}$+6.49, $R^2$=0.94.

the scale-down methodology incorporating CSD Versions-1 and 2 to provide quantities of representative material for process integration studies was confirmed.

### 4.3.3 Centrifuge Characterisation: Filter Performance

In a typical mAb harvest process the unit operation subsequent to centrifugation is normally depth filtration. If an accurate centrate mimic was to be developed, it had to show equivalent filtration properties to that of the centrate obtained at scale. Figure 4.9 shows the pressure and turbidity profiles generated during the operation of the X0HC depth filter

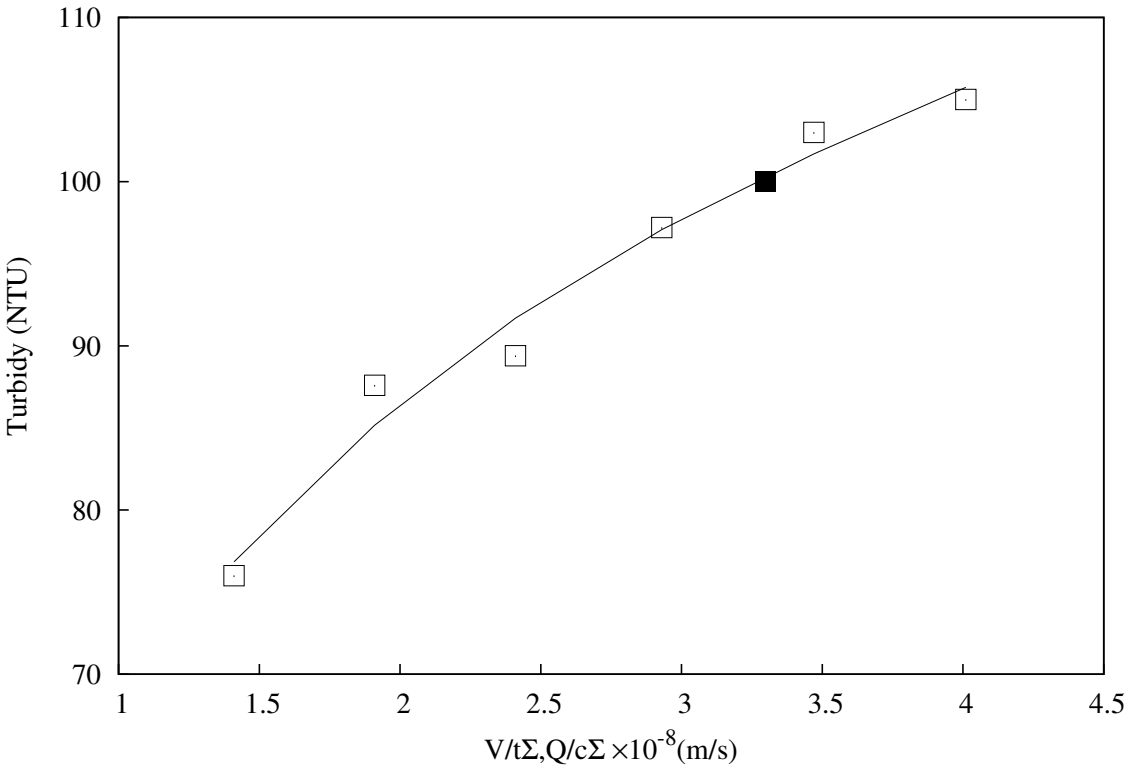


**Fig. 4.5:** Study examining turbidity upon centrifugation of cell culture material (Culture-P 4.1) passed through CSD Version-2 at a range of $V/t\Sigma_{lab}$ (□) so as to mimic the turbidity of LAPX-404 centrate generated whilst operated at 7,900g and flow rate of 120L/hr (■). CSD condtioned cell culture was generated by passing Culture-P at an EDR of $2.5 \times 10^5$ W/Kg through the CSD Version-2 and centrifuged at desired $V/t\Sigma_{lab}$ values in a lab-scale centrifuge.

when challenged with two feeds: the BTPX-305 centrate and the mimic sourced from the scale-down method. The samples generated via the scale-down method showed pressure and turbidity profiles that matched closely those of the BTPX-305. This indicated that the scale-down mimic had similar filtration properties to the BTPX-305 centrate, confirming the utility of the CSD Version-1 and the lab-scale centrifuge.

### 4.3.4 Influnce of Feed Flow Rate on Feed Zone Shear

The $Q/\Sigma$ of a given disk-stack centrifuge can be altered through changes in bowl speed and flow rate. Previous studies have shown that increases in bowl speed lead to higher levels

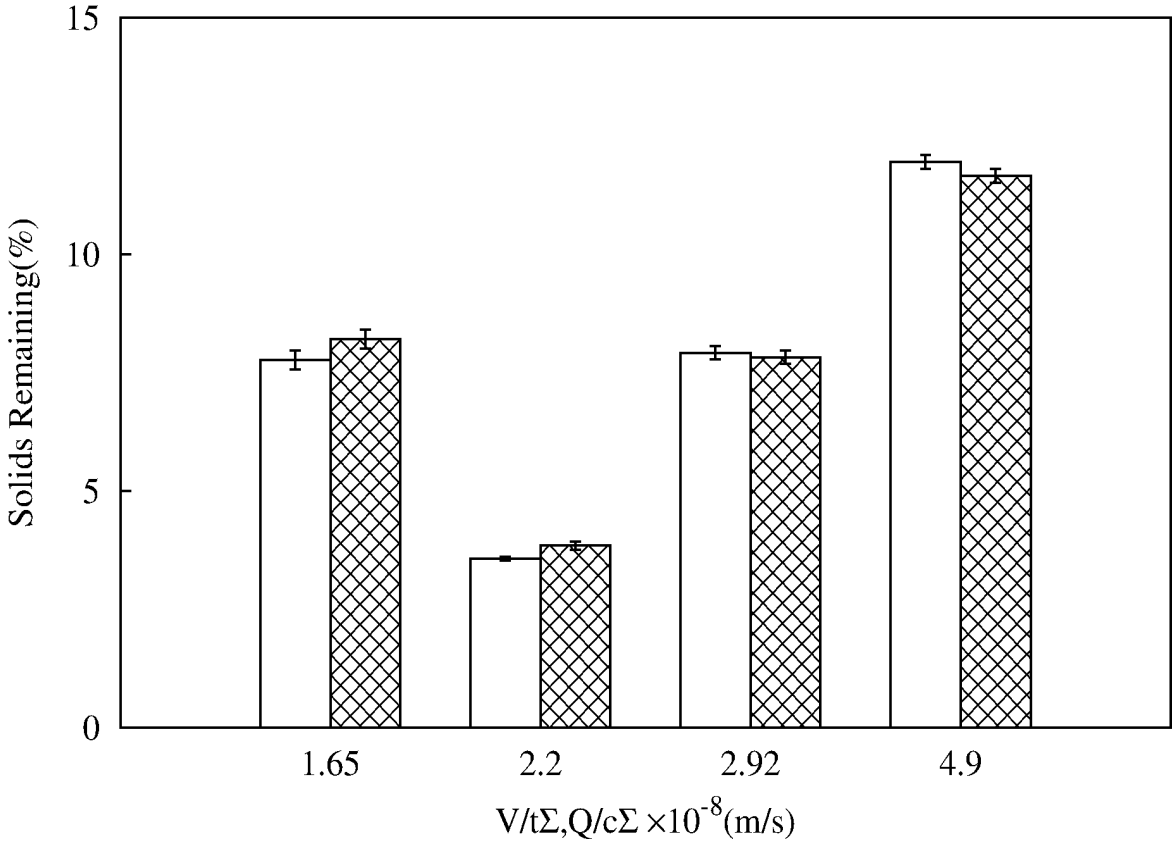


**Fig. 4.6:** Comparison of solids remaining in centrate generated using the scale down methodology employing CSD Version-1 mimicking LAPX-404 and BTPX-305 at a range of conditions (Table 4.2) ☒ and solids remaining from pilot scale centrifuge runs (□). Centrates generated in the LAPX-404 were sourced from Culture-H (Table 4.1) while the BTPX-305 centrate was sourced from Culture-I (Table 4.1). The values plotted are the average of 5 data points.

of shear as quantified through LDH release [Figure 4.2]. This study explored the effect of flow rate at a fixed bowl speed on shear damage. Figure 4.10 shows there was a decrease in the levels of LDH release in the centrifuge with increasing flow rates (0.3-0.9 L/min). This suggested that higher flow rates did not result in higher levels of shear and that the speed of the centrifuge bowl was predominately responsible for the shear imposed on the cells. The decrease in LDH release observed could be as a result of the lower residence times seen with increasing flow rates. A similar phenomenon was also observed in previous small scale studies utilising the rotating shear device where increased residence time in the RSD yielded an increased level of exposure to shear for shear sensitive mammalian

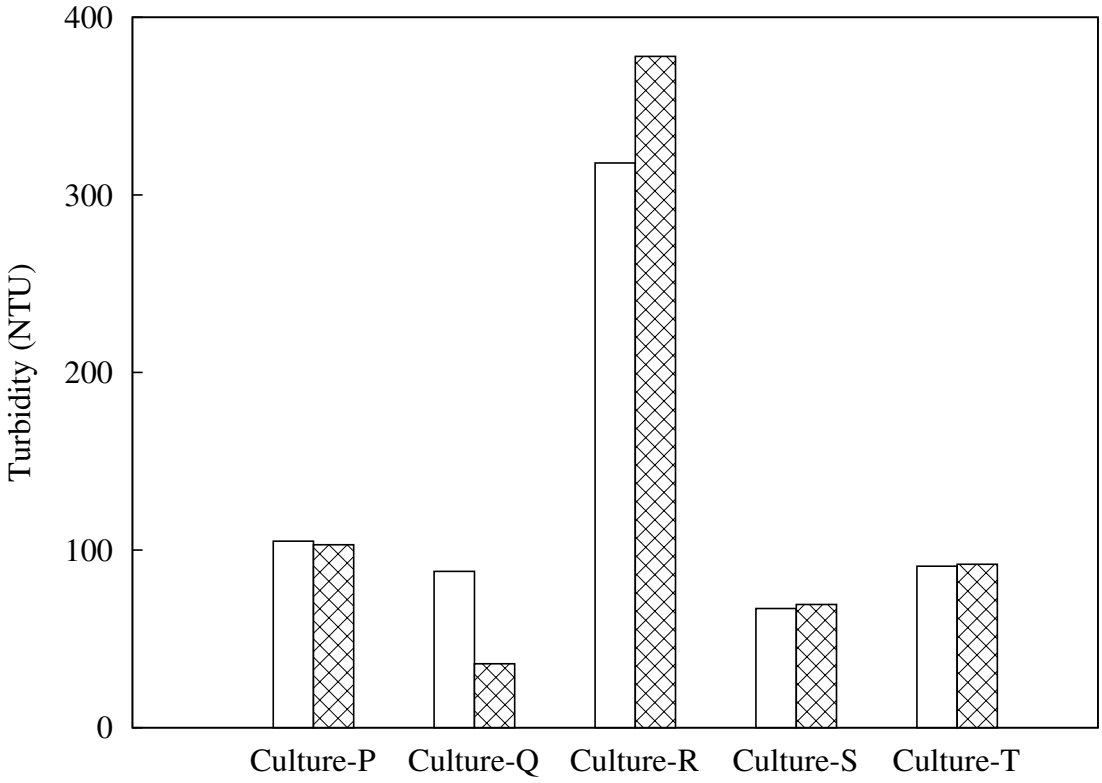


**Fig. 4.7:** Comparison of Turbidity generated using the scale down methodology (☒) incorporating CSD Version-2 mimicking LAPX-404 at 7,900g and flow rate of 120L/hr and turbidity centrate from the pilot scale machine (□). Cell culture material for this study were sourced from Culture P, Q, R, S and T (Table 4.1)

cells [Hutchinson *et al.*, 2006]. Furthermore, values of LDH released in this study were ≈ 10% which was consistent with the earlier study of quantifying the prevailing levels of shear in the Westfalia SO1 (Oelde, Germany).

### 4.3.5 Effect of Flux on Depth and Sterile Filtration

With the utility of the scale down method incorporating CSD Version-1 and 2 to create samples that mimic the characteristics of a pilot scale centrifuge confirmed, the device was then used as a means to generate large pools of sample for process studies. A typical bioprocess harvest platform incorporates centrifugation, depth filtration and sterile filtration. Depth filters are often operated at a defined flux to utilise efficiently the filter

area. This study examined the impact of flux on the X0HC depth filter and subsequent SHC sterile filtration operations. Typically at higher fluxes the filter area is not utilised efficiently and hence pressure build up in the filter occurs more rapidly. Lower filter capacities are often associated with higher fluxes. In this study [Figure 4.11] it was found that with a given centrate an increase in flux from 50 LMH to 200 LMH had no significant effect on the capacity of the subsequent depth filter. The flux decline profiles [Figure 4.12] for the SHC suggested that X0HC filtrates created at the two fluxes examined (50 and 200 LMH) had similar fouling propensities. The conclusion that increasing flux did not affecting filter performance is unlikely to be universal and must be applied on a case by case basis since not all centrates will have the fouling propensities akin to the centrate derived from Culture-L.

### 4.3.6 Effect of Centrifugation Conditions on Filtration

Process development requires scoping and understanding centrifuge performance at a range of $Q/\Sigma$ values. Typically poor centrifuge performance results in the carry over of cell debris to the centrate [Jain *et al.*, 2005]. These cell debris can cause subsequent fouling in later chromatographic processes, resulting in high column pressures and accompanied reductions in column lifetime and efficiency [Kempken *et al.*, 1995]. In order to avoid chromatographic column fouling, depth filtration is often used immediately after centrifugation to remove these sub-micron particles [Yigzaw *et al.*, 2006]. Typically characterization of centrifugation and filtration at pilot-scale requires 50L of cell culture. Having established that CSD Version-1 could be used to prepare large quantities of sheared material for integrated process studies, the impact of the combination of centrifugation and depth filtration operating conditions on the performance of the primary recovery train was examined. Figure 4.13 shows the solids remaining and the X0HC and SHC capacities for samples mimicking the LAPX-404 centrifuge at a range of conditions [Table 4.2].

Unsurprisingly the increase in capacities of both X0HC and SHC were inversely related to the levels of solids remaining. This study set the template for the preparatory CSD Version-1 to be utilised for harvest characterisation studies. It enabled the user to work at the 5 L bioreactor scale to characterise the harvest process instead of utilising a 50 L bioreactor hence saving material.

### 4.3.7 Impact of Culture Conditions on the Harvest Sequence

This study focused on the impact of cell culture conditions on the performance of a sequence comprising centrifugation, depth filtration and sterile filtration. The cell cultures examined represented differing extremes of harvest challenge; a difficult to harvest material and a relatively easy to recover broth. The former was from a bioreactor producing a high cell density, low viability cell culture. Figure 4.14 shows the separation behaviour when either of the cultures sheared using CSD Version-1 at a range of shear conditions. Culture representing the difficult harvest conditions showed steeper response surface compared to the culture representing easy harvest conditions. The results show that high cell density, low viability material was far more sensitive to shear, making subsequent centrifugation especially difficult.

This study also showed that processing difficult to harvest cultures negatively impacted the ability of the centrifuge to remove solids [Figure 4.15]. This form of material is challenging for harvest operations as there is a high solid content, leading to the centrifuge bowl filling up rapidly and requiring a high frequency of discharge. Another challenge was the low viability of the material. Such broths will contain large populations of cell debris which are small in size and have a lower density than viable cells. The removal of such cell debris by centrifugation is difficult and these particles often end up in the centrate resulting in a poor separation. However, the easy to harvest broth had a lower solid content

and a greater population of large viable cells, which facilitated separation. Furthermore, it may be expected that high cell viability may lead to healthy cells with intact cell walls and consequently are more resistant to shear damage within the centrifuge feed zone. This would be expected to yield a centrate of high clarity and fewer cell debris particles being passed on to subsequent filtration processes hence requiring much lower filter area when processing easy to harvest cultures [Figure 4.15] while those representing difficult to harvest conditions yielded a low quality centrate with larger amount of % solids carry over. This goes on to affect subsequent filtration steps resulting in much lower capacities to that of the culture representing easy to harvest conditions.

Figure 4.16 shows the X0HC pressures and turbidity profiles for centrates derived from both culture materials. Upon filtration, the centrate material from difficult harvest conditions showed significant increases in both the pressure and turbidity profiles (Δ15.5 psi, Δ8.7 NTU) compared to that of the easy to harvest material (Δ6.0 psi, Δ2.8 NTU). This can be directly attributed to the higher levels of smaller debris in the centrate of the high cell density culture causing a more rapid rate of pore blockage. As noted in Figure 4.15, processing of the difficult to harvest culture yielded lower SHC capacities compared to the easy to harvest culture. This was attributed to the larger amount of small particles carried through from the high cell density culture which in turn lead to a more rapid rate of pore blockage and flux decline [Figure 4.17].

### 4.3.8 Effect of Pre-Harvest Conditions on Centrifugation

Leaps in upstream development have lead to increased titres. This has also resulted in high cell density cell culture streams and elevated levels of process-related impurities, which increase the burden on subsequent purification operations. To address this conditions of the cell culture broth pre harvest may be altered through changes in pH conditions or

broth temperature in order to improve the performance of subsequent unit operations [Westoby *et al.*, 2011a]. This study utilised the CSD to characterize the influence of hold time, temperature and shear on centrifugation separation.

Figure 4.18 showed there to be clear increase in turbidity with increasing levels of shear. Statistical analysis of the data revealed shear to be the most influential parameter (P-Value=0.003) affecting the turbidity of the centrate. This was not surprising as higher levels of shear result in higher levels cell rupture and subsequent generation of fine particulates which are difficult to remove through centrifugal separation. Figure 4.18 **(A)** suggests longer hold times at lower temperatures ($5^oC$) had a negative effect on separation performance. This is due to the higher viscosities that are expected with colder temperatures ($5^oC$) which hinder centrifugal separation. Higher temperatures ($35^oC$) are expected to yield better clarification with an increased hold time. However, in this study higher temperatures over an increased hold time resulted in the rapid reduction in viability of the material (0 Hours: 93.7%, 3 Hours: 60.0%, 6 Hours: 16.90%). At lower viabilities there was an increased population of fine particulates which were difficult to remove through centrifugation and hence resulted in high turbidity centrates.

Typical centrifuge processes platforms operate at fixed bowl speeds and as a result changes in shear are very unlikely but there is a potential for the cell culture broth under certain circumstances to be held before processing over an extended period of time. This study identified that the hold time and the temperature can each have a significant influence on the performance of the centrifugation step.

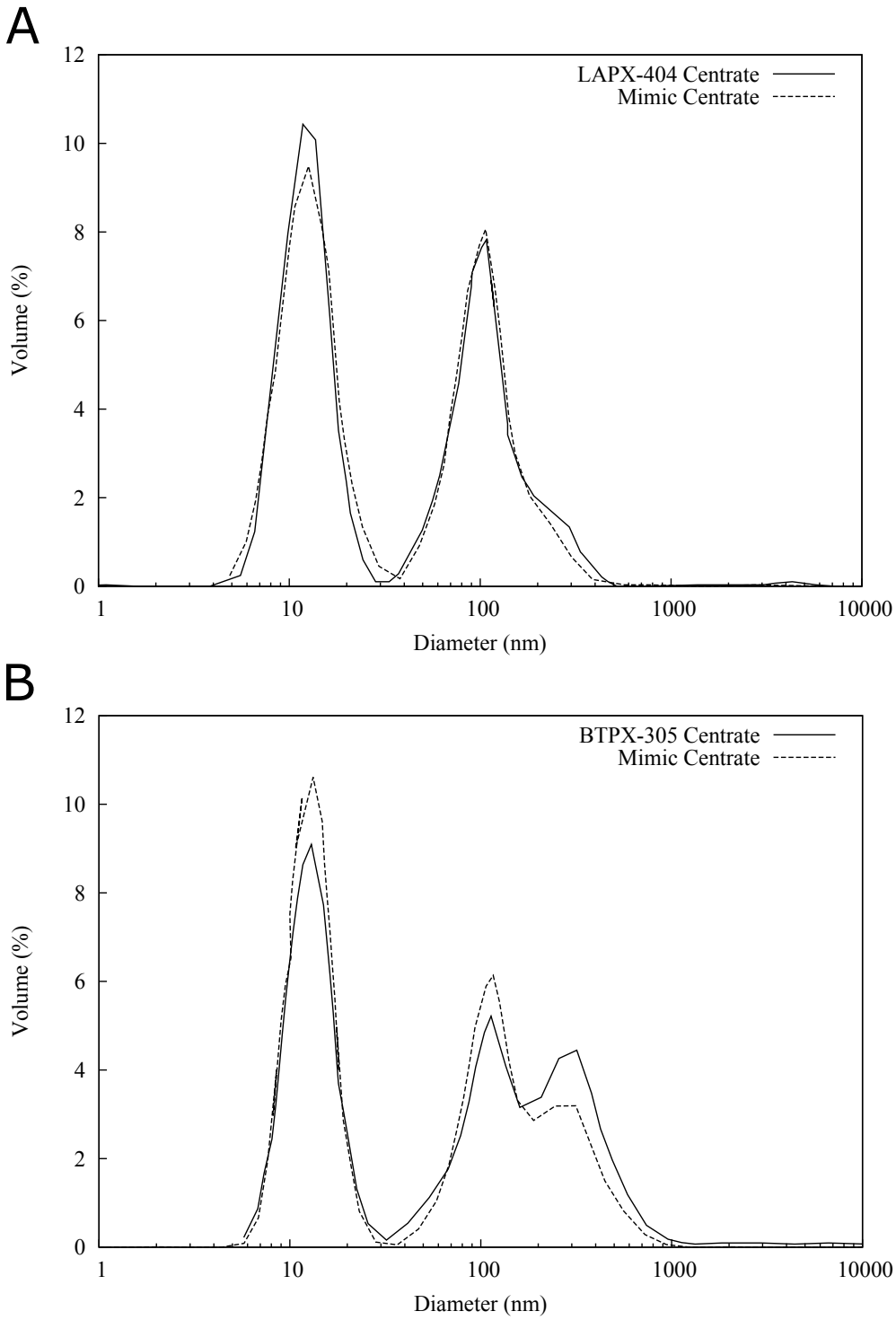


**Fig. 4.8:** Comparison of particle size distributions between the samples sourced from CSD Version-1 based scale down method and pilot-scale machine. **(A)** LAPX-404 centrate at condition 7,900 g and its respective mimic generated through the use of the CSD and lab-scale centrifuge **(B)** BTPX-305 centrate at 12,500 g and its respective mimic generated through the use of the CSD and lab-scale centrifuge. Centrates for for this study were sourced from Culture H and I (Table 4.1) respectively.

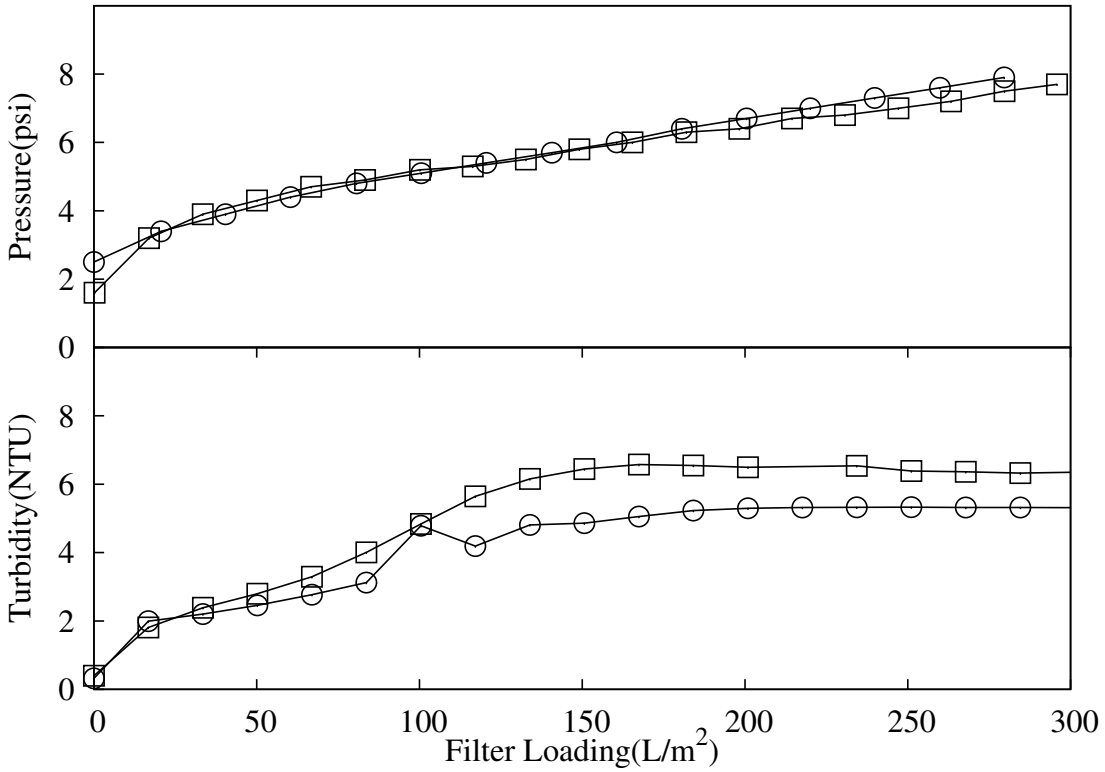


**Fig. 4.9:** A study comparing the pressure and turbidity profiles for 0.1-2.0 $\mu$m X0HC depth filter when filtering centrate from the BTPX-305 machine (◯) and the mimic centrate (□) generated from the scale-down methodology presented in the chapter. BTPX-305 centrate for this study was generated at a $V/t\Sigma_{lab}$ of $2.20\times10^{-8}$ m/s. Preparatory CSD centrate was processed to mimic the BTPX-305 at 12,500g and a flow rate of 480 L/h. The material for this experiment was sourced from Culture-I (Table 4.1) and filtration for this study was operated at 200 LMH.

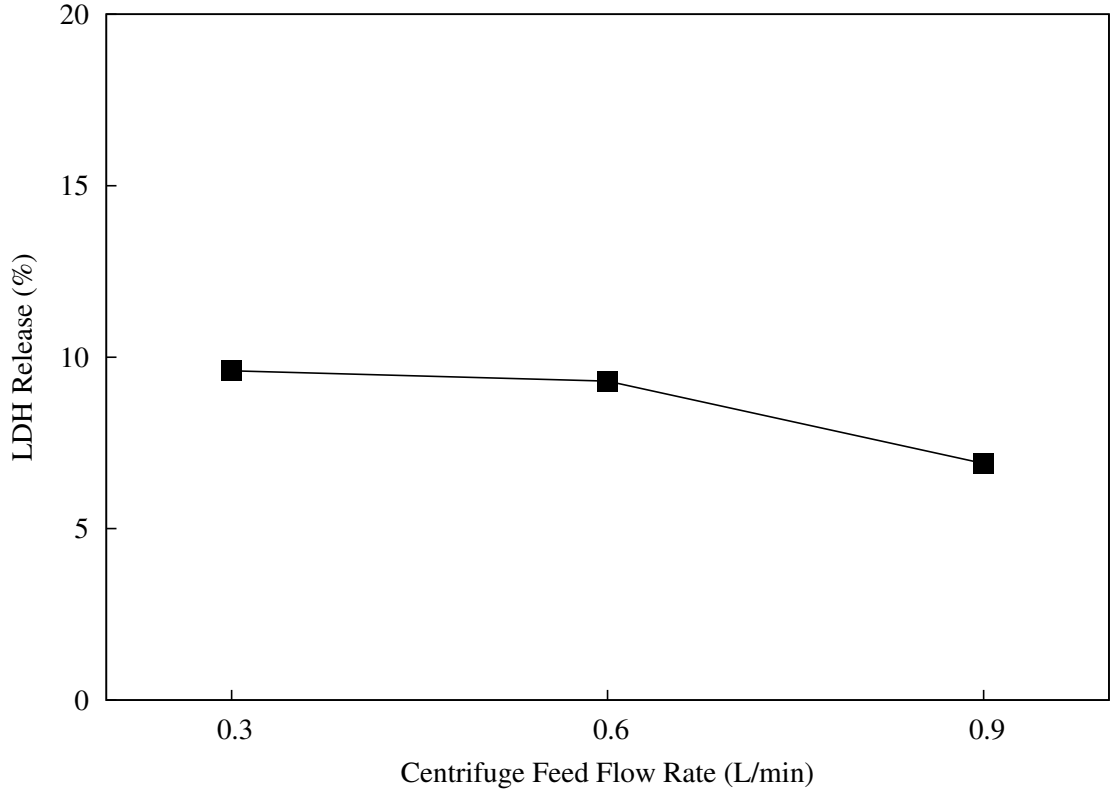


**Fig. 4.10:** Study examining the levels of LDH released at a range of feed flow rates (0.3-0.9 L/hr) while operating the Wesfalia SO1-06-107 while bowl speed of pilot-scale machine is maintained at 11,000 RPM. Culture-K (Table 4.1) was used as feed material during this study.

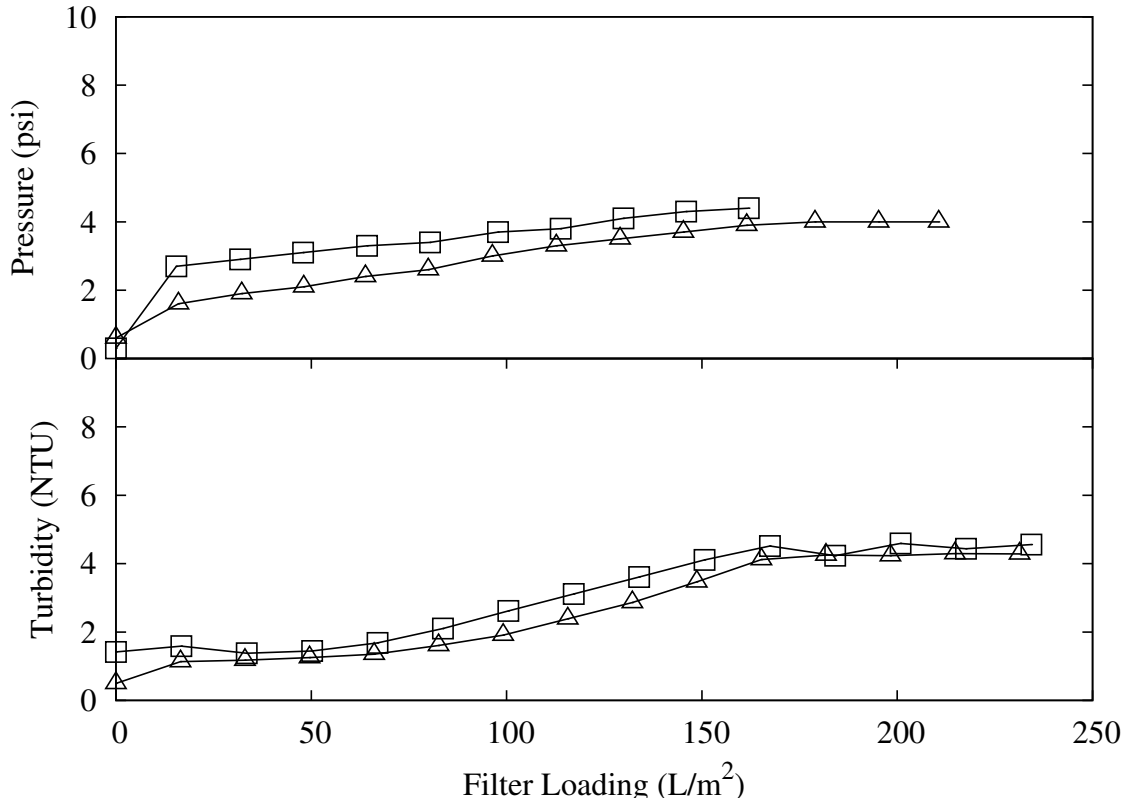


**Fig. 4.11:** Study comparing the pressure and turbidity profiles for 0.1-2.0 $\mu$m X0HC depth filter operated at 200 LMH (□) and 50 LMH (◯) when challenged with identical centrates. Centrates for this study were generated using the scale down method incorporating a combination of CSD Version-1 and lab-scale centrifuge to mimic the LAPX-404 at Q/Σ of $2.92\times10^{-8}$ m/s. Cell culture for this study was sourced from Culture-L (Table 4.1)

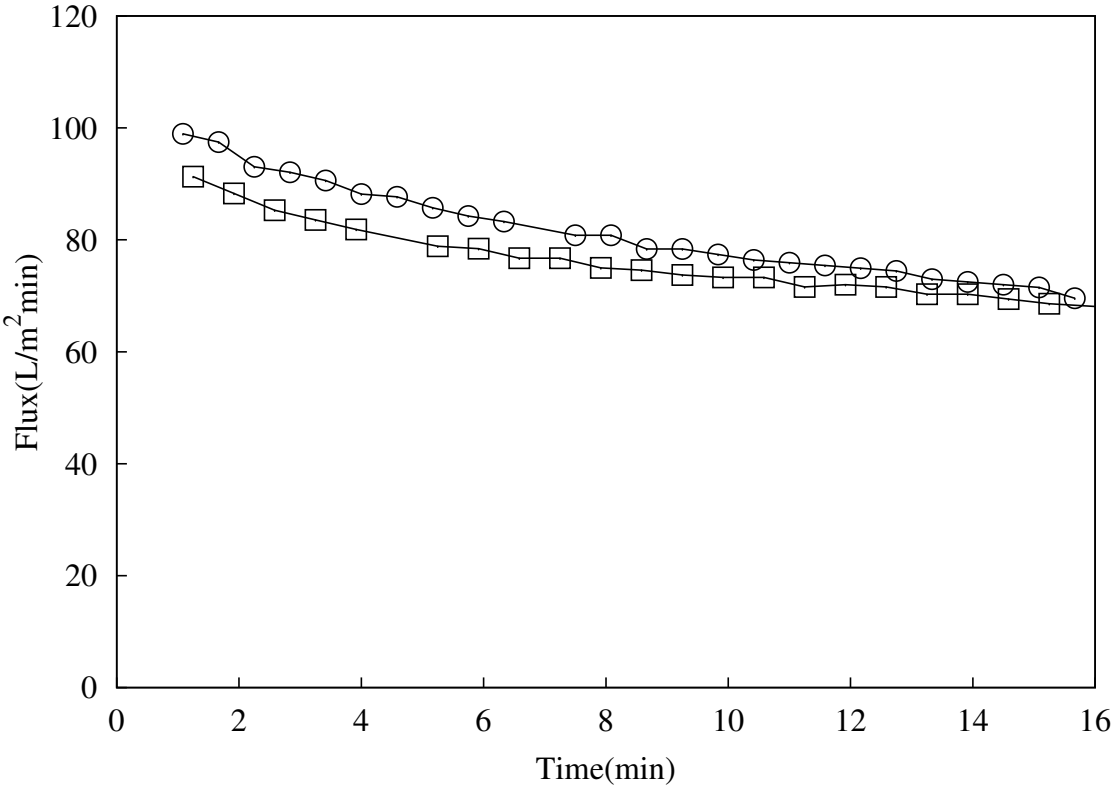


**Fig. 4.12:** Study examining the SHC sterile filter (0.2 $\mu$m) flux decline when challenged with filtrates sourced from X0HC depth filter operated at 200 LMH (□) and 50 LMH (◯). The materials used to conduction the filtration at 50 and 200 LMH at the X0HC stage was generated using the scale down methodology so as to mimic the pilot scale LAPX-404 centrifuge at Q/Σ of $2.92\times10^{-8}$ m/s. Cell culture material for this study was sourced from Culture-L (Table 4.2).

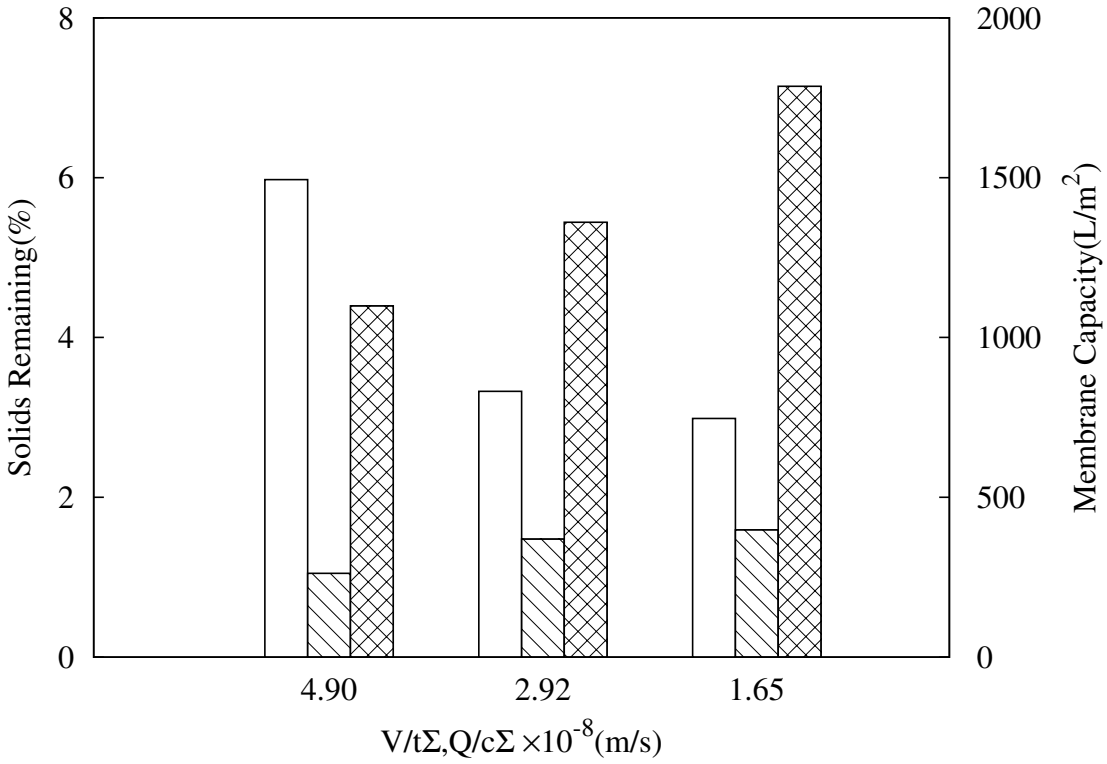


**Fig. 4.13:** Summary of a study examining the effect centrifugal operating conditions have on the harvest sequence with markers of % solids remaining examining centrifugation performance of the LAPX-404 and capacities of 0.1-2.0 $\mu$m X0HC depth filter (▧) and 0.2 $\mu$m SHC sterile filter (▩) quantifying filtration performance. Sample material to mimic a range of Q/Σ values by the pilot-scale LAPX-404 was obtained through processing culture M (Table 4.1) through CSD Version-1 and centrifuging the sheared material using a lab-scale centrifuge under the conditions described in (Table 4.2).

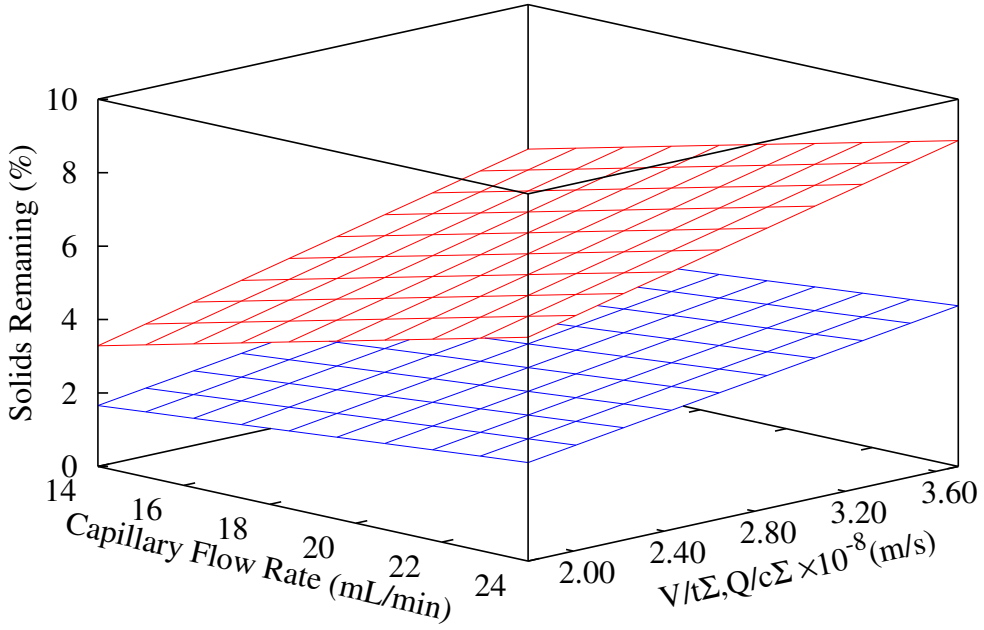


**Fig. 4.14:** Study examining the combined effect of shear damage and centrifugal separation on % solids remaining for two separate cell cultures. The cell cultures tested represented an easy (Culture-O, ⊞, Table 4.1) and difficult to harvest (Culture-N, ⊞, Table 4.1). Shear damage to cells were applied by processing either culture through CSD Version-1 at a range of flow rates and centrifugal separation at a range of $V/t\Sigma_{\text{lab}}$ was obtained through a lab-scale centrifuge.

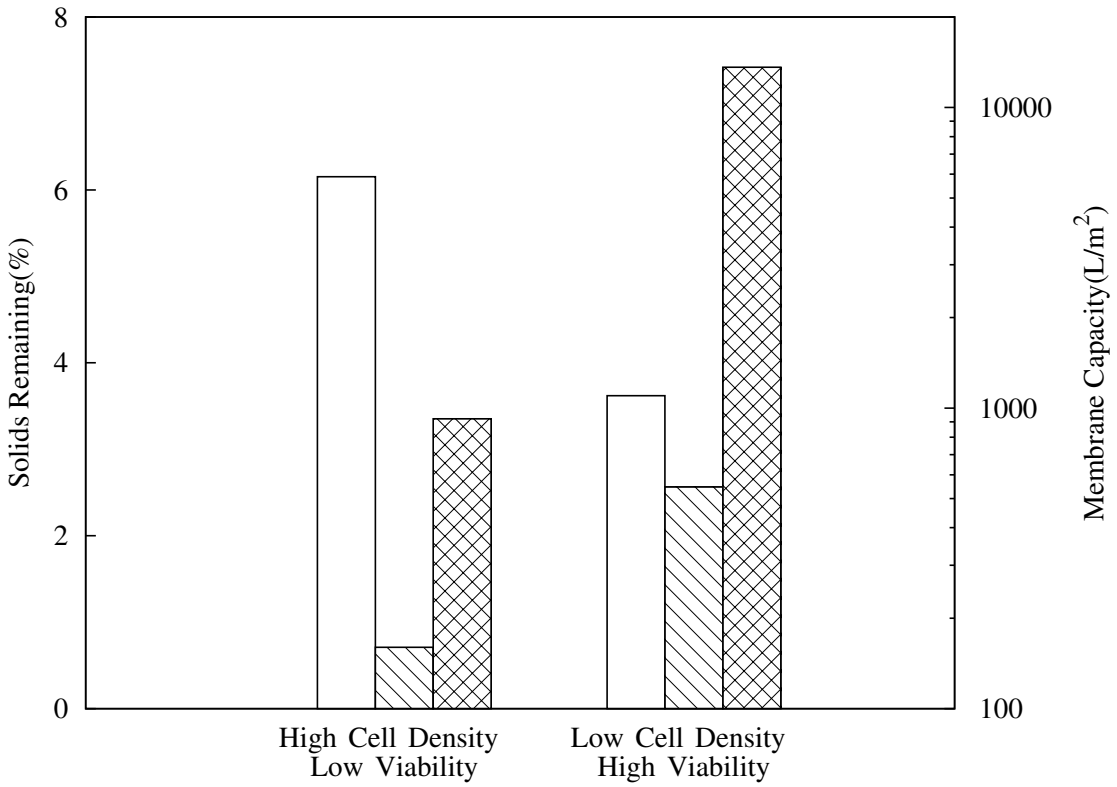


**Fig. 4.15:** Study comparing process performance at different stages of the primary recovery sequence. Feed stream was from two cell cultures representing difficult to harvest material (Culture-N) and easy to harvest material (Culture-O). The culture properties for these materials are listed in Table 4.1. (□) Post centrifugation mimicking LAPX-404 at a V/tΣ of $2.92\times10^{-8}$ m/s (Table 4.2; (▨) capacity of 0.1-2.0 $\mu$m depth filter (X0HC) at 200 LMH; (▩) capacity of 0.2 $\mu$m sterile filter (SHC) at 10 psi.

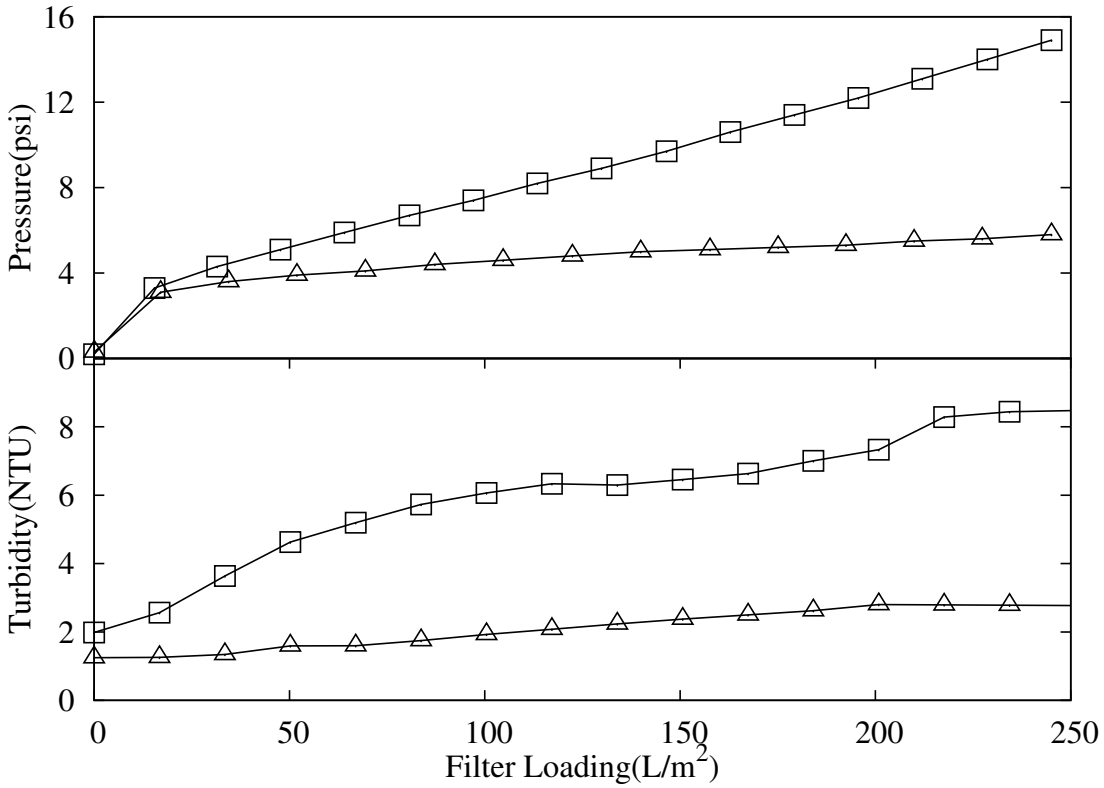


**Fig. 4.16:** Study comparing pressure and turbidity profiles generated by operating 0.1-2.0 $\mu$m depth filter (X0HC) processing samples obtained via the scale-down methodology incorporating a combination of CSD Version-1 and lab-scale centrifuge. The material used to challenge the depth filter represented difficult to harvest material (Culture-N, □, Table 4.1) and easy to harvest material (Culture-O, △, Table 4.1). The scale-down method was calibrated to mimic the centrates from LAPX-404 operated at V/t$\Sigma$ of $2.92\times10^{-8}$ m/s (Table 4.2).

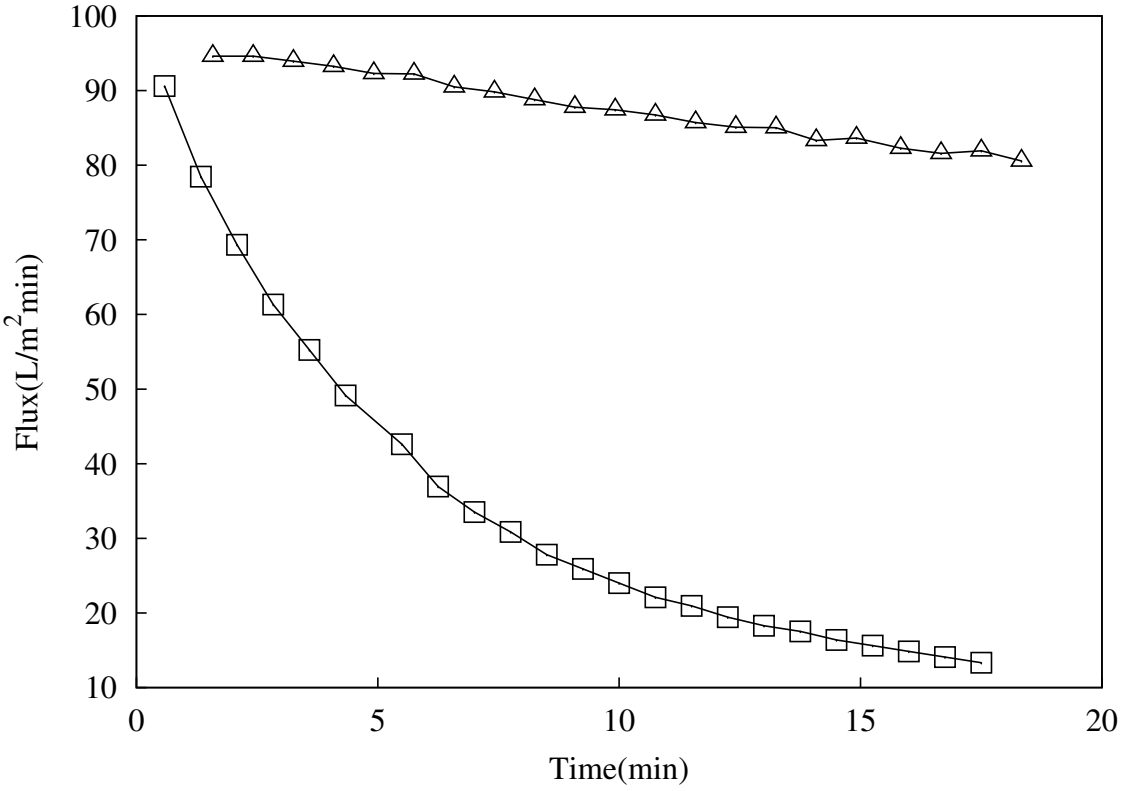


**Fig. 4.17:** Comparison of 0.2 $\mu$m sterile filter (SHC) flux decline for two cell cultures, difficult to harvest material (Culture-N, □, Table 4.1) and easy to harvest material (Culture-O, △, Table 4.1). The filtrate was generated through conditioning either cultures using the scale-down methodology incorporating CSD Version-1 to mimic the LAPX-404 at V/tΣ of $2.92\times10^{-8}$ m/s (Table 4.2) and processing the centrate through a 0.1-2.0 $\mu$m depth filter (X0HC) at 200LMH.

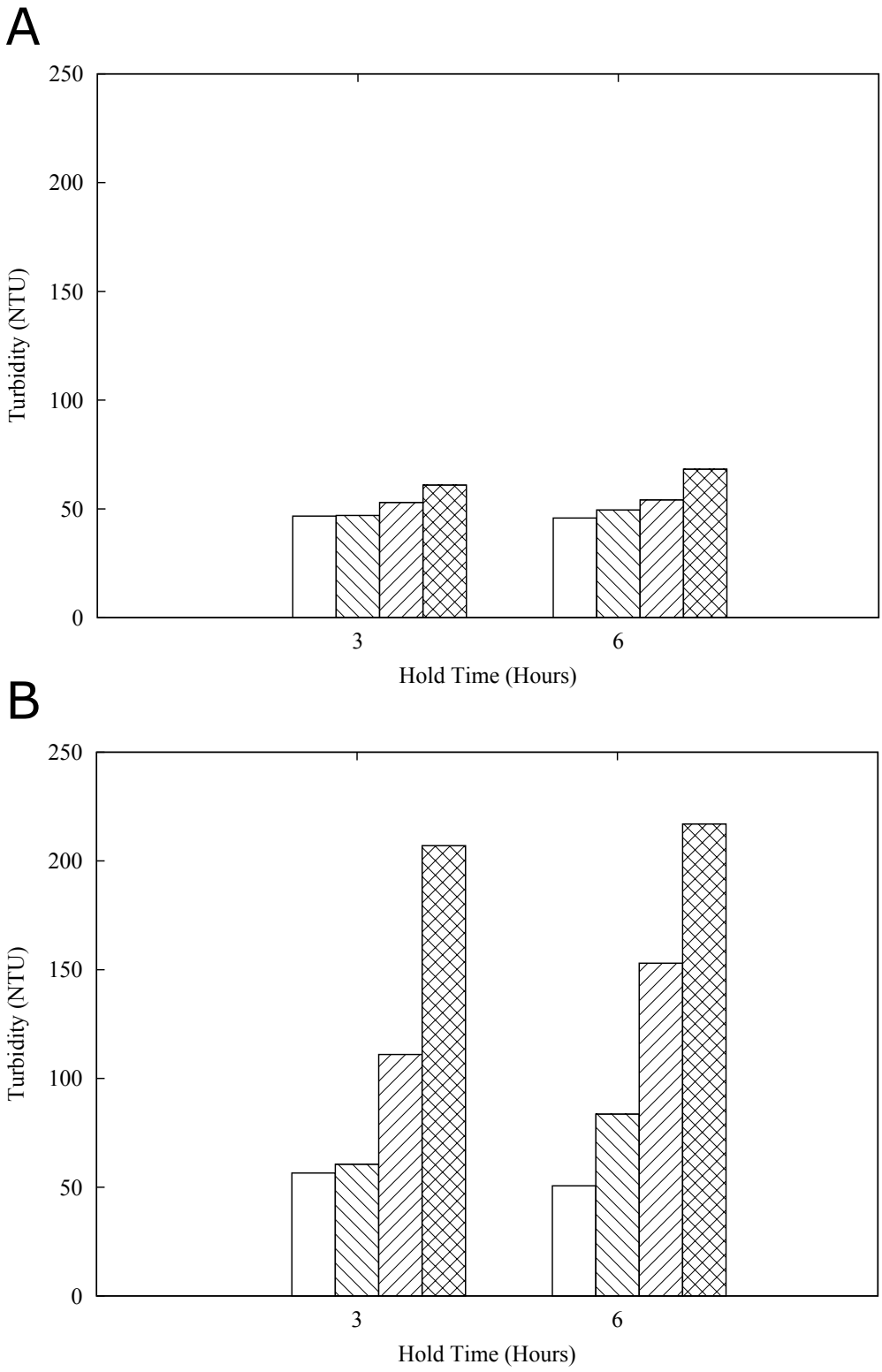


**Fig. 4.18:** Examining the effects of cell culture hold at a range of temperatures; (**A**) 5 and (**B**) $35^{o}$C , hold times; 3 & 6 Hours and EDRs; 0 (□), 1.84 (▧), 11.85 (▨) and 31.89 (▩) $\times 10^{5}$ (W/Kg)on centrate turbidity. Culture-J (Table 4.1) was used as source material and centrifuged at V/tΣ 2.41 $\times 10^{-8}$ m/s to generate the centrates for subsequent turbidity measurements.

## 4.4 Conclusion

This chapter aimed to utilise capillary shear devices (CSD) Version 1 and Version 2 with the scale-down frame work to mimic the performance of a pilot scale centrifuge. The shear within the Alfa Laval LAPX-404, BTPX-305 and Westfalia SO1 machines were all characterised using Version 1 and Version 2 of the CSD at flow rates and energy dissipation rates (EDRs) which were found to be similar to those quoted in literature. CSD Version 1 was further utilised as a tool to understand better the design space throughout the harvest step. This allowed an insight into understanding the positive influence of better centrifugal separation ($Q/\Sigma$) resulting in the improved performance of subsequent filtration steps through increased filter capacity. Other studies explored the potential of filter flux increases from 50 LMH to 200 LMH affecting depth filter capacity. Here no significant influences on XOHC filter capacity or subsequent sterile filter capacity were seen. With the impact of harvest unit operations and influence of their process parameters on overall performance of the primary recovery explored, experiments were conducted to examine the effect posed by cell culture properties. It was found that cultures with a combination of low viability and high cell densities created challenges in both centrifugation and filtration steps through poor solids clearance and increased reduction in filter capacities respectively. Additionally, it was found that high temperatures and lengthy hold times had a negative influence on centrifugation performance producing centrates with high turbidities.

The proposed scale down methodology developed in this chapter enables the user to calibrate and confirm the operating conditions of the CSD Versions 1 and 2 with a bench centrifuge that would allow for predictive capabilities of the pilot-scale centrifuge and subsequent polishing filter performance. Multiple studies demonstrated that the scale-down methodology could be utilised successfully to predict large-scale performance

by matching a range of centrate properties. This adds to the toolbox of available small scale models for high throughput characterization of mammalian cell culture processes.

Often times, at early stages of bioprocess development material availability is limited, and the pilot-scale disk stack centrifuge is not characterised at this stage. Additionally, subsequent filtration steps are also not characterised due to the lack of representative feed materials to challenge such steps. However, with the methods developed in this chapter it allows for the creation of unlimited feed material for the characterisation of subsequent filtration steps. The method described also provides a route to generate centrate representative of the disk stack centrifuge for more accurate characterisation of later polishing chromatographic steps in the process platform. Having developed a scale down method to reduce the material requirement for better understanding the process performance of the disk-stack centrifuge, Chapter 5 seeks to develop a method that will enable a reduction in the material required for material intensive filter rating studies.

# Chapter 5

# Scale-Down Depth Filtration Process Development

## 5.1 Introduction

Depth filtration is an adaptable and scalable unit operation that is typically used for the clarification of mammalian cell culture broth both pre and post-centrifugation. Estimating the optimum filter sizing of this key unit operation is however a difficult decision. Over-sizing of the filter is uneconomical and under-sizing of the filter can result in process related issues such as increased fouling in subsequent chromatographic stages thus shortening column lifetime and efficiency [Kempken *et al.*, 1995] or filter blockage resulting in loss of material. For constant flow operation the optimum filter area or capacity is defined as the cumulative volume of material filtered until a maximum pressure is reached [Yavorsky *et al.*, 2003] whereas the capacity for constant pressure is determined as the volume of material processed before a minimum flow rate is reached [Badmington, 1995]. The optimum capacity of this unit operation is difficult to estimate due to the influence of a large number of parameters, including mode of operation, type of cell line, level of aggregates, cell culture conditions and centrifuge operating conditions. Typically in

an industrial environment, depth filtration is performed in constant flow mode. Experiments are often conducted at a smaller-scale to best mimic the capacities observed at commercial-scale for each material tested. One of the problems of this approach is that although the method allows for capacity predictions at large-scale, it is time-consuming and material intensive, particularly in comparison to capacity predictions performed in constant pressure mode. However, little work has been carried out on the translation between these two modes of operation.

Significant research has been carried out on the characterisation of depth filtration through the development of fouling mechanisms to predict the observed flux decline or pressure increase in either modes of operation. The four classical fouling models outlined in the literature are referenced as complete fouling, standard fouling, cake filtration and intermediate fouling. Combination fouling models are also investigated where these fouling models incorporate two or more of the classical models in conjunction. Both types of models are described in detail in the theory section [Section 5.2] of this chapter. These have been shown to describe better the observed fouling in filters where classical models fail [Bolton *et al.*, 2006]. The type of fouling is specific to the membrane permeability and resistance due to filter type and filtrate material. To date most research on fouling has been based on constant pressure filtration [Mulder & Gimbel, 1991, Nakamura & Matsumoto, 2006, Duclos-Orsello *et al.*, 2006, Ho & Zydney, 2000, Palacio *et al.*, 2002] while relatively less work has explored fouling behaviour of operations under constant flow. Hlavacek & Bouchet [1993] explored the fouling behaviours at constant flow and demonstrated the ability of the intermediate model to fit the pressure increase of BSA solutions filtered through various different membrane types. Ho & Zydney [2002] modelled constant flow microfiltration of protein, while Chellam & Xu [2006] used fouling laws to analyze the

constant flow microfiltration of colloids.

The ability to translate across constant flow and constant pressure models would be a major step and result in significant savings of time and valuable test materials for filter sizing studies. Bolton [2006] investigated the transition between these two modes of operation through characterisation of a BSA foulant on a membrane filter. They found that the parameter coefficients of various theoretical models used to fit the flux decline during constant pressure operation could be used within the constant flow model to predict the observed pressure increase. However, the drawback of this method is that either the initial pressure drop for constant flow operation or the initial flux decline for constant pressure operation is required to calculate predictions in the different modes of operation.

This chapter provides a methodology to predict accurately the capacity of two unique dead end filters (D0HC & X0HC) operated under constant flow utilising constant-pressure flux decline data. The flux decline of a wide range of industrially relevant centrates was characterised under constant pressure operation by evaluating the fit of various theoretical fouling models. Constant flow experiments were conducted on the same material and the capacity measured. A correlation between the fouling coefficients calculated for constant pressure operation and the observed capacity at the same equivalent pressure was developed. The correlation related the observed fouling at constant pressure to that of constant flow operation. The model was subsequently validated through additional experiments performed at constant pressure and constant flow demonstrating accurate prediction of capacity. The approach enabled future prediction of constant flow capacities of materials with a wide range of fouling propensities using a minimum amount of material. This method may be highly beneficial at an early stage of development, a point at which material for process studies are often in short supply.

## 5.2 Theoretical Considerations

When operating filters in constant pressure mode the rate of filter fouling can be described by the generalised form of Darcy's Law:

$$J_v = \frac{1}{A}\frac{dV}{dt} = \frac{R_{filter}\Delta P}{\mu} \tag{5.1}$$

where $J_v$ is the permeate flux defined by the flow rate per unit area of $A$ with $V$ and $t$ represents volume and time respectively. The pressure drop across the filter, $\Delta P$, depends on the viscosity of the material, $\mu$, and the specific filter resistance, $R_{filter}$.

Both the viscosity and equivalent filter resistance are specific to the filtered material and the filter utilised. This can result in a large range of flux declines for constant pressure operation and highly varied pressure profiles for constant flow operation.

The primary fouling models used to define the various observed fouling of depth filters for constant pressure are defined by Bowen *et al.* [1995] as complete fouling, intermediate fouling, standard fouling and cake filtration. Complete fouling occurs when each particle arriving at the filter participates in fouling the pores of the membrane and is defined as:

$$\text{Complete fouling model} \quad J_v(t) = J_v(0)e^{-K_{Com}J_v(0)t} \tag{5.2}$$

Where $K_{Com}$ is the fouling coefficient for the Complete fouling model. Cake filtration occurs when the particles form a resistant layer on top of the filter, this cake layer formation increases as new particles arrive at the filter and is defined as:

$$\text{Cake filtration model} \quad J_v(t) = \frac{J_v(0)}{\sqrt{1 + K_C J_v(0)t}} \tag{5.3}$$

Where $K_C$ is the fouling coefficient for the Cake fouling model. Intermediate fouling assumes that some particles arriving at the filter will directly block a portion of the available area while other particles will only participate in partial blockage of the pores and is defined as:

$$\text{Intermediate fouling model} \quad J_v(t) = \frac{J_v(0)}{1 + K_I J_v(0)\, t} \tag{5.4}$$

Where $K_I$ is the fouling coefficient for the Intermediate fouling model. Standard fouling assumes that particles deposit onto the internal walls of the pores, as further particles arrive the internal diameter of the pore wall is further constricted and over time will result in the complete blockage of the pore and the this mechanism is defined as:

$$\text{Standard fouling model} \quad J_v(t) = \frac{J_v(0)}{(1 + K_S J_v(0)\, t)^2} \tag{5.5}$$

Where $K_S$ is the fouling coefficient for the Standard fouling model. In addition to the four classic models, additional fouling models have been generated including an adsorptive fouling model that assumes particle deposition on the filter follows zeroth-order kinetics and is defined by Bolton [2006] as:

$$\text{Adsorptive fouling model} \quad J_v(t) = J_v(0)(1 - K_A J_v(0)\, t)^4 \tag{5.6}$$

Where $K_A$ is the fouling coefficient for the Adsorption fouling model. One of the major problems with fitting a single fouling model is the assumption of a single fouling mechanism in action when in reality membrane fouling is often far more complicated and is usually better characterised using a combination of models [Bolton *et al.*, 2006; Sampath

*et al.*, 2014]. Examples of two different combined models are:

$$\begin{aligned} \text{Intermediate-Cake fouling model} &= \frac{J_v(0)}{(1+K_I J_v(0)\,t)(\sqrt{1+K_C J_v(0)\,t})} \\ \text{Standard-Adsorption fouling model} &= \frac{J_v(0)}{(1+K_S J_v(0)\,t)^2((1+K_A J_v(0)\,t)^4)} \end{aligned} \tag{5.7}$$

The above fouling models are defined for constant pressure mode and model the flux decline as a function of time. For constant flow operation, the inverse of the above mentioned fouling models applies. The requirement becomes the need to model the increase in pressure as a function of time by replacing $J_v(0)$ with $P_0$ as the initial pressure during constant flow mode.

## 5.3 Materials and Methods

### 5.3.1 Cell Culture

The cell culture material utilised in these experiment was generated using CHO cell lines expressing a range of mAb products. The cultures were produced in bench (3 and 5 L) and pilot scale (500 L) bioreactors and harvested during the decline phase of growth (days 11-14). The harvested broths had a range of cell culture properties summarised in Table 5.1.

### 5.3.2 Pilot-scale Centrifugation

The centrates were generated by processing cell culture broths [Table 5.1] though a Westfalia SO1 disk-stack centrifuge at a range Q/Σ where the bowl speed was maintained at 10,000 RPM and flow rates were varied between 0.3-0.9 L/min. Details of centrate properties and centrifugal operating conditions can be found in Table 5.2.

**Table 5.1:** Summary of cell culture properties of material used for constant flow and constant pressure experiments.

| Product | Material ID | Bio Reactor Size (L) | Cell Density $\times 10^6$(cells/mL) | Cell Viability (%) |
|---|---|---|---|---|
| Culture-U | Centrate-1 | 500 | 25 | 68 |
| Culture-V | Centrate-2 | 5 | 20 | 75 |
| Culture-V | Centrate-3 | 5 | 20 | 75 |
| Culture-V | Centrate-4 | 5 | 20 | 75 |
| Culture-W | Centrate-5 | 500 | 24 | 90 |
| Culture-W | Centrate-6 | 500 | 24 | 90 |
| Culture-AA | | 3 | 26 | 39 |
| Culture-AB | | 3 | 30 | 39 |
| Culture-AC | | 3 | 31 | 49 |
| Culture-AD | | 3 | 11 | 25 |
| Culture-AE | | 3 | 11 | 88 |
| Culture-AF | | 3 | 11 | 19 |
| Culture-AG | | 3 | 13 | 89 |
| Culture-AH | | 3 | 17 | 44 |
| Culture-AI | | 3 | 9 | 53 |
| Culture-AJ | | 3 | 10 | 60 |
| Culture-AK | | 3 | 15 | 47 |
| Culture-AL | | 3 | 12 | 46 |

### 5.3.3 Filtration

Constant pressure and constant flow filtration experiments were both conducted using 23 $cm^2$ Millistack X0HC and D0HC depth filter capsules (EMD Millipore, Massachusetts, USA) with a nominal pore size ranging from 0.5-0.1 and 5-0.2 $\mu$m respectively. Figure 5.4 shows the experimental setup to conduct filtration under constant flow mode. The X0HC filter was first wetted with RO water at 200 LMH for 20 minutes and subsequently aired for 10 minutes to remove any residual water. The centrate was well mixed using a magnetic flea and pumped through the aired filter at 100 LMH with pressure recorded for the duration of the experiment. The D0HC depth filter was wetted under the same conditions to that of the X0HC filter. However, the material challenging the D0HC filter

**Table 5.2:** Summary of the centrifugal operational settings for processing of cell cultures (Table 5.1) and the resultant centrate turbidity.

| Material ID | Centrifuge Flow Rate (L/min) | Turbidity (NTU) |
|---|---|---|
| Centrate-1 | 0.3 | 234 |
| Centrate-2 | 0.3 | 215 |
| Centrate-3 | 0.6 | 331 |
| Centrate-4 | 0.9 | 560 |
| Centrate-5 | 0.3 | 102 |
| Centrate-6 | 0.9 | 106 |

was processed at 30 LMH.

Identical materials were used to challenge X0HC and D0HC filters filter in both constant pressure and constant flow approaches. A range of pressures [Table 5.3] were tested. Figure 5.4 shows the experimental schematic where centrate was sealed inside a feed vessel and pressurised to the set pressure using compressed air. Throughout the filtration studies collected volume was recorded with time. The same experimental methodology to that of the X0HC constant pressure approach was utilised for operations using the 3.5 $cm^2$ Millipore SHC sterile filters (EMD Millipore, Massachusetts, USA). The pressure was set at 10 psi for all SHC experiments.

## 5.4 Results

### 5.4.1 Resource Requirements for Constant Pressure and Flow Studies

It is common practice in industry when sizing depth filters at constant flow to measure capacity at a pressure drop of 20 psi. These studies often are time consuming and material intensive. Whilst depth filter sizing at constant pressure is not common place, this mode

**Table 5.3:** Centrate turbidity and experimental conditions for constant flow and constant pressure studies.

| Material ID | Constant Pressure Operating Conditions (psi) | Constant Flow Operating Conditions (LMH) |
|---|---|---|
| Centrate-1 | 10,15,20,25 | 100 |
| Centrate-2 | 15,20,25 | 100 |
| Centrate-3 | 10,15,20,25 | 100 |
| Centrate-4 | 15,20,25 | 100 |
| Centrate-5 | 10,15 | 100 |
| Centrate-6 | 10,15,20 | 100 |
| Culture-AA | 15 | 30 |
| Culture-AB | 10,15 | 30 |
| Culture-AC | 10 | 30 |
| Culture-AD | 5 | 30 |
| Culture-AE | 5 | 30 |
| Culture-AF | 10 | 30 |
| Culture-AG | 10 | 30 |
| Culture-AH | 5 | 30 |
| Culture-AI | 5 | 30 |
| Culture-AJ | 10 | 30 |
| Culture-AK | 10 | 30 |
| Culture-AL | 10 | 30 |

of operation has the advantage of processing samples faster than when operating under constant flow. This saving of experimental time is highlighted in Figure 5.1A where a range of process materials (≈ 100mL) were challenged under both modes of operation. Figure 5.1A suggests for the range of process materials tested [Table 5.1] there was on average a 80% reduction in the experimental time required for those lab-scale depth filter studies operated at constant pressure mode compared to those operated at constant flow mode [Figure 5.4]. In addition to the time savings, constant pressure operations also reduce process material requirements for studies. Figure 5.1B suggests there is on a average a 70% reduction in the process material requirement, this is an advantage at an early stage

of bioprocess development when material availability is scarce.

### 5.4.2 Depth Filters Fouling at Constant Pressure and Flow Mode

This study utilised multiple cell cultures broths that were processed at a variety of centrifuge operating conditions provided a ranging centrates with characteristics as typical to those of a multi-product mammalian cell culture facility. The characteristics of all centrates displayed in Tables 5.1 and 5.2 were defined in terms of their respective cell densities, cell viabilities and turbidities. With such a varied range of turbidities characterising each centrate, they were each expected to foul in a distinct manner and hence generate a broad range of experimental capacities [Figure 5.2]. Similar to the constant flow experiments [Figure 5.2A] when identical centrates were passed through a depth filter at constant pressure each centrate exhibited highly unique flux decline [Figure 5.2B] for each centrate. This was most likely due to the differing rates of membrane fouling which was specific to each material. The specific nature of fouling observed at constant pressure and the corresponding capacities achieved at constant flow was the basis to develop a correlation between both modes of operations. The following section describes in detail the strategy used to develop such a correlation for both X0HC and D0HC depth filters.

### 5.4.3 X0HC Flux Decline

This study produced distinct flux declines corresponding to the six identical centrates were passed through the X0HC depth filter at constant pressure. The unique flux profiles for each centrate are shown in Figure 5.2B highlighting the differing rates of membrane fouling specific to each material. Characterising the fouling mechanisms observed during both modes of operation is routinely achieved through the application of various mathematical models as summarised in the earlier section of theoretical considerations. In

this work the observed fouling during constant pressure operation of centrates 1-6 was characterised using classical (intermediate, cake, standard, complete, adsorption) and combined models (cake-adsorption, cake-intermediate, complete-standard, intermediate-standard, complete-adsorption, cake-complete, intermediate-complete, cake-standard and standard-adsorption). A global optimisation function was utilised to generate the optimum coefficients that minimised the error between the experimental and theoretical flux declines. The goodness of fit was quantified using the coefficient of determination ($R^2_{fit}$) and is summarised in Table 5.4. Of the classical models tested the cake and adsorption fouling models were the most representative and were found to model accurately the majority of the different flux profiles. Similarly for the combined models; cake-adsorption, cake-intermediate, cake-complete and cake-standard were shown to model accurately the observed fouling of each centrate at the different pressures investigated. Table 5.4 highlights the challenge with fitting theoretical models to a wide range of centrates and the inability of some of the classical models to capture the observed complex fouling mechanisms. The complexity of the fouling involved here was highlighted by some cases where it was not possible accurately to describe the flux decline by a single fouling mechanism but required a combination of two fouling mechanisms. In the study when characterising the fouling of the X0HC filter the cake-adsorption model for example was the only model able to capture the abnormal fouling profile observed for centrate-2 at 10 and 15 psi [Table 5.4]. This is consistent with the work conducted by Sampath *et al.* [2014] who investigated various combined models in addition to the four classic models and concluded that none of the models could consistently fit the various flux declines generated from *Pichia pastoris* fermentations.

**Table 5.4:** Summary of the classical and mixed fouling model fits ($R^2$) for centrates 1-6 (Table 5.2) at the range of pressures tested (Table 5.3).

| CP Pressure | Inter | Cake | Stan | Comp | Adsorp | Cake-Adsorp | Cake-Inter | Comp-Stan | Inter-Stan | Inter-Adsorp | Comp-Adsorp | Cake-Comp | Inter-Comp | Cake-Stan | Stan-Adsorp |
|---|---|---|---|---|---|---|---|---|---|---|---|---|---|---|---|
| **Centrate-1** | | | | | | | | | | | | | | | |
| 10 psi | 0.98 | 0.96 | 0.95 | 0.87 | 0.79 | 0.96 | 0.99 | 0.95 | 0.98 | 0.98 | 0.87 | 0.99 | 0.98 | 0.99 | 0.95 |
| 15 psi | 0.99 | 0.97 | 0.98 | 0.94 | 0.9 | 0.97 | 0.99 | 0.98 | 0.99 | 0.99 | 0.93 | 1 | 0.99 | 0.99 | 0.98 |
| 20 psi | 1 | 0.97 | 0.99 | 0.95 | 0.91 | 0.97 | 1 | 0.99 | 1 | 1 | 0.84 | 1 | 1 | 1 | 0.99 |
| 25 psi | 1 | 0.97 | 0.99 | 0.96 | 0.92 | 0.97 | 1 | 0.99 | 1 | 1 | 0.96 | 1 | 1 | 1 | 0.99 |
| Mean | 0.99 | 0.96 | 0.98 | 0.93 | 0.88 | 0.96 | 0.99 | 0.98 | 0.99 | 0.99 | 0.9 | 1 | 0.99 | 0.99 | 0.98 |
| **Centrate-2** | | | | | | | | | | | | | | | |
| 10 psi | 0.05 | 0.5 | 0 | 0 | 0 | 0.89 | 0.5 | 0 | 0.05 | 0.05 | 0 | 0.5 | 0.05 | 0.5 | 0 |
| 15 psi | 0.05 | 0.48 | 0 | 0 | 0 | 0.92 | 0.48 | 0 | 0.05 | 0.05 | 0 | 0.48 | 0.05 | 0.48 | 0 |
| 20 psi | 0.69 | 0.87 | 0.54 | 0.35 | 0.23 | 0.96 | 0.87 | 0.54 | 0.69 | 0.69 | 0.23 | 0.87 | 0.69 | 0.87 | 0.54 |
| 25 psi | 0.82 | 0.86 | 0.78 | 0.73 | 0.7 | 0.87 | 0.86 | 0.78 | 0.82 | 0.82 | 0.73 | 0.86 | 0.82 | 0.86 | 0.78 |
| Mean | 0.4 | 0.68 | 0.33 | 0.27 | 0.23 | 0.91 | 0.68 | 0.33 | 0.4 | 0.4 | 0.24 | 0.68 | 0.4 | 0.68 | 0.33 |
| **Centrate-3** | | | | | | | | | | | | | | | |
| 10 psi | 0.59 | 0.78 | 0.44 | 0.23 | 0.11 | 0.78 | 0.78 | 0.44 | 0.59 | 0.59 | 0.03 | 0.78 | 0.59 | 0.78 | 0.44 |
| 15 psi | 0.89 | 0.97 | 0.83 | 0.73 | 0.67 | 1 | 0.97 | 0.83 | 0.89 | 0.89 | 0.71 | 0.97 | 0.89 | 0.97 | 0.83 |
| 20 psi | 0.96 | 0.99 | 0.94 | 0.91 | 0.89 | 0.99 | 0.99 | 0.94 | 0.96 | 0.96 | 0.91 | 0.99 | 0.96 | 0.99 | 0.94 |
| 25 psi | 0.86 | 0.92 | 0.81 | 0.76 | 0.74 | 0.97 | 0.92 | 0.81 | 0.86 | 0.86 | 0.76 | 0.92 | 0.86 | 0.92 | 0.81 |
| Mean | 0.83 | 0.91 | 0.75 | 0.66 | 0.6 | 0.93 | 0.91 | 0.75 | 0.83 | 0.82 | 0.6 | 0.91 | 0.83 | 0.91 | 0.75 |
| **Centrate-4** | | | | | | | | | | | | | | | |
| 10 psi | 0.99 | 0.92 | 0.97 | 0.86 | 0.76 | 0.92 | 0.99 | 0.97 | 0.99 | 0.99 | 0.86 | 0.99 | 0.99 | 0.99 | 0.97 |
| 15 psi | 1 | 0.96 | 0.98 | 0.9 | 0.82 | 0.96 | 1 | 0.98 | 1 | 1 | 0.9 | 1 | 1 | 1 | 0.98 |
| 20 psi | 0.99 | 0.97 | 0.95 | 0.82 | 0.7 | 0.97 | 1 | 0.95 | 0.99 | 0.99 | 0.79 | 1 | 0.99 | 1 | 0.95 |
| 25 psi | 1 | 0.97 | 0.96 | 0.85 | 0.75 | 0.97 | 1 | 0.96 | 1 | 1 | 0.83 | 1 | 1 | 1 | 0.96 |
| Mean | 0.99 | 0.96 | 0.96 | 0.86 | 0.76 | 0.96 | 1 | 0.96 | 0.99 | 0.99 | 0.84 | 1 | 0.99 | 1 | 0.96 |
| **Centrate-5** | | | | | | | | | | | | | | | |
| 10 psi | 0.38 | 0.53 | 0.27 | 0.14 | 0.07 | 0.66 | 0.53 | 0.27 | 0.38 | 0.37 | 0.14 | 0.53 | 0.38 | 0.53 | 0.27 |
| 15 psi | 0.6 | 0.74 | 0.5 | 0.4 | 0.34 | 0.97 | 0.74 | 0.5 | 0.6 | 0.6 | 0.4 | 0.74 | 0.6 | 0.74 | 0.5 |
| Mean | 0.49 | 0.63 | 0.39 | 0.27 | 0.2 | 0.81 | 0.63 | 0.39 | 0.49 | 0.48 | 0.27 | 0.63 | 0.49 | 0.63 | 0.39 |
| **Centrate-6** | | | | | | | | | | | | | | | |
| 10 psi | 0.96 | 0.92 | 0.98 | 0.98 | 0.97 | 0.92 | 0.97 | 0.98 | 0.98 | 0.97 | 0.97 | 0.98 | 0.98 | 0.98 | 0.98 |
| 15 psi | 0.95 | 0.99 | 0.93 | 0.88 | 0.86 | 0.99 | 0.99 | 0.93 | 0.95 | 0.95 | 0.88 | 0.99 | 0.95 | 0.99 | 0.93 |
| 20 psi | 0.96 | 0.98 | 0.95 | 0.93 | 0.92 | 0.98 | 0.98 | 0.95 | 0.96 | 0.96 | 0.93 | 0.98 | 0.96 | 0.98 | 0.95 |
| Mean | 0.96 | 0.96 | 0.95 | 0.93 | 0.92 | 0.96 | 0.98 | 0.95 | 0.96 | 0.96 | 0.93 | 0.98 | 0.96 | 0.98 | 0.95 |
| **Overall mean** | 0.78 | 0.85 | 0.73 | 0.65 | 0.6 | 0.93 | 0.87 | 0.73 | 0.78 | 0.78 | 0.63 | 0.87 | 0.78 | 0.87 | 0.73 |

### 5.4.4 X0HC Model Development

The coefficients generated by each model in Table 5.4 were subsequently correlated with the corresponding capacity achieved during constant flow at the specific pressures performed during constant pressure operation. A pictographic illustration of the strategy utilised is shown in Figure 5.4. For the classical models, containing a single coefficient, a simple exponential relationship generated the strongest correlation between the constant flow capacities. This type of relationship was selected across all of the classical models based on minimising the coefficient of determination ($R^2_{Cal}$) of the calibration data sets (Centrates 1-5). For the combined models, containing two coefficients, a quadratic linear regression model that considered the interaction between the two terms was assumed and a stepwise regression approach which implemented both forward addition and backward elimination was used to generate the final model. The selection criteria for the finalised combined model was the same as for the classical models. In addition to determining the $R^2_{Cal}$, K-Fold cross verification ($R^2_{Cross}$) was implemented to assess the ability of the models to make predictions for an independent data set. A summary of the finalised models are given in Table 5.6. Of the classical models the cake model resulted in the highest $R^2_{Cal}$ calibration and $R^2_{Cross}$ for cross verification. However, the best overall model was found to be the cake-adsorption model with an average $R^2$ equal to 0.93. This model was shown previously as the model to fit best the wide range of flux profiles generated by each centrate. This fouling mechanism indicated that some of the foulant initially deposited on to the filter with a gradual build up of a cake layer that increases the resistance to flow. Table 5.6 demonstrates that the cake-adsorption model was the most robust model and resulted in the best predictions. The exponential and polynomial relationship generated by the cake and cake-adsorption model are shown in Table 5.5.

**Table 5.5:** Summary of cake and cake-adsorption model structure and coefficients for fitting constant pressure data to constant flow capacities

| Model | Mode Structure | Definition |
|---|---|---|
| Cake | $\mathrm{CF}_{cap_i} = ae^{bK_{C,i}}$ (5.8) | $CF_{cap_i}$ : predicted capacity at pressure (i)<br>$K_C$ : Cake coefficient at pressure (i)<br>$a$ : Exponential coefficient = 425.0<br>$b$ : Exponential coefficient= -7.19×$10^5$ |
| Cake-Adsorption | $\mathrm{CF}_{cap_i} = \alpha_0 + \alpha_1 K_{C_i} + \alpha_2 K_{A_i} + \alpha_3 K_{C_i}^2$ (5.9) | $K_{C_i}$ : Cake coefficient at pressure (i)<br>$K_{A_i}$ : Adsorption coefficient at pressure (i)<br>$\alpha_0$ = 296, $\alpha_1$ = -1.12×$10^8$, $\alpha_2$ = 6.12×$10^9$<br>$\alpha_3$ = 9.91×$10^{12}$ |

**Table 5.6:** Fouling model type and $R^2$ value for both classical and mixed models. The $R^2$ value was calculated based on the model predictions using the coefficients determined at each pressure and the corresponding experimental capacities. In the model structure, $K_I$, $K_C$ $K_S$, $K_{Com}$ and $K_A$ represent the model coefficients of the intermediate, cake, standard, complete and adsorption models respectively and a and $b$ are the model coefficients related to the exponential function. In the combined models, $\alpha_0$ is the intercept term and $\alpha_{1,2,3,4}$ represent the parameter coefficients of the regression model.

| Model | Model structure | $R^2_{Fit}$ | $R^2_{Cal}$ | $R^2_{Cross}$ | Average |
|---|---|---|---|---|---|
| Intermediate | $ae^bK_I$ | 0.75 | 0.81 | 0.78 | 0.78 |
| Cake | $ae^bK_C$ | 0.81 | 0.83 | 0.82 | 0.82 |
| Standard | $ae^bK_S$ | 0.70 | 0.78 | 0.74 | 0.74 |
| Complete | $ae^bK_{Com}$ | 0.64 | 0.74 | 0.69 | 0.69 |
| Adsorp | $ae^bK_A$ | 0.59 | 0.59 | 0.59 | 0.59 |
| Cake-Adsorption | $CF_{cap_i} = \alpha_0 + \alpha_1 K_{C_i} + \alpha_2 K_{A_i} + \alpha_3 K_{C_i}^2$ | 0.93 | 0.86 | 0.89 | 0.89 |
| Cake-Intermediate | $\alpha_0 + \alpha_1 K_C + \alpha_2 K_I + \alpha_3 K_I^2$ | 0.82 | 0.76 | 0.79 | 0.79 |
| Comp-Standard | $\alpha_0 + \alpha_1 K_S + \alpha_2 K_S^2$ | 0.70 | 0.74 | 0.72 | 0.72 |
| Intermediate -Standard | $\alpha_0 + \alpha_1 K_I + \alpha_2 K_I^2$ | 0.75 | 0.77 | 0.76 | 0.76 |
| Intermediate-Adsorption | $\alpha_0 + \alpha_1 K_I + \alpha_2 K_I^2$ | 0.72 | 0.78 | 0.75 | 0.75 |
| Complete-Adsorption | $\alpha_0 + \alpha_1 K_{Com} + \alpha_2 K_A + \alpha_3 K_{Com}^2 + \alpha_4 K_{Com} K_A$ | 0.45 | 0.41 | 0.43 | 0.43 |
| Cake-Complete | $\alpha_0 + \alpha_1 K_C + \alpha_2 K_{Com} + \alpha_3 K_C K_{Com}$ | 0.82 | 0.81 | 0.81 | 0.81 |
| Intermediate-Complete | $\alpha_0 + \alpha_1 K_I + \alpha_2 K_I^2$ | 0.75 | 0.77 | 0.76 | 0.76 |
| Cake-Standard | $\alpha_0 + \alpha_1 K_C + \alpha_2 K_S + \alpha_3 K_C K_S + \alpha_4 K_C K_S$ | 0.82 | 0.78 | 0.80 | 0.80 |
| Standard-Adsorption | $\alpha_0 + \alpha_1 K_S + \alpha_2 K_S^2$ | 0.70 | 0.74 | 0.72 | 0.72 |

### 5.4.5 X0HC Model Verification

To validate the developed correlations, constant flow capacity of an independent material not included in the model calibration data set was utilised as source material to provide an external verification set. The predictions were calculated during constant pressure operation utilizing the coefficients from cake ($K_C$) and cake-adsorption ($K_C$ and $K_A$) fouling models [Table 5.5] to identify the capacity at constant flow operation and to identify the capacity under constant flow operation. A summary outlining this methodology is shown in Figure 5.4. The predictions of a subset of these models is shown in Figure 5.6. These models provide an accurate prediction of the capacities for centrate-6 at 10, 15 and 20 psi. Figure 5.6 illustrates a good level of agreement (± 14 %, n=3) between the predicted capacities and the experimental recorded capacities for Centrate 6 and as a result validates the relation developed in Table 5.5.

In addition to quantifying depth filter capacity it is important when creating an alternative method for filter rating that the properties of the filtrates produced by either method of operation (either constant flow or constant pressure) be comparable. To test the ability of each method to create essentially identical filtrates, the product of the constant flow and constant pressure modes of operation were taken forward for SHC sterile filter studies. Figure 5.5A suggests both modes of filtration produced filtrates with similar turbidities post X0HC and subsequent SHC filtration steps. Furthermore, Figure 5.5B shows that identical flux decline profiles were generated when operating the SHC sterile filter using material from X0HC filtrates operated at constant pressure and constant flow conditions. The data obtained from Centrate-6 validated the correlation developed and suggested that the developed methodology based on constant pressure operation could be utilised to characterize subsequent sterile filtration operations. However, this is unlikely to be

universal and must be applied in a case by case basis as other centrates may not have fouling properties akin to those of Centrate-6.

### 5.4.6 D0HC Capacity Prediction Stratergy

D0HC depth filters are typically employed as primary filters post fermentation and require characterization in a similar vein to that of the X0HC filter. This study describes a strategy to generate a predictive model of D0HC filter capacity at constant flow. A similar strategy to that employed with the model development for the X0HC filter was used for capacity prediction at constant flow for the D0HC. Firstly the fouling fits for all the classical fouling models were tested to identify the model with the best fit during operation at constant pressure. Equations 5.10 - 5.13 are linearized forms of the complete, cake, intermediate and standard fouling models. The linearity of these equations were tested for a range of materials [Culture AA-AI, Table 5.1] so as to identify the model with the best fit. Summary of all fits can be found in Table 5.7. The standard model provided the best fit with an average of $R^2$ value of 0.99 [Table 5.7]. Primary depth filters akin to the D0HC are made of a matrix that is tortuous. This allows for sieving of a wide variety of particulate sizes. Hence it enables, in the case of the materials tested, cells and cell debris to fill these tortuous pores. This may lead fouling to occur under the standard mechanism. This could explain the high level of fit of the standard fouling model when processing cell culture material through the D0HC depth filter. With the best fit studies conducted the second part of the strategy involves the correlation of the fouling coefficient from the aforementioned study with capacities obtained at constant flow. The following sections of this chapter describe this part in further detail.

$$\text{Complete Fouling} \Rightarrow \frac{dV}{dt} = K_{Com} V \tag{5.10}$$

**Table 5.7:** Summary of $R^2$ when fitting all classical models (Equations 5.10 - 5.13) for a range of cell culture materials (Table 5.1) when D0HC filter was operated at constant pressure.

| Culture-ID | Intermediate $R^2$ | Standard $R^2$ | Cake $R^2$ | Complete $R^2$ |
|---|---|---|---|---|
| Culture-AA | 0.85 | 0.99 | 0.59 | 0.81 |
| Culture-AB | 0.73 | 0.99 | 0.59 | 0.52 |
| Culture-AC | 0.87 | 0.99 | 0.62 | 0.78 |
| Culture-AD | 0.99 | 0.99 | 0.99 | 0.99 |
| Culture-AE | 0.98 | 0.99 | 0.95 | 0.85 |
| Culture-AF | 0.91 | 0.99 | 0.98 | 0.94 |
| Culture-AG | 0.97 | 0.99 | 0.92 | 0.98 |
| Culture-AH | 0.72 | 0.99 | 0.76 | 0.82 |
| Culture-AI | 0.98 | 0.99 | 0.94 | 0.98 |
| Culture-AJ | 0.96 | 0.99 | 0.89 | 0.97 |

$$\text{Cake Fouling} \Rightarrow \frac{t}{V} = K_C V \tag{5.11}$$

$$\text{Intermediate Fouling} \Rightarrow \frac{dt}{dV} = K_I V \tag{5.12}$$

$$\text{Standard Fouling} \Rightarrow \frac{t}{V} = K_S t \tag{5.13}$$

### 5.4.7 D0HC Correlation Development

Fouling coefficients ($K_{Com}$, $K_C$, $K_I$ and $K_S$) were quantified using Equations 5.10 - 5.13. The coefficients were utilized to develop a correlation against the capacities obtained during constant flow when a given pressure was reached. Table 5.7 shows a summary of the fits when developing correlations based on a classical model′s fouling coefficients and the equation structures used to obtain such a correlation. A linear correlation based around the standard fouling mechanism′s coefficient ($K_S$) provided the best calibration fit at an $R^2$ of 0.92 [Table 5.8]. The fouling mechanisms showed that the logarithmic

**Table 5.8:** Summary of fouling fit ($R^2_{Fit}$) using all classical fouling models and calibration fit ($R^2_{Cal}$) between constant pressure fouling constant and constant flow capacity where $g$ is the coefficient for linear and logarithmic model structures and $h$ is the intercept.

| Model | Model Structure | $R^2_{Fit}$ | $R^2_{Cal}$ | $R^2_{Ave}$ |
|---|---|---|---|---|
| Intermediate | $gK_S + h$ | 0.89 | 0.92 | 0.91 |
| Standard | $gK_S + h$ | 0.99 | 0.92 | 0.96 |
| Cake | $gK_S + h$ | 0.82 | 0.38 | 0.60 |
| Complete | $gK_S + h$ | 0.86 | 0.61 | 0.74 |
| Intermediate | $g\ln(K_S) + h$ | 0.89 | 0.92 | 0.91 |
| Standard | $g\ln(K_S) + h$ | 0.99 | 0.92 | 0.96 |
| Cake | $g\ln(K_S) + h$ | 0.82 | 0.38 | 0.60 |
| Complete | $g\ln(K_S) + h$ | 0.86 | 0.61 | 0.74 |

models did not provide the same level as fit as those found for linear fits. However, further experiments would be required to confirm that the standard linear model is the best fit for the fouling constants beyond the data sets tested. The correlation developed between the standard fouling model coefficient and experimental constant flow capacity for the D0HC filter was described using Equation 5.14 below. This equation was used to predict the capacity of the D0HC filter when operated at constant flow when processing independent cell culture material.

$$CF_{cap_i} = gK_{S,i} + h \tag{5.14}$$

Where:

$CF_{cap_i}$ : predicted capacity at pressure (i)

$K_S$ : Standard coefficient at pressure (i)

$g$ : Linear coefficient = $9.77 \times 10^3$

$h$ : intercept = $1.76 \times 10^2$

### 5.4.8 D0HC Model Verification

Utilizing the linear fit identified in the earlier section [Equation 5.14] an independent run was conducted to confirm the validity of the developed model. The capacity obtained ex-

perimentally and the predictions made using the novel method developed in this chapter is illustrated in Figure 5.4. This shows there to be a strong predictive capability achieved using the novel method. Typical variability between depth filter capacities when processing a given material is ±30% [Yavorsky *et al.*, 2003]. This is mainly due to the difficulties in manufacturing a cellulocis porous matrix. The predictions of capacities made using the model was ± 14.4%, $n$ =3. This was within the regions quoted in literature Yavorsky *et al.* [2003] and hence verifies the developed model's ability to predict constant flow capacities using constant pressure data.

## 5.5 Alternate Methods

This chapter has described the development of a scale-down method that is capable of predicting constant flow filtration capacity using constant pressure filtration data. This method was verified by the prediction of capacity for two separate depth filters types (D0HC and X0HC) operated at constant flow. Strictly however the successful method was borne out of a series of less illuminating studies the detailed results of which were not included in this chapter. Three main experimental methods prior were investigated to the method described in this chapter. An introduction into each method and reasons for the methods failure are described below.

### 5.5.1 Method 1

This method involved correlating the pressure of operation and the $V_{max}$ value of the material when operated at constant pressure to the capacity at constant flow. It was very difficult to create a model based on those variables for two reasons. The first being the use of TECAN based USD filtration system. This system required cutting filters and subsequently placing them inside the filtration rigs. Then placing the material on top of

the filter and creating a vacuum on the permeate side of the filter to draw material through it. There were number of issues mainly related to the reliability of data. Replicates were difficult to obtain because there were filter to filter variability and some of the rigs had leakages that meant that the correct pressure was not being applied. This meant that any constant pressure data obtained from this device were highly unreliable.

The second issue with this method was with regards to the assumptions made when calculating $V_{max}$. The $V_{max}$ method assumes that the filter is fouled via the pore constriction method. From later studies this was found not to be the case [Table 5.6]. The main lesson learned from this method was comparing filters of separate sizes designed in different ways was unlikely to produce the desirable outcome. Furthermore, use of a TECAN based USD filtration method would be required to show scalability to show similar performance when operated at constant pressure using a 23cm$^2$ depth filter. So the decision was made only to use 23cm$^2$ filters for constant pressure studies.

### 5.5.2 Method 2

Method 2 was based on the utility of extrapolated the flux decline data observed from constant pressure when filtering material to predict the capacity at constant flow operation. The flux was extrapolated to quantify the capacity at 100 LMH. This capacity value was then correlated against the capacity obtained at constant flow. Extrapolation was initially based on fitting simple logarithmic models to predict the capacity at 100 LMH. Unfortunately, there was no correlation observed between the capacity at constant flow compared to the capacity at constant pressure. Subsequently, fouling models were incorporated to predict of the capacity at 100 LMH through modelling the flux decline. However, the predicted capacity at constant pressure did not correlate with the capacity at constant flow.

### 5.5.3 Method 3

Another method of predicting constant flow capacity was done through creating a model based on the material turbidity and the $V_{max}$ value of the material passed through at constant pressure. However, it was found that though turbidity is used throughout industry to describe centrate quality in the current work it did not provide the best representation of centrate quality. If many small particulates were present in the system when compared to a single large particle both were found to create a similar level of obscurity presenting similar turbidity values. Figure 5.9 shows centrate-5 and centrate-6 with similar turbidities of 102 NTU and 106 NTU respectively. However, both materials produced vastly different flux declines. This made it difficult to make correlations using turbidity values to predict constant flow capacity.

## 5.6 Conclusion

Large volumes of centrates (5,000-10,000 L) are typically processed by depth filters in mAb process platforms operated in constant flow mode. The filter area required for this task is determined at the very early stages of process development using small scale studies to identify filter capacity but typically this will require large volumes of material (>1 L). The use of constant pressure over constant flow operation for sizing enables significant savings in time and material [Figure 5.1]. This allows for faster process development times in industry for depth filter sizing studies. This chapter described a method that utilises constant pressure fouling data to predict capacity during constant flow processes.

The method described in this chapter was used to predict the capacity of multiple depth filter types when tested against a range of feed materials. When comparing these predictions operated at constant pressure against experimental capacities obtained by

means of constant flow there were a good level of agreement for both Millipore X0HC (± 14%, $n$ =3) and D0HC (± 14%, $n$ =3) depth filters, a level of agreement in line with previous predictions published in literature [Yavorsky *et al.*, 2003]. Additionally the method described in this chapter also enables a 70% reduction of material required for typical X0HC filter sizing studies and furthermore reduces the time required such studies by 80%. It was also found that the X0HC filtrate generated from both modes of filter operation produced filtrates that had similar qualities in terms of turbidity and subsequent sterile filter fouling propensities. The method described could be used to produce a library of correlations for multiple filters so that filter screening can be conducted more rapidly. Furthermore, it could be utilized in a high throughput manner to understand filter capacity for a range of material without an investment of a large volume of feed material. This will enable faster and more robust process characterisation studies to be conducted at a very early stage of process development.

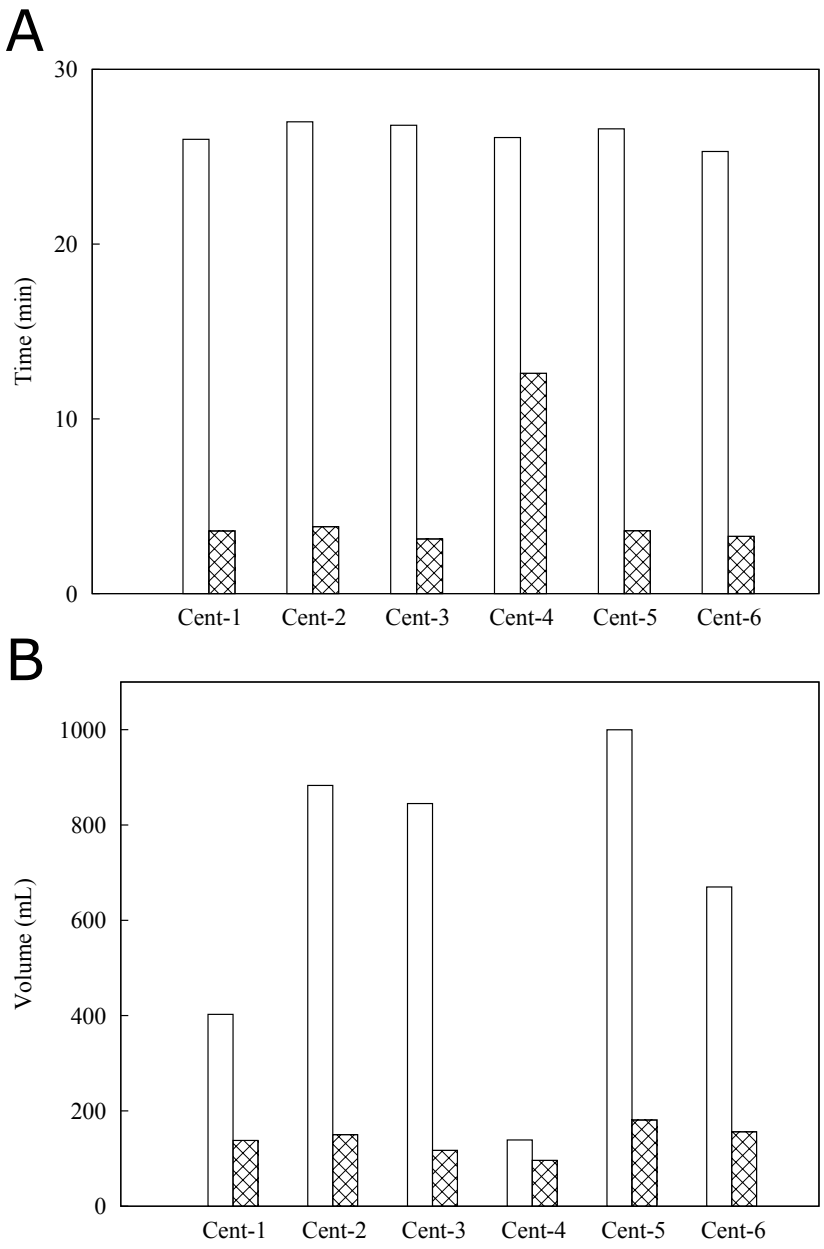


**Fig. 5.1:** Examining experimental time when processing 100mLs and process material volume requirements for either mode of filtration; constant pressure (☒) and constant flow (☐). Centrates used for these studies were sourced from multiple cell culture broths (Table 5.1) and processed through a pilot scale centrifuge at a range of conditions (Table 5.2).

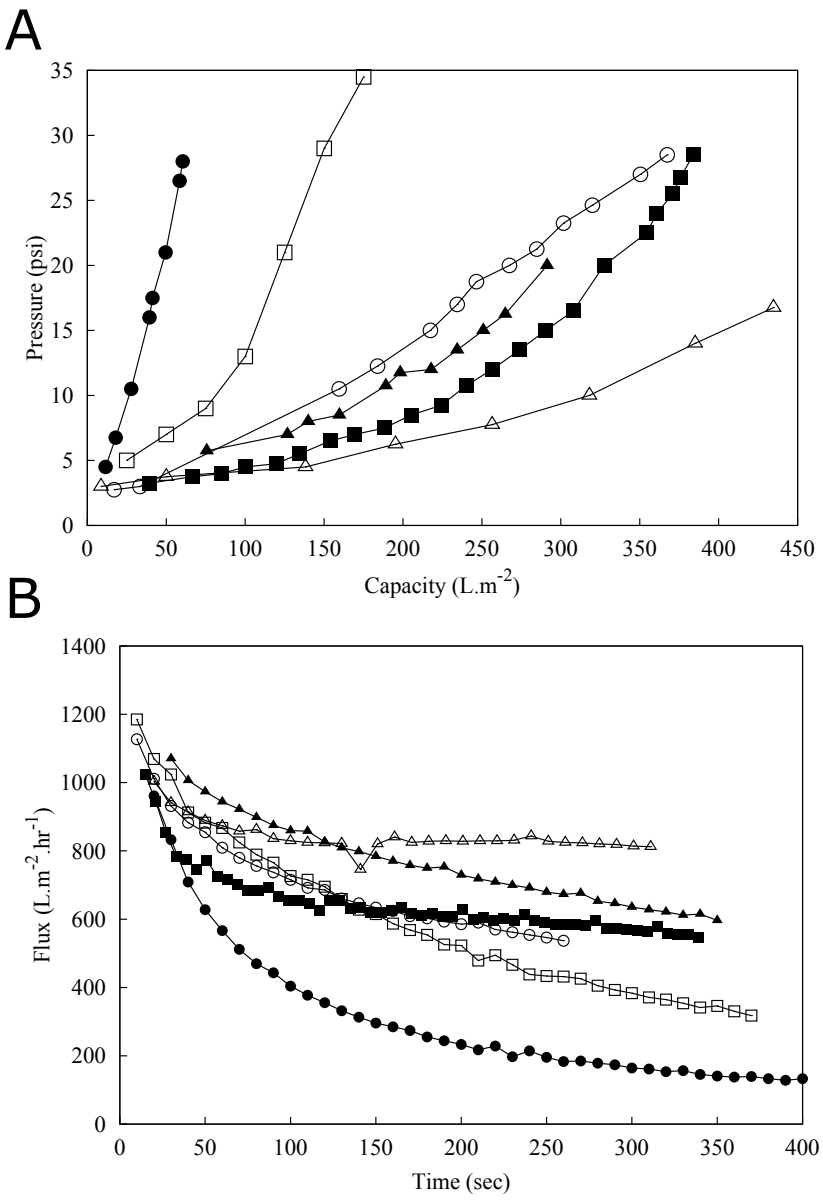


**Fig. 5.2:** Study examining the A)X0HC filter pressure profiles when operated at constant flow at 100 LMH and B) X0HC filter flux decline when operated at a pressure of 15 psi. A range centrates (1□, 2■, 3◯, 4●, 5△, 6▲) were used as source materials for this study (Table 5.2).

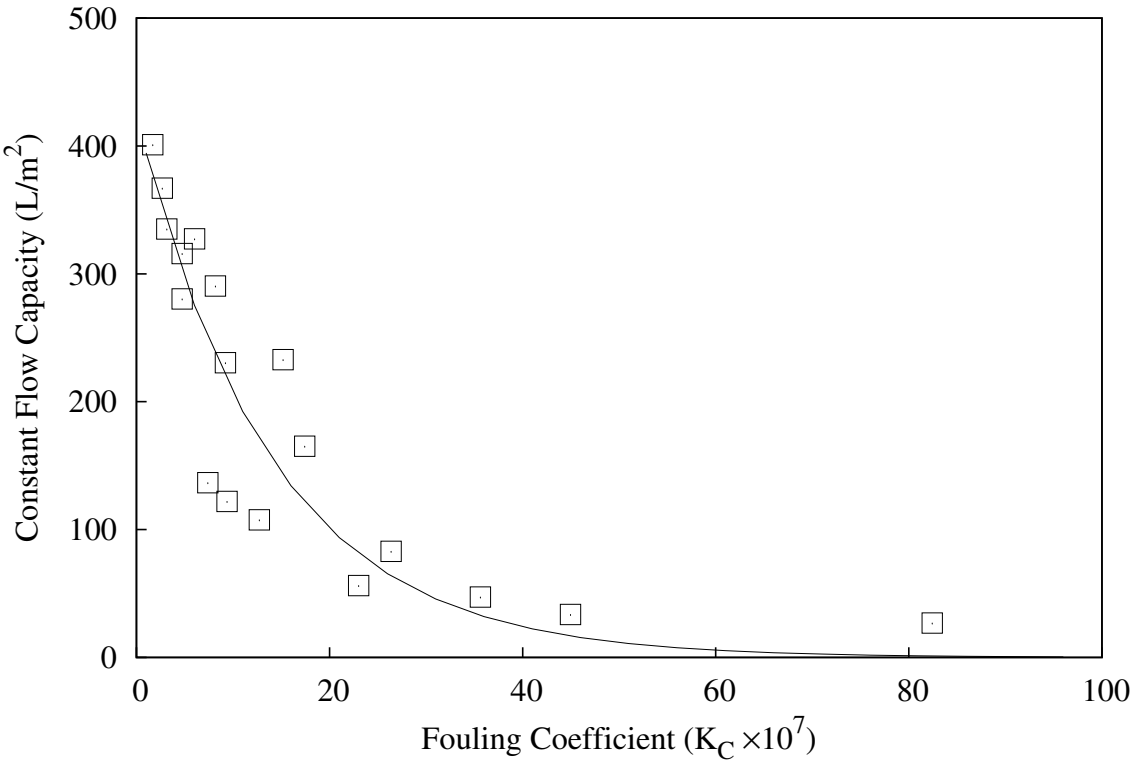


**Fig. 5.3:** Study developing the correlation between the fouling coefficients at constant pressure and capacity at constant flow when operating a X0HC depth filter. A range of centrates were used as source material for this study (Table 5.2).

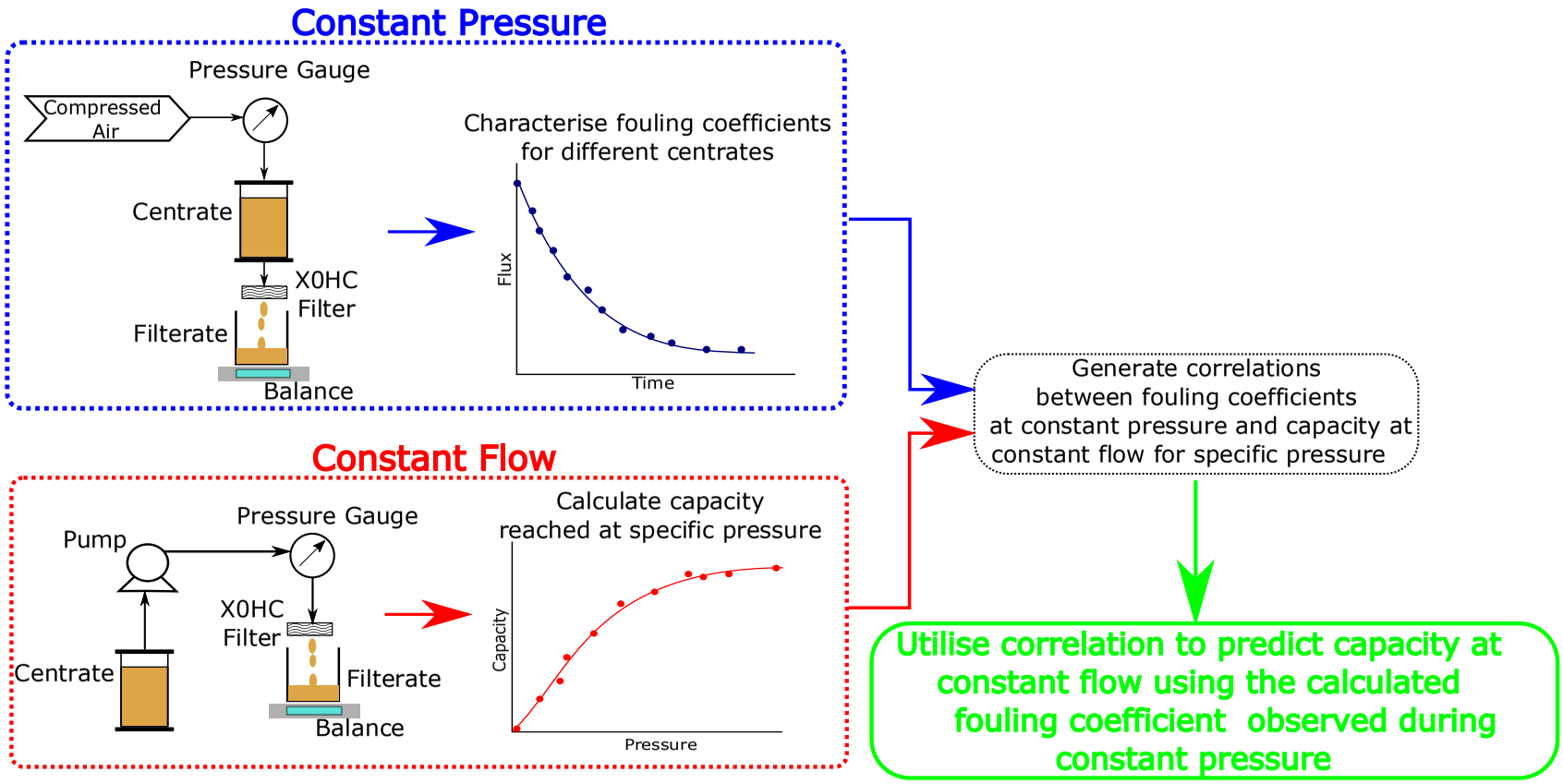


**Fig. 5.4:** Pictorial of flow diagram summarising the strategy for the development of the correlation to predict constant flow capacity from constant pressure flux decline data

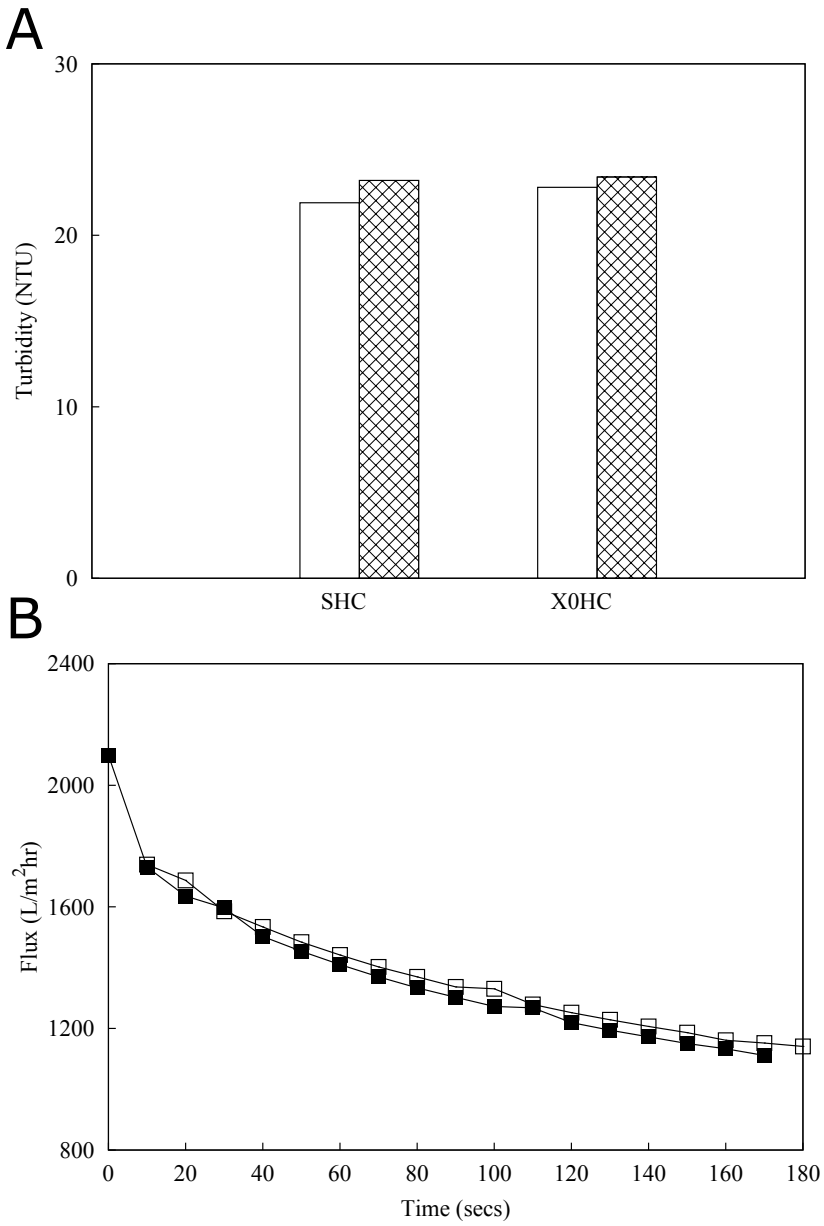


**Fig. 5.5:** Study examining A) filtrate turbidities post SHC and X0HC filtration using experimental constant flow □ operation and predictive constant pressure methods ☒ when processing Centrate-6 B) Study examining flux decline using a SHC sterile filter when processing filtrate post X0HC generated via the predictive constant pressure □ methods and experimental constant flow ■ for the processing of Centrate-6.

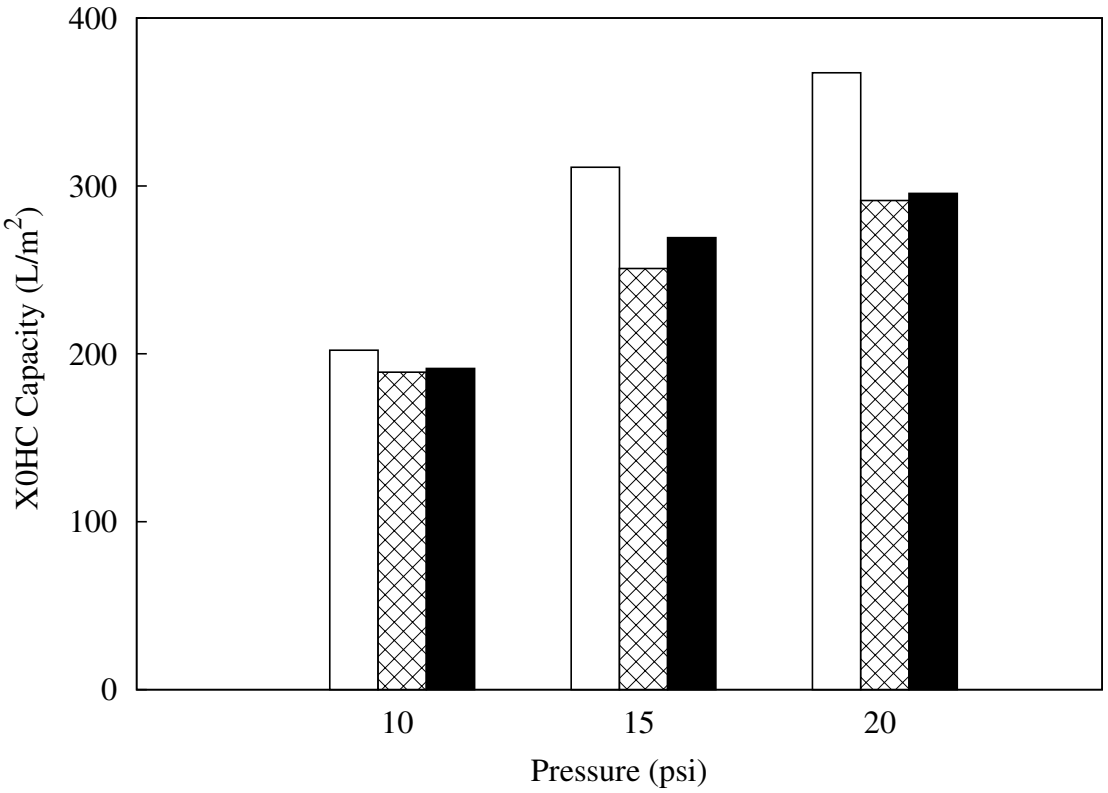


**Fig. 5.6:** Study comparing the mathematical model predictions made through the constant pressure methodology based on the cake (□) and cake-adsorption (■) models at a range of pressures and experimental values (⊠) of constant flow capacities when operated at 100 LMH. Culture-6 was used as source material for this study.

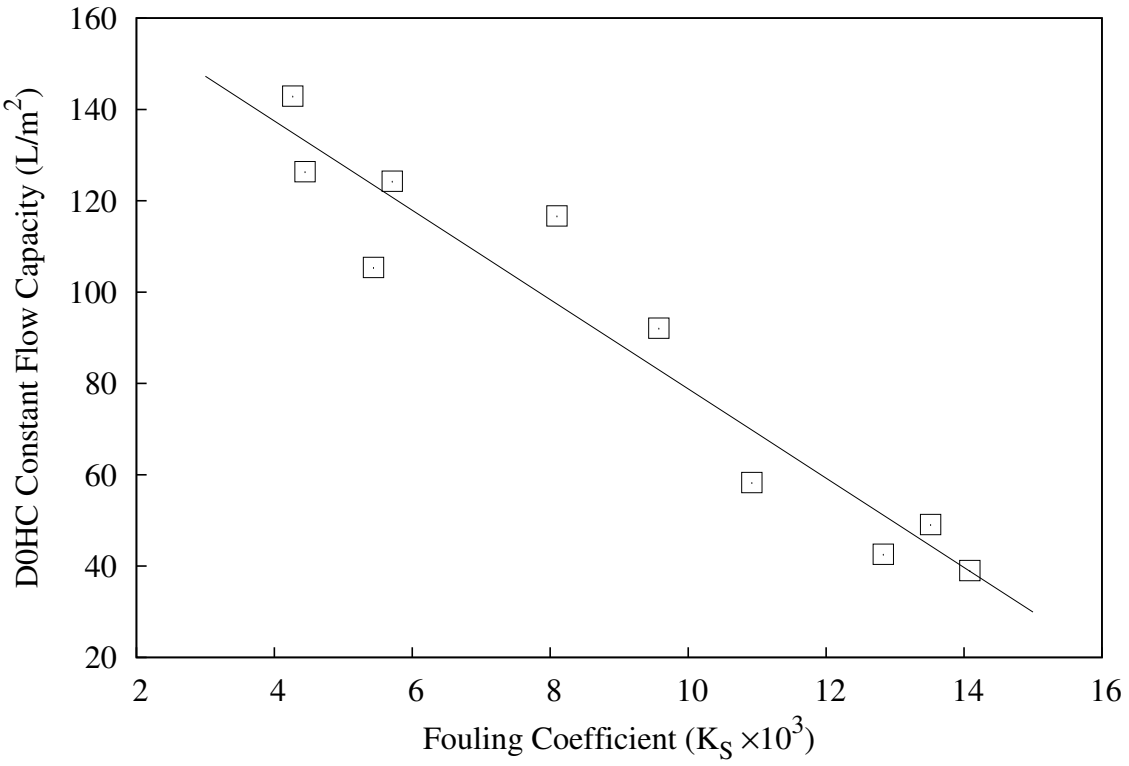


**Fig. 5.7:** Study developing the correlation between the fouling coefficients at constant pressure and capacity at constant flow when operating a D0HC depth filter at 30 LMH (Table 5.3). A wide range of materials were used for this study (Culture AA-AI, Table 5.1).

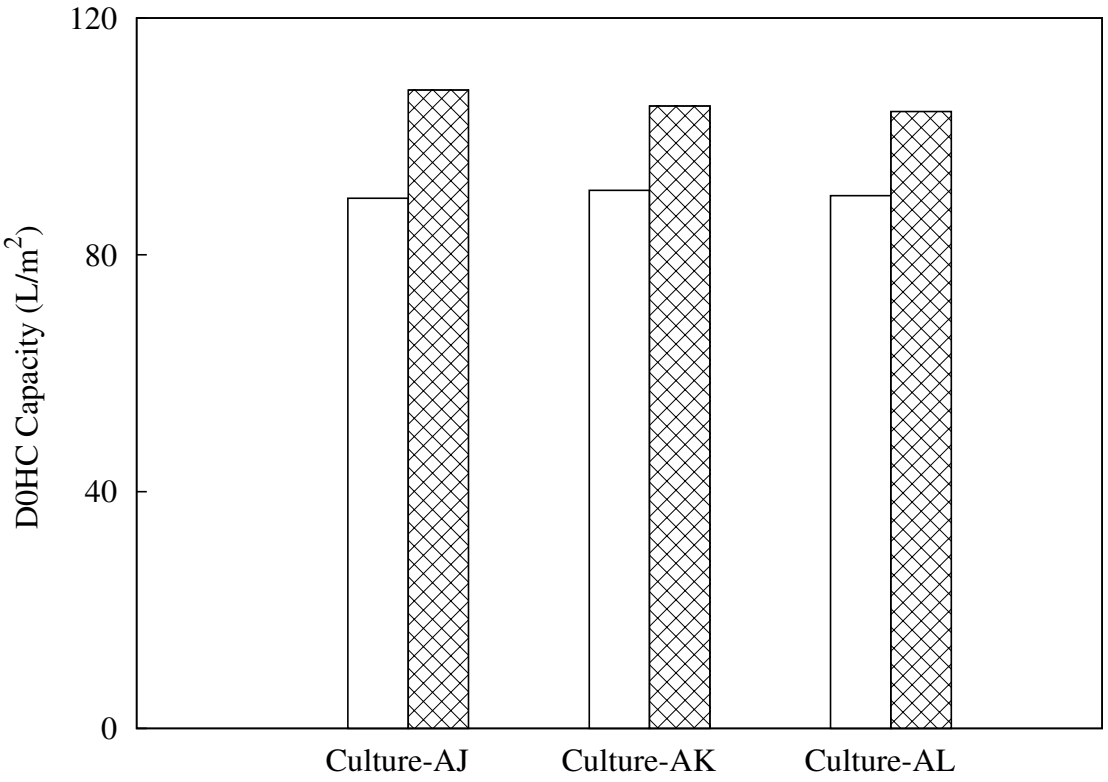


**Fig. 5.8:** Study comparing the mathematical standard fouling model predictions (☒) made utilizing the constant pressure methodology at a range of pressures and experimental values (☐) of constant flow capacities when operated at 30 LMH. Cultures AJ, AK & AL (Table 5.1) were used as source material for this study.

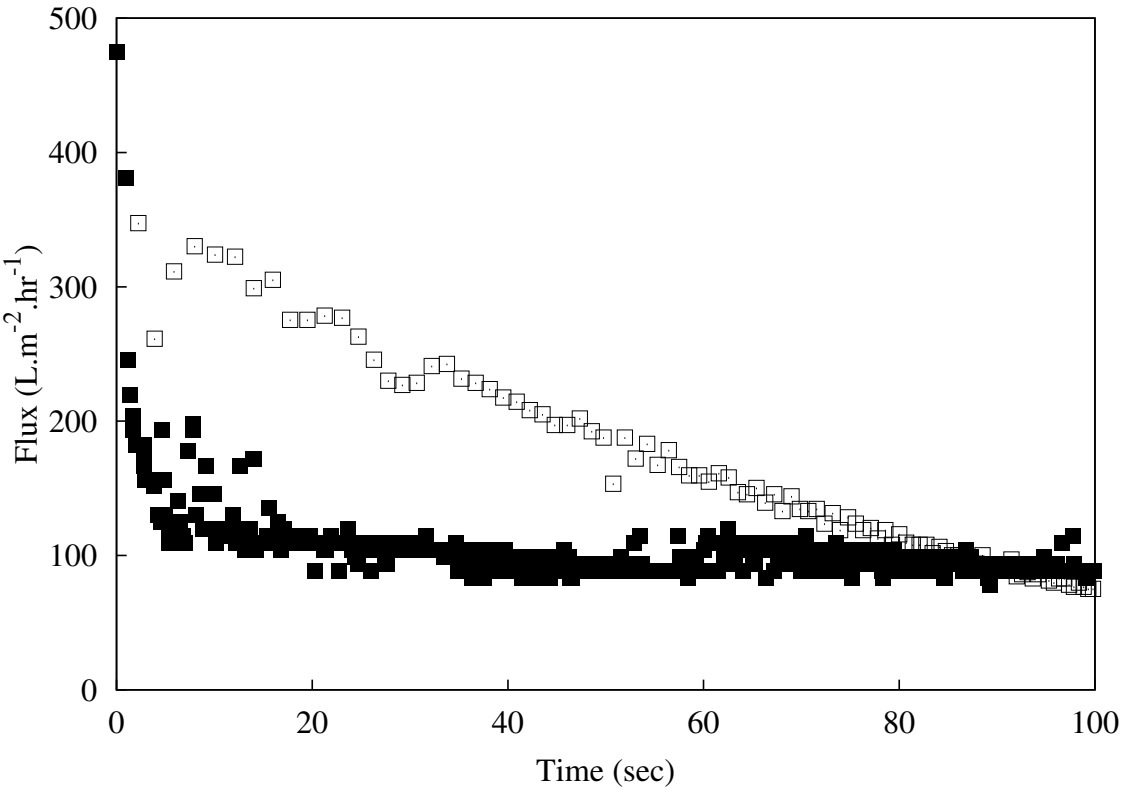


**Fig. 5.9:** X0HC filter flux decline when operated at a pressure of 5 psi challenged with Centrate-5 □ and Centrate-6 ■ (Table 5.2).

# Chapter 6

# Validation

The overall aim of this thesis was to devise methods that allow for more efficient development and characterization of scalable harvest processes and to involve the creation of scale-down tools and methods that enable prediction of pilot-scale predictions. Typical process development efforts for the harvest step are often resource and time intensive. Process development of the centrifugation step in the harvest sequence typically requires 50L cell culture for full characterisation. However, volumes of this nature are only available relatively late in the process development making process development at an early stage difficult. Additionally the testable parameters at pilot-scale with 50L is often very narrow and in order to obtain a thorough understanding of the design space multiple 50L batches are required. This is neither economically efficient nor is it practical when the main role of the pilot-facility early on in development is to produce multiple lots of products for toxicology studies.

An accurate scale-down method should allow for an understanding of the effects and interactions of process inputs on a unit operation without the burden of running at pilot-scale. Scale-down devices use significantly less material and hence allow for multiple experiments to be conducted at an accelerated rate. This allows for a better understanding

of the process design space. The utility of scale-down tools has been utilized successfully for multiple operations both upstream and down-stream. However, little work has been done on the scaling down of the sequence. This thesis describes scale-down methods and tools that enable mimicking of process performance of pilot-scale harvest unit operations. These scale-down tools can be leveraged to conduct process development studies at an earlier stage of process development. This allows companies to accelerate process development times. Process development is often a critical part of bringing a drug to market. Faster development times would enable bringing a product to market allowing faster access to patients for novel monoclonal antibody therapies.

MedImmune Gaithersburg (USA) focuses its development work on novel antibody-based therapeutics for patients. This thesis was conducted within a division of MedImmune which concentrates on process development and creating material for toxicology batches during cycle 1 development. The typical validation challenges faced in early stage development revolves around validating the material and processes used in lab scale and pilot scale to determine KCCPs and identifying CQAs at the very early stages of candidate screening. The processes would involve all the unit operations typically found in a mAb process platform and the methods which those processes run. The materials to be validated would include raw materials, resins and disposables such as filters.

Fulfilling Quality by Design (QbD) regulatory initiatives over the last decade has required that biopharmaceutical manufacturers develop a thorough understanding of a product′s quality attributes and its process of manufacture through the generation of design spaces. High throughput scale-down techniques now enable the rapid generation of high volumes of experimental data, both in the upstream and downstream manufacturing process. Such large experimental data sets generated through these techniques

in principle allows for better decision-making to help identify the effects and critical interactions of the input parameters on the process performance and product quality.

The validation issues that currently loom for my project are based around the validation of the scale-down methods developed. These methods will have to show that they are representative of the large scale processes of centrifugation and depth filtration. One of my main aims was to create a validation document for the scale down devices by initially assessing the CQAs (Critical Quality Attributes) and then conducting experiments to identify how well they match the CQAs  PPAs (Process Performance Attributes).

In the past no CQAs were discussed when presenting reproducibility of a scale-down devices in the majority of literature. They mainly discussed process performance attributes (PPAs) such as solids remaining and capacities for centrifugation and depth filtration respectively. The main reason for this could be that these processes are not seen as ones that do not affect CQAs. This could be due to the fact that during process development primary recovery is seen as an intermediary step and there is hence a lack of process knowledge in terms of understanding the design space. More recently publications are starting to look at typical CQAs such as HCPs, hcDNA and titre with respect to changes in the primary recovery region and hence could potentially create a drive towards understanding the design space better.

This thesis focused mainly on validating the scale-down methods developed and heavily focused on matching the PPAs observed at pilot-scale. Chapter-3 showed that the scale down method was able to mimic the pilot-scale centrifuges process performance attributes. These include turbidity, particle size distribution and filterability of the material generated through the scale-down methodology. The scale-down method developed to

match the pilot-scale centrifuge also matches a CQA in the levels of LDH released. This CQA is typically used in industry to quantify the levels of shear generated in the disk-stack centrifuge. Chapter-4 focused on matching the capacity values of depth filtration studies conducted at pilot-scale using a scale down method.

A potential problem of the utility of scale-down tools could be that it places a heavy burden on the analytical teams to quantify particle size distribution and LDH levels. A way around this would be to require more FIO (For Information Only) assays for the CQAs so that the process development scientist can understand the design space and only submit a smaller quantity of samples for validated assays for the ranges that the process will operate under.

Usually the development of fermentation processes is lengthy and requires many stages of optimisation. The scale down method may have to be simplified in order to mimic the worst case scenario seen through the primary recovery process. This could mean instead of testing the entire harvest design space for each cell culture, only test the condition that the commercial scale machine would be operated at. This would minimize the number of experiments conducted as well as provide a material that best represents the eventual commercial scale process for subsequent chromatographic studies.

Scale-down devices can enable production of large quantities of experimental data, if combined with appropriate analytical methods. Creating documents to best show the data generated would be another potential problem with such devices. Though it may be interesting to the scientists it may not be all relevant to the regulatory agencies like the FDA. A document template would have to be created so that it summarises the key take

home messages from the experiments.

Validation of the operation methods of the scale-down would be essential to produce reproducible results. This would provide scientists with SOPs so that the device can be best utilized. The SOPs designed will need to have the user in mind and take into consideration ease of use, label printing for large experimental samples sets so that assay requests can be conducted more smoothly, methods for storing samples and data upon experiment completion.

# Chapter 7

# Conclusions and Future Work

The aim of this thesis was to create tools that enable more efficient development and characterization of the unit operations in the harvest sequence. This aim was achieved through the development of novel scale-down methodologies and tools that enabled the prediction of pilot-scale centrifugation and depth filtration performance.

The scale down method developed for centrifugation had the ability to predict the process of performance of multiple disk stack machines. This prediction was achieved through the use of a novel shear device which had the ability to develop levels of shear present in disk-stack centrifuges. This work built upon existing knowledge from published work by Westoby *et al.* [2011b] and Boychyn *et al.* [2004] so as to create a simple method with the ability to produce unlimited amounts of sheared material for subsequent filter rating studies. The scale down filtration method developed in this thesis had the ability to translate constant pressure data to predict constant flow performance for depth filters. This was an alternative method to those described in literature and was shown to be accurate across a range of materials and depth filters. The methods described in this thesis facilitate high throughput experimentation with an increased number of experiments conducted with a minimal material requirement. This allows for a more thorough

understanding of the process design space for harvest operations.

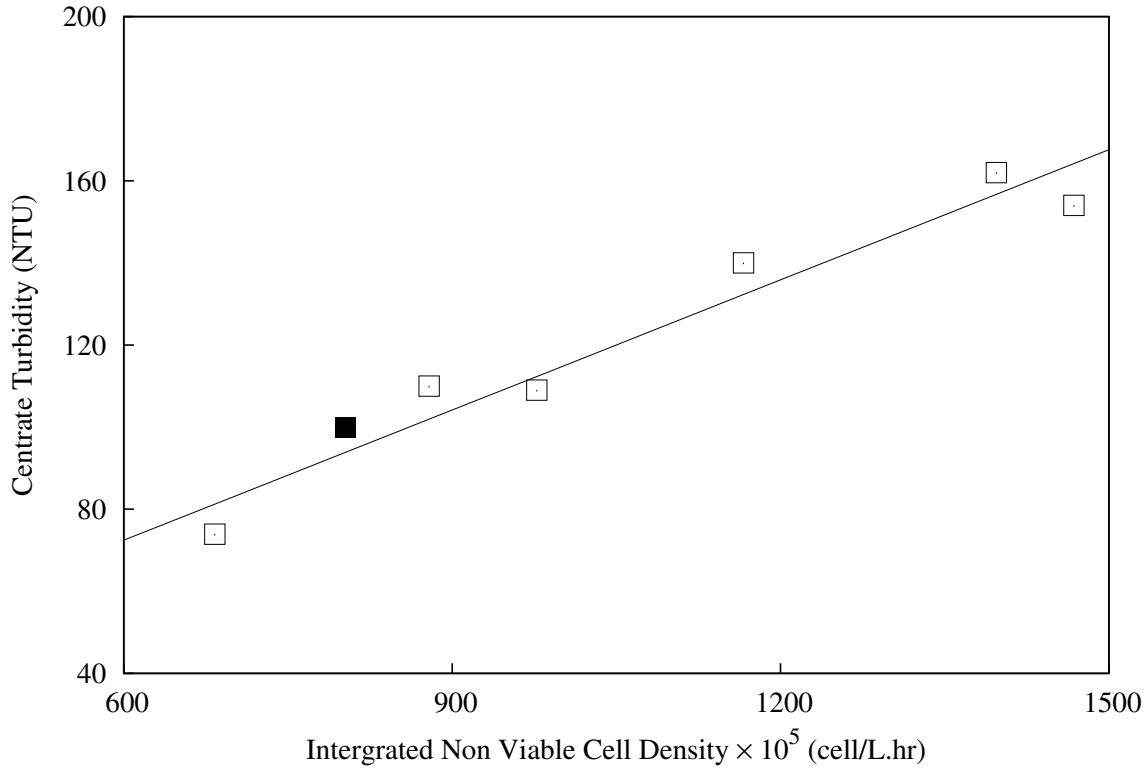


**Fig. 7.1:** The modelling datasets (□) was generated by shearing cell culture material using the CSD Version-2 and centrifuged using a lab-scale centrifuge to mimic the LAPX-404. Regression analysis (—) was used to determine the following relationship between the integrated non viable cell density ($INVCD$) and Turbidity ($Turb$) to identify the centrate turbidity obtained using the pilot-scale centrifuge: (■): $Turb$=0.11($INVCD$)+9.02, $R^2$=0.94. The turbidity of the LAPX-404 centrifuge was determined experimentally when processing an independent cell culture material.

The methods described in this thesis can also be leveraged to identify the correlations between cell culture conditions and process performance of harvest operations. Figure 7.1 shows with increasing levels of integrated non-viable cell density there is an increase in centrate turbidity. This is expected as there are often higher levels of small particulates with increased levels of integrated non viable cell densities. These increased populations are often difficult to remove through the centrifugation step and hence results in higher resultant turbidities in the centrate. The effect of cell culture conditions on depth filtration

operations was not tested exhaustively in this work but would be an obvious future target. Filter performance is known to change dramatically for primary depth filters. Increasing cell density typically causing faster rates of fouling reducing the filter capacity. Understanding of the influence of cell culture conditions on primary recovery operations is an important aspect of process development. The typical parameters used to characterize cell culture conditions are cell density and cell viability. These parameters are cell specific; two cell lines with identical cell density and cell viability may potentially demonstrate very different separation performances and as such an alternative method of characterization is required to quantify the cell culture broth. Particle size distribution describes the number of particulates in the medium as a function of the size range. These readings could potentially be utilized to predict the performance of the harvest operation. However, instruments that are able to measure particles across a wide region from sub-micron to 10 microns are difficult to find. Furthermore, PSD devices are known to produce highly variable results making analysis between readings difficult.

Furthermore, the developed methodology for the prediction of depth filtration performance is based on identifying the fouling model that best fits a given material and filter. In the case of the tested D0HC and X0HC filters a standard model was found to fit the D0HC while a cake/cake-adsorption was found to fit the X0HC filters. The developed model could be worked on to identify why there is such a deviation between filter types of different structures.

When developing this model a wide range of conditions were tested however there are occasions where the materials that conform to this methodology could be out of range. In these cases the model will have to be further developed to add more data points to make

the model more robust and include a wider range of material conditions.

In addition to centrifugation and depth filtration there is a polishing sterile filter step that removes any fine particulates that escapes the depth filter. These filters are also sized during the harvest development step. A scale-down approach to sterile filter sizing and rating was considered by Kong *et al.* [2010] utilising the TECAN platform. The production of commercial 96 well filter plates could also be leveraged in order to conduct high through put filter sizing studies. Subsequent to the sterile filter in the typical monoclonal antibody process platform chromatographic polishing steps are utilized to separate and concentrate the product of interest from a pool of aggregates, fragments, HCPs and hcDNAs. The TECAN platform has been leveraged to quantify chromatography process performance at an early stage of process development where small quantities of material available for such studies. The development of scale down tools for the harvest process enables production of material for the chromatographic step. Additionally scale-down devices could be utilized to test the influence of a wide variety of post harvest materials on the performance of the chromatography step. A platform approach to identify the output parameters that would most influence the chromatographic process would be ideal in understanding key interactions between harvest and chromatographic processes.

The future of biotechnology will involve greater automation and less human input for process characterization. Currently the bottleneck in running a fully automated scale-down processes is the harvest step. However, the methods and techniques developed in this thesis are automation-ready and could potentially be integrated with liquid handling platforms (TECAN). A more automated scale-down process development strategy is likely to result in large volumes of data being generated. With such levels of data there will also be a requirement to process the data through screening and data analytic techniques. The

processed data could be utilized along with a user interactive software to create designs spaces and process flow diagrams so as to better understand the process.

The aim of this thesis was to develop tools that enable more efficient development and characterization of the harvest step. This aim was achieved and the methods developed in this thesis have been integrated into process development efforts by the industrial sponsor (MedImmune LLC, Gaithersburg,USA) of this program. Furthermore, the work conducted in this thesis has resulted in multiple publication efforts.

# References


AGGARWAL, S. (2011). What's fueling the biotech engine 2010 to 2011. *Nature Biotechnology*, **29**, 1083–1089.

AMBLER, C.M. (1959). The theory of scaling up laboratory data for the sedimentation type centrifuge. *Journal of Biochemical and Microbiological Technology and Engineering*, **1**, 185–205.

AXELSSON, H. (2002). *Cell Separation, Centrifugation*. John Wiley & Sons, Inc.

BADMINGTON, W.R.P.M.H.E.S., F. (1995). Vmax testing for practical microfiltration train scale-up in biopharmaceutical processing. *Pharmaceutical technology*, **19**, 64–76.

BIRCH, B.R., J. & WOOD, L. (1985). Bulk production of monoclonal antibodies in fermenters. *Trends in Biotechnology*, **3**, 162 – 166.

BIRD, R., STEWART, W. & LIGHTFOOT, E. (1960). Transport phenomena, wiley, new york.

BOLTON, B.A.L.M., G. (2006). The effects of flow rate on membrane capacity: Development and application of adsorptive membrane fouling models. *Journal of Membrane Science*, **279**, 625 – 634.

BOLTON, G., LACASSE, D. & KURIYEL, R. (2006). Combined models of membrane fouling: Development and application to microfiltration and ultrafiltration of biological fluids. *Journal of Membrane Science*, **277**, 75 – 84.

BOWEN, W., CALVO, J. & HERNÁNDEZ, A. (1995). Steps of membrane blocking in flux decline during protein microfiltration. *Journal of Membrane Science*, **101**, 153 – 165.

BOYCHYN, M., YIM, S., SHAMLOU, P.A., BULMER, M., MORE, J. & HOARE, M. (2001). Characterization of flow intensity in continuous centrifuges for the development of laboratory mimics. *Chemical Engineering Science*, **56**, 4759 – 4770.

BOYCHYN, M., YIM, S., BULMER, M., MORE, J., BRACEWELL, D. & HOARE, M. (2004). Performance prediction of industrial centrifuges using scale-down models. *Bioprocess and Biosystems Engineering*, **26**, 385–391.

BRENNER, C., S. MILSTEIN (1966). Origin of antibody variation. *Nature*, **211**, 242–243.

CHAMPION, K., MADDEN, H., DOUGHERTY, J. & SHACTER, E. (2005). Defining your product profile and maintaining control over it, part 2. *BioProcess Int*, **3**, 52–57.

CHAN, G., BOOTH, A., MANNWEILER, K. & HOARE, M. (2006). Ultra scale-down studies of the effect of flow and impact conditions during e. coli cell processing. *Biotechnology and Bioengineering*, **95**, 671–683.

CHANDLER, M. & ZYDNEY, A. (2004). High throughput screening for membrane process development. *Journal of membrane science*, **237**, 181–188.

CHELLAM, S. & XU, W. (2006). Blocking laws analysis of dead-end constant flux microfiltration of compressible cakes. *Journal of Colloid and Interface Science*, **301**, 248 – 257.

DEPALMA, A. (2004). Large scale biomanufacturing operations. *GEN*, **24**, 2004.

DUCLOS-ORSELLO, C., LI, W. & HO, C.C. (2006). A three mechanism model to describe fouling of microfiltration membranes. *Journal of Membrane Science*, **280**, 856 – 866.

FARID, S. (2001). *Decision support tool for simulating the process and business perspective of biopharmaceutical manufacture*. Ph.D. thesis, Advanced Center for Biochemical Engineering, UCL.

FARID, S.S. (2008). Economic drivers and trade-offs in antibody purification processes. *BioPharm International*, **21**, 37.

FLATMAN, S. (2011). Impurities in biotechnology products –experience of setting specifications. [Online; accessed 26-April-2016].

GERBA, C.P. & HOU, K. (1985). Endotoxin removal by charge-modified filters. *Applied and environmental microbiology*, **50**, 1375–1377.

GHOSE, S., ALLEN, M., HUBBARD, B., BROOKS, C. & CRAMER, S.M. (2005). Antibody variable region interactions with protein a: Implications for the development of generic purification processes. *Biotechnology and Bioengineering*, **92**, 665–673.

GOETZE, A.M., SCHENAUER, M.R. & FLYNN, G.C. (2010). Assessing monoclonal antibody product quality attribute criticality through clinical studies. *mAbs*, **2**, 500—507.

HIRSCHLER, B. (2010). Factbox-world's top-selling drugs in 2014 vs 2010. [Online; accessed 26-April-2016].

HLAVACEK, M. & BOUCHET, F. (1993). Constant flowrate blocking laws and an example of their application to dead-end microfiltration of protein solutions. *Journal of Membrane Science*, **82**, 285 – 295.

HO, C.C. & ZYDNEY, A.L. (2000). A combined pore blockage and cake filtration model for protein fouling during microfiltration. *Journal of Colloid and Interface Science*, **232**, 389 – 399.

HO, C.C. & ZYDNEY, A.L. (2002). Transmembrane pressure profiles during constant flux microfiltration of bovine serum albumin. *Journal of Membrane Science*, **209**, 363 – 377.

HOWARD, L. (2011). Challenges in the cgmp manufacturing of hescs: Lessons learned from monoclonal antibodies, bioprocess technology consultants. [Online; accessed 27-April-2016].

HUTCHINSON, N., BINGHAM, N., MURRELL, N., FARID, S. & HOARE, M. (2006). Shear stress analysis of mammalian cell suspensions for prediction of industrial centrifugation and its verification. *Biotechnology and Bioengineering*, **95**, 483–491.

JACKSON, N.B., LIDDELL, J.M. & LYE, G.J. (2006). An automated microscale technique for the quantitative and parallel analysis of microfiltration operations. *Journal of membrane science*, **276**, 31–41.

JAGSCHIES, G., GRÖNBERG, A., BJÖRKMAN, T., LACKI, K. & JOHANSSON, H.J. (2006). Technical and economical evaluation of downstream processing options for monoclonal antibody (mab) production. *Biopharm international*.

JAIN, M., PARANANDI, M., ROUSH, D., GÖKLEN, K. & KELLY, W.J. (2005). Using cfd to understand how flow patterns affect retention of cell-sized particles in a tubular bowl centrifuge. *Industrial Engineering Chemistry Research*, **44**, 7876–7884.

JEFFERIS, R. (2009). Recombinant antibody therapeutics: the impact of glycosylation on mechanisms of action. *Trends in Pharmacological Sciences*, **30**, 356 – 362.

JUNGBAUER, A. & GÖBEL, U. (2012). Biopharmaceutical process development–shortcut to market: An interview with rolf werner from boehringer ingelheim. *Biotechnology journal*, **7**, 14–16.

KELLY, B. (2009). Industrialization of mab production technology:the bioprocessing industry at a crossroads. *mAbs*, **1**, 443 – 452.

KEMPKEN, R., PREISSMANN, A. & BERTHOLD, W. (1995). Assessment of a disc stack centrifuge for use in mammalian cell separation. *Biotechnology and Bioengineering*, **46**, 132–138.

KONG, S., AUCAMP, J. & TITCHENER-HOOKER, N.J. (2010). Studies on membrane sterile filtration of plasmid {DNA} using an automated multiwell technique. *Journal of Membrane Science*, **353**, 144 – 150.

KRISHNA, R. (2012). *Applications of Pharmacokinetic principles in drug development*. Springer Science & Business Media.

KUNERT, R. & REINHART, D. (2016). Advances in recombinant antibody manufacturing. *Applied Microbiology and Biotechnology*, **100**, 3451–3461.

LAU, E.C., KONG, S., MCNULTY, S., ENTWISLE, C., MCILGORM, A., DALTON, K.A. & HOARE, M. (2013). An ultra scale-down characterization of low shear stress primary recovery stages to enhance selectivity of fusion protein recovery from its molecular variants. *Biotechnology and Bioengineering*, **110**, 1973–1983.

LEVY, M., COLLINS, I., YIM, S., WARD, J., TITCHENER-HOOKER, N., SHAMLOU, P.A. & DUNNILL, P. (1999). Effect of shear on plasmid dna in solution. *Bioprocess Engineering*, **20**, 7–13.

LI, F., ZHOU, J.X., YANG, X., TRESSEL, T. & LEE, B. (2007). Current therapeutic antibody production and process optimization. *Bioprocessing journal*, **5**, 16.

LIU, H.F., MA, J., WINTER, C. & BAYER, R. (2010). Recovery and purification process development for monoclonal antibody production. *mAbs*, **2**, 480–499, pMID: 20647768.

LIU, J.K. (2014). The history of monoclonal antibody development – progress, remaining challenges and future innovations. *Annals of Medicine and Surgery*, **3**, 113 – 116.

LOONEY, W. (2016). 2016: A biopharma market in flux. *Pharmaceutical Executive*, **36**.

MA, N., KOELLING, K.W. & CHALMERS, J.J. (2002). Fabrication and use of a transient contractional flow device to quantify the sensitivity of mammalian and insect cells to hydrodynamic forces. *Biotechnology and Bioengineering*, **80**, 428–437.

MARICHAL-GALLARDO, P. & ALVAREZ, M. (2012). State-of-the-art in downstream processing of monoclonal antibodies: Process trends in design and validation. *Biotechnology progress*, **28**, 899–916.

MAYBURY, J.P., HOARE, M. & DUNNILL, P. (2000). The use of laboratory centrifugation studies to predict performance of industrial machines: Studies of shear-insensitive and shear-sensitive materials. *Biotechnology and Bioengineering*, **67**, 265–273.

MCCAFFERTY, J. (2010). The long and winding road to antibody therapeutics. In *mAbs*, vol. 2, 459–460, Taylor & Francis.

MCCAMISH, M. & WOOLLETT, G. (2012). The state of the art in the development of biosimilars. *Clinical Pharmacology & Therapeutics*, **91**, 405–417.

MCGLAUGHLIN, M.S. (2010). An emerging answer to the downstream bottleneck. *BioProcess Int*, **10**, 58–61.

MICHELETTI, M. & LYE, G.J. (2006). Microscale bioprocess optimisation. *Current Opinion in Biotechnology*, **17**, 611 – 618, chemical biotechnology / Pharmaceutical biotechnology.

MOSQUEIRA, F.G., HIGGINS, J.J., DUNNILL, P. & LILLY, M.D. (1981). Characteristics of mechanically disrupted bakers' yeast in relation to its separation in industrial centrifuges. *Biotechnology and Bioengineering*, **23**, 335–343.

MULDER, T. & GIMBEL, R. (1991). Application of permeable collectors in deep-bed filtration. *Separations Technology*, **1**, 153 – 165.

NAKAMURA, K. & MATSUMOTO, K. (2006). Properties of protein adsorption onto pore surface during microfiltration: Effects of solution environment and membrane hydrophobicity. *Journal of Membrane Science*, **280**, 363 – 374.

OZATO, K., MAYER, N. & SACHS, D. (1980). Hybridoma cell lines secreting monoclonal antibodies to mouse h-2 and ia antigens. *The Journal of Immunology*, **124**, 533–540.

PALACIO, L., HO, C.C. & ZYDNEY, A.L. (2002). Application of a pore-blockage—cake-filtration model to protein fouling during microfiltration. *Biotechnology and Bioengineering*, **79**, 260–270.

PETERSEN, J.F., MCINTIRE, L.V. & PAPOUTSAKIS, E. (1988). Shear sensitivity of cultured hybridoma cells (crl-8018) depends on mode of growth, culture age and metabolite concentration. *Journal of Biotechnology*, **7**, 229 – 246.

Pharmaceuticals, 2012 (2012). Should patents on pharmaceuticals be extended to encourage innovation? The Wall Street Journal, [Online; accessed 26-April-2016].

Pharmaceuticals, 2014 (2014). The price of failure. The Economist.

PILBROUGH, W., MUNRO, T.P. & GRAY, P. (2009). Intraclonal protein expression heterogeneity in recombinant cho cells. *PloS one*, **4**, e8432.

PINHEIRO, H. (1993). *Centrifugation*. Cabral JMS editors.

PISANO, G.P. (1997). *The development factory: unlocking the potential of process innovation*. Harvard Business Press.

PRESTA, L.G. (2008). Molecular engineering and design of therapeutic antibodies. *Current Opinion in Immunology*, **20**, 460 – 470, host–Pathogen Interactions / Antibody TherapeuticsEdited by Tsuneyasu Kaisho and Hermann Wagner / Edited by Paul Parren and Jan van de Winkel.

RATHORE, A. & MHATRE, R. (2011). *Quality by Design for Biopharmaceuticals: Principles and Case Studies*. Wiley Series in Biotechnology and Bioengineering, Wiley.

REICHERT, J. & VALGE-ARCHER, V. (2007). Development trends for monoclonal antibody cancer therapeutics. *Nature Reviews Drug Discovery*, **6**, 349–356.

REICHERT, J.M., ROSENSWEIG, C.J., FADEN, L.B. & DEWITZ, M.C. (2005). Monoclonal antibody successes in the clinic. *Nature Biotech*, **23**, 1073 – 1078.

ROUSH, Y., DAVID J. LU (2008). Advances in primary recovery: Centrifugation and membrane technology. *Biotechnology Progress*, **24**, 488–495.

SAMARANAYAKE, H., WIRTH, T., SCHENKWEIN, D., RÄTY, J.K. & YLÄ-HERTTUALA, S. (2009). Challenges in monoclonal antibody-based therapies. *Annals of medicine*, **41**, 322–331.

SAMPATH, M., SHUKLA, A. & RATHORE, A.S. (2014). Modeling of filtration processes—microfiltration and depth filtration for harvest of a therapeutic protein expressed in pichia pastoris at constant pressure. *Bioengineering*, **1**, 260.

SCHIRMER, E.B., KUCZEWSKI, M., GOLDEN, K., LAIN, B., BRAGG, C., CHON, J., CACCIUTTOLO, M. & ZARBIS-PAPASTOITSIS, G. (2010). Primary clarification of very high-density cell culture harvests by enhanced cell settling. *BioProcess Int*, **8**, 32–39.

SCHLICHTING, H. & GERSTEN, K. (2003). *Boundary-layer theory*. Springer Science & Business Media.

SHIRATO, M., MURASE, T., IWATA, M. & NAKATSUKA, S. (1986). The terzaghi-voigt combined model for constant-pressure consolidation of filter cakes and homogeneous semi-solid materials. *Chemical Engineering Science*, **41**, 3213–3218.

SHUKLA, A.A. & KANDULA, J.R. (2008). Harvest and recovery of monoclonal antibodies from large-scale mammalian cell culture. *BioPharm International*, **21**, 34.

SINGH, N., PIZZELLI, K., ROMERO, J.K., CHROSTOWSKI, J., EVANGELIST, G., HAMZIK, J., SOICE, N. & CHENG, K. (2013). Clarification of recombinant proteins from high cell density mammalian cell culture systems using new improved depth filters. *Biotechnology and bioengineering*, **110**, 1964–1972.

SOMMERFELD, S. & STRUBE, J. (2005). Challenges in biotechnology production—generic processes and process optimization for monoclonal antibodies. *Chemical Engineering and Processing: Process Intensification*, **44**, 1123–1137.

TAIT, A., AUCAMP, J., BUGEON, A. & HOARE, M. (2009). Ultra scale-down prediction using microwell technology of the industrial scale clarification characteristics by centrifugation of mammalian cell broths. *Biotechnology and Bioengineering*, **104**, 321–331.

TAIT, A., HOGWOOD, C., SMALES, C. & BRACEWELL, D. (2012). Host cell protein dynamics in the supernatant of a mab producing cho cell line. *Biotechnology and Bioengineering*, **109**, 971–982.

TITCHENER-HOOKER, N., DUNNILL, P. & HOARE, M. (2008). Micro biochemical engineering to accelerate the design of industrial-scale downstream processes for biopharmaceutical proteins. *Biotechnology and Bioengineering*, **100**, 473–487.

TJANDRA, J.L., RAMADI, L. & MCKENZIE, I.F. (1990). Development of human anti-murine antibody (hama) response in patients. *Immunology & Cell Biology*, **68**.

TREXLER-SCHMIDT, M., SZE-KHOO, S., COTHRAN, A.R., THAI, B.Q., SARGIS, S., LEBRETON, B., KELLEY, B. & BLANK, G.S. (2009). Purification strategies to process 5 g/l titers of monoclonal antibodies. *BioPharm Intl Supplement March*, 8–15.

VANDEZANDE, P., GEVERS, L.E., PAUL, J.S., VANKELECOM, I.F. & JACOBS, P.A. (2005). High throughput screening for rapid development of membranes and membrane processes. *Journal of membrane science*, **250**, 305–310.

VICKROY, B., LORENZ, K. & KELLY, W. (2007). Modeling shear damage to suspended cho cells during cross-flow filtration. *Biotechnology Progress*, **23**, 194–199.

WALSH, G. (2014). Biopharmaceutical benchmarks 2014. *Nature Biotechnology*, **32**, 992–1000.

WERNER, R.G. (2004). Economic aspects of commercial manufacture of biopharmaceuticals. *Journal of biotechnology*, **113**, 171–182.

WESTOBY, M., CHROSTOWSKI, J., DE VILMORIN, P., SMELKO, J.P. & ROMERO, J.K. (2011a). Effects of solution environment on mammalian cell fermentation broth properties: Enhanced impurity removal and clarification performance. *Biotechnology and Bioengineering*, **108**, 50–58.

WESTOBY, M., ROGERS, J.K., HAVERSTOCK, R., ROMERO, J. & PIERACCI, J. (2011b). Modeling industrial centrifugation of mammalian cell culture using a capillary based scale-down system. *Biotechnology and Bioengineering*, **108**, 989–998.

YAVORSKY, D., BLANCK, R., LAMBALOT, C. & BRUNKOW, R. (2003). The clarification of bioreactor cell cultures for biopharmaceuticals. *Pharmaceutical Technology*, **27**, 62–67.

YIGZAW, Y., PIPER, R., TRAN, M. & SHUKLA, A.A. (2006). Exploitation of the adsorptive properties of depth filters for host cell protein removal during monoclonal antibody purification. *Biotechnology Progress*, **22**, 288–296.

ZYDNEY, A.L. & HO, C.C. (2002). Scale-up of microfiltration systems: fouling phenomena and vmax analysis. *Desalination*, **146**, 75 – 81.

# Appendix A

# Publications

ARTICLE

BIOTECHNOLOGY and BIOENGINEERING

# A Scale-Down Mimic for Mapping the Process Performance of Centrifugation, Depth, and Sterile Filtration

**Adrian Joseph,[1] Brian Kenty,[2] Michael Mollet,[2] Kenneth Hwang,[2] Steven Rose,[2] Stephen Goldrick,[1] Jean Bender,[2] Suzanne S. Farid,[1] Nigel Titchener-Hooker[1]**

[1]The Advanced Centre of Biochemical Engineering, Department of Biochemical Engineering, University College London, Bernard Katz Building, London, WC1E 6BT, United Kingdom; telephone: +44207 679 9586; fax: +44207 916 3943; e-mail: nigelth@ucl.ac.uk

[2]MedImmune LLC Gaithersburg Headquarters, One MedImmune Way, Gaithersburg, Maryland

**ABSTRACT:** In the production of biopharmaceuticals disk-stack centrifugation is widely used as a harvest step for the removal of cells and cellular debris. Depth filters followed by sterile filters are often then employed to remove residual solids remaining in the centrate. Process development of centrifugation is usually conducted at pilot-scale so as to mimic the commercial scale equipment but this method requires large quantities of cell culture and significant levels of effort for successful characterization. A scale-down approach based upon the use of a shear device and a bench-top centrifuge has been extended in this work towards a preparative methodology that successfully predicts the performance of the continuous centrifuge and polishing filters. The use of this methodology allows the effects of cell culture conditions and large-scale centrifugal process parameters on subsequent filtration performance to be assessed at an early stage of process development where material availability is limited.

Biotechnol. Bioeng. 2016;113: 1934–1941.



**KEYWORDS:** centrifugation; continuous centrifugation; scale-down; primary recovery; mammalian cell; disk-stack centrifuge; depth filter; capillary shear; filter capacity



Abbreviations: CSD, capillary shear device; RSD, rotating shear device; USD, ultra scale down; LDH, lactate dehydrogenase; mAb, monoclonal antibody; NADH, nicotinamide adenine dinucleotide; PEEK, polyetheretherketone; QbD, quality by design.

Correspondence to: N. Titchener-Hooker
Received 20 October 2015; Revision received 19 February 2016; Accepted 24 February 2016
Accepted manuscript online 1 March 2016;
Article first published online 16 March 2016 in Wiley Online Library (http://onlinelibrary.wiley.com/doi/10.1002/bit.25967/abstract).
DOI 10.1002/bit.25967

## Introduction

Quality by Design (QbD) regulatory initiatives over the last decade have required that biopharmaceutical manufacturers develop a thorough understanding of a product's quality attributes and manufacturing process through the generation of design spaces (Rathore, 2009). High throughput scale-down techniques now enable the rapid generation of extensive experimental data representative of large-scale performance, both in the upstream and downstream manufacturing process. Such large experimental data sets generated through these techniques allow for better identification of the effects and interactions of the input parameters on the process performance and product quality (Titchener-Hooker et al., 2008).

Continuous flow disk-stack centrifugation is often used to harvest commercial-scale cell culture processes because of its robustness and relatively low running costs (Axelsson, 2002). The intermittent discharge provided by the disk-stack centrifuge enables removal of a considerable quantity of cells and large cellular debris in a semi continuous fashion. However, one of the disadvantages of disk-stack centrifugation is that in many designs the cells enter the centrifuge through a feed zone in which high levels of shear are present. This shear can damage shear-sensitive mammalian cells resulting in the generation of submicron particles which are carried over to the centrate (Jain et al., 2005). These fine particles can cause subsequent fouling in later chromatographic processes, resulting in high column pressures and accompanied reductions in column lifetime and efficiency (Kempken et al., 1995). In order to avoid chromatographic column fouling, depth filtration is often used immediately after centrifugation to remove these submicron particles (Yigzaw et al., 2006). Hence, a typical process sequence for a mammalian cell culture process might begin with the removal of cells and cell debris achieved through a combination of a centrifugal step followed by a depth filtration step (Shukla and Kandula, 2008).

In order to scale among different types of centrifuges, correction factors are used to account for the deviations from

 

ideal conditions such as those caused by differences in flow patterns (Mosqueira et al., 1981). Typically, Sigma theory is used to scale centrifuges irrespective of size, geometry, and type (Ambler, 1959). However, Sigma theory does not take into account the generation of small particles through cell damage in the high shear regions of centrifuge feed zones. In order to capture accurately these effects at laboratory-scale, the shear generated in the feed zone needs to be mimicked (Boychyn et al., 2001). A Rotating Shear Device (RSD) has been developed to reproduce the prevailing shear conditions in such feed zones (Boychyn et al., 2001). Operated in combination with a bench-top centrifuge, this has been shown to successfully predict the clarification efficiency of mammalian cell culture in a pilot-scale disk-stack centrifuge (Hutchinson et al., 2006). The RSD has also been used in conjunction with micro well plates using sub-millilitre volumes to successfully model pilot-scale centrifugation performance (Tait et al., 2009).

In the routine development of primary recovery operations, the performances of both centrifugal and filtration processes need to be characterized. The RSD was developed as an ultra scale-down (USD) tool to investigate under well-controlled and -defined conditions using small quantities of feedstock. Extensive publications have shown the utility of the RSD to understand the impact of exposure to various levels of shear as might be experienced in the centrifugal step at pilot to manufacturing scale (Boychyn et al., 2001; Hutchinson et al., 2006; Tait et al., 2009). However, in order to test secondary depth filter capacity, large quantity ($\approx$1 L) of centrate is required. The RSD is limited to shearing a maximum of 20 mL of material per run hence restricting its ability to provide the quantity of feedstock needed to characterize subsequent filtration performance. The Capillary Shear Device (CSD) has also shown to be a preparative device with the ability to mimic feed zone shear. Flow through the capillary enables the generation of energy dissipation rates (EDR) equivalent to those found in disk-stack centrifuges (Westoby et al., 2011). Furthermore, this methodology has shown that it can generate centrates with a particle size distribution equivalent to that from a large-scale centrifuge (Westoby et al., 2011). In theory, such a device can be used to produce unlimited quantities of sheared material. To date no comparison between the characteristics of the material prepared by the CSD and the established RSD has been published.

In this paper, a combination of scale-down devices was used to explore the impact of centrifugal separation on filter capacity so as to determine the best integration between the steps of centrifugal solids removal and submicron particulate elimination by depth filtration ahead of packed bed high resolution steps of purification. It explores the utility of the CSD to create a pool of sheared feed material for centrifugal separation and the creation of a realistic centrate pool for the subsequent characterization of the following depth filtration step. In this sense, it is proposed to use the CSD as a preparatory method for filtration studies greater than 1 L or more of feed material. Critical to the success of this approach is the quality of the CSD material. The process characteristics and properties of the CSD preparatory scale material are compared against the RSD as a proven method for scale-down studies.

## Materials and Methods

### Theoretical Considerations

A detailed discussion of scale-down centrifugation is given in prior studies (Boychyn et al., 2001; Hutchinson et al., 2006). In essence by maintaining the ratio of flow rate to equivalent settling area and accounting for deviations from ideal flow conditions, Sigma theory enables the direct comparison of clarification efficiencies between centrifuges of different sizes and geometries (Ambler, 1959). Hence, this methodology can be applied to predict the clarification performance of a disk-stack centrifuge using a laboratory bench-top centrifuge:

$$\frac{\frac{Q_{ds}}{c_{ds}\Sigma_{ds}}}{} = \frac{\frac{V_{lab}}{t_{lab}c_{lab}\Sigma_{lab}}}{}, \quad (1)$$

where $Q_{ds}$ is the volumetric flow rate into the disk-stack centrifuge, $V_{lab}$ is the volume of material used in the laboratory centrifuge, $t_{lab}$ is the centrifugation time, and $c_{ds}$ and $c_{lab}$ are correction factors that account for the non-ideal flow properties in the disk-stack and laboratory scale centrifuges, respectively. The correction factor for the disk-stack centrifuge is quoted to be $\approx$0.4 by (Pinheiro and Cabral, 1993) while the correction factor for the laboratory scale centrifuge is 1. Here, the relationship determined by Maybury et al. (2000) is used to describe the equivalent settling area of a laboratory-scale centrifuge ($\Sigma_{lab}$):

$$\Sigma_{lab} = \frac{V_{lab}\,\omega^2(3-2x-2y)}{6g\,\ln\,(2R_2/(R_2+R_1))}, \quad (2)$$

$\omega$ is the angular velocity of the rotor; $x$ and $y$ are the fractional acceleration and deceleration times. $R_1$ is the distance from the top of the liquid level of the centrifuge tube to the center of the laboratory-scale centrifuge's axis of rotation, while $R_2$ is the distance from the bottom of the centrifuge tube to the center of the axis of rotation. The equivalent settling area for a disk-stack centrifuge ($\Sigma_{ds}$) is described by:

$$\Sigma_{ds} = \frac{2}{3g}\pi\, z\,\omega^2\cot\theta\left(r_2{}^3 - r_1{}^3\right), \quad (3)$$

where $z$ is the total number of disks, $\theta$ is the half disk angle, $r_1$ and $r_2$ are the inner and outer disk radii, respectively.

### Cell Culture

Cell culture used in the experiments were generated using CHO cell lines expressing monoclonal antibody products. The cultures produced had a range of cell densities and viabilities measured at the day of harvest as summarized in Table I. Bench-scale cell culture was conducted in 3 L fed batch bioreactors while pilot-scale culture was performed in 50, 100, and 2000 L stainless steel bioreactors. All cultures are harvested between days 11 and 14 during the decline phase of growth.

### Rotating Shear Device (RSD)

The design, theory, and application of the rotating shear device to mimic levels of shear found in centrifuge feed zones has been

**Table I.** Cell culture properties.

| Material | Bio reactor size (L) | Cell density $\times 10^6$ (cells/mL) | Cell viability (%) |
|---|---|---|---|
| Culture-A | 100 | 24.5 | 68 |
| Culture-B | 100 | 26.8 | 58 |
| Culture-C | 2000 | 14.9 | 74 |
| Culture-D | 2000 | 16 | 70 |
| Culture-E | 2000 | 12.2 | 45 |
| Culture-F | 3 | 30.8 | 31 |
| Culture-G | 50 | 11.6 | 72 |

thoroughly covered in previous studies (Boychyn et al., 2004; Hutchinson et al., 2006; Maybury et al., 2000). The material to be sheared is held in a cylindrical chamber with a diameter of 50 mm and a height of 10 mm. A rotating disk located within the chamber creates the shear and has a diameter of 40 mm and a thickness of 1 mm. The correlation of the rotating speed of the disk to the levels of energy dissipation has been developed in previous studies (Boychyn et al., 2004). In the experiments conducted for this study, the rotating shear device was run at a range of speeds in order to identify the equivalent shear generated in both the Capillary shear device (CSD) and the pilot-scale centrifuge. Material was subjected to shear in the chamber for 20 s to ensure that the total content was equally exposed to shear generated by the rotating disk (Hutchinson et al., 2006).

## Capillary Shear Device (CSD)

The use of capillary based shear systems to mimic levels of energy dissipation experienced in disk-stack centrifugal processes have been extensively described in literature (Aucamp et al., 2014; Chan et al., 2006; Westoby et al., 2011). The CSD described in this publication consisted of a Harvard syringe pump (Cambridge, UK), 0.01″ ID 10 cm long Polyetheretherketone (PEEK) tubing, 10 mL glass syringe, and check valves as set out in Figure 1. The cell culture was delivered from a vessel to the glass syringe via a check valve (ID-2). Subsequently, the flow through the capillary was achieved through another check valve (ID-3) with the syringe pump in infuse mode. Varying the level of shear was achieved by adjusting the flow rate through the capillary. This relationship has been developed in more detail in previous studies (Ma et al., 2002; Mollet et al., 2004, 2007). The culture was kept well mixed using a stir plate and stir bar. The sheared material was collected in a sealed vessel.

## Identification of Pilot-Scale Centrifuge Shear

In order to identify the levels of shear at a range of different flow rates through the CSD, the lactate dehydrogenase (LDH) concentration of the cell culture was measured before and after shearing. The relationship between the level of LDH increase as a function of flow rate (Q) was established and used to calculate the capillary flow rate that resulted in an equivalent level of cell lysis in the preparative CSD to that of the standard ultra scale-down RSD. This provided the necessary bridging study between the RSD, preparative CSD, and the pilot-scale centrifuge.

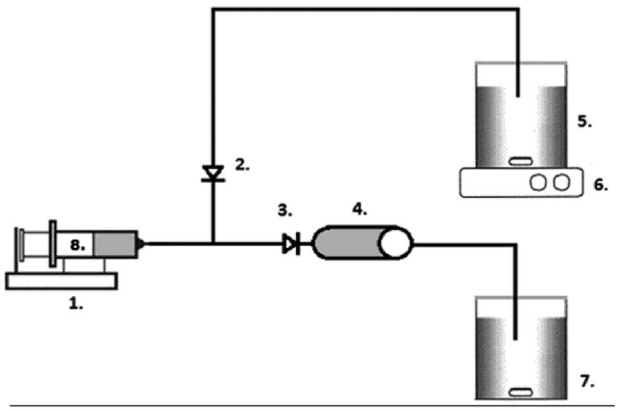


| ID | Make | Description |
|---|---|---|
| 1 | Harvard PHD Ultra | Syringe Pump |
| 2 | IDEX Health & Science | Check Valve |
| 3 | IDEX Health & Science | Check Valve |
| 4 | IDEX Health & Science | 10cm 0.01" ID High Pressure PEEK Tubing |
| 5,7 | Kimex | Beaker |
| 6 | Thermo Scientific Cimarec | Laboratory Stirrer/Hotplate |
| 8 | ILS | 10mL Glass Syringe |

**Figure 1.** Preparative CDS apparatus schematic and parts list.

## Identification of Pilot-Scale Centrifuge Separation Efficiency

Correction factors of ≈0.4 have been used to describe industrial disk-stack centrifuges; however, not all centrifuges behave identically. To estimate the correction factor of the pilot-scale centrifuges examined in this study, material was generated using the preparative CSD under conditions which corresponded to the level of shear observed in the centrifuge as verified by the RSD data. Subsequently, the sheared material was centrifuged in a bench top centrifuge at a range of $V/t\Sigma$. The supernatants from the range of centrifuged samples were analyzed for the extent of solids remaining. This data set was used to identify the best value for the effective centrifuge correction factor.

## Centrifuge Experiments and Protocols

### *Floor Swing-Out Rotor Centrifuge*

In order to generate large quantities of centrate required for depth filtration experiments, it was necessary to explore the preparative characteristics of the CSD. Immediately following exposure to capillary shear, the sheared cell culture material was placed into a series of 50 mL polypropylene tubes and centrifuged at 2600*g* with varying liquid height and for varying durations in order to generate the required range of $V/t\Sigma$. Centrifugation was conducted in a Beckman J-HC centrifuge with a JS 4.2A rotor (Brea, CA). The Optical Density (OD) of the supernatant was measured following each run at a wavelength of 600 nm.

### *Pilot-Scale Centrifuge*

Continuous flow Alfa Laval LAPX-404 and BTPX-305 disk-stack centrifuges (Lund, Sweden) were used to clarify the cell culture at large-scale. In the experiments conducted with the LAPX-404 flow

rates were set at 90–120 L/h and the rotational speed of the bowl was varied to generate between 6000 and 10,000 g while the larger BTPX-305's flow rate and bowl speed were maintained at 480 L/h and 12,500 g, respectively.

### Depth and Sterile Filtration Protocols

The centrate clarification experiments were conducted using a Millistak+ X0HC depth filter (EMD Millipore, Billerica, MA) with a nominal pore size ranging from 0.1 to 2 μm. Sterilizing grade SHC filters (EMD Millipore) were used to filter the depth filtered material. The SHC has a bilayer structure with a pore size rating of 0.5/0.2 μm.

Depth filtration capacity ($L/m^2$) was identified by observing the change in filter pressure at a constant flow rate. This approach is known as the $P_{max}$ methodology (Yavorsky et al., 2003). In this study, $P_{max}$ was defined as the capacity at which a pressure drop of 10 psi was reached. The experimental runs were conducted using a 23 $cm^2$ filter capsule at 200 LMH. Pressure drops and filtrate turbidities (NTU) were recorded for the duration of the experiment. In cases where the feed pool of centrate had been exhausted and a pressure of 10 psi had not been attained an intermediate pore blockage model was linearized (Eq. 4) to predict theoretically the volume of filtrate per filter area ($V$) required to reach a pressure ($\Delta P$) of 10 psi (Hlavacek and Bouchet, 1993). In the linearized equation, $a''$ and $b''$ were used as dimensionless coefficients.

$$\ln(\Delta P) = a''V + b'', \tag{4}$$

The capacity of SHC sterile filters required to filter the X0HC filtrate was established through the $V_{max}$ methodology (Badmington et al., 1995). Experiments were conducted with a 3.5 $cm^2$ at a constant pressure of 10 psi and the flux decline was monitored over time. The $V_{max}$ method is a linearized form (Eq. 5) of the pore constriction model used to compute theoretically the maximum volume of filtrate per unit filter area ($V_{max}$) that can be obtained before complete fouling through plugging occurs (Kong et al., 2010; Lau et al., 2013; Zydney and Ho, 2002).

$$\frac{t}{V} = \frac{1}{Q_0} + \left(\frac{1}{V_{max}}\right)t, \tag{5}$$

where $V$ is the total volume of filtrate volume per unit filter area collected over time ($t$) and $Q_0$ is the initial specific volumetric filtrate flow rate per unit filter area.

### Solids Remaining

The performance of a centrifuge in removing solids at any given set of operating conditions may be described by calculating the percentage of solids remaining in the supernatant ($S$).

$$S = \left(\frac{OD_s - OD_o}{OD_f - OD_o}\right) \times 100\%, \tag{6}$$

where $OD_s$ is the filtrate clarity post depth filtration, $OD_o$ is the base line for a well clarified centrate (obtained by extended centrifugation for 30 min at 16,000$g$ (Tait et al., 2009)) $OD_f$ refers to the clarity of the feed stream prior to depth filtration. All optical densities were measured at 600 nm.

### Characterization of Cell Lysis

Lactate dehydrogenase (LDH) is an intracellular enzyme that is only released during cell rupture. LDH increase was used to characterize the extent of cell lysis occurring during the centrifugation process (Ma et al., 2002; Petersen et al., 1988). It was also used to establish comparability between the established scale-down method for generating defined levels of shear (RSD) and the preparative CSD method explored in this study for the generation of filter feed volumes. Following assay protocols provided in the BioVision Kit (Milpitas, CA) samples that had been exposed to shear in *either* device were immediately centrifuged at 10,000$g$ for 15 min for the separation of cell debris from the sample. The supernatant was removed and combined with Nicotinamide adenine dinucleotide (NADH) and pyruvate solutions. The sample mixture was then aliquoted into a microwell plate and a microplate reader used to measure the absorbance change. The LDH increase ($LDH_{INC}$) was used calculated by dividing the change in LDH activity in the non-sheared sample ($LDH_{NS}$) and sheared sample ($LDH_{NS}$) by that of the non-sheared sample.

$$LDH_{INC} = \left(\frac{LDH_{SS} - LDH_{NS}}{LDH_{NS}}\right) \times 100\% \tag{7}$$

## Results and Discussion

Extensive work has been published on the use of the Rotating shear device (RSD) to understand the consequence of shear stress placed on cell culture materials and thus predicting the impact of similar levels of exposure prevailing in the feed zones of pilot-scale centrifuges. By the use of such a scale-down device it has been possible to approximate the levels of energy dissipation in both hydro and non-hydro hermetically sealed centrifuges (Boychyn et al., 2004). In this study, the need to prepare large quantities of sheared material so as to satisfy the feed requirements for subsequent filtration experiments was met by use of a Capillary shear device (CSD). Integral to this was the need to compare the product of this device to that of the RSD to demonstrate comparability in the amount of shear stress generated and of the resultant material properties. Figure 2 shows the LDH increase for a typical cell culture broth sheared using the CSD at flowrates from 12 to 20 mL/min and the RSD at rotational speeds between 6000 and 9000 RPM. A linear increase in LDH release is observed in both cases and the data from both systems overlap each other suggesting similar levels of energy dissipation can be generated using the two devices. These results encompass the flow rates reported in literature to mimic the shear in a hydro-hermetically sealed centrifuge for operation of a CSD (Westoby et al., 2011) and the range of rotational speeds used in the RSD to achieve the same mimic (Boychyn et al., 2004).

Having established the comparability of the two devices, the next step was to mimic the process performances of the pilot-scale centrifuges; Alfa Laval LAPX-404 and BTPX-305. The CSD was used

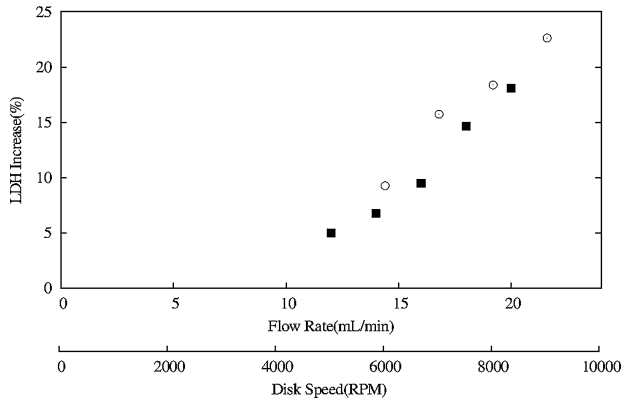


**Figure 2.** Comparison of LDH increase for Culture-A (Table I) sourced centrates generated using the preparative scale capillary shear device (CSD, ■) and rotating shear device (RSD, ○). The ranges tested for the rotational speed and flow rate incorporate literature values that have been shown previously to mimic the shear damage generated in a centrifuge equipped with a hyrdo-hermetic feed-zone.

as a proxy to approximate the levels of shear to which material is exposed inside the centrifuge at 6000, 7900, and 10,000*g* for the LAPX-404 and at 12,500*g* for the BTPX-305. Data shown in Figure 3 provided a correlation connecting the operating flow rate within the CSD to the conditions of operation in the LAPX-404 centrifuge (Table II) via levels of LDH increase ($LDH_{INC}$). Regression analysis of the modeling dataset and matching of the LDH increase showed that the levels of shear in the feed zone of the LAPX-404 and BTPX-305 were equivalent to the levels of shear created at a flow rate range of 16.6–18.0 mL/min in the CSD. This result is consistent with earlier published data (Westoby et al., 2011).

The next step of predicting the pilot-scale centrifuges' process performance was to identify the centrifuge correction factors. The

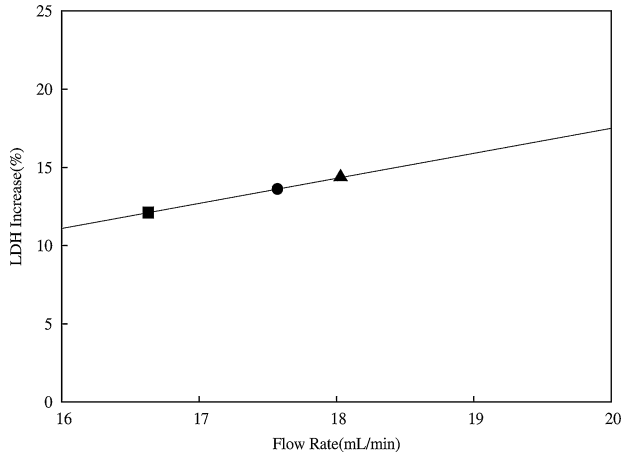


**Figure 3.** LDH increase for the modeling datasets generated by shearing material (Culture-B(—)) (Table I) using the preparatory CSD to identify the shear in the LAPX-404 centrate at conditions 1 (■), 2 (●), and 3 (▲) (Table II). Regression analysis was used to determine the following relationship between LDH increase ($LDH_{INC}$) and flowrate (Q) for Culture-B: $LDH_{INC} = 1.60\,Q - 14.49$, $R^2 = 0.98$.

relationship between solids remaining (S) and $V/t\Sigma$ was empirically determined ($S = 7.1 \times \ln(V/t\Sigma) - 130.3$, $R^2 = 0.99$) and the correction faction of the Alfa Laval LAPX-404 was found to be approximately 0.27 while a correction factor of 0.55 was established to describe the BTPX-305 (modeling data set: $S = 2.5 \times \ln(V/t\Sigma) - 48.0$, $R^2 = 0.99$). These results and other independent studies using multiple cell culture samples determined the correction factor of the LAPX-404 to be in the range of 0.27–0.31, confirming the correction factor values indicated were representative of the centrifuge's attributes. The preparative methodology based on the CSD was then used to mimic a set of $Q/c\Sigma$ in the LAPX-404 and BTPX-305 machines (Table II). The solids remaining in centrates generated using the CSD closely matched the solids remaining in centrates generated by the pilot-scale centrifuges (Fig. 4). This confirmed the validity of the approach to provide quantities of representative material for process integration studies.

In a typical mAb harvest process, the unit operation subsequent to centrifugation is depth filtration. If an accurate centrate mimic was to be developed, it had to show equivalent filtration properties to that of the centrate obtained at scale. Figure 5 shows the pressure and turbidity profiles generated during the operation of the X0HC depth filter provided with two feeds: the BTPX-305 centrate and the centrate from the preparative CSD approach calibrated against the established RSD scale-down tool. The CSD centrate showed pressure and turbidity profiles that closely matched those of the BTPX-305. This indicated that the CSD centrate had similar filtration properties to the BTPX-305 centrate, confirming utility of the preparative CSD.

Having established that the CSD can be used to prepare large quantities of sheared material for integrated process studies, the impact of the combination of centrifugal and depth filtration operating conditions on the performance of the primary recovery train was examined. Figure 6 shows the solids remaining and the X0HC and SHC capacities for centrates mimicking the LAPX-404 centrifuge at a range of conditions (Table II). Unsurprisingly, the increase in capacities of both X0HC and SHC are inversely related to the levels of solids remaining.

When the impact of flux on the X0HC depth filter and subsequent SHC sterile filtration operations was examined, it was found that with the given centrate an increase in flux from 50 to 200 LMH had no significant effect on the capacity of the depth filter (50 LMH: 407 $L/m^2$, 200 LMH: 435 $L/m^2$). The flux decline profiles (Fig. 7) for the SHC suggested that X0HC filtrates created at the two fluxes examined (50 and 200 LMH) had similar fouling propensities.

Subsequent studies focused on the impact of cell culture conditions on the performance of a harvest operation comprising centrifugation, depth filtration, and sterile filtration. The cell cultures examined represented differing extremes of harvest challenge; a difficult to harvest material and a relatively facile to recover broth. The former was from a bioreactor producing a high cell density, low viability cell culture whereas the latter was characterized by relatively low cell density and high cell viability.

It was shown that processing difficult to harvest cultures negatively impacted the ability of the centrifuge to remove solids (Fig. 8A). This form of material is challenging for harvest operations as there is a high solid content, leading to the centrifuge bowl filling up rapidly and requiring a high frequency of discharge. Another challenge was the low viability of the material. Such broths

**Table II.** Operational settings for pilot-scale centrifuge and corresponding CSD settings.

| | Pilot-scale centrifuge | | | Capillary shear device (CSD) | |
|---|---|---|---|---|---|
| Condition | Centrifuge | Flow rate (L/h) | Relative centrifugal force (g) | $Q/c\Sigma$, $V/t\Sigma \times 10^{-8}$ (m/s) | CSD flowrate (mL/min) |
| 1 | LAPX-404 | 90 | 6000 | 4.9 | 16.63 |
| 2 | LAPX-404 | 105 | 7900 | 2.92 | 17.57 |
| 3 | LAPX-404 | 120 | 10,000 | 1.65 | 18.03 |
| 4 | BTPX-305 | 480 | 12,500 | 2.2 | 17.08 |

will contain large populations of cell debris which are small in size and have a lower density than viable cells. The removal of such cell debris by centrifugation is difficult and these particles often end up in the centrate resulting in a poor separation. However, the easy to harvest broth has a lower solid content and a greater population of large viable cells, which facilitates separation. Furthermore, it may be expected that high cell viability may lead to healthy cells with intact cell walls and consequently, more resistant to shear damage within the centrifuge feed zone. This would be expected to yield a centrate of high clarity and fewer cell debris particles being passed on to subsequent filtration processes hence requiring much lower capacities when processing easy to harvest cultures (Fig. 8A). Figure 8B shows the X0HC pressures and turbidity profiles for centrates derived from both culture materials. Upon filtration, the centrate material from difficult harvest conditions showed significant increases in both the pressure and turbidity profiles ($\Delta$15.5 psi, $\Delta$8.7 NTU) compared to that of the easy to harvest material ($\Delta$6.0 psi, $\Delta$2.8 NTU). This can be directly attributed to the higher levels of smaller debris in the centrate of the high cell density culture causing a more rapid rate of pore blockage.

As noted in Figure 8A, processing of the difficult to harvest culture yielded lower SHC capacities compared to the easy to harvest culture. This was attributed to the larger amount of small particles carried through from the high cell density culture which in turn lead to a more rapid rate of pore blockage and flux decline (Fig. 8C).

## Conclusion

This work examines the impact of primary recovery process parameters and cell culture conditions on the performance of subsequent centrifugal harvest and both depth and sterile filtration as a process sequence. In order to characterize the process sequence, the ability to prepare adequate volumes of sheared samples was necessary. This study commenced by establishing the conditions of operation for a preparative device based on capillary shear to create levels of shear damage similar to the industrially accepted standard RSD used routinely for scale-down studies.

Experiments were conducted to determine the flow rates through the preparative CSD to generate equivalent levels to the shear developed in the standard RSD which has already been shown to match shear levels found in the feed zone of industrial disk-stack centrifuges. The centrates generated were then filtered. In the process of filtration, equivalent turbidity and pressure profiles were observed to those obtained when filtering centrate generated from a large-scale disk stack centrifuge.

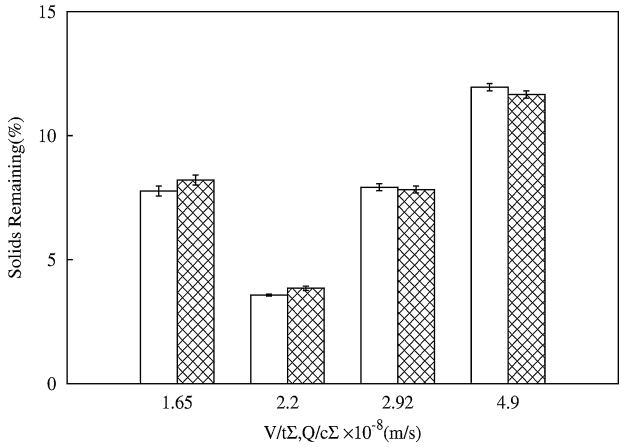


**Figure 4.** Comparison of solids remaining in centrate generated using the preparative CSD mimicking LAPX-404 and BTPX-305 at a range of conditions (Table II) marked in ☒ and solids remaining from pilot, scale centrifuge runs marked in □. Centrates generated for LAPX-404 were sourced from Culture-B (Table I) while the BTPX-305 centrate was sourced from Culture-C (Table I). The values plotted are shown as mean ± SD ($n = 3$).

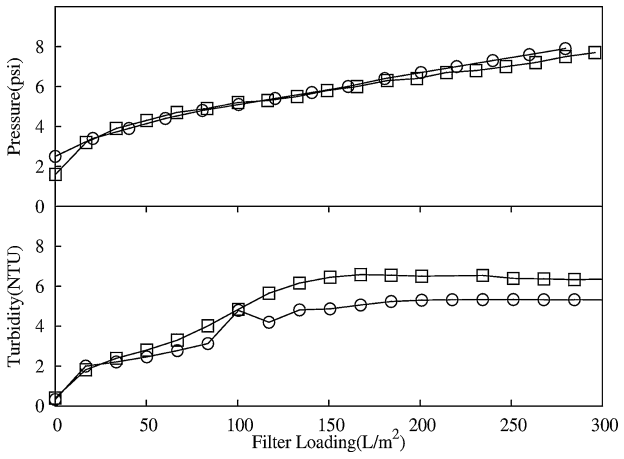


**Figure 5.** Comparison of pressure and turbidity profiles for 0.1–2.0 μm X0HC depth filter when filtering centrate from the BTPX-305 machine (○) and the mimic centrate (□) generated applying the preparative methodology presented in the paper. BTPX-305 centrate for this study was generated at a relative centrifuge force of 12,500*g*. Preparatory CSD centrate was processed to mimic the large-scale centrifuge. The material for this experiment was sourced from Culture-C (Table I) and filtered at 200 LMH.

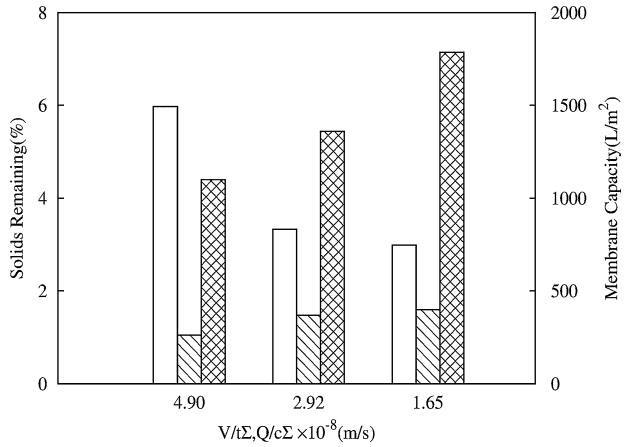


**Figure 6.** Comparison of solids remaining post centrifugation (□), and filter capacities of 0.1–2.0 μm X0HC depth filter (▽) and 0.2 μm SHC sterile filter (⊠). Data obtained from preparatory CSD centrate mimicking the LAPX-404 at a range of centrifugal conditions (Table II). All centrates and filtrates were generated from processing Culture-D (Table I).

The preparative methodology was then applied to explore how culture conditions impact primary recovery. One feed was from a culture producing high cell densities and low viabilities. This feed had a negative effect on the performance of a typical bioprocess sequence reducing the centrifuge capability to clear solids and also reducing the capacity of subsequent depth and sterile filtration processes. Altering the centrifugal operating conditions to produce centrates with lower solids remaining yielded higher capacities of both depth and sterile filters.

The proposed preparative methodology enables the user to calibrate and confirm the operating conditions of the CSD and bench centrifuge that would allow for predictive small-scale

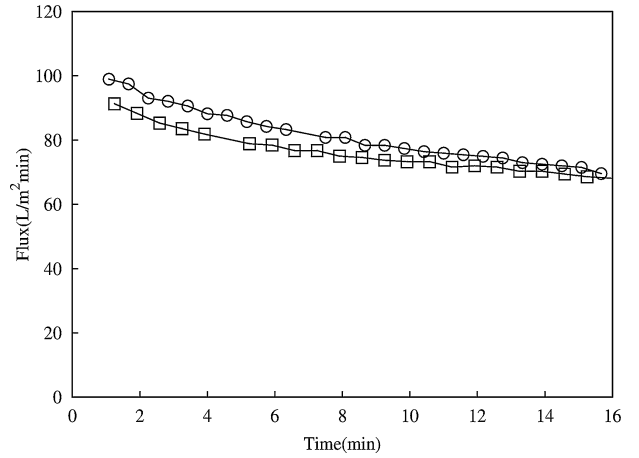


**Figure 7.** Comparison of 0.2 μm SHC sterile filter flux decline at 10 psi. Feed was from a 0.1 to 2.0 μm depth filter (X0HC) operated at 200 LMH (□) and 50 LMH (○). Both filtrates generated from processing Culture-E (Table I) using the preparatory CSD mimicking LAPX-404 at a *V*/tΣ of $2.92 \times 10^{-8}$ (m/s) (Table II).

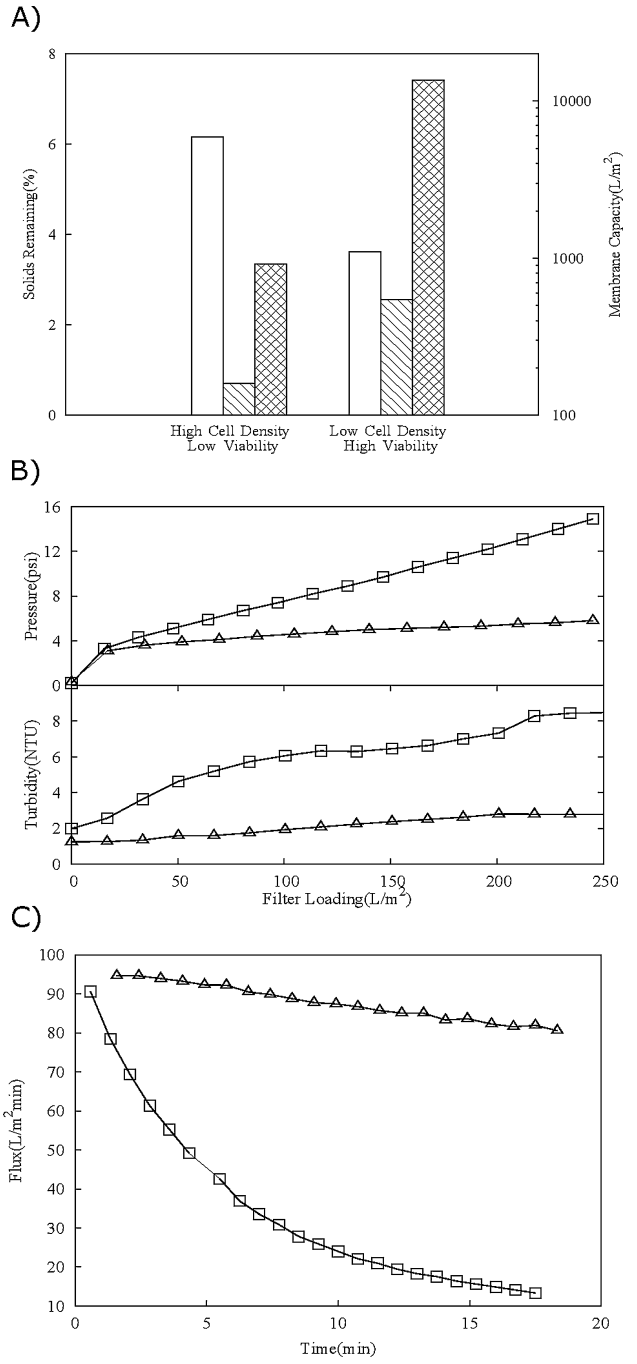


**Figure 8.** Comparison of process performance at different stages of the primary recovery sequence. Feed streams were sourced from two cell cultures representing difficult to harvest material (Culture-F) and easy to harvest material (Culture-G). The culture properties for this are listed in Table I. (**A**) (□) Post centrifugation mimicking LAPX-404 at a *V*/tΣ of $2.92 \times 10^{-8}$ (m/s) (Table II); (▽) capacity of 0.1–2.0 μm depth filter (X0HC) at 200 LMH; (⊠) capacity of 0.2 μm sterile filter (SHC) at 10 psi. (**B**) Comparison of pressure and turbidity profiles generated operating 0.1–2.0 μm depth filter (X0HC) processing centrate obtained via the preparative methodology using Culture-F (□) and Culture-G (△). Centrate generated to mimic the LAPX-404 operated at *V*/tΣ of $2.92 \times 10^{-8}$ (m/s). (**C**) Comparison of 0.2 μm sterile filter (SHC) flux decline for Culture-F (□) and Culture-G (△). The filtrate was generated through conditioning both cultures using the preparative methodology to mimic the LAPX-404 at *V*/tΣ of $2.92 \times 10^{-8}$ (m/s) and processing the centrate through a 0.1–2.0 μm depth filter (X0HC) at 200 LMH.

centrifuge and polishing filter performance. It was demonstrated that the scale-down methodology can successfully predict large-scale performance. This adds to the toolbox of available small-scale models for high throughput characterization of mammalian cell culture processes. Future work should leverage the methodology developed in this publication to incorporate a wider range of cell culture broths and other models of disk-stack centrifuges.

## Nomenclature

| | |
|---|---|
| $a''$, $b''$ | dimensionless coefficients for the linearized intermediate pore blockage model |
| c | correction factor to allow for flow conditions not considered in the theoretical derivation of $\Sigma$ for large-scale centrifuges |
| $LDH_{NS}$ | absorbance of no shear sample at 450 nm |
| $LDH_{SS}$ | absorbance of sheared sample at 450 nm |
| $OD_f$ | optical density of feed at 600 nm |
| $OD_o$ | optical density of well spun sample at 600 nm |
| $OD_s$ | optical density of supernatant at 600 nm |
| $P_{max}$ | predicted capacity at 10 psi for constant flow operations ($L/m^2$) |
| $Q_0$ | initial volumetric filtrate flow rate (L/h) |
| $Q_{ds}$ | flow rate of pilot scale disk-stack centrifuge (L/h) |
| $r_1$ | inner radius of centrifuge discs (m) |
| $r_2$ | outer radius of centrifuge discs (m) |
| $R_1$ | radius to sample surface in an individual tube (m) |
| $R_2$ | radius to sample base in an individual (m) |
| S | solids remaining in processed samples (%) |
| t | filtration time (h) |
| $t_{lab}$ | laboratory centrifugation time (h) |
| V | total filtrate volume per filter area ($L/m^2$) |
| $V_{lab}$ | volume of suspension in individual tubes (L) |
| $V_{max}$ | predicted maximum volume filtered per unit area for constant pressure operations ($L/m^2$) |
| x | fraction of overall centrifugation time for deceleration phase |
| y | fraction of overall centrifugation time for acceleration phase |
| z | number of discs in disc-stack centrifuge |
| $\sum_{ds}$ | equivalent disk stack centrifuge settling area ($m^2$) |
| $\sum_{lab}$ | equivalent laboratory centrifuge settling area ($m^2$) |
| $\omega$ | angular velocity ($s^{-1}$) |

## References


Ambler CM. 1959. The theory of scaling up laboratory data for the sedimentation type centrifuge. J Biochem Microbiol Technol Eng 1(2):185–205.

Aucamp JP, Davies R, Hallet D, Weiss A, Titchener-Hooker NJ. 2014. Integration of host strain bioengineering and bioprocess development using ultra-scale down studies to select the optimum combination: An antibody fragment primary recovery case study. Biotechnol Bioeng 111(10):1971–1981.

Axelsson H. 2002. Cell separation, centrifugation. In: Flickinger MC, Drew SW, editors. Encyclopedia of bioprocess technology. New York: Wiley. p 513–531.

Badmington F, Wilkins R, Payne M, Honig ES. 1995. Vmax testing for practical microfiltration train scale-up in biopharmaceutical processing. Pharm Technol 19(9):64–76.

Boychyn M, Yim S, Bulmer M, More J, Bracewell D, Hoare M. 2004. Performance prediction of industrial centrifuges using scale-down models. Bioprocess Biosyst Eng 26(6):385–391.

Boychyn M, Yim S, Shamlou PA, Bulmer M, More J, Hoare M. 2001. Characterization of flow intensity in continuous centrifuges for the development of laboratory mimics. Chem Eng Sci 56(16):4759–4770.

Chan G, Booth A, Mannweiler K, Hoare M. 2006. Ultra scale-down studies of the effect of flow and impact conditions during *E. coli* cell processing. Biotechnol Bioeng 95(4):671–683.

Hlavacek M, Bouchet F. 1993. Constant flowrate blocking laws and an example of their application to dead-end microfiltration of protein solutions. J Membr Sci 82(3):285–295.

Hutchinson N, Bingham N, Murrell N, Farid S, Hoare M. 2006. Shear stress analysis of mammalian cell suspensions for prediction of industrial centrifugation and its verification. Biotechnol Bioeng 95(3):483–491.

Jain M, Paranandi M, Roush D, Göklen K, Kelly WJ. 2005. Using cfd to understand how flow patterns affect retention of cell-sized particles in a tubular bowl centrifuge. Ind Eng Chem Res 44(20):7876–7884.

Kempken R, Preissmann A, Berthold W. 1995. Assessment of a disc stack centrifuge for use in mammalian cell separation. Biotechnol Bioeng 46(2):132–138.

Kong S, Aucamp J, Titchener-Hooker NJ. 2010. Studies on membrane sterile filtration of plasmid dna using an automated multiwell technique. J Membr Sci 353(1–2):144–150.

Lau EC, Kong S, McNulty S, Entwisle C, Mcilgorm A, Dalton KA, Hoare M. 2013. An ultra scale-down characterization of low shear stress primary recovery stages to enhance selectivity of fusion protein recovery from its molecular variants. Biotechnol Bioeng 110(7):1973–1983.

Ma N, Koelling KW, Chalmers JJ. 2002. Fabrication and use of a transient contractional flow device to quantify the sensitivity of mammalian and insect cells to hydrodynamic forces. Biotechnol Bioeng 80(4):428–437.

Maybury JP, Hoare M, Dunnill P. 2000. The use of laboratory centrifugation studies to predict performance of industrial machines: Studies of shear-insensitive and shear-sensitive materials. Biotechnol Bioeng 67(3):265–273.

Mollet M, Godoy-Silva R, Berdugo C, Chalmers JJ. 2007. Acute hydrodynamic forces and apoptosis: a complex question. Biotechnol Bioeng 98(4):772–788.

Mollet M, Ma N, Zhao Y, Brodkey R, Taticek R, Chalmers JJ. 2004. Bioprocess equipment: Characterization of energy dissipation rate and its potential to damage cells. Biotechnol Prog 20(5):1437–1448.

Mosqueira FG, Higgins JJ, Dunnill P, Lilly MD. 1981. Characteristics of mechanically disrupted bakers' yeast in relation to its separation in industrial centrifuges. Biotechnol Bioeng 23(2):335–343.

Petersen JF, McIntire LV, Papoutsakis E. 1988. Shear sensitivity of cultured hybridoma cells (crl-8018) depends on mode of growth, culture age and metabolite concentration. J Biotechnol 7(3):229–246.

Pinheiro H, Cabral JMS. 1993. Centrifugation. In: Kennedy JF, Cabral JMS, editors. Recovery processes for biological materials. Chichester: John Wiley & Sons Ltd. p 145.

Rathore AS. 2009. Roadmap for implementation of quality by design (qbd) for biotechnology products. Trends Biotechnol 27(9):546–553.

Shukla AA, Kandula JR. 2008. Harvest and recovery of monoclonal antibodies: Cell removal and clarification. In: Gottschalk U, editor. Process scale purification of antibodies. Hoboken, New Jersey: John Wiley & Sons, Inc. p 53–78.

Tait A, Aucamp J, Bugeon A, Hoare M. 2009. Ultra scale-down prediction using microwell technology of the industrial scale clarification characteristics by centrifugation of mammalian cell broths. Biotechnol Bioeng 104(2):321–331.

Titchener-Hooker N, Dunnill P, Hoare M. 2008. Micro biochemical engineering to accelerate the design of industrial-scale downstream processes for biopharmaceutical proteins. Biotechnol Bioeng 100(3):473–487.

Westoby M, Rogers JK, Haverstock R, Romero J, Pieracci J. 2011. Modeling industrial centrifugation of mammalian cell culture using a capillary based scale-down system. Biotechnol Bioeng 108(5):989–998.

Yavorsky D, Blanck R, Lambalot C, Brunkow R. 2003. The clarification of bioreactor cell cultures for biopharmaceuticals. Pharm Technol 27(3):62–67.

Yigzaw Y, Piper R, Tran M, Shukla AA. 2006. Exploitation of the adsorptive properties of depth filters for host cell protein removal during monoclonal antibody purification. Biotechnol Prog 22(1):288–296.

Zydney AL, Ho CC. 2002. Scale-up of microfiltration systems: Fouling phenomena and Vmax analysis. Desalination 146(1–3):75–81.

Biotech Method

# An Automated Laboratory-scale Methodology for the Generation of Sheared Mammalian Cell Culture Samples

Adrian Joseph[1], Stephen Goldrick[1], Michael Mollet[3], Richard Turner[2], Jean Bender[3], David Gruber[2], Suzanne S Farid[1], Nigel Titchener-Hooker [1]

[1]The Advanced Centre of Biochemical Engineering, Department of Biochemical Engineering, University College London, Gordon Street, London, WC1H 0AH, UK

[2]MedImmune, Milstein Building, Granta Park, Cambridge, CB21 6GH, UK

[3]MedImmune Gaithersburg Headquarters, One MedImmune Way, Gaithersburg, MD 20878, USA

**Correspondence:** Professor Nigel Titchener-Hooker, The Advanced Centre of Biochemical Engineering, Department of Biochemical Engineering, University College London, Gordon Street, London WC1H 0AH, United Kingdom

- **E-mail:** nigelth@ucl.ac.uk

**Keywords:** Capillary shear; Disk-stack centrifuge; Energy dissipation rate; Mammalian cell; Scale-down

**Abbreviations: CSD,** capillary shear device; **CFD,** computational fluid dynamics; **EDR,** energy dissipation rates; **LDH,** Lactate dehydrogenase; **mAb,** monoclonal antibody; **PSD,** particle size distribution; **QbD,** quality by design; **RSD,** rotating shear device



This is the author manuscript accepted for publication and has undergone full peer review but has not been through the copyediting, typesetting, pagination and proofreading process, which may lead to differences between this version and the Version of Record.
Please cite this article as doi: 10.1002/biot.201600730.

Submitted: 14-Dec-2016
Revised: 12-Feb-2017
Accepted: 12-Feb-2017

Abstract

Continuous disk-stack centrifugation is typically used for the removal of cells and cellular debris from mammalian cell culture broths at manufacturing-scale. The use of scale-down methods to characterise disk-stack centrifugation performance enables substantial reductions in material requirements and allows a much wider design space to be tested than is currently possible at pilot-scale. The process of scaling down centrifugation has historically been challenging due to the difficulties in mimicking the Energy Dissipation Rates (EDRs) in typical machines. This paper describes an alternative and easy-to-assemble automated capillary-based methodology to generate levels of EDRs consistent with those found in a continuous disk-stack centrifuge. Variations in EDR were achieved through changes in capillary internal diameter and the flow rate of operation through the capillary. The EDRs found to match the levels of shear in the feed zone of a pilot-scale centrifuge using the experimental method developed in this paper ($2.4\times10^5$ W/Kg) are consistent with those obtained through previously published computational fluid dynamic (CFD) studies ($2.0\times10^5$ W/Kg). Furthermore, this methodology can be incorporated into existing scale-down methods to model the process performance of continuous disk-stack centrifuges. This was demonstrated through the characterisation of culture hold time, culture temperature and EDRs on centrate quality.

## 1 Introduction

Understanding a product's key quality attributes and its process of manufacture through the use of design spaces is a regulatory requirement for biopharmaceutical manufacturers [1]. In typical mammalian cell culture purification platforms multiple unit operations each with individual process parameters affect the critical quality attributes of a product. Adoption of a Quality by Design (QbD) approach can help in defining the design space especially when combined with high throughput scale-down techniques to generate considerable quantities of data that mimic commercial-scale unit operations [2]. These extensive experimental datasets enable a thorough understanding of the effect input parameters have on process performance and the product's critical quality attributes [3]. Monoclonal antibody (mAb) manufacturing platforms often begin with the processing of cell culture material for the removal of cells and cellular debris. Disk-stack centrifuges are typically used at manufacturing-scale because of their capacity to handle a wide variety of feedstock [4]. They also enable processing in a continuous fashion by utilizing the functionality of a semi-continuous solids discharge [5]. However, most disk-stack centrifuge designs suffer from high levels of shear being present in the feed zones. This results in breakage of shear-sensitive mammalian cells creating sub-micron particles. In order to understand the potential effects of sub-micron particles on subsequent unit operations, pilot-scale studies (>50L harvest material) are often conducted.

Pilot-scale studies are material, time and resource-intensive. Scale-down methods potentially allow for the reduction of these requirements and enable such studies to be conducted at laboratory-scale. Methods incorporating Sigma Theory [6] facilitate such scaling down and hence enable subsequent comparisons between centrifuges of varying geometries and sizes. These methods however do not consider the effect of shear experienced in the feed zones, typically associated with disk-stack centrifugation [7].

Many studies have shown the exposure of mammalian cells to shear through flow constriction [8,9] or through the use of rheometers [10-12] can have a detrimental effect on cell viability. A number of

devices described in the literature were shown to generate levels of shear comparable to those prevailing in the feed zone of typical disk-stack centrifuges [7,13-16]. Most devices are based upon either the Rotating disk shear device (RSD) or the Capillary shear device (CSD). The RSD developed at University College London [7,13-14] mimics the prevailing shear in disk-stack centrifuge feed zones. The capillary shear device developed by Westoby et al., [15] has also shown the ability to generate levels of shear similar to those of a disk-stack centrifuge feed zone. Additionally, the combination of both devices (RSD and CSD) with a laboratory-scale centrifuge have been shown to create centrates with comparable levels of solids remaining to those from a disk-stack centrifuge [7,13-16]. This publication develops an automated experimental methodology based upon the CSD capable of generating a range of shear levels typically produced in the feed zone of a disk-stack centrifuge in addition to quantifying the back pressure enabling calculation of the EDRs. EDR is the irreversible rate of increase in internal energy within a system. The effect of EDR on cell culture has been used in previous studies to characterise bioprocess-related scenarios such as centrifugation [7,13-15] and cross flow filtration [17]. The unique feature of the approach described in this paper lies in the ability to use commonly available laboratory equipment to enable these functionalities and facilitate high throughput experimentation. The methodology is based on a simple setup utilizing standard downstream processing laboratory equipment. The method requires a Fast protein liquid chromatography (FPLC) instrument to act as the delivery system which enables high flow rates to be reached at high back pressures and has the added utility of generating performance feedback through back pressure readings. This provides a preparative bench top route for the exposure of samples to defined levels of shear ahead of rating studies of typical clarification steps e.g. centrifugation and depth filtration.

## 2 Materials and methods

### 2.1 Energy dissipation rate (EDR)

EDR is the irreversible rate of increase in internal energy within a system. It is measured in terms of unit of power per unit volume or mass. Under laminar flow conditions within a capillary, the maximum energy dissipation ($\varepsilon_{max}$) occurs at the capillary wall. This can be described (Equation 1) as a function

of pressure increase ($\Delta P$), where; $l$ and $D$ are the length and diameter of the capillary; $\mu$ and $\rho$ are the viscosity and density of the process fluid [15].

$$\varepsilon_{max} = \frac{D^2 \Delta P^2}{16 l^2 \mu \rho} \quad (1)$$

**2.2 Cell culture**

The cell culture material was generated using CHO cell lines expressing mAb products. The cultures were produced at bench-scale (5 L) and pilot-scale (100 L) bioreactors and were harvested during the decline phase of growth (days 11-14). Table 1 summarises the cell culture properties at time of harvest. Cell density and cell viability of the culture were measured through an industrial standard trypan blue dye exclusion method [18]. The ViCell (Beckman Coulter, High Wycombe, UK) was also used to provide Particle Size Distribution (PSD) data based on trypan blue stained images.

**2.3 Fast protein liquid chromatography (FPLC) instrument and super loop**

An AKTA Explorer (GE Life Sciences, Uppsala, Sweden) was used as the FPLC system. Through the use of accurate piston pump devices this system is capable of delivering flow rates up to 100 mL/min with an accuracy of ±2%. It is also configured with monitors for multi-wavelength detection, conductivity and pressure. Superloops (GE Life Sciences) are often used in a chromatographic setting for sample injection and collection while in this paper they were used for the injection of cell culture material through the capillary. A method was developed that comprised of two parts; first the sample is loaded into the Superloop using the peristaltic (low shear) sample pump. Once loaded the piston pumps displace the feed from the Superloop though the capillary and into a collection vessel (Figure 1). Using the Unicorn control software's scouting functionality and this method, multiple conditions (different feed material, flow rates, capillaries sizes etc.) could be queued and run sequentially without manual intervention.

**2.4 Capillary shear device (CSD)**

Adjusting the flow rate of the piston pump and altering the stainless steel capillary diameter of the CSD allowed varying levels of shear to be imposed on the cell culture material. Previous studies have established the relationship between shear, flow rate and capillary diameter in detail [15,19-21].

### 2.5 Analytical techniques

#### 2.5.1 LDH release

Lactate dehydrogenase (LDH) is an enzyme that is released during cell rupture. In this paper % LDH release ($LDH_{REL}$) was used as a measure of the shear levels experienced at varying flow rates [17] of the CSD and during operation of the pilot-scale centrifuge. Assay protocols (Abcam, Cambridge, UK) provided by the supplier were followed to identify % LDH release. $LDH_{REL}$ was calculated by dividing the difference between LDH release from the sheared sample ($LDH_{SS}$) and the no shear sample ($LDH_{NS}$) by the difference between the total LDH release ($LDH_{TR}$) sample and the no shear sample. The total LDH release sample was generated through mixing the non-sheared cell culture sample with a lysis solution at 1/10 dilution which was subsequently incubated for 30 minutes. This ensured all cell membranes were ruptured and provided the total amount of LDH present. The % LDH release ($LDH_{REL}$) following exposure to shear in the CSD was calculated using Equation 2.

$$LDH_{REL} = \left(\frac{LDH_{SS} - LDH_{NS}}{LDH_{TR} - LDH_{NS}}\right) \times 100 \quad (2)$$

#### 2.5.2 Turbidity

The performance of the centrifuge for the removal of cell and cellular debris was quantified offline by measuring the turbidity of the centrate in an Orion Thermo Scientific (Waltham, MA, USA) turbidity meter. Centrates were placed in clear 10 mL glass vials and illuminated at a wavelength of 450 nm. The intensity of transmitted light received by the detector was quantified in nephelometric turbidity units (NTU). Centrates with high cell debris content translated to >100 NTU and similarly low cell debris levels translated to <100 NTU.

### 2.6 Pilot-scale and laboratory-scale centrifugation

A continuous GEA Westfalia SO1-06-107 (Oelde, Germany) disk-stack centrifuge was used to generate centrates at pilot-scale. These experiments were conducted at a set bowl speed of 10,000 RPM and flow rates were varied between 0.3-0.9 L/min. A laboratory-scale Beckman J-HC centrifuge with a JS 4.2A rotor (Brea, CA, USA) was used to process material following exposure to shear in the CSD.

### 2.6.1 Identification of pilot-scale centrifugation shear

The levels of shear corresponding to a range of different EDRs generated in the CSD were estimated by measurement of the LDH concentration of the cell culture measured before and after shear (Equation 2). The relationship between the levels of LDH release as a function of maximum energy dissipation rate ($\varepsilon_{max}$) was established. The level of shear in the pilot-scale centrifuge was quantified by matching the level of % LDH release in the centrate to the existing relationship between % LDH release and maximum energy dissipation rate ($\varepsilon_{max}$).

## 3 Results and discussion

### 3.1. CSD characterisation

This section summarises the performance of the methodology developed to enable a range of EDRs relevant to the feed zone of disk-stack centrifugation to be investigated in an automated and high throughput manner. A key advantage of using a FPLC instrument as a delivery system was that it enabled higher flow rates to be reached when compared to typical syringe pumps [16] which were unable to maintain a set flow rate at high back pressures. Furthermore, the FPLC instrument had the utility of generating performance feedback through back pressure readings which enabled the calculation of EDRs (Equation 1). With this functionality Figure 2A examines the effect of changes in capillary diameter and operational flow rates on the back pressures and EDRs developed. The relationship between capillary internal diameter and pressure increase is very well understood [22] and experimentally explored in a previous study [15], as expected it was found that increasing operational flow rate resulted in higher back pressures. The relationship between flow rate and back pressure becomes more pronounced with narrower internal capillary diameters. Furthermore, the pressures found in this experiment were within the range quoted by Westoby et al., [15] when processing mammalian cell culture through a capillary with an internal diameter of 0.01" confirming consistency with earlier published data.

Higher levels of cellular damage are associated with high levels of cellular debris, leading to increased centrate turbidities [15]. Figure 2Bi shows the extent of small cellular debris created as assessed through centrate turbidity for two capillaries of different diameters. An increase in turbidity was expected with increased CSD flow rates for both capillaries but there was significantly more damage when the material was passed through the 0.007" capillary compared to the 0.01" capillary (Figure 2Bi). This was due to the higher levels of energy dissipation (Figure 2Bii) created using the narrower 0.007" capillary which resulted in higher levels of breakage and hence an increase in centrate turbidity post shear. Figure 2Bi also suggests that in order for the 0.01" capillary to generate equivalent amounts of energy dissipation to that of the 0.007" capillary, and hence generate the same levels of damage the operational flow rate through the 0.01" capillary would be required to increase significantly.

Figure 3A shows the effect of increased EDR on the PSD of cell culture material. With increased levels of EDR there was a reduction of counts for particles greater than 20μm. This suggests the breakup of viable and non-viable cells into finer particulates. Particles below 6 μm are below the detection limit of the ViCell hence the build-up of <6μm fines could not be quantified but had to be inferred. Trypan blue stained images obtained from the ViCell showed large quantities of small particulates present in cell culture samples exposed to increased EDRs using the CSD (Figure 3Bi-iv).

A correlation (Figure 4A) was developed between the levels of LDH release through operation of the CSD at a range of EDRs ($1.2\times10^5$-$10.7\times10^5$ W/Kg). Regression analysis of the dataset showed that LDH release from the centrifuge was equivalent to an EDR of $2.4\times10^5$ (W/Kg) created using the CSD with a 0.01" capillary. The values found in this study match closely those from earlier published data [7,23] where CFD analysis of a similar non-hermetic GEA Westfalia SAOOH disk-stack centrifuge (Oelde, Germany) reported an EDR of $2.0\times10^5$ (W/Kg). As such these results validate the methodology developed to identify levels of shear prevailing within a centrifuge.

The process performance of a given disk-stack centrifuge can be altered through changes in bowl speed and flow rate. A previous study [16] has shown that increases in bowl speed lead to higher levels of shear, as quantified through LDH release. In the present study (Figure 4B) the effect of flow rate, at a fixed bowl speed on shear damage was explored. Figure 4B shows there was a decrease in the levels of LDH release with increasing flow rate (0.3-0.9 L/min). The operation of disc-stack centrifuges at low flow rates can lead to prolonged exposure of shear sensitive mammalian cells to the high shear feed-zone region [24,25]. The decrease in LDH release observed could be as a result of the lower residence times which accompany the operation of the centrifuge at an increased flow rate [26]. Furthermore, the levels of LDH release in the centrate from this experiment (10%) was consistent with the values obtained in earlier experiments which quantified the prevailing levels of shear in a GEA Westfalia SO1-06-107 disk-stack machine (Oelde, Germany).

**3.2 Industrial case study**

Upstream developments in mammalian cell culture have led to increased titres often resulting in high cell density cell culture streams with elevated levels of host-cell impurities (e.g. host-cell proteins, DNA), which increase the burden on subsequent purification operations [27]. To address these levels of impurities, non-chromatographic techniques to alter cell culture broth conditions pre-harvest are increasingly commonplace [28]. These alterations typically involve changes in pH conditions or broth temperature so as to improve the performance of subsequent unit operations [29]. The CSD based method developed in this paper was integrated with existing scale-down centrifugation methods [15,16] to characterize the influence of hold time, temperature and levels of shear on the performance of the disk-stack centrifugation step. Figure 4C shows there is a clear increase in supernatant turbidity with increasing levels of shear as would be expected. Statistical analysis of the variables hold time, temperature and level of shear revealed shear to be the most influential parameter (P-Value=0.003) that affected the turbidity of the centrate. This is not surprising as higher levels of shear result in higher levels of cell rupture and subsequent generation of fine particulates which are difficult to remove through centrifugal separation. Figure 4Ci suggests longer hold times at lower temperatures ($5^{O}C$) had a negative effect on separation performance. This is likely due to the higher viscosities that

are expected when operating at lower temperatures ($5^{O}C$) which hinders centrifugal separation. Conversely higher temperatures ($35^{O}C$) are expected to yield better levels of clarification with an increased hold time. However, in this experiment higher temperatures and increased hold time resulted in the rapid reduction in viability of the material from 94% at the start of the experiment to 60% at 3 hours and subsequently to 17% at 6 hours. At lower viabilities there was an increased population of fine particulates which were difficult to remove through centrifugation and hence resulted in high turbidities being present in the centrate potentially challenging latter filtration operations. Typical continuous disk-stack centrifuge processes platforms operate at a fixed bowl speed. Changes in shear as a result of alterations to the bowl speed are therefore unlikely but there is a potential for the cell broth under certain circumstances to be held before processing over an extended period of time. This study identified that hold time and temperature can each have a significant influence on the performance of the centrifugation step.

**4 Concluding remarks**

The purpose of this work was to develop an alternative methodology to those available in the literature in order to characterize the shear generated when utilizing continuous disk-stack centrifugation and enable high-throughput experimentation. Studies were conducted to show that the Capillary shear device (CSD) using the automated methodology developed in this paper had the ability process cell culture to create multiple levels of shear simply through changes in capillary diameter and operational flow rates. The developed method also had the ability to quantify back pressure hence having the ability to estimate Energy dissipation rates (EDR). Furthermore, the CSD had the ability to generate the levels of shear created in the feed zone of a pilot-scale disk-stack centrifuge. The EDR values obtained in this publication describing non-hermetic centrifuges matched closely those developed in the literature using Computational fluid dynamics (CFD) for a pilot-scale centrifuge with a similar design. The methodology was also used in combination with existing scale-down centrifugation protocols to give an insight into the negative influence of high temperatures and lengthy hold times on centrifugation through increases in centrate turbidity which would result in a potential reduction in the ease of filtration for the subsequent depth and sterile filtration steps.

**Acknowledgement**

Financial support from the UK Engineering and Physical Sciences Research Council (EPSRC) and MedImmune for the Engineering Doctorate studentship for A. Joseph is gratefully acknowledged. The work presented is associated with the joint UCL-MedImmune Centre of Excellence for predictive multivariate decision-support tools in the bioprocessing sector and the EPSRC Centre for Innovative Manufacturing in Emergent Macromolecular Therapies hosted by the UCL Biochemical Engineering. Grant code: EP/G034656/1.

**5 References**

[1] Luciani, F., Galluzzo, S., Gaggioli, A., et al. Implementing quality by design for biotech products: Are regulators on track? *mAbs*. 2015, *7*, 451-455.

[2] Rathore, A. S., Mhatre, R., Quality by design for biopharmaceuticals: principles and case studies. *Considerations for biotechnology product quality by design*, John Wiley & Sons, 2011, pp. 9-27.

[3] Titchener-Hooker, N., Dunnill, P., Hoare, M., Micro biochemical engineering to accelerate the design of industrial-scale downstream processes for biopharmaceutical proteins. *Biotechnology and Bioengineering*. 2008, *100*, 473-487.

[4] Russell, E., Wang, A., and Rathore, A., Harvest of a Therapeutic Protein Product from High Cell Density Fermentation Broths. *Process Scale Bioseparations for the Biopharmaceutical Industry*, CRC Press, 2006, pp 1 -58.

[5] Axelsson, H., Cell Separation, Centrifugation, *Encyclopedia of Industrial Biotechnology* John Wiley & Sons, 2010, pp 1–21.

[6] Ambler, C. M., The theory of scaling up laboratory data for the sedimentation type centrifuge. *Journal of Biochemical and Microbiological Technology and Engineering*. 1959, *1*, 185-205.

[7] Boychyn, M., Yim, S., Shamlou, P. A., Bulmer, M., More, J., Hoare M., Characterization of flow intensity in continuous centrifuges for the development of laboratory mimics. *Chemical Engineering Science*. 2001, *56*, 4759-4770.

[8] Born, C., Zhang, Z., Al-Rubeai, M., Thomas, C. R., Estimation of disruption of animal cells by laminar shear stress. *Biotechnology and Bioengineering*, 1992, *40*, 1004-1010.

[9] Garcia-Briones, M. A., Chalmers, J. J., Flow parameters associated with hydrodynamic cell injury. *Biotechnology and Bioengineering*. 1994, *44*, 1089-1098.

[10] Kretzmer, G., Schugerl, K., Response of mammalian cells to shear stress. *Applied Microbiology and Biotechnology*. 1991, *34*, 613–616.

[11] Abu-Reesh, I., Kargi, F., Biological responses of hybridoma cells to defined hydrodynamic shear stress. *Journal of Biotechnology*. 1989, *9*, 167-178.

[12] Petersen, J. F., McIntire, L. V., Papoutsakis, E. T., Shear sensitivity of cultured hybridoma cells (CRL-8018) depends on mode of growth, culture age and metabolite concentration. *Journal of Biotechnology*. 1988, *7*, 229-246.

[13] Hutchinson, N., Bingham, N., Murrell, N., Farid, S. et al., Shear stress analysis of mammalian cell suspensions for prediction of industrial centrifugation and its verification. *Biotechnology and Bioengineering*. 2006, *95*, 483–491.

[14] Tait, A., Aucamp, J., Bugeon, A., Hoare, M., Ultra scale-down prediction using microwell technology of the industrial scale clarification characteristics by centrifugation of mammalian cell broths. *Biotechnology and Bioengineering*. 2009, *104*, 321-331.

[15] Westoby, M., Rogers, J. K., Haverstock, R., Romero, J., Pieracci, J., Modeling industrial centrifugation of mammalian cell culture using a capillary based scale-down system. *Biotechnology and Bioengineering*. 2011, *108*, 989-998.

[16] Joseph, A., Kenty, B., Mollet, M., Hwang, K., Rose, S., Goldrick, S., Bender, J., Farid, S. S., Titchener-Hooker, N., A scale-down mimic for mapping the process performance of centrifugation, depth and sterile filtration. *Biotechnology and Bioengineering*. 2016, *113*, 1934–1941.

[17] Vickroy B., Lorenz K., Kelly W., Modeling shear damage to suspended CHO cells during crossflow filltration, *Biotechnology Progress*. 2007, *23*, 194-199.

[18] Stoddart, M., "Mammalian cell viability: methods and protocols." *Methods in Molecular Biology*. 2011, 740, pp 1-6.

[19] Chan, G., Booth, A., Mannweiler, K., Hoare, M., Ultra scale-down studies of the effect of flow and impact conditions during *E.coli* cell processing. *Biotechnology and Bioengineering*. 2006, *95*, 671-683.

[20] Ma, N., Koelling, K. W., Chalmers, J. J., Fabrication and use of a transient contractional flow device to quantify the sensitivity of mammalian and insect cells to hydrodynamic forces. *Biotechnology and Bioengineering*. 2002, *80*, 428-437.

[21] Mollet, M., Ma, N., Zhao, Y., Brodkey, R., Taticek, R., Chalmers, J. J., Bioprocess equipment: Characterization of energy dissipation rate and its potential to damage cells. *Biotechnology progress*. 2004, *20*, 1437-1448.

[22] Bird, R., Stewart, W., Lightfoot, E., *Transport Phenomena*. Wiley International edition, Wiley, 2007.

[23] Boychyn, M., Yim, S., Bulmer, M., More, J., Bracewell, D., Hoare, M., Performance prediction of industrial centrifuges using scale-down models. *Bioprocess and Biosystems Engineering*. 2004, *26*, 385-391.

[24] Han, X., Hewig, A., Vedantham, G., Recovery and Purification of Antibody. *Antibody Expression and Production*. Springer Verlag. 2011, pp 305-320.

[25] Russell, E., Wang, A., Rathore, A. S., Harvest of a therapeutic protein product from high cell density fermentation broths: Principles and Case study. *Process scale bioseparations for the biopharmaceutical industry*. CRC press. 2006, pp 1-59.

[26] Bender, J., Brown, A., Winter, C., Scale-up of a disc stack centrifuge for CHO harvest, *Downstream Gab '02 abstracts*. Amersham Biosciences. 2002, pp 10–11.

[27] Gupta, S. Implementation of CQA (Critical Quality Attribute) based approach for development of biosimilars*, Continuous Processing in Pharmaceutical Manufacturing*, Wiley-VCH Verlag GmbH & Co. KGaA, Weinheim, Germany. 2014, pp 357-383.

[28] Shukla A., Thömmes J., Recent advances in large-scale production of monoclonal antibodies and related proteins. *Trends in Biotechnology*. 2010, *28,* 253-261.

[29] Westoby, M., Chrostowski, J., de Vilmorin, P., Smelko, J. P., Romero, J. K., Effects of solution environment on mammalian cell fermentation broth properties: Enhanced impurity removal and clarification performance. *Biotechnology and Bioengineering*. 2011, *108*, 50-58.

**Tables**

**Table 1. Properties of cell culture materials used in CSD studies**

| Material | Bio Reactor Size (L) | Cell Density×$10^6$ (cells/mL) | Cell Viability (%) |
|---|---|---|---|
| Culture-A | 100 | 23.9 | 90 |
| Culture-B | 100 | 20.3 | 96 |
| Culture-C | 5 | 30.8 | 31 |

**Figure legends**

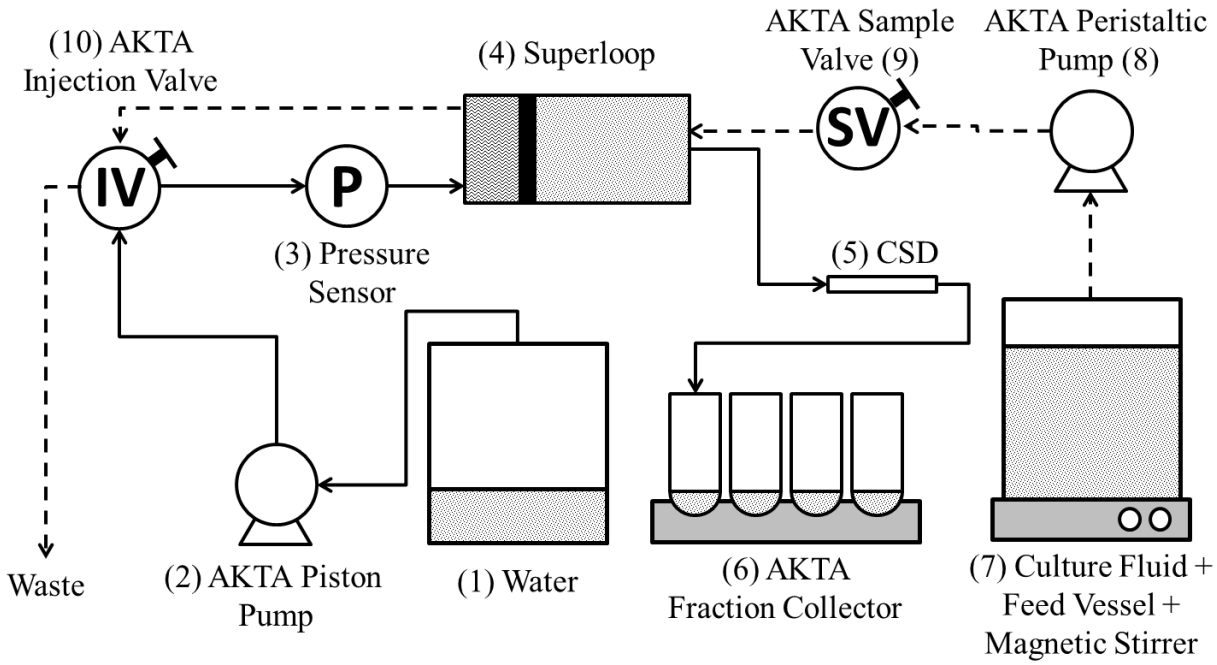


| Description | Supplier | ID |
|---|---|---|
| AKTA Piston Pump (P-901) | GE Life Sciences (Little Chalfont, UK) | 2 |
| Pressure Sensor (P-901) | GE Life Sciences (Little Chalfont, UK) | 3 |
| Superloop (18-1113-81) | GE Life Sciences (Little Chalfont, UK) | 4 |
| 10cm 0.01" ID Steel Capillary (U112) | IDEX Health & Science (Oak Harbor, WA, USA) | 5 |
| Fraction Collector (Frac-950) | GE Life Sciences (Little Chalfont, UK) | 6 |
| AKTA Peristaltic Pump (P-960) | GE Life Sciences (Little Chalfont, UK) | 8 |
| AKTA Sample Valve (INV-907) | GE Life Sciences (Little Chalfont, UK) | 9 |
| AKTA Injection Valve (INV-907) | GE Life Sciences (Little Chalfont, UK) | 10 |

**Figure 1.** Schematic of CSD apparatus, parts description and supplier information. Loading phase of CSD is indicated with dashed lines (– –) while shearing phase of the CSD is indicated with the solid lines (——).

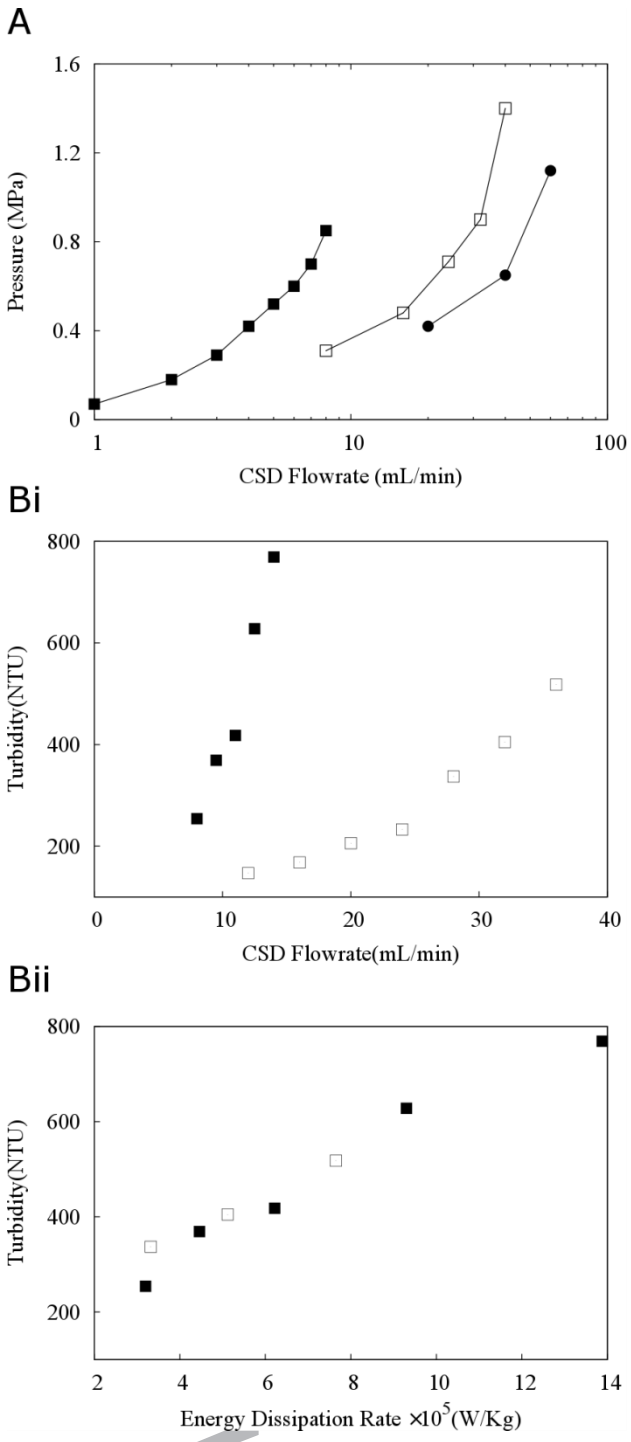


**Figure 2. A)** Study examining the effect of capillary size over a flow rate range of 1-60 mL/min on the back pressure produced by the CSD. Capillary sizes: 0.007" (■), 0.01" (○) and 0.02" (●). **B)** Examining the effect of (**Bi)** flow rates and **(Bii)** EDR on centrate turbidity using capillary sizes 0.007" (■) and 0.01" (□). A range of EDRs were generated using the CSD apparatus by processing Culture-C. The sheared material was subsequently centrifuged at V/tΣ $2.41\times10^{-8}$ (m/s) to quantify centrate turbidity.

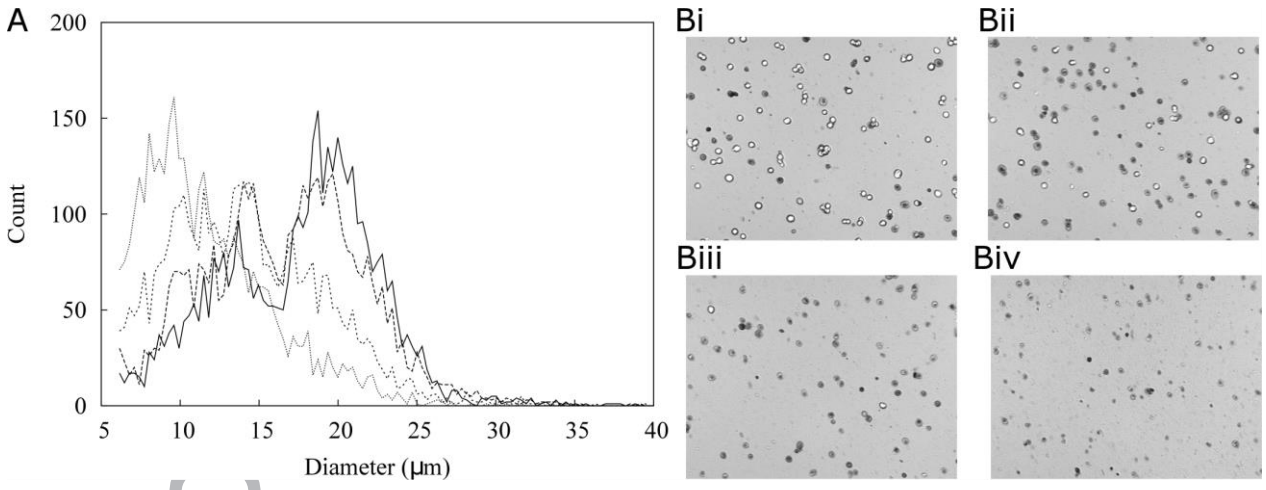


**Figure 3. A)** Comparison of particle size distribution of Culture-B when passed through the CSD at EDRs of 0 (——), 1.84 (— —), 11.85 (- - -) and 31.89 (.....) $\times 10^5$ (W/Kg) **B)** Vi-Cell XR Coulter Counter images of Culture-B sheared using the CSD at EDRs of 0**(Bi)**, 1.84**(Bii)**, 11.85**(Biii)** and 31.89**(Biv)** $\times 10^5$ (W/Kg).

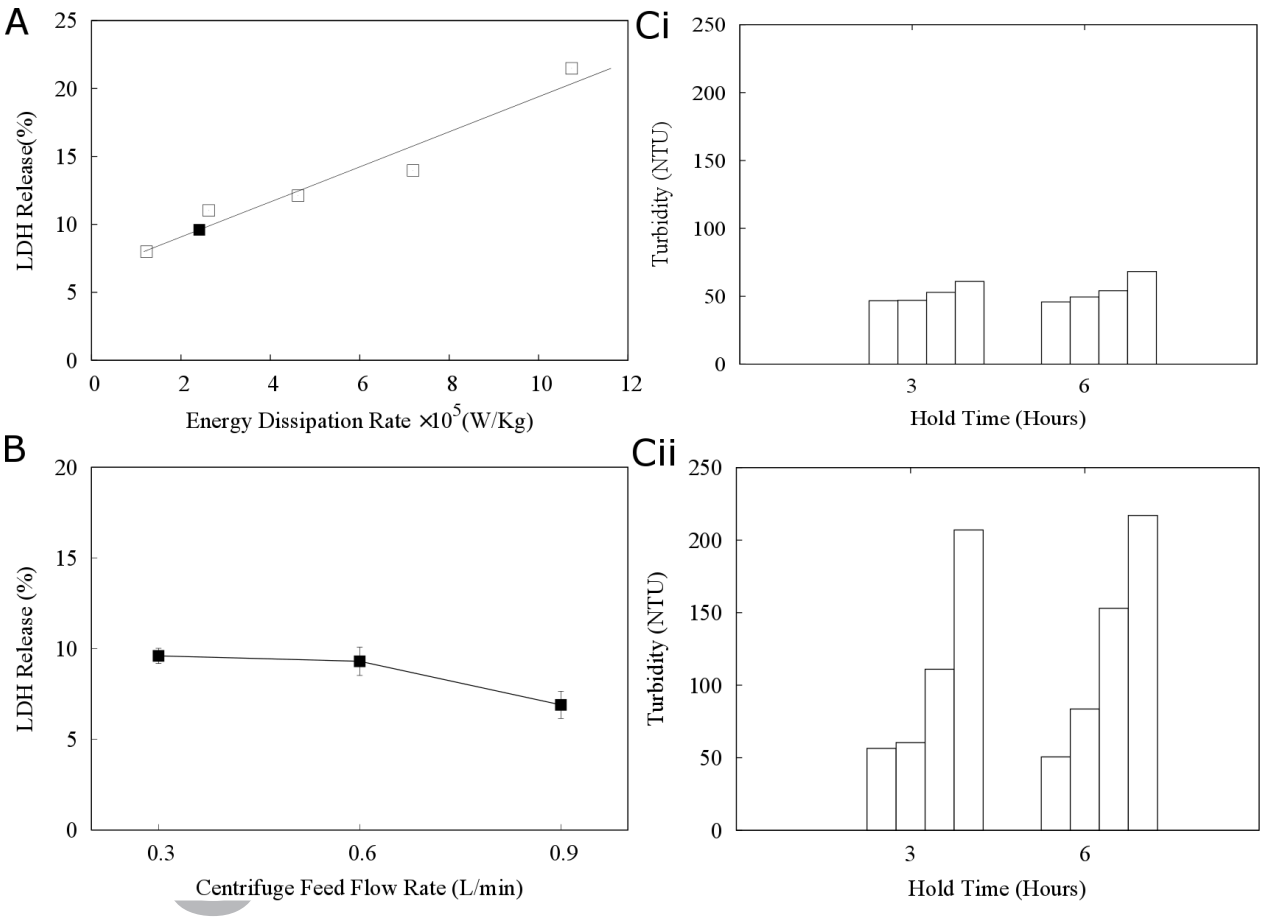


**Figure 4. A)** Study examining the correlation between the % LDH release (Measure of cell rupture) and EDR of CSD so that cell damage in the feed zone of the GEA Westfalia SO1-06-107 can be quantified. LDH release for the modelling datasets (□) was generated by shearing material (Culture-A, Table 1) using the CSD. Regression analysis (▬) was used to determine the following relationship between LDH Release ($LDH_{Rel}$) and EDR ($\varepsilon_{max}$) to identify the levels of shear generated in the GEA Westfalia SO1-06-107 centrate (■):$LDH_{Rel}$ =1.29 $\varepsilon_{max}$ +6.49, $R^2$=0.94. **B)** Study examining the levels of LDH released at a range of feed flow rates (0.3-0.9 L/hr) while the bowl speed of the Westfalia SO1-06-107 was maintained at 10,000 RPM. Culture-B (Table 1) was used as feed material during this study. The values plotted are shown as mean ± SD ($n$ = 3). **C)** Examining the effects of cell culture hold at a range of temperatures; **(Ci)** 5 and **(Cii)** 35 $^{O}$C, hold times; 3 and 6 Hours and EDRs; 0 (□), 1.84 (▨), 11.85 (▨) and 31.89 (▩)×$10^5$ (W/Kg) on centrate turbidity. Culture-B was used as source material and centrifuged at V/tΣ 2.41×$10^{-8}$ (m/s) to generate the centrates for subsequent turbidity measurements.

# Predicting Performance of Constant Flow Depth Filtration using Constant Pressure Filtration Data

Stephen Goldrick [a,1], Adrian Joseph[a,1], Michael Mollet[b], Richard Turner[c], David Gruber[c], Suzanne S. Farid[a] and Nigel J. Titchener-Hooker[a]*

[a] The Advanced Centre of Biochemical Engineering, Department of Biochemical Engineering, University College London, Gordon Street, WC1H 0AH, London, United Kingdom

[b] MedImmune, One MedImmune Way, Gaithersburg, MD 20878, United States of America

[c] MedImmune, Milstein Building, Granta Park, Cambridge, CB21 6GH, United Kingdom

[1] Both authors contributed equally to this work

**Correspondence*:** Professor Nigel Titchener-Hooker, The Advanced Centre of Biochemical Engineering, Department of Biochemical Engineering, University College London, Bernard Katz Building, London, WC1E 6BT, United Kingdom

**E-mail:** nigelth@ucl.ac.uk



# Highlights

- Identifies optimum classic and combined fouling models describing depth filtration
- Utilisation of constant pressure flux decline data to predict constant flow capacity
- Proposed method reduces material and time requirements for filter sizing studies
- Method verified for centrates processed at different scales across multiple products
- Robust methodology demonstrated for capacity predictions of X0DC and D0HC filters

# Abstract

This paper describes a method of predicting constant flow filtration capacities using constant pressure datasets collected during the purification of several monoclonal antibodies through depth filtration. The method required characterisation of the fouling mechanism occurring in constant pressure filtration processes by evaluating the best fit of each of the classic and combined theoretical fouling models. The optimised coefficients of the various models were correlated with the corresponding capacities achieved during constant flow operation at the specific pressures performed during constant pressure operation for each centrate. Of the classic and combined fouling models investigated, the Cake-Adsorption fouling model was found to best describe the fouling mechanisms observed for each centrate at the various different pressures investigated. A linear regression model was generated with these coefficients and was shown to predict accurately the capacities at constant flow operation at each pressure. This model was subsequently validated using an additional centrate and accurately predicted the constant flow capacities at three different pressures (0.69, 1.03 and 1.38 bar). The model used the optimised Cake-Adsorption model coefficients that best described the flux decline during constant pressure operation. The proposed method of predicting depth filtration performance proved to be faster than the traditional approach whilst requiring significantly less material, making it particularly attractive for early process development activities.





# Keywords

Constant flow; Constant pressure; Depth filtration; Filter sizing; Mammalian cell; fouling models.

# 1. Introduction

The market for therapeutic monoclonal antibodies (mAb) has seen unprecedented growth in recent years and this expansion is predicted to continue over the next decade [1]. To meet product supply for this increasing market and to ensure potential new drug candidates are manufactured effectively, pharmaceutical and biotechnology companies are required to operate across a wide range of scales, including large-scale manufacturing performed in vessels up to 20,000 L in addition to research development activities carried out using small or micro-scale systems. One of the challenges of operating at multiple scales is the need for flexible and scalable downstream processing unit operations. Depth filtration is an adaptable and scalable unit operation that has gained wide acceptance as the technique of choice for the clarification of mammalian cell culture broth post-centrifugation [2]. Accurate estimations of the optimum filter sizing of this key unit operation are critical. Over-sizing of the filter is uneconomic and under-sizing of the filter can result in process-related issues such as increased fouling in subsequent chromatographic stages thus shortening column lifetime and efficiency [3, 4] or filter blockage resulting in loss of material. For constant flow operation the optimum filter area or capacity is defined as the cumulative volume of material filtered until a maximum pressure is reached [5] whereas the capacity for constant pressure is determined as the volume of material processed before a minimum flow rate is reached [6]. The optimum capacity of this unit operation is difficult to predict and can be influenced by a large number of parameters, including mode of operation, type of cell line, level of aggregates, cell culture conditions and centrifuge operating conditions [2]. Typically in an industrial environment, depth filtration trials are performed in constant flow mode on a scale-down mimic that predicts the capacity at large-scale for each material tested. One of the problems of this approach is that it is time-consuming and material-intensive, particularly in comparison to capacity predictions

performed in constant pressure mode. Fundamentally constant pressure and constant flow are operated differently. In constant flow operation a positive displacement pump is required to ensure the constant flow is maintained throughput the run. The pressure drop across the filter increases to maintain this constant flow due to foulant build up with time. In contrast, during constant pressure operation the initial flux through the filter is relatively high and decreases gradually as the filter fouls resulting in the hydrodynamic conditions at the filter surface changing over time [7]. This initial high flux can result in severe fouling [8] and therefore subsequently reduce the overall capacity of the filter. Hence the majority of biopharmaceutical processes operate in constant flow mode to maximize the available filter area. Miller et al. [7] demonstrated comparable fouling behavior between constant flow and constant pressure operation during dead-end ultrafiltraion of an emulsified oil for low constant flow operation (<62 LMH) with deviations between the modes of operation found for flows about this value. However, Bolton et al. [9] and Chellam and Xu [10] demonstrated comparable fouling characteristics between the two modes of operation during the dead-end ultrafiltration of various materials ranging from antibody preparations to bacteria. Little research has investigated the conversion of constant pressure to constant flow operation for depth filtration.

Understanding membrane fouling remains a major challenge due to the multiple factors influencing this highly complex mechanism. Upstream processing conditions including cell viability and centrifuge operation can greatly influence the feed material onto a primary recovery depth filter resulting in significantly varied filtration properties [11]. Furthermore, the filters typically have an anisotropic pore structure resulting in various fouling mechanisms from deposition to adsorption of solutes to the membrane surface, cake layer formation, concentration

polarization and build-up of osmotic pressure [7]. In an attempt to simplify these highly complicated mechanisms various mathematical models have been applied to quantify the observed fouling. A limitation of these blocking models is that they are semi-empirical and assume the fouling mechanism is solely related to the physical blockage of the pores or inner pore walls as a result of the particles depositing onto the surface [12]. However, his generalisation has been widely implemented and successfully approximated the observed fouling during dead-end microfiltration [8, 13, 14, 15], ultra-filtration [16,17] and depth-filtration [18, 19]. The four classic models outlined in the literature are referenced as Complete blocking, Standard blocking, Cake filtration and Intermediate blocking [15]. Combination models have also been investigated which incorporate two or more of the classic models in conjunction. These have been shown to describe better the observed fouling in filters where classic models fail [17]. Most research has focused on the application of these mathematical models to define the fouling properties of proteins in dead-end microfiltration systems during constant pressure operation [9, 13, 15] or ultra-filtration [17, 18]. Depth filtration operates slightly differently than these absolute filters and mainly retains the particles in the filter media, however these fouling models have been successfully demonstrated to model the observed fouling [19]. Sampath et al. [15] showed that these mathematical models can characterise the fouling of depth filters during the loading of a *Pichia pastoris* fermentation during constant pressure operation. Hlavacek and Bouchet [16] implemented the models to explore the fouling behaviours at constant flow and demonstrated the ability of the intermediate model to fit the pressure increase of bovine serum albumin (BSA) solutions filtered through various different membrane types. Similarly, Ho and Zydney [13] modelled constant flow microfiltration of protein, while Chellam and Xu [10] used these blocking laws to analyse the constant flow microfiltration of colloids. As depth filtration post centrifugation is the primary

clarification method for large-scale mammalian cell manufacturing there is a need to investigate the various fouling modes that occur during both constant flow and constant pressure operation.

The ability to translate across constant flow and constant pressure models in filtration studies would be a major step forward and result in significant savings of time and valuable test materials for filter sizing studies. Bolton et al. [9] investigated the transition between these two modes of operation on dead-end microfiltration through characterisation of a bovine serum albumin foulant on a membrane filter. They found that the parameter coefficients of various theoretical models used to fit the flux decline during constant pressure operation could be used within the constant flow model to predict the observed pressure increase. However, with this method some models require calculation of the initial pressure drop for constant flow operation or the initial flux decline for constant pressure operation to generate predictions in the different mode.

Our study provides a methodology to accurately predict the capacity of depth filtration operated under constant flow utilising only constant pressure flux decline data. The flux decline of a wide range of industrially relevant centrates was characterised under constant pressure operation by evaluating the fit of various theoretical fouling models. Subsequently, constant flow experiments were conducted to determine the capacity of each of the centrates investigated. The model was found to be highly robust based on a low root mean square error for cross-validation. Additional experiments were performed to validate further the model and demonstrate its ability to predict accurately capacity at constant flow using data performed at constant pressure while also using significantly less material. This method may be highly beneficial at an early stage in the development of new molecules or proteins where material and time resources for process studies are often in short supply.

# 2. Theoretical considerations

In depth filtration the rate of filter fouling can be described by the generalised form of Darcy's Law:

$$J_v = \frac{1}{A}\frac{dV}{dt} \approx \frac{\Delta P}{R_{filter}\mu} \quad (1)$$

Where $J_v$ is the permeate flux defined by the flow rate per unit area of $A$ with $V$ and $t$ representing the volume and time respectively. The pressure drop across the filter, $\Delta P$, depends on the viscosity of the material, $\mu$, and the specific filter resistance, $R_{filter}$. During constant flow operation ($\Delta J_v$=0), the increase in pressure during fouling is represented as:

$$\Delta P = J_v R_{filter}\mu \quad (2)$$

Whereas during constant pressure operation ($\Delta P$ is fixed) the decrease in flux is represented by:

$$\Delta J_v = \frac{\Delta P}{R_{filter}\mu} \quad (3)$$

Both the viscosity and equivalent filter resistance are specific to the material being filtered and dependent on the filter type and pore size. In both modes of operation the increase in filter resistance ($R_{filter}$) during dead-end filtration relates to filter fouling as a result of particle retention on the surface and inner walls of the filter, cake layer formation, concentration polarisation in addition to other microscopic fouling mechanisms. The increase in filter resistance results in a reduction in flux during constant pressure operation whereas a pressure increase is observed during constant flow operation. To characterise the observed fouling, researchers have relied on four classical fouling models; Cake filtration, Complete, Intermediate and Standard blocking. These models are semi-empirical and are highly dependent on the ratio of the particle size of the cell culture material to filter pore size [20]. Filter resistance is increased by large particles retained on the surface that completely block (Complete blocking) or partially block the

available pores (Intermediate blocking). This filter foulant can increase with time as more material is filtered and the particles can form a cake layer (Cake filtration) further increasing the filter resistance. Small particles in the material relative to the filter pore size can deposit within the pore structure (Standard blocking or Adsorption) reducing the radius of the pore and therefore restricting the volume throughput of the filter.

The primary blocking models were originally defined by Hermans and Bredee [21] in 1935 and have more recently gained significant interest based on their application to dead-end microfiltration of protein solutions by Bowen et al [15] and Ho and Zydney [13]. These models are defined by Bowen et al. [9] as Complete blocking, Intermediate blocking, Standard blocking and Cake filtration.

Complete blocking occurs when each particle arriving at the filter participates in blocking the pores of the membrane and is defined by Eq. 2 where $K_{Com}$ is the fouling coefficient for the Complete blocking model and $J_v(0)$ is the initial permeate flux.

$$\text{Complete blocking model: } J_v(t) = J_v(0)e^{-K_{Com}J_v(0)t} \quad (2)$$

Cake filtration occurs when the particles form a resistant layer on top of the filter, this layer increases in depth as new particles arrive at the filter and is defined as Eq. 3 where $K_C$ is the fouling coefficient for the Cake filtration model.

$$\text{Cake filtration model: } J_v(t) = \frac{J_v(0)}{\sqrt{1+K_C J_v(0)t}} \quad (3)$$

Intermediate blocking assumes that some particles arriving at the filter will directly block a portion of the available area while other particles will only participate in partial blockage of the pores and is defined as Eq. 4 where $K_I$ is the fouling coefficient for the Intermediate blocking model.

$$\text{Intermediate blocking model: } J_v(t) = \frac{J_v(0)}{1+K_I J_v(0) t} \quad (4)$$

Standard blocking assumes that particles deposit onto the internal walls of the pores. As further particles arrive the internal diameter of the pore wall is further constricted and over time will result in the complete blockage of the pore. The mechanism is defined as Eq. 5 where $K_S$ is the fouling coefficient for the Standard blocking model.

$$\text{Standard blocking model: } J_v(t) = \frac{J_v(0)}{(1+K_S J_v(0) t)^2} \quad (5)$$

In addition to the four classic models, additional fouling models have been generated including an adsorptive fouling model that assumes particle deposition on the pore walls of the filter follows zeroth-order kinetics and is defined by Bolton et al. [9] as Eq. 6 where $K_A$ is the fouling coefficient for the Adsorption fouling model.

$$\text{Adsorptive model: } J_v(t) = J_v(0)(1 - K_A J_v(0) t)^4 \quad (6)$$

For constant flow operation, the inverse of the above mentioned fouling models applies and can model the increase in pressure as a function of time by replacing $J_v(0)$ with $P_0$ as the initial pressure during constant flow mode [9].

One of the major problems with fitting a single blocking model is the assumption of a single fouling mechanism in action when in reality membrane fouling is often far more complicated and is usually better characterised using a combination of models [17, 18]. The combination models enable 2 of the 5 previously discussed fouling mechanisms to act in parallel resulting in an additional ten combination fouling models to be considered. In total there were 15 different fouling models that were examined in this work and are outlined in Table 4.

To characterise the dominant fouling mechanism during constant pressure operation, a global optimisation function was implemented to find the optimum classic and combined fouling coefficients. The optimisation function minimised the summed squared error (*f(x)*) between the experimental flux decline ($J_{v,exp}$) generated at constant pressure and the predicted theoretical flux decline ($J_{v,pred}$) generated from the 15 (primary and combined) previously discussed fouling models. The optimisation function is subject to the constraint of non-negative fouling coefficients and is defined as:

Minimise: $f(x) = \sum(J_{v,exp} - J_{v,pred})^2$ subject to $K_C$, $K_s$, $K_{Com}$, $K_I$ , $K_A \geq 0$ (6)

The dominant fouling mechanism was quantifed by the coefficient of determination ($R_{fit}^2$), calculated based on the difference between of the experimental constant pressure flux decline compared to theoretical fouling model. The coefficient of determination was defined here as:

$$R_{fit}^2 = 1 - \frac{\sum_{t=0}^{t=t}(J_{v,exp}(t) - J_{v,pred}(t))^2}{\sum_{t=0}^{t=t}(J_{v,exp}(t) - \overline{J_{v,exp}(t)})^2} \quad (7)$$

Where $\overline{J_{v,exp}(t)}$ defines the mean value of the flux.

The theoretical model that best describes the observed flux decline typically defines the dominant fouling mechanism for the material. However, the fouling can often be described by multiple

fouling mechanisms where the combined fouling models are typically a better fit. To demonstrate this Fig.1 highlights an example of two experimental flux declines recorded on a depth filter for two centrates (Centrate 4 and 5) operated at constant pressure equal to 0.69 bar. The optimum theoretical flux for each experimental flux decline is shown by the solid line. Centrate 4 represented by the large pink circles was adequately described by the Cake filtration model with an $R^2_{fit}$ equal to 0.99. The primary fouling models could not accurately approximate the flux decline of Centrate 5, however the combined Cake-Adsorption combined fouling model resulted in an excellent fit with $R^2_{fit}$ equal to 0.97.

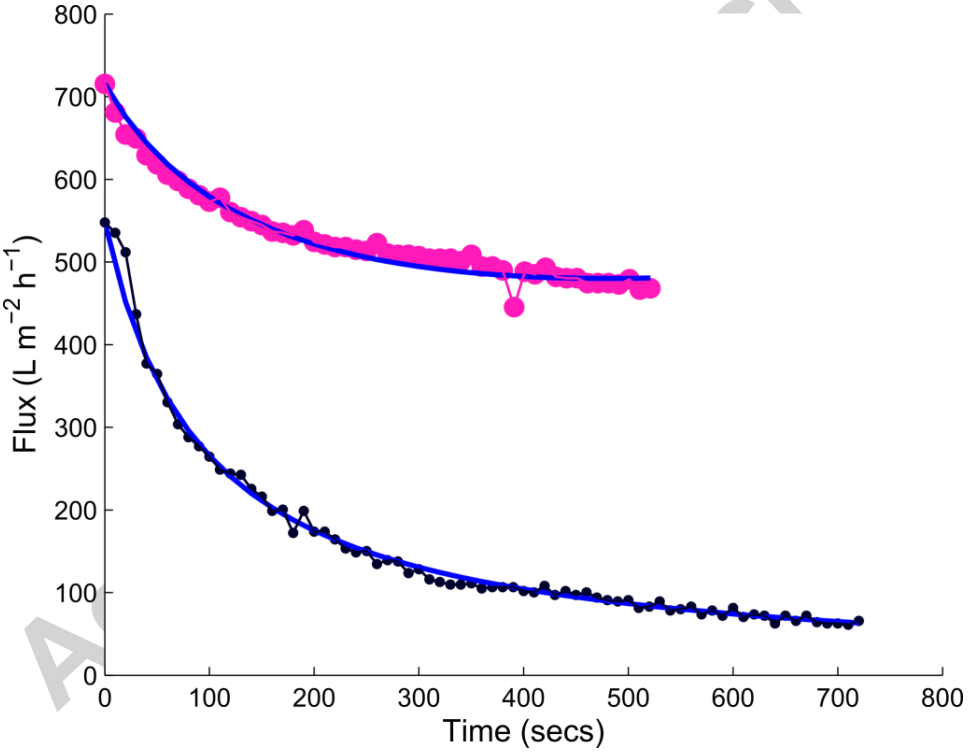


**Fig. 1:** Comparison of theoretical flux decline compared to experimental flux decline data generated from constant pressure studies using a small-scale (23 cm$^2$) depth filter. The flux decline represented by • is the experimental flux decline of Centrate 4 operated at constant pressure equal to 0.69 bar and ● represents the experimental flux decline of Centrate 5 operated at the same constant pressure. The flux represented by — equals the optimum theoretical flux decline with the highest coefficient of determination. The best fouling model fit for Centrate 4 was the Intermediate model with $K_I$ equal to 1.942x10$^{-5}$ m$^2$ L$^{-1}$. Similar the best fouling fit model for Centrate 5 was equal to the Cake-Adsorption model with $K_C$ and $K_A$ equal to 1.085x10$^{-5}$ and 2.6x10$^{-7}$ m$^2$ L$^{-1}$.

# 3. Experimental materials and methods

## 3.1. Cell culture

The cell culture material utilised in these experiments was generated using Chinese Hamster Ovary (CHO) cell lines expressing a range of monoclonal antibodies (mAb) products. The cultures were produced in bench (5 L) and pilot scale (500 L) bioreactors and harvested during the decline phase of growth (days 11-14). The harvested broths had a range of cell culture properties summarised in Table 1. The cell density and cell viability were identified using an automated Trypan blue dye exclusion method (ViCell, Beckman Coulter, High Wycombe, UK).

**Table 1:** Cell culture properties of material used for constant flow and constant pressure experiments.

| Product | Material ID | Bioreactor size (L) | Cell density $\times 10^6$(cells/mL) | Cell viability (%) |
|---|---|---|---|---|
| mAb-A | Centrate-1 | 500 | 25 | 68 |
| mAb-B | Centrate-2 | 5 | 20 | 75 |
| mAb-B | Centrate-3 | 5 | 20 | 75 |
| mAb-B | Centrate-4 | 5 | 20 | 75 |
| mAb-C | Centrate-5 | 500 | 24 | 90 |
| mAb-C | Centrate-6 | 500 | 24 | 90 |

## 3.2. Large scale centrifugation

The centrates were generated by processing the cell culture broths though a Westfalia SO1-06-107 (Odele, Germany) disk-stack centrifuge operated at 10,000 RPM and flow rates were varied between 0.3-0.9 L/min. The centrifugal operating conditions and the subsequent turbidities of the centrates are summarised in Table 2. The turbidity values recorded in this study were measured using a HACH 2100P turbidity meter (Loveland, CO, USA).

**Table 2:** Centrifugal operational settings for processing of cell cultures and the resultant centrate turbidity.

| Material ID | Centrifuge flow rate (L/min) | Turbidity (NTU) |
|---|---|---|
| Centrate-1 | 0.3 | 234 |
| Centrate-2 | 0.3 | 215 |
| Centrate-3 | 0.6 | 331 |
| Centrate-4 | 0.9 | 560 |
| Centrate-5 | 0.3 | 102 |
| Centrate-6 | 0.9 | 106 |

Note: NTU-Normalised turbidity units

## 3.3. Filtration

Constant pressure and constant flow filtration experiments were conducted using a 23 $cm^2$ Millistack X0HC depth filter capsule (EMD Millipore, MA, USA) with a nominal pore size ranging from 0.1-2 μm. The depth filter was first wetted with RO water at 200 L $m^{-2}$ $h^{-1}$ (LMH) for 20 minutes and subsequently aired for 10 minutes to remove any residual water. The centrate was well mixed using a magnetic flea and pumped through the aired filter at 100 LMH with pressure recorded for the duration of the experiment. Identical materials were used to challenge the filter in both constant pressure and constant flow approaches. During constant pressure experiments the centrate was sealed inside a feed vessel and pressurised to the set pressure using compressed air. Throughout the experiment the filtrate was collected and the volume recorded with time. A similar methodology was implemented for constant pressure operation of a 3.5 $cm^2$ Millipore SHC sterile filters (EMD Millipore, MA, USA). The pressure was set at 0.69 bar for all sterile filter experiments. A summary of the pressure set points for constant pressure operation and flowrate set point during constant flow operation are shown in Table 3.

**Table 3:** Experimental conditions for constant flow and constant pressure studies.

| Material ID | Constant pressure operation conditions (bar) | Flowrate (LMH) |
|---|---|---|
| Centrate 1 | 0.69, 1.03, 1.38, 1.72 | 100 |
| Centrate 2 | 0.69, 1.03, 1.38, 1.72 | 100 |
| Centrate 3 | 0.69, 1.03, 1.38, 1.72 | 100 |
| Centrate 4 | 0.69, 1.03, 1.38, 1.72 | 100 |
| Centrate 5 | 0.69, 1.03 | 100 |
| Centrate 6 | 0.69, 1.03, 1.38 | 100 |

# 4. Results and discussion

The capacity of depth filters at any scale is primarily determined by the fouling properties of the material. Understanding these characteristics faster and accurately can provide an efficient method by which to determine depth filter capacity. Capacity predictions can be performed through constant pressure operation or constant flow operation. In order to highlight the advantages of constant pressure operation compared to constant flow operation the depth filter performance was evaluated in both modes of operation using a wide range of processed materials. Processing multiple cell culture broths at a variety of centrifuge operating conditions provided a range of centrates with various fouling properties.

It is common practice in industry to quantify the capacity during constant flow operation as the total volume passed through the filter up until a given pressure drop is reached (typically 1.38 bar). This practice is however, time-consuming and material-intensive. Whilst depth filter sizing at constant pressure is not common practice, this mode of operation has the advantage of processing samples more quickly than when operating at constant flow mode. The savings of experimental process time are highlighted in Fig. 2A where the time to filter 100 mL of each centrate under both constant pressure and constant flow operation is shown. As expected all of the centrates were processed by the 23 $cm^2$ filter in approximately 26 minutes during constant flow operation. Constant pressure operation allows the material to be processed significantly faster, with on average an 80% reduction in processing time observed for the majority of the centrates compared to constant flow operation. Additionally, the total volume required to conduct experiments under both modes of operations is summarised in Fig. 2B and highlights an average of 70% savings of material to perform these experiments at constant pressure operation. The processing time and

volume required to filter Centrate 4 with an NTU value of 560 is shown here to behave abnormally in comparison to the other five centrates. This high NTU value is atypical and resulted in rapid fouling of the filter in both modes of operation. However, filtering this turbid material under constant pressure operation mode was still faster than constant flow operation.

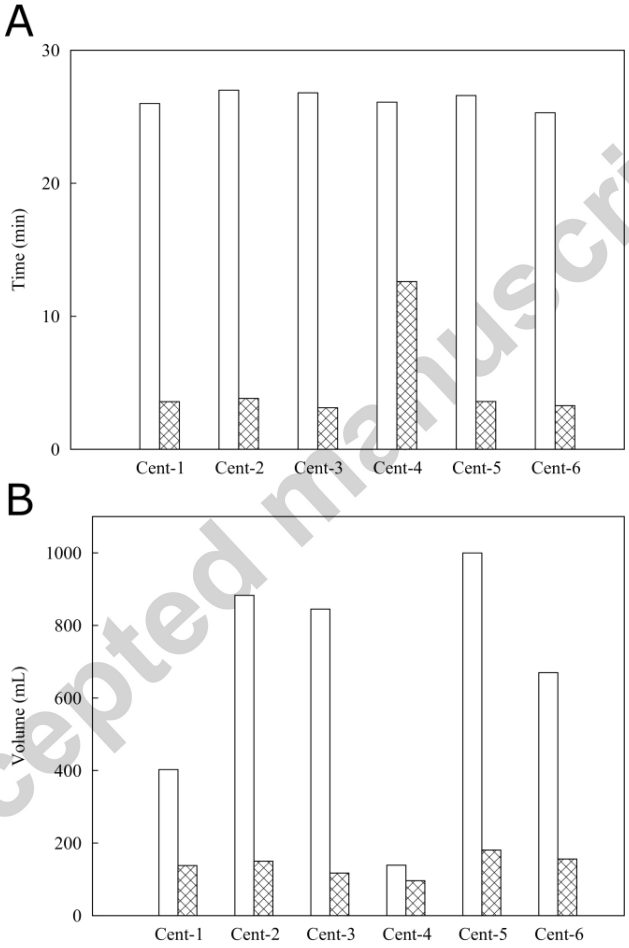




**Fig. 2:** Comparison of constant flow and constant pressure modes of operation on **(A)** experimental time to process 100 mL of material and **(B)** total process material volume requirements across multiple centrates. Centrates used by these studies were sourced from multiple cell culture broths (Table 1) and processed through a pilot scale centrifuge at a range of conditions (Table 2). Constant pressure represented as ☒ and constant flow as □.

The significant savings in material and processing time achieved during constant pressure operation provided the impetus for developing a constant pressure operation based method to enable accurate predictions of capacity for constant flow operations. Little research has been carried out on the ability to utilise constant pressure data to enable accurate predictions of process performance of depth filters when operated at constant flow. The methodology reported in this paper analysed both constant pressure and constant flow depth filtration performance data. The study utilised a wide range of centrates generated from three different products and two scales as summarised in Table 1. The varied range of turbidities and process characteristics of the six centrates generated a broad range of experimental capacities when operated at constant flow as shown in Fig. 3. The turbidity post centrifugation was recorded here as a quick and simple measurement to quantify centrifuge performance, similar to practices in industry [22]. It can also give a broad indication of a centrates fouling propensity during depth filtration.

As highlighted by Fig. 3, Centrate 4 with the highest turbidity (560 NTU) was shown to be the most difficult material to filter. Similarly, Centrate 5 with the lowest turbidity (102 NTU) was easily filtered and displayed a significantly higher subsequent filter capacity than the other centrates. However, Centrate 6 (106 NTU) with a similar NTU value to Centrate 5 displayed a very different level of filterability. This suggests no obvious correlation can be determined between the filterability of the centrate and its recorded turbidity. Thus the large range of observed capacities posed a real challenge in the optimum sizing of this key unit operation.

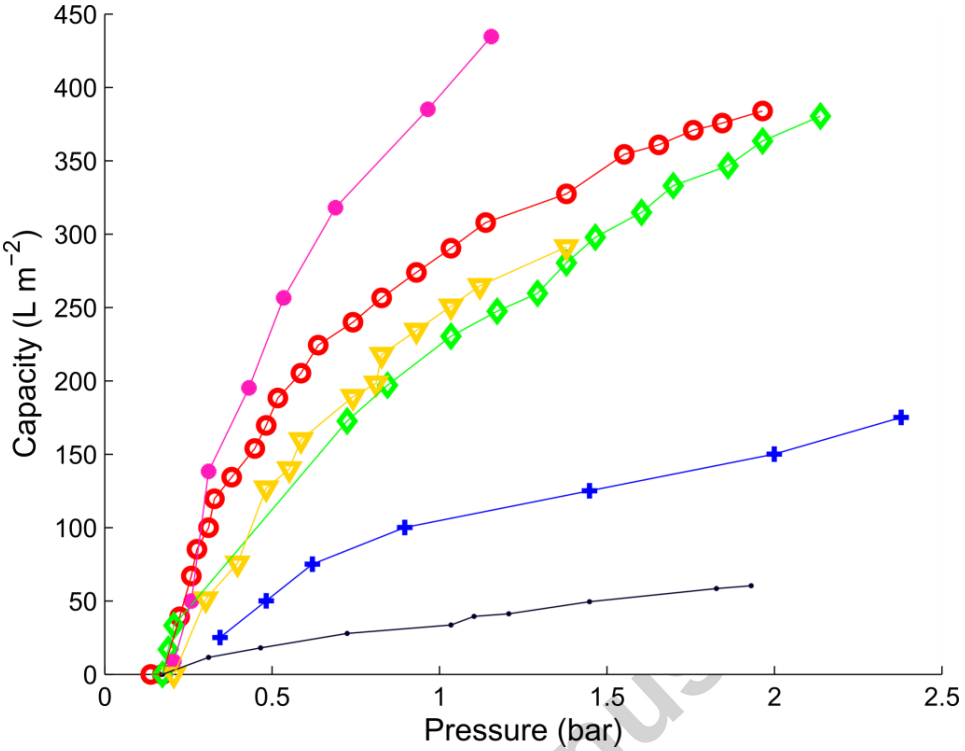


**Fig. 3:** Experimental pressure profile data generated from constant flow studies using a small-scale (23 cm$^2$) depth filter operated at 100 LMH with Centrate 1 represented as +, Centrate 2 as **O**, Centrate 3 as ♦, Centrate 4 as •, Centrate 5 as ● and Centrate 6 as▼.

Comparable variation was observed when the six centrates were passed through the depth filter at constant pressure. The unique flux profiles for each centrate are shown in Fig. 4 highlighting the differing rates of membrane fouling specific to each material. Similar to the work carried out by Sampath et al. [18] on depth filtration of a therapeutic product expressed in a *Pichia pastoris* fermentation under constant pressure, no correlation was determined between the filterability of the centrate and the recorded turbidity. The initial flux ($J_v(0)$) of each centrate was shown to increase (Fig. 4) with pressure of operation due to the incompressible nature of the depth filter over the experimental pressure range of 0.69 -1.72 bar. Similar observations were seen by Ho and

Zydney [13] during microfiltration studies of bovine serum albumin solutions and by Chellam and Xu [10] during microfiltration of bacteria, colloidal silica and treated natural waters.

Characterising the fouling mechanisms observed during both modes of operation are routinely defined through the application of various mathematical fouling models as summarised in Section 2 of theoretical considerations. In this work the observed fouling during constant pressure operation of Centrates 1-6 was characterised using the classic and combined fouling models.

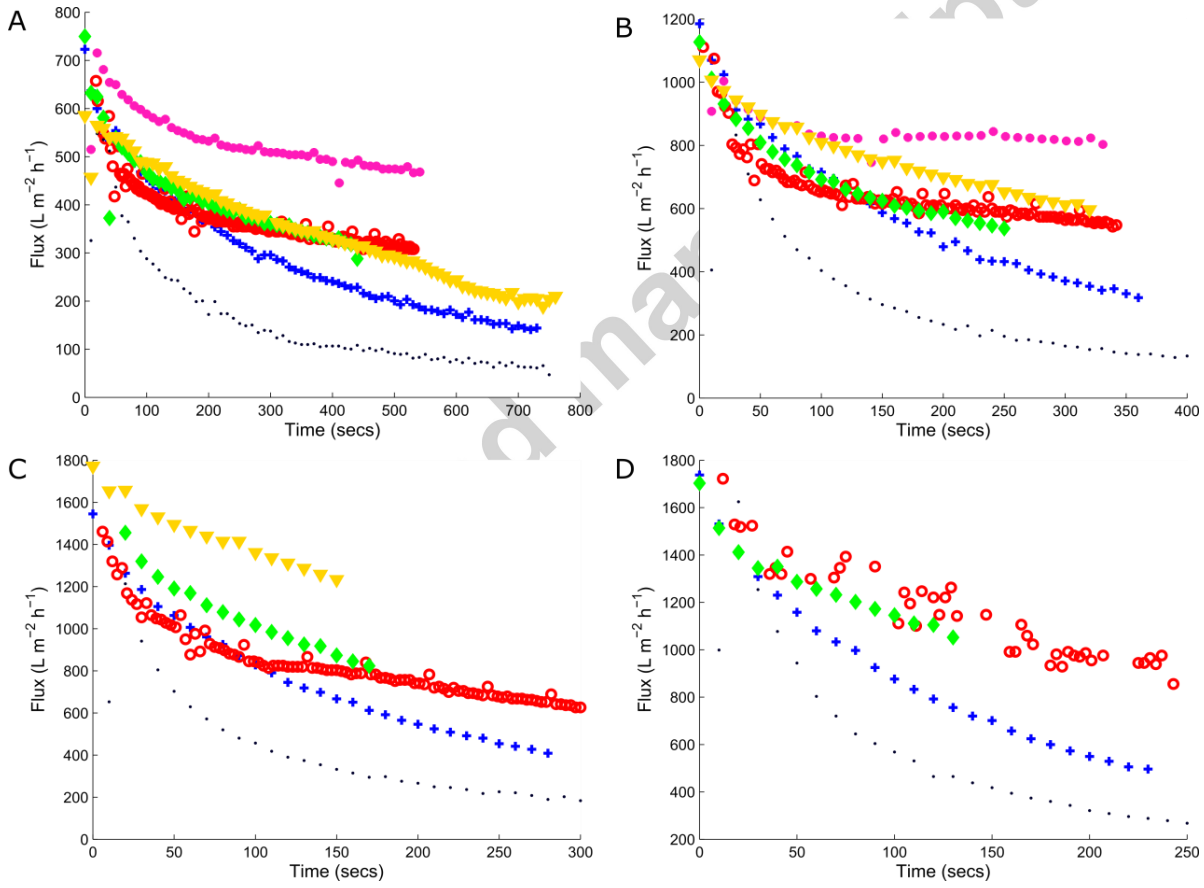


**Fig. 4:** Experimental data generated from constant pressure studies using a small-scale (23 cm$^2$) depth filter for Centrates 1-6 at pressures equal to **(A)** 0.69 bar, **(B)** 1.03 bar, **(C)** 1.38 bar and **(D)** 1.72 bar. Centrate 1 represented as blocking **+**, Centrate 2 as **o**, Centrate 3 as ♦, Centrate 4 as •, Centrate 5 as ● and Centrate 6 as ▼.

A global optimisation function was utilised to generate the optimum coefficients of the fouling models that minimised the error between the experimental and theoretical flux declines. The goodness of fit was quantified using the coefficient of determination ($R_{fit}^2$) and is summarised in Table 4. Of the classic models the Cake and Intermediate models were the dominant fouling mechanism found to model accurately the majority of the different flux profiles. Similarly, for the combined models, the Cake-Adsorption, Cake-Intermediate, Cake-Complete and Cake-Standard were shown to model effectively the observed fouling of each centrate at the different pressures investigated. Table 4 highlights the challenge with fitting theoretical fouling models to a wide range of centrates and the inability of some of the classic models to capture the observed complex fouling mechanisms. Furthermore, some of the centrates were adequately described by two or more of the classic fouling models demonstrating the similarly between the theoretical flux declines generated by the different fouling models.

Interestingly in Table 4, the pressure was also shown to influence the blocking mechanism observed for each material. At the lower pressures where particles would be depositing onto the filter surface at a slower rate the Cake filtration model, the dominant fouling model for these materials, failed to describe adequately the fouling. This implies that in addition to the formation of the cake resistance layer there was a second type of fouling occurring. The complex fouling observed for Centrate-2 and Centrate-5 could not be described by a single fouling mechanism at the lower pressures. The Cake-Adsorption model was the only model that could adequately describe the fouling profiles observed for these centrates across all of the pressures investigated. Sampath et al. [18] reported similar findings and concluded that neither of the classic or combined fouling models could consistently fit the various flux declines for different depth filters. Although, the Cake-Adsorption model was not investigated in their work.

**Table 4:** Summary of the classic and combined fouling model fits for Centrates 1-6 (Table 2) at the range of pressures tested (Table 3).

| CP Pressure (bar) | Intermediate | Cake | Standard | Complete | Adsorption | Cake-Adsorption | Cake-Intermediate | Complete-Standard | Intermediate-Standard | Intermediate-Adsorption | Complete-Adsorption | Cake-Complete | Intermediate-Complete | Cake-Standard | Standard-Adsorption |
|---|---|---|---|---|---|---|---|---|---|---|---|---|---|---|---|
| Centrate 1 | | | | | | | | | | | | | | | |
| 0.69 | 0.98 | 0.96 | 0.95 | 0.87 | 0.79 | 0.96 | 0.99 | 0.95 | 0.98 | 0.98 | 0.87 | 0.99 | 0.98 | 0.99 | 0.95 |
| 1.03 | 0.99 | 0.97 | 0.98 | 0.94 | 0.90 | 0.97 | 0.99 | 0.98 | 0.99 | 0.99 | 0.64 | 1.00 | 0.99 | 0.99 | 0.98 |
| 1.38 | 1.00 | 0.97 | 0.99 | 0.95 | 0.91 | 0.97 | 1.00 | 0.99 | 1.00 | 1.00 | 0.94 | 1.00 | 1.00 | 1.00 | 0.99 |
| 1.72 | 1.00 | 0.97 | 0.99 | 0.96 | 0.92 | 0.96 | 1.00 | 0.99 | 1.00 | 1.00 | 0.96 | 1.00 | 1.00 | 1.00 | 0.99 |
| Mean | 0.99 | 0.96 | 0.98 | 0.93 | 0.88 | 0.96 | 0.99 | 0.98 | 0.99 | 0.99 | 0.85 | 1.00 | 0.99 | 0.99 | 0.98 |
| Centrate 2 | | | | | | | | | | | | | | | |
| 0.69 | 0.05 | 0.50 | 0.00 | 0.00 | 0.00 | 0.89 | 0.50 | 0.00 | 0.02 | 0.05 | 0.00 | 0.50 | 0.05 | 0.50 | 0.00 |
| 1.03 | 0.05 | 0.48 | 0.00 | 0.00 | 0.00 | 0.92 | 0.48 | 0.00 | 0.05 | 0.05 | 0.00 | 0.48 | 0.05 | 0.48 | 0.00 |
| 1.38 | 0.69 | 0.87 | 0.54 | 0.35 | 0.23 | 0.90 | 0.87 | 0.54 | 0.69 | 0.00 | 0.35 | 0.87 | 0.69 | 0.87 | 0.54 |
| 1.72 | 0.82 | 0.86 | 0.78 | 0.73 | 0.70 | 0.87 | 0.86 | 0.78 | 0.81 | 0.82 | 0.00 | 0.86 | 0.82 | 0.86 | 0.78 |
| Mean | 0.40 | 0.68 | 0.33 | 0.27 | 0.23 | 0.90 | 0.68 | 0.33 | 0.39 | 0.23 | 0.09 | 0.68 | 0.40 | 0.68 | 0.33 |
| Centrate 3 | | | | | | | | | | | | | | | |
| 0.69 | 0.59 | 0.78 | 0.44 | 0.23 | 0.11 | 0.77 | 0.78 | 0.44 | 0.58 | 0.59 | 0.22 | 0.78 | 0.59 | 0.78 | 0.44 |
| 1.03 | 0.89 | 0.97 | 0.83 | 0.73 | 0.67 | 0.99 | 0.97 | 0.83 | 0.89 | 0.89 | 0.73 | 0.97 | 0.89 | 0.97 | 0.83 |
| 1.38 | 0.96 | 0.99 | 0.94 | 0.91 | 0.89 | 0.99 | 0.99 | 0.94 | 0.96 | 0.96 | 0.91 | 0.99 | 0.96 | 0.99 | 0.94 |
| 1.72 | 0.86 | 0.92 | 0.81 | 0.76 | 0.74 | 0.97 | 0.92 | 0.81 | 0.86 | 0.86 | 0.70 | 0.92 | 0.86 | 0.92 | 0.81 |
| Mean | 0.83 | 0.91 | 0.75 | 0.66 | 0.60 | 0.93 | 0.91 | 0.75 | 0.82 | 0.83 | 0.64 | 0.91 | 0.82 | 0.91 | 0.75 |
| Centrate 4 | | | | | | | | | | | | | | | |
| 0.69 | 0.99 | 0.92 | 0.97 | 0.86 | 0.76 | 0.92 | 0.99 | 0.97 | 0.99 | 0.99 | 0.85 | 0.99 | 0.99 | 0.99 | 0.97 |
| 1.03 | 1.00 | 0.96 | 0.98 | 0.90 | 0.82 | 0.96 | 1.00 | 0.98 | 1.00 | 1.00 | 0.90 | 1.00 | 1.00 | 1.00 | 0.98 |
| 1.38 | 0.99 | 0.97 | 0.95 | 0.82 | 0.70 | 0.97 | 1.00 | 0.95 | 0.99 | 0.99 | 0.81 | 1.00 | 0.99 | 1.00 | 0.95 |
| 1.72 | 1.00 | 0.97 | 0.96 | 0.85 | 0.75 | 0.97 | 1.00 | 0.96 | 1.00 | 1.00 | 0.00 | 1.00 | 1.00 | 1.00 | 0.96 |
| Mean | 0.99 | 0.96 | 0.96 | 0.86 | 0.76 | 0.96 | 1.00 | 0.96 | 0.99 | 0.99 | 0.64 | 1.00 | 0.99 | 1.00 | 0.96 |
| Centrate 5 | | | | | | | | | | | | | | | |
| 0.69 | 0.60 | 0.74 | 0.50 | 0.40 | 0.34 | 0.97 | 0.74 | 0.50 | 0.59 | 0.60 | 0.40 | 0.74 | 0.59 | 0.74 | 0.50 |
| 1.03 | 0.00 | 0.00 | 0.00 | 0.00 | 0.00 | 0.70 | 0.00 | 0.00 | 0.00 | 0.00 | 0.00 | 0.00 | 0.00 | 0.00 | 0.00 |
| Mean | 0.30 | 0.37 | 0.25 | 0.20 | 0.17 | 0.83 | 0.37 | 0.25 | 0.30 | 0.30 | 0.20 | 0.37 | 0.30 | 0.37 | 0.25 |
| Centrate 6 | | | | | | | | | | | | | | | |
| 0.69 | 0.98 | 0.93 | 0.99 | 0.99 | 0.98 | 0.93 | 0.99 | 0.99 | 0.99 | 0.99 | 0.99 | 0.99 | 0.99 | 0.99 | 0.99 |
| 1.03 | 0.95 | 0.99 | 0.93 | 0.88 | 0.86 | 0.99 | 0.99 | 0.93 | 0.95 | 0.95 | 0.86 | 0.99 | 0.95 | 0.99 | 0.93 |
| 1.38 | 0.96 | 0.98 | 0.95 | 0.93 | 0.92 | 0.98 | 0.98 | 0.95 | 0.96 | 0.96 | 0.93 | 0.98 | 0.96 | 0.98 | 0.95 |
| Mean | 0.96 | 0.97 | 0.95 | 0.93 | 0.92 | 0.97 | 0.98 | 0.95 | 0.97 | 0.97 | 0.92 | 0.99 | 0.97 | 0.99 | 0.95 |
| Overall mean | 0.75 | 0.81 | 0.70 | 0.64 | 0.59 | 0.93 | 0.82 | 0.70 | 0.75 | 0.72 | 0.45 | 0.82 | 0.75 | 0.82 | 0.70 |

Note: The fit is quantifed by the coefficient of determination ($R_{fit}^2$), calculated based on the difference between of the experimental constant pressure flux decline compared to theoretical fouling model. CP Pressure stands for pressure set in constant pressure mode

The optimised fouling coefficients that best described the constant pressure flux decline of Centrates 1-5 (shown in Fig. 4) were selected as the calibration dataset. The coefficients were normalised by pressure and correlated with the corresponding capacity achieved during constant flow (shown in Fig. 3) at the specific pressure investigated. For the classic models, containing a single coefficient, a simple exponential relationship generated the strongest correlation between the constant flow capacities and enabled accurate predictions. This type of relationship was selected across all of the classic models based on minimising the coefficient of determination ($R_{Cal}^2$) between the predicted and experimentally recorded capacity at constant flow for the calibration datasets (Centrates 1-5). The robustness of the correlation model was estimated by a cross validation method that estimated the performance of the model trained with one of the centrates removed from the calibration dataset and is defined in Table 5 as $R_{Cross}^2$. For the combined models, containing two coefficients, a quadratic linear regression model that considered the interaction between the two terms was assumed and a stepwise regression approach implementing both forward addition and backward elimination was used to generate the final model. The selection criteria for the finalised combined model was the same as for the classic models. A summary of the finalised correlation models of both the classic and combined models outlining their structure and prediction accuracy are shown in Table 5.

**Table 5:** Correlation model structure and $R^2$ values for both classic and combined models.

| Fouling model | Correlation model structure | $R_{Cal}^2$ | $R_{Cross}^2$ |
|---|---|---|---|
| Intermediate | $ae^{bK_I}$ | 0.81 | 0.78 |
| Cake | $ae^{bK_C}$ | 0.83 | 0.82 |
| Standard | $ae^{bK_S}$ | 0.78 | 0.74 |
| Complete | $ae^{bK_{Com}}$ | 0.74 | 0.69 |
| Adsorption | $ae^{bK_A}$ | 0.59 | 0.59 |
| Cake-Adsorption | $\alpha_0 + \alpha_1 K_C + \alpha_2 K_A + \alpha_3 K_C^2$ | 0.86 | 0.89 |
| Cake- Intermediate | $\alpha_0 + \alpha_1 K_C + \alpha_2 K_I + \alpha_3 K_I^2$ | 0.76 | 0.79 |
| Comp-Standard | $\alpha_0 + \alpha_1 K_S + \alpha_2 K_S^2$ | 0.74 | 0.72 |
| Intermediate- Standard | $\alpha_0 + \alpha_1 K_I + \alpha_2 K_I^2$ | 0.77 | 0.76 |
| Intermediate- Adsorption | $\alpha_0 + \alpha_1 K_I + \alpha_2 K_I^2$ | 0.78 | 0.75 |
| Complete-Adsorption | $\alpha_0 + \alpha_1 K_{Com} + \alpha_2 K_A + \alpha_3 K_{Com}^2 + \alpha_4 K_{Com} K_A$ | 0.41 | 0.43 |
| Cake-Complete | $\alpha_0 + \alpha_1 K_C + \alpha_2 K_{Com} + \alpha_3 K_C K_{Com}$ | 0.81 | 0.81 |
| Intermediate-Complete | $\alpha_0 + \alpha_1 K_I + \alpha_2 K_I^2$ | 0.77 | 0.76 |
| Cake-Standard | $\alpha_0 + \alpha_1 K_C + \alpha_2 K_S + \alpha_3 K_C K_S + \alpha_4 K_C K_S$ | 0.78 | 0.80 |
| Standard-Adsorption | $\alpha_0 + \alpha_1 K_I + \alpha_2 K_S^2$ | 0.74 | 0.72 |

Note: $R_{Cal}^2$ was the coefficient of determination between the predicted and experimentally recorded capacity of the calibration dataset (Centrates 1-5). $R_{Cross}^2$ was taken as the cross validation coefficient of determination of the calibration dataset. In the correlation model structure, $K_I$, $K_C$, $K_S$, $K_{Com}$ and $K_A$ represent the model coefficients of the Intermediate, Cake, Standard, Complete and Adsorption models respectively and $a$ and $b$ are the model coefficients related to the exponential function. In the combined models, $\alpha_0$ is the intercept term and $\alpha_{1,2,3,4}$ represent the parameter coefficients of the model.

Table 5 suggests that of the classic models the correlation generated from the Cake model fouling coefficients enabled the best prediction of the constant flow capacity. However, the correlation generated from the Cake-Adsorption combined model gave a better prediction of the capacity at constant flow. This fouling mechanism suggests the dominant mechanism involves an initial deposition of the foulant onto the filter with a gradual build-up of a cake layer increasing the resistance to flow. Table 5 demonstrates that in addition to the Cake-Adsorption model, some of the other models were comparable in terms of their respective fits and power of prediction. The exponential relationship generated by the Cake model is defined in Eq. 9 where $CF_{cap,i}$ is the predicted filter capacity at pressure $i$ when operated at constant flow. $K_{C,i}$ is the Cake filtration coefficient calculated from the flux decline data when operated at constant pressure. $a$ and $b$ are calculated model coefficients.

$$CF_{cap,i} = ae^{bK_{C,i}} \quad (9)$$

Whereas the Cake-Adsorption model and is defined as Eq. 10 where $K_{C,i}$ and $K_{A,i}$ are the cake and adsorptive model coefficients calculated from flux decline data when operated at constant pressure. $\alpha_0$, $\alpha_1$, $\alpha_2$ and $\alpha_3$ are the calculated model coefficients.

$$CF_{cap,i} = \alpha_0 + \alpha_1 K_{C,i} + \alpha_2 K_{A,i} + \alpha_3 {K_{C,i}}^2 \quad (10)$$

All of the models were found to be robust through cross validation analysis of the five centrates resulting in a high cross validation ($R_{Cross}^2$) value as summarised in Table 5. To verify further the accuracy of both models in this work, the constant flow capacity data of Centrate-6 (not included in the model calibration dataset) was implemented as an external validation dataset. The predictions were made using the calculated fouling coefficients of each model that best fitted the pressure flux profile of the Centrate-6 at 0.69, 1.03 and 1.38 bar during constant pressure operation shown in Fig. 4 A, B and C. The generated fouling coefficients were then inserted into equations 9 and 10 to predict the capacity at each pressure analysed. Fig. 5 shows the predicted capacities at constant flow operation obtained from both of the correlation models. Although the Cake model is shown to predict adequately the capacity at constant flow for this centrate, the Cake-Adsorption model generates a more accurate prediction. The constant pressure flux profile generated at 1.38 bar for Centrate-6 was generated in 2.5 minutes and required a total of 140 mL of centrate. Filtering Centrate-6 through constant flow operation took a total of 173 minutes and required 670 mL to generate a capacity prediction up to 1.38 bar. Therefore, for this particular centrate the constant

pressure methodology was almost 70 times quicker and required only a fraction (1/5) of the material needs of the constant flow approach.

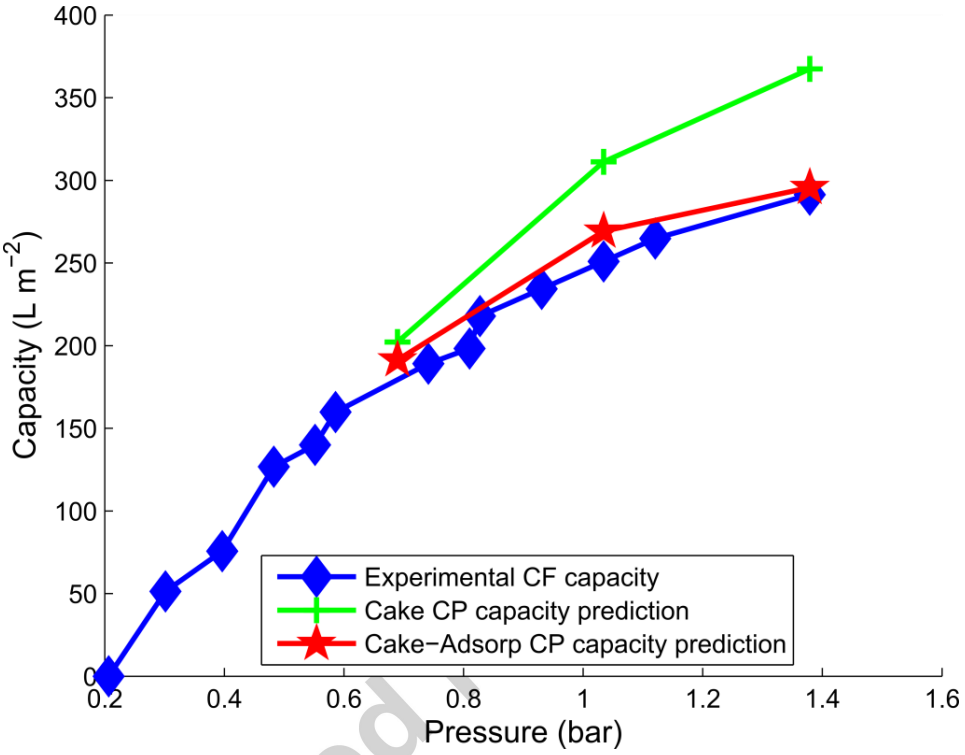


**Fig. 5:** Capacity predictions of the Cake and Cake-Adsorption fouling models for Centrate 6 at constant flow using constant pressure data recorded at 0.69, 1.03 and 1.38 bar. The experimental capacity for Centrate 6 generated in constant flow mode is shown for comparison and represented as ♦. The Cake model predictions are represented as + and the Cake-Adsorption model as ⋆. The symbols represent the experimental data points. The *a* and *b* coefficients in the Cake model were equal to 424 L m$^{-2}$ h and -7.18×10$^{5}$ L m$^{-2}$, respectively and the Cake filtration coefficients recorded at constant pressure were 1.03×10$^{-6}$ ,4.32×10$^{-7}$ and 2.01×10$^{-7}$ for each pressure investigated. For the Cake-Adsorption model, $\alpha_0$, $\alpha_1$, $\alpha_2$, $\alpha_3$ were equal to 296 L m$^{-2}$ h$^{-1}$, -1.12×10$^{8}$ L$^{2}$ m$^{-4}$ h$^{-1}$, 6.12×10$^{9}$ L$^{2}$ m$^{-4}$ h$^{-1}$ and 9.91×10$^{12}$ L$^{4}$ m$^{-6}$ h, respectively. The fouling Cake-Adsorption coefficients for each pressure were equal to 1.03×10$^{-6}$,0; 5.32×10$^{-7}$, 4.86×10$^{-9}$; 2.73×10$^{-7}$, 4.80×10$^{-9}$. All fouling coefficient units are equal to m$^{2}$ L$^{-1}$.

It is important when creating an alternative method for filter rating that the properties of the filtrates produced by either method of operation (constant flow or constant pressure) be comparable in terms of subsequent processing. To test the ability of each method to create

essentially identical filtrates, the filtrate of Centrate 6 operated at constant flow and constant pressure modes of operation were taken forward for sterile filtration. The recorded turbidites post depth filter operated at constant flow resulted in a filtrate with a turbidity equal to 23.4 NTU and at constant pressure equal to 22.8 NTU. Furthermore, Fig. 6 shows that identical flux decline profiles were generated when operating the sterile filter using material from the depth filtration step operated at both conditions. The external validation of this methodology data was carried out using Centrate 6 and validated the correlation developed. It also suggests that the developed methodology based on constant pressure operation can be utilised to characterise subsequent sterile filtration operations.

A summary outlining the new methodology is shown in Fig. 7. Firstly, the fouling coefficients for the different centrates at various constant pressures are calculated. The dominant fouling mechanism is then calculated by analysing the optimum fit of each of the classic and combined fouling models. Subsequently the capacity using the same centrates are calculated for constant flow operation up to a predefined pressure (typically 1.38 bar). A correlation is developed between the fouling coefficient of the dominant fouling mechanism and the subsequent capacity at each pressure investigated. Correlations involving the classic models can be generated using an exponential function and a linear regression model can be used for the combined model coefficients. The generated correlations can be used to predict the capacity at constant flow operation by calculating the fouling coefficient during constant pressure operation. The reduction of experimental runs and the minimisation of material requirements are the key aspect of the methodology described in Figure 7. This study used 5 distinct feed stocks at a range of pressures to develop the correlation to successfully predict the capacity of the X0HC filter at constant flow. A possible limitation of the study is the application of a brute force modelling approach to

characterise the dominant fouling mechanism based on the available classical and combined fouling models. However, this methodology was found to be valid for the filtration of multiple highly varied centrate materials and across multiple operating conditions. Although, previous reports have demonstrated significant deviations in the fouling observed between constant pressure and constant flux operation for high initial pressure fluxes [7]. The methodology reported here was found to be very robust and was verified for constant flux operation at 100 LMH. Therefore, the proposed methodology is highly suited to predict constant flux capacity for industrial depth-filtration operations that are typically operated at 100 LMH up to a maximum pressure differential pressure equal to 1.38 bar.

To further verify the method described in this publication an additional study on a D0HC depth filter (EMD Millipore, MA, USA) with a wider nominal pore size was conducted. The study utilized a wide range of cell culture material as feed-stock to challenge the depth filter. Fig. 1 Supplementary information highlights a strong correlation between the capacities reached at 0.69 bar for the D0HC depth filter when operated at constant flow and the standard fouling coefficients calculated for the constant pressure operation recorded at 0.69 bar. The developed correlation successfully predicted the D0HC capacities when processing three independent cell culture materials at constant flow as shown in Fig. 2 Supplementary information. The results from this study demonstrates the robustness and applicability of this methodology to work across a range of filter types and feed stocks. Furthermore, the accurate predictions of capacity at constant flow generated through constant pressure experimentation enables significant reductions in material and time requirements for various filtration studies.

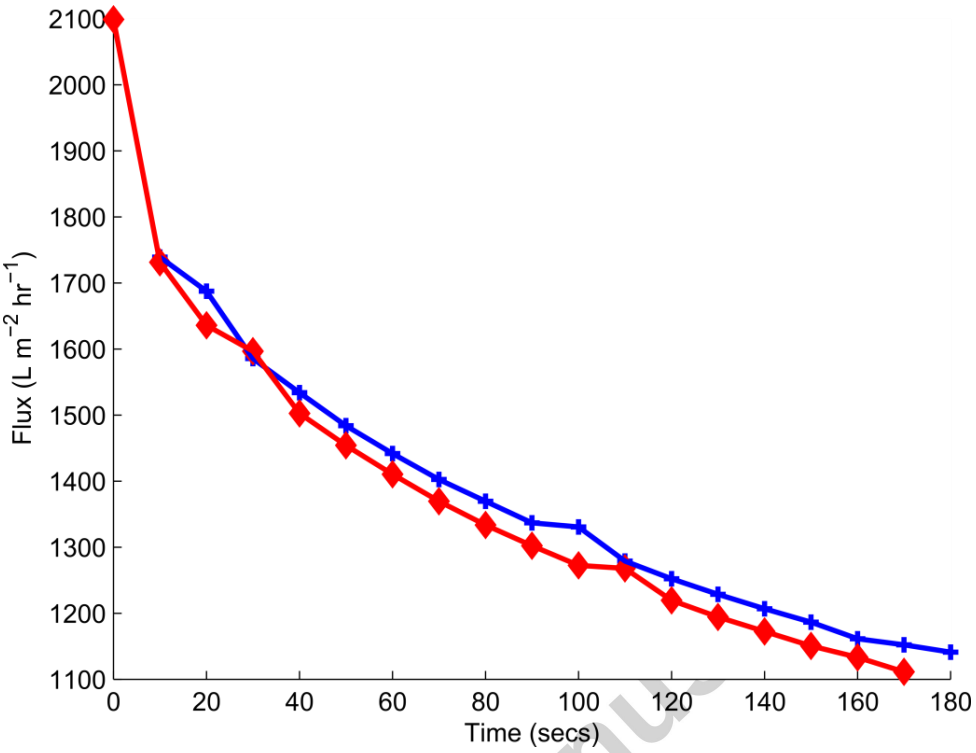


**Fig. 6:** Comparison of flux declines generated from a sterile filter when processing Centrate 6 filtrate post depth filter generated at constant pressure operation ♦ and at constant flow operation **+** .

**Fig. 7:** Flow diagram summarising the development of the correlation model to predict constant flow capacity from constant pressure flux decline data

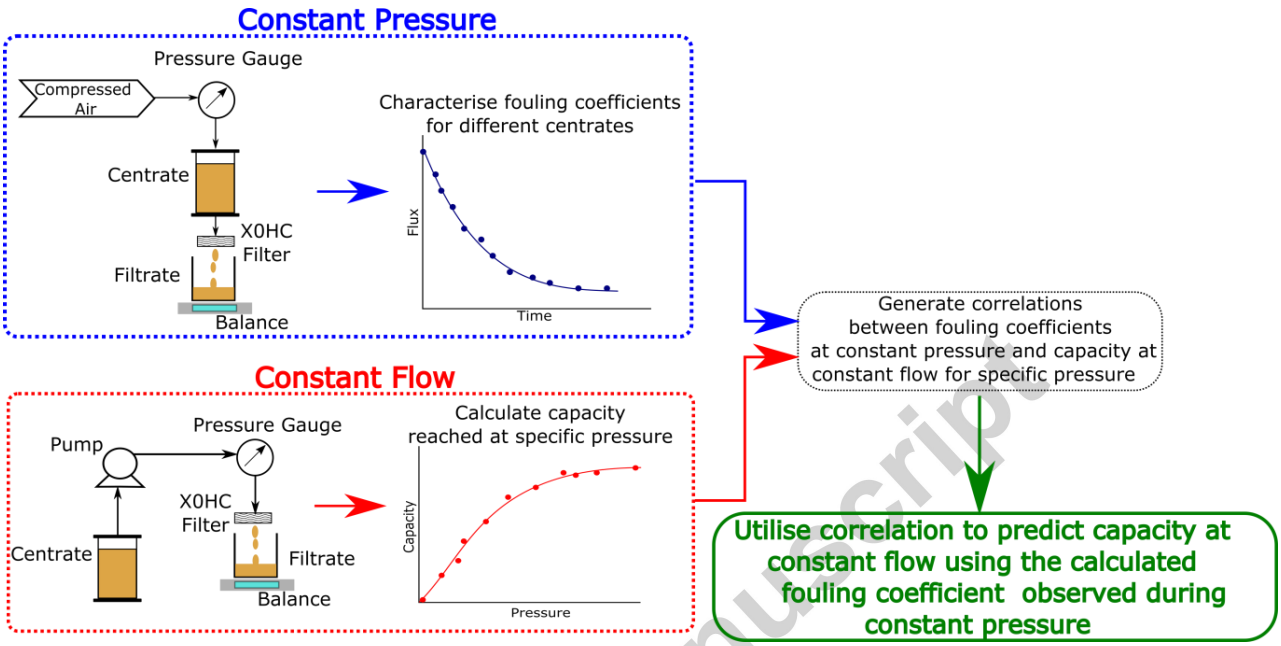


# 5. Conclusion

This publication describes the development and testing of a methodology to utilise constant pressure fouling data to predict capacity during constant flow processes of depth filters using mammalian cell culture material with a range of fouling propensities. The Cake-Adsorption fouling model was found to represent accurately the dominant fouling mechanism for the wide variety of centrates analysed across the multiple pressures. The calculated coefficients of this model were highly correlated ($R_{Cal}^2$=0.86) with the capacity at constant flow for the equivalent pressure. The correlation model can be implemented to provide an accurate prediction of the

capacity during constant flow operation at a specific pressure utilising the fouling coefficient calculated for the constant pressure flux profile at the specific pressure investigated. The correlation was found to be robust through cross-validation and was externally validated resulting in accurate capacity predictions of constant flow operation. The method described in this publication was also utilised to successfully predict the capacity of an alternate depth filter with a wider nominal pore size when operated at constant flow, further verifying the utility of the methodology developed. Additionally, it was also found that the filtrate generated from both modes of operation had similar qualities in terms of turbidity and subsequent sterile filter fouling propensities. The use of constant pressure over constant flow operation enabled significant savings in time and material requirements allowing for faster process development times in industry for depth filtration characterisation.

# Nomenclature

$a$ cake model coefficient (L $m^{-2}$)

$b$ cake model exponential coefficient (m)

$A$ available membrane frontal area ($m^2$)

$CF_{Cap,i}$ filter capacity at constant flow for a given pressure (L $m^{-2}$)

$J$ flux (L $m^2$ $h^{-1}$)

$J_v(0)$ initial flux (L $m^2$ $h^{-1}$)

$J_v(t)$ flux relative to available membrane area (L $m^2$ $h^{-1}$)

$K_A$ complete blocking constant ($m^2$ $L^{-1}$)

$K_C$ cake filtration constant ($m^2$ $L^{-1}$)

$K_{Com}$ complete blocking constant ($m^2$ $L^{-1}$)

$K_I$ intermediate blocking constant ($m^2$ $L^{-1}$)

$K_S$ standard blocking constant ($m^2$ $L^{-1}$)

$LMH$ liters per meter per hour (L $m^{-2}$ $h^{-1}$)

$P$ pressure (bar)

$R_{filter}$ specific resistance to filtration ($m^{-1}$)

$R^2$ coefficient of determination

$t$ time (h)

$V$ volume filtered ($m^3$)

## Greek letters

$\alpha_0$ Cake-Adsorption model coefficient (L $m^{-2}$ $h^{-1}$)

$\alpha_{1,2,}$ Cake-Adsorption model coefficients ($L^2$ $m^{-4}$ $h^{-1}$)

$\alpha_{3,4}$ Cake-Adsorption model coefficients ($L^4$ $m^{-6}$ h)

$\mu$ solution viscosity (Pa s)

# Acknowledgement

Financial support from the UK Engineering and Physical Sciences Research Council (EPSRC) and MedImmune for the Engineering Doctorate studentship for A. Joseph is gratefully acknowledged. This research is associated with the joint UCL-MedImmune Centre of Excellence for predictive multivariate decision-support tools in the bioprocessing sector and financial support from MedImmune and UCL for S. Goldrick is gratefully acknowledged. Grant code: EP/G034656/1.

# References

[1] A.D. Bandaranayake, S.C. Almo, Recent advances in mammalian protein production, FEBS Letters. 588 (2014) 253-260.

[2] D.J. Roush, Y. Lu, Advances in primary recovery: Centrifugation and membrane technology, Biotechnol. Prog. 24 (2008) 488-495.

[3] Y. Yigzaw, R. Piper, M. Tran, and A.A. Shukla, Exploitation of the adsorptive properties of depth filters for host cell protein removal during monoclonal antibody purification, Biotechnol. Prog. 22 (2006) 288-296

[4] R. Kempken, A. Preissmann, W. Berthold, Assessment of a disc stack centrifuge for use in mammalian cell separation, Biotechnol. Bioeng. 46 (1995) 132-138.

[5] D. Yavorsky, R. Blanck, C. Lambalot, R. Brunkow, The clarification of bioreactor cell cultures for biopharmaceuticals, Pharm. Biotechnol. 27 (2003) 62-67.

[6] F. Badmington, R. Wilkins, M. Payne, E.S. Honig, Vmax testing for practical microfiltration train scale-up in biopharmaceutical processing, Pharm. Biotechnol. 19(1995) 64-76.

[7] D. J. Miller, S. Kasemset, D.R. Paul, & B.D. Freeman, Comparison of membrane fouling at constant flux and constant transmembrane pressure conditions, J. Membrane Sci. 454 (2014) 505-515.

[8] D.M. Kanani R. Ghosh, A constant flux based mathematical model for predicting permeate flux decline in constant pressure protein ultrafiltration, J. Membrane Sci. 290 (2007) 207-15.

[9] G.R. Bolton, A.W. Boesch, M.J. Lazzara, The effects of flow rate on membrane capacity: Development and application of adsorptive membrane fouling models, J. Membrane Sci. 279 (2006) 625-634.

[10] S. Chellam, W. Xu, Blocking laws analysis of dead-end constant flux microfiltration of compressible cakes, J. Colloid Interface Sci. 301 (2006) 248-257.

[11] A. Joseph, B. Kenty, M. Mollet, K. Hwang, S. Rose, S. Goldrick, J. Bender, S.S. Farid, and N. Titchener-Hooker, A scale-down mimic for mapping the process performance of centrifugation, depth and sterile filtration, Biotechnol. Bioeng. 113 (2016) 1934-1941.

[12] Tien C, Ramarao BV. Revisiting the laws of filtration: An assessment of their use in identifying particle retention mechanisms in filtration, J. Membrane Sci. 383 (2011) 17-25.

[13] C-C. Ho, A.L. Zydney, A combined pore blockage and cake filtration model for protein fouling during microfiltration, J. Colloid Interface Sci. 232 (2000) 389-399.

[14] M. Hlavacek and F. Bouchet, Constant flowrate blocking laws and an example of their application to dead-end microfiltration of protein solutions, J. Colloid Interface Sci. 82 (1993) 285-295.

[15] W. Bowen, J. Calvo, A. Hernández, Steps of membrane blocking in flux decline during protein microfiltration, J. Colloid Interface Sci. 101 (1995) 153-165.

[16] M. Said, A. Ahmad, A.W. Mohammad, M.T. Nor, S.R. Abdullah, Blocking mechanism of PES membrane during ultrafiltration of POME, J. Ind. Eng. Chem. 21 (2015) 182-188.

[17] G. Bolton, D. LaCasse, R. Kuriyel, Combined models of membrane fouling: development and application to microfiltration and ultrafiltration of biological fluids, J. Membrane Sci. 277 (2006) 75-84.

[18] M. Sampath, A. Shukla, A.S. Rathore, Modelling of filtration processes—microfiltration and depth filtration for harvest of a therapeutic protein expressed in pichia pastoris at constant pressure, Bioeng. 1 (2014) 260-277.

[19] M.E. Laska, R.P. Brooks, M. Gayton and N,S. Pujar, Robust scale-up of dead end filtration: Impact of filter fouling mechanisms and flow distribution. Biotechnol. Bioeng. 92 (2005) 308-320.

[20] C. Tien, B.V. Ramarao, Revisiting the laws of filtration: An assessment of their use in identifying particle retention mechanisms in filtration. J. Membrane Sci. 383 (2011) 17-25.

[21] P.H. Hermans, H.L. Bredee, Zur kenntnis der filtrationsgesetze, Recl. Trav. Chim. Pays-Bas. 54 (1935) 680-700.

[22] M. Westoby, J.K. Rogers, R. Haverstock, J. Romero, J. Pieracci, Modelling industrial centrifugation of mammalian cell culture using a capillary based scale-down system, Biotechnol. Bioeng. 108 (2011) 989-998.



# Graphical abstract